VARIES ASPECTS OF LATEX FILM FORMATION IN THE PRESENCE OF ADDITIVES

by

Ewa Odrobina

A thesis submitted in conformity with the requirements
for the degree of Doctor of Philosophy
Graduate Department of Chemistry
University of Toronto

ABSTRACT

VARIES ASPECTS OF LATEX FILM FORMATION IN THE PRESENCE OF ADDITIVES

Ewa Emilia Odrobina, Ph.D. Thesis (2000)

Department of Chemistry, University of Toronto

This thesis examines the interaction of small macromolecules, like surfactants and oligomers, with poly(butyl methacrylate) (PBMA) latex particles. In this work, we mostly concentrated on nonionic surfactants, with the general structure R-$(EO)_n$, where, R represents the hydrophobic moiety, and $(EO)_n$ is the hydrophilic moiety consisting of n units of ethylene oxide. We also performed a number of experiments with other low molecular weight species, such as BMA oligomers and oligo(ethylene glycols) (PEG) as well as with a two ionic surfactants, sodium dodecyl sulfate (SDS) and dihexyl sulfosuccinate (C_{941}).

Binding isotherms for a series of nonylphenyl ether surfactants NP-$(EO)_n$ with PBMA latex reveal that the interactions between latex particles and nonionic surfactants decreases drastically with increasing EO chain length. We found that nonionic surfactants and PEG oligomers have very limited miscibility with PBMA at room temperature, but the miscibility increases with increasing temperature and decreasing EO chain length. The low molecular weight species which are not miscible with polymeric matrix phase separate to form domains in the latex films. The movement of surfactant to the surface (exudation) upon annealing is connected with the existence of micrometer-diameter channels leading to the film surface.

From polymer diffusion and miscibility measurements, we learned that when surfactant or oligomer stays in the film as a separate domains, it retards polymer diffusion, but when it is fully miscible with the polymeric matrix, it can act as a traditional plasticizer, and promote polymer diffusion by introducing free volume into the system. In this case the Fujita–Doolitle free volume theory is able to describe the effect of additive on the polymer diffusion rate. The effect of NP-$(EO)_{20}$ surfactant and BMA oligomers can be described in this way.

To investigate the influence of soft filler domains on polymer diffusion in latex films, we developed a model system consisting of cross-linked soft PBA latex particles dispersed in PBMA latex films. These experiments, show that the overall effect of added soft particles on polymer diffusion (retardation or enhancement) depends on a combination of different contributions: obstacle effects, wetting phenomena and changes in the morphology of the film.

Acknowledgements

I would like to express my deep appreciation to Professor Mitchell A. Winnik for being a great supervisor and teacher. Due to his understanding, patience, and believe in me as a growing scientist, I was able to successfully finish my Ph.D. studies while being mother of two young children. In his group, I not only obtained scientific knowledge, but learned how to work independently as well as in a team, how to make decisions and effectively communicate with people. I was also given the chance to collaborate with industry, and participate in conferences, both of which influenced my self-development.

My special thanks go to Dr. Jianrong Feng, for precious discussions, and a long successful collaboration, as well to Dr. Seigou Kawaguchi, Dr. Yuansheng Liu, Dr. Hung Pham, Dr. Ronghua Liu, Ms Olga Vorobova, Ms Valentina Stoyeva, Dr. Simon Bystryak, for various collaborations, and Dr. Matthew Moffitt for participation in the proof reading of my thesis. Thanks are extended to Dr. Theodore Provder for financial support to work at ICI, as well to Dr. Michael Neag, Dr. Edwin F. Meyer and Ms Candy Michalski at ICI for their wonderful assistance in carrying out the MDSC experiments during my visits to their lab.

I would also like to thank all members of Professor Winnik's laboratory for many valuable discussions, and the friendly environment they have created.

I also acknowledge the Ontario Center for Material Research (OCMR) for two years of scholarship funding, which enable me to collaborate with the industrial partners. Various scholarships offered by University of Toronto during my graduate studies are also appreciated.

I owe my deep thanks to my husband and mother for their help, encouragement and love. I would like to dedicate my thesis to them and to my beloved father who is no longer among us, but who dreamed of my scientific career.

TABLE OF CONTENTS

ABSTRACT ii

ACKNOWLEDGEMENTS iv

LIST OF TABLES viii

LIST OF FIGURES x

1 INTRODUCTION 1
1.1 Latex Film Formation 1
1.1.1 Description of the process 1
1.1.2 Drying Process. 2
1.1.3 Particle Deformation Mechanism and Packing Structure. 3
1.1.4 Polymer Diffusion. 4
1.1.5 Materials 5
1.2 Polymer Diffusion Measurements in Latex Films by Direct Energy Transfer (DET) method. 6
1.2.1 Polymer Diffusion Across Interface 6
1.2.2 Direct Non-radiative Energy Transfer 10
1.2.3 Analysis of Polymer Diffusion by DET 14
1.2.4 Fluorescence Decay Measurements 19
1.3 Free volume theory 19
1.3.1 Historical background 19
1.3.2 Concept of free volume 19
1.4 References 22

2 BINDING ISOTHERMS OF NP-$(EO)_n$ SURFACTANTS 26
2.1 Introduction 26
2.2 Experimental 27
2.3 Results and Discussion 28
2.3.1 Influence of size of the PBMA latex on the binding isotherm for NP-20 28
2.3.2 Influence of EO chain length on the binding isotherm of NP surfactants 29
2.3.3 Effect of the nature and size of hydrophobe part of surfactant on binding isotherm 31
2.3.4 Conformation of NP-$(EO)_n$ surfactant molecules bound to the PBMA latex surface 31
2.4 Conclusion 33
2.5 References 34

3 THE EFFECT OF POST-ADDED SURFACTANTS ON POLYMER INTERDIFFUSION PROCESS IN LATEX FILMS 35
3.1 Introduction 35
3.2 Experimental 37
3.2.1 Sample Preparation and Fluorescence Decay Measurement 37
3.3 Results and discussion 39

3.3.1 Influence of surfactants on diffusion of high molecular weight PBMA latex 39
3.3.2 Application of free volume theory to the high molecular weight polymer and nonionic surfactant system. 42
3.3.3 Influence of nonionic surfactants on diffusion of low molecular weight PBMA. 45
3.3.3.1 Starting point for measurements of diffusion parameters for low M PBMA films. 45
3.3.3.2 Film formation and diffusion of low M PBMA in the presence of nonionic surfactants at room temperature. 46
3.3.3.3 Diffusion of low M PBMA in the presence of nonionic surfactants at elevated temperatures 49
3.4 Conclusions 53
3.5 References 54

4 EFFECT OF OLIGOMERS ON THE POLYMER DIFFUSION RATE IN POLY(BUTYL METHACRYLATE) LATEX FILMS 56
4.1 Introduction 56
4.2 Experimental 56
4.2.1 Preparation of Oligomers 56
4.2.2 Film formation and Characterization 57
4.3 Results and Discussion 58
4.3.1 Characterization of the Latex Polymer. 58
4.3.2 Characterization of the oligomeric species. 60
4.4 Effect of oligomer on PBMA diffusion. 67
4.5 Conclusions 71
4.6 References 72

5 LOCATION OF NONIONIC SURFACTANTS AND PEG OLIGOMERS IN PBMA LATEX FILM 73
5.1 Introduction. 73
5.2 Experimental 73
5.2.1 Materials 73
5.2.2 Sample Preparation 75
5.2.3 Modulated Differential Scanning Calorimetry (MDSC) Measurements. 76
5.2.4 Laser Scanning Confocal Fluorescence Microscopy (LSCFM). 76
5.2.5 Fluorescence Decay Measurements 77
5.3 Results and discussion. 77
5.3.1 Latex films in the presence of NP-20. 77
5.3.2 DET in Nascent Films containing NP-20. 78
5.3.3 Miscibility of PBMA with NP-20 and PEO oligomers examined by MDSC 79
5.3.4 Mixtures of PBMA with EO_{10} and EO_{20} Examined by MDSC 84
5.3.5 DET investigation of the effects of An-EO_{38} in latex films 87
5.3.6 Morphology of PBMA films with AnEO_{38} in the light of Laser Scanning Confocal Fluorescence Microscopy(LSCFM). 93

5.3.6.1 Images for freshly formed films and films annealed at 50 °C. 93
5.3.6.2 Images for films annealed at 90 °C. 94
5.3.7 Effect of EO_n on Interdiffusion in PBMA Latex Films 98
5.4 Conclusions 103
5.5 References. 106

6 THE F_M VS $T^{1/2}$ AND F_M VS $T^{1/4}$ DEPENDENCE OBSERVED IN POLYDISPERSED LATEX FILMS. 107
6.1 Introduction 107
6.2 Experimental 107
6.3 Results and disscusion 108
6.4 Conclusions 113
6.5 References 113

7 THE EFFECT OF SOFT POLYMER FILLER PARTICLES ON POLYMER DIFFUSION IN PBMA LATEX FILMS. 114
7.1 Introduction 114
7.2 Experimental 116
7.2.1 Latex samples 116
7.1.2 Modulated Differential Scanning Calorimetry (MDSC) Measurements. 117
7.1.3 Film formation and measurements 118
7.3 Results and Discussion. 119
7.3.1 Initial Energy Transfer in Nascent Films. 119
7.3.2 Maximum Energy Transfer in Well-Mixed Films. 121
7.3.3 Effect of the size of soft PBA particles on diffusion rate of high Mw PBMA. 122
7.3.4 Effect of soft PBA particles on high M PBMA diffusion. Varying the blend composition. 126
7.3.5 DET as a method for probing local morphology in latex films. 133
7.3.6 Latex film morphology in the presence of soft PBA filler. 135
7.3.7 Obstacle vs. Free Volume models. 138
7.3.8 Influence of Soft PBA Particles on low M PBMA. 139
7.3.9 MDSC Measurements of the Glass Transition Temperature T_g in the PBMA + PBA blends. 140
7.4 Conclusions 144
7.5 References 145

APPENDIX A 147
The theory of modulated differential Calorimetry 147

LIST OF TABLES

Table 1-1	Recipe for the preparation of labeled PBMA latex.	6
Table 2-1	Adsorption data of NP-$(EO)_n$ surfactant on PBMA latex (d=393 nm).	30
Table 2-2	Dissociation constants for NP-$(EO)_n$ bound to the PBMA latex. The values were obtained form fitting experimental data to the Langmuir isotherms.	30
Table 3-1	Latex particle characteristics –high M PBMA.	37
Table 3-2	Latex particle characteristics –low M PBMA.	37
Table 3-3	List of investigated surfactants.	38
Table 3-4	Latex characteristics.	43
Table 3-5a	The change in the area under the fluorescence decay curves for various aging times at 23 °C, for a pure PBMA film and for a film containing 5 wt % NP-10.	47
Table 3-5b	The change in the area under the fluorescence decay curves for various aging times at 23 °C, for a pure PBMA film and for a film containing 5 wt % $C^{=}_{8}$-EO_7.	47
Table 4-1	Latex characteristics.	58
Table 5-1a	Latex particle characteristics –high M PBMA.	74
Table 5-1b	Latex particle characteristics –low M PBMA.	74

Table 5-1c	High M PBMA latex + An-$(EO)_{38}$ characteristics. (DET measurements).	74
Table 5-1d	High M PBMA latex + An-$(EO)_{38}$ characteristics. (LSCFM) measurements.	75
Table 5-2	Summary of T_g values for PBMA and PBMA + 2 wt% NP-20 blends.	83
Table 5-3	Summary of T_m values[a] for NP-20 and T_g values[b] for PBMA (in °C) for NP-20 and for mixtures of PBMA with various amounts of NP-20.	83
Table 5-4	Summary of T_g and T_m values (in ° C) for EO_{20}, and (PBMA + EO_{20})	85
Table 5-5	Summary of T_g and T_m values (in °C) for EO_{10}, and (PBMA + EO_{10})	87

Table 7-1	Recipe for the preparation of crosslinked PBA latex.	116
Table 7-2	Characteristics of PBMA latexes.	117

LIST OF FIGURES

Figure 1-1	Representation of latex film formation process.	2
Figure 1-2	Schematic drawing depicting the concentration profile C(r,t) of polymers confined to a one latex particle with radius R at t = 0 and at some later time t.	8
Figure 1-3	Minor chain reptation model[31]; a) diffusion along the tube and disengagement of a chain from its initial tube, b) the growth of minor chains up to reptation time T_r, where chains disengage from the initial tube and taking a new conformation.	9
Scheme 1-4	The deexcitation pathways of an excited donor (D) in the presence of an acceptor (A) chromophore.	11
Figure 1-5	The examples of fluorescence decay for PBMA films: (1) containing only phenantrene (Phe); (2) for freshly formed film containing Phe as a donor and An as a acceptor with ratio Phe/An =1:1; (3) for the same film like in (2) but annealed at 80 °C for 4 hours; (4) for the same film like in (2) but fully mixed.	14
Figure 1-6	Dependence of $k_{1/4}$ vs φ for PBMA + BMA oligomers.	17
Figure 1-7	The changes of: a) $\log(D_{app})$, and b) $k_{1/4}$ vs. volume fraction of BMA oligomer φ in the PBMA film.	18
Figure 1-8	The changes of: a) $\log(D_{app})$, and b) $k_{1/4}$ vs. volume fraction of soft filler φ in the PBMA film.	18

Figure 2-1	Schematic representation of the adsorption equilibrium of	26

surfactant on latex.

Figure 2-2 Binding isotherms of NP-20 with different diameters d of PBMA latex: (○) d=393 nm, (●) d=261 nm, (△) d=141 nm. 28

Figure 2-3 Binding isotherms of NP-$(EO)_n$ surfactants with PBMA latex (latex diameter d = 393 nm): (○) NP-10, (●) NP-20, (□) NP-40, (■) NP-100. 29

Figure 2-4 Dependence of the amount of bound surfactant per surface area at saturation Γ_{sat} vs. molecular weight of $(EO)_n$ – hydrophilic part of surfactant. 32

Figure 3-1 Dependence of extent of mixing (f_m) on annealing time (diffusion time) for pure high M PBMA film (○) and films with 5 wt % of different surfactants: NP-20 (●), A-20 (□), Ocenol-12 (■), Ocenol-40 (Δ), SDS (▲), C-941 (▽); (a) short time behavior, (b) long time behavior. The annealing temperature is 72 °C. 40

Figure 3-2 Dependence of extent of mixing (f_m) on annealing time for pure high M PBMA film (○) and films with the presence of 5 wt % Ocenol-9 (□), and Ocenol-15 (●). The annealing temperature was 76 °C. 41

Figure 3-3 Plots of f_m vs. square-root of annealing time at the different NP-surfactants at 90°C. (○) 0 wt% NP; (■) NP-100, 15 wt%; (□) NP-40, 14.6 wt%; (▲) NP-20, 15.0 wt%, and (●) Np-10, 17.8 wt%. 41

Figure 3-4 Plots of apparent diffusion coefficient (D_{app}) vs. extent of mixing 44

(f_m) in the presence of NP-20 surfactant at 90 °C: (○) 0 wt%, (●) 3.34 wt%, (Δ) 9.9 wt%, (▲) 15 wt% NP-20.

Figure 3-5 Master curve of D_{app} vs. f_m. The Master Curve was constructed from the data in Figure 3-4 using equation 3-1, and the values f_p(90 °C)= 0.089 and $\beta(t) = 0.20$ The symbols are the same as those in Figure 3-4. 44

Figure 3-6 Efficiency of energy transfer Φ_{ET} vs. time of film formation for low M PBMA films. The data was taken from reference 18. After 40 min the process of water evaporation is finished and Φ_{ET} does not change with time up to 100 min. 46

Figure 3-7 Efficiency of energy transfer Φ_{ET} vs. annealing time for pure low M PBMA film (○) and films with the presence of 5 wt% NP-10 (●), and Octene-7 ($C^{=}_{8}$-EO_7) (□). The diffusion process takes place at room temperature. 47

Figure 3-8 Dependence of extent of diffusion f_m (a) and apparent diffusion coefficient D_{app} (b) on annealing time (diffusion time) for low M PBMA film (○) and films with 5 wt % of NP surfactants: (●) NP-6, (□) NP-20, (■) NP-40. Annealing temperature is 60 °C. 50

Figure 3-9 Dependence of extent of diffusion f_m on annealing time (diffusion time) for low M PBMA film (○) and films with 5 wt % of NP surfactants: (▲) NP-6, (□) NP-10, (◆) NP-20. Annealing temperature is 50 °C. 50

Figure 3-10 Dependence of extent of diffusion f_m (a), and apparent diffusion coefficient D_{app} (b) on annealing time (diffusion time) for low 51

molecular weight PBMA film (○) and films with 5 wt % of the following surfactants: (●) $C^{=}_{11}$-EO_{40}, (□) $C^{=}_{11}$-EO_{15}, (▲) $C^{=}_{8}$-EO_{14}, (▼) OCENOL-EO_{16}, (▽) $C^{=}_{8}$-EO_{7}. The annealing temperature was 50 °C.

Figure 4-1 GPC (RI) curves for an unlabeled PBMA sample with (1) and without (2) cleaning. 59

Figure 4-2 GPC curves for a labeled (An-PBMA) sample: curve (1) refractive index (RI) signal, (2) fluorescence (FL) signal. 59

Figure 4-3 GPC signal for BMA oligomer separated from PBMA latex (Figure 4-4a) by centrifugation, then dried and dissolved in THF. 61

Figure 4- 4 GPC (RI) curves for (a) crude PBMA sample with oligomers (a), and (b) the same sample after cleaning by ion exchange. The two traces are normalized to the same peak height for the polymer peak at t = 16 min. (c) The difference signal obtained by subtracting curve (b) from curve (a). 62

Figure 4-5 ^{1}H NMR spectrum of poly(butyl methacrylate) in $CDCl_3$. 65

Figure 4-6 ^{1}H NMR spectrum of a freeze-dried sample of the oligomer in $CDCl_3$. 65

Figure 4-7 (top) ^{1}H NMR spectrum of a freeze-dried sample of the oligomer fraction employed in the experiments described above. The sample is dissolved in DMSO-d6 to which a trace of DMSO is added as a reference. (bottom) ^{1}H NMR spectrum of the same sample to which a few drops of pyridine have been added. The inset presents the aliphatic region of this spectrum on an expanded scale. 66

Figure 4-8	GPC signals for 1:1 mixture of the Phe- and An-labeled PBMA without (1) and with (2) post-added oligomers (9 wt %).	68
Figure 4-9	Comparison of diffusion rates for PBMA (M_W=370K) at 76°C without post-addition (■) and with addition of 3 wt% (□), 6 wt% (●), and 9 wt% (○) of BMA oligomers. In (a) and (b) the plots of extent of mixing (f_m) vs. time (in min) and the mean diffusion coefficient (D_p, in nm^2/s) vs. fm, respectively, are shown.	69
Figure 4-10	Plot of $1/Ln[D_p(T,\Phi_a)/D_p(T,0)]$ vs $1/\Phi_a$.	71
Figure 4-11	Master curve of D_p vs. f_m for PBMA latex films with 0 wt% (■), 3 wt% (□), 6 wt% (●), and 9 wt% (○) of BMA oligomers.	71
Figure 5-1	Plots of Area(0) values (obtained from integration of the normalized Phe fluorescence decay profiles) vs. concentration of Np-20 surfactant molecules.	78
Figure 5-2	Plots of heat flow (1), nonreversing heat flow (2), and reversing heat flow (3) vs. temperature for pure PBMA. The reversing heat flow shows a glass transition at 34 °C. The peak in the scan of nonreversing heat flow is due to enthalpy relaxation reflecting prior sample history.	79
Figure 5-3	(a) MDSC first scan (heating) for pure PBMA (1), PBMA + 5 wt% NP-20 (2), and 10 wt% NP-20 (3). (b) MDSC scans (first heating (1), second cooling (2), and third reheating (3) for pure NP-20 surfactant.	80
Figure 5-4	Plot of total heat flow vs. temperature (three scans) for: (a) PBMA + 5 wt % NP-20, and (b) PBMA + 10 wt % NP-20. We identify	82

the peak exotherm at – 40 °C in the cooling scans with the crystallization of NP-20 after it demixes from the polymer. In case (b) we also observe broad NP-20 crystallization peak at 15 °C indicating that not all surfactant became molecularly mixed with polymer matrix.

Figure 5-5 Plots of reversing heat flow (W/g) for the cooling scan vs. temperature for PBMA (1), PBMA + 2 wt % (2), PBMA + 5 wt % NP-20 (3), and PBMA + 10 wt % NP-20 (4). 84

Figure 5-6 Plots of total heat flow for cooling scans vs. temperature for PBMA samples with 3.8 wt %, 5 wt %, and 10 wt % PEG_{20}. The two crystallization peaks observed in these scans are approximately at –30 °C and 25 °C. The peak at 25 °C is the crystallization peak of pure PEG_{20} (not mixed with PBMA). The peak at –30 °C is the crystallization peak of PEG_{20} after it demixes from the polymer. 85

Figure 5-7 Plots of total heat flow for first heating scans vs. temperature for PBMA samples with 0 wt %, 1.7 wt %, 3.8 wt %, 5 wt %, and 10 wt % PEG_{10}. The peak around 0 °C is the melting peak of PEG_{10}. The peak at 35 °C is due to enthalpy relaxation, and obscures the PBMA glass transition region. 87

Figure 5-8 The schematic representation of An-labeled PEG domains (An-EO_{38}) in the Phe-labeled latex film. The energy transfer takes place between donor-labeled latex particles and acceptor labeled PEG domains. 88

Figure 5-9 Area under the fluorescence decay (a), and efficiency of energy 89

transfer Φ_{ET} (b) vs. An-EO_{40} concentration for PBMA + An-EO_{38}: (○) freshly formed films, (■) films annealed for 30 hours at 50 °C.

Figure 5-10 The area under the fluorescence decay (a), and the efficiency of energy transfer Φ_{ET} (b) versus annealing time at 50 °C for films with: 20 wt% (●), 25 wt% (□), and 30 wt% (■) An-EO_{38} in the Phe-PBMA latex film. 90

Figure 5-11 The efficiency of energy transfer versus annealing time at 90° C for Phe-PBMA films containing: 5 wt% (○), 10 wt% (●), 15 wt% (□), 25 wt% (■), and 30 wt% (Δ) An-EO_{38}. 92

Figure 5-12 Confocal images of freshly formed PBMA sample with 30 wt% of An$(EO)_{38}$. The top right image is the surface of the sample, next ones are the subsequent slices with the depth interval 5μm. The size of each image is 73.1 x 73.1 μm. 94

Figure 5-13 Images of PBMA sample with 7 wt% of AnEO_{38}, annealed at 90 °C, 3 hours. The images are from the surface (right top) of the film into the bulk with 2 μm depth interval. The size of each image is 73.1 x 73.1 μm. 95

Figure 5-14 Images of PBMA sample with 15 wt% of AnEO_{38}: (A) annealed at 90 °C for 3 hours, (B) for freshly formed film. The images are from the surface (right top) of the film into the bulk at 5 μm depth intervals. The size of each image is 73.1 x 73.1 μm. 96

Figure 5-15 Images of PBMA sample with 30 wt% of AnEO_{38}, annealed at 90 °C, 3 hours. The images are from the surface (right top) of the film 97

into the bulk at 5 μm depth intervals. The size of each image is 73.1 x 73.1 μm.

Figure 5-16 Images of PBMA sample with 30 wt% of $AnEO_{38}$, annealed at 90 °C for 3 hours, and immersed in silicon oil. The images are from the surface (right top) of the film into the bulk at 5 μm depth intervals. The size of each image is 73.1 x 73.1 μm. 98

Figure 5-17 Dependence of extent of diffusion f_m (a) and apparent diffusion coefficient D_{app} (b) on annealing time (diffusion time). (c) Dependence of diffusion coefficient on extent of mixing for pure PBMA film (●) and films with the presence of 5 wt % PEG of different molecular weight (○) EO_{10}, (△) EO_{20}, (□) EO_{68}, (◆) EO_{100}. Annealing temperature: 76 °C. 99

Figure 5-18 Plots of Area(0) vs. concentration of EO_{20} in the PBMA films. 101

Figure 5-19 Dependence of extent of diffusion f_m (a) and apparent diffusion coefficient D_{app} (b) on annealing time (diffusion time). (c) Dependence of diffusion coefficient on extent of mixing for pure PBMA film (●) and films with the presence of 5 wt % PEG of different molecular weight (○) EO_{10}, (△) EO_{20}, (□) EO_{68}, (◆) EO_{100}. Annealing temperature: 90 °C. 101

Figure 5-20 Dependence of extent of diffusion (f_m) on annealing time (diffusion time) for pure low M PBMA film (●) and films with the presence of 5 wt % PEG of different molecular weight (○) EO_{10}, (▲) EO_{45}. Annealing temperature: 60 °C. 102

Figure 5-21 Model of NP-20 surfactant distribution in PBMA latex films with varying surfactant content. (a) For PBMA films with 2 wt % or 104

less of NP-20 surfactant. Before annealing, the surfactant is distributed only in the top surface of the polymer. After annealing, the surfactant is uniformly distributed in the film. (b) For PBMA films with 5+ wt % NP-20 surfactant. Before annealing, the surfactant is distributed only in the top surface of the polymer. During annealing at 90 °C, the surfactant diffuses uniformly inti the polymer phase. Upon cooling, part of the surfactant remains in the polymer phase, but the rest of the NP-20 phase separates and forms local domains in the film.

Figure 6-1 Dependence of $\ln(f_m)$ vs. $\ln(t)$ (f_m is the extent of mixing, and t is the annealing time) for three different latex film samples prepared from the low molecular weight ($M_w = 3.5x10^4$) PBMA particles, annealed at 60 °C. 108

Figure 6-2 Dependence of $\ln(f_m)$ vs. $\ln(t)$ (f_m is the extent of mixing, and t is the annealing time) for high molecular weight ($M_w = 4x10^5$) PBMA sample and its blends, annealed at 70 °C: (○) in the absence of presence of crosslinked poly(butylacrylate) (PBA) microspheres, (●) 10 % PBA, (□) 30 % PBA, (■) 60 % PBA. 109

Figure 6-3 Dependence of $\ln(f_m)$ vs. $\ln(t)$ for samples from Figure 2: a) expanded region for $f_m \leq 0.2$, (○) pure PBMA (slope = 0.41), (●) 10 % PBA (slope = 0.4), (□) 30 % PBA (slope = 0.56), (■) 60 % PBA (slope = 0.55); b) expanded region for $f_m > 0.2$, (○) pure PBMA (slope = 0.20), (●) 10 % PBA (slope = 0.22), (□) 30 % PBA (slope = 0.27), (■) 60 % PBA (slope = 0.28). 110

Figure 6-4 Dependence of $\ln(f_m)$ vs. $\ln(t)$ in the range of f_m parameters $0< f_m \leq 0.2$ for high molecular weight ($M_w = 4x10^5$) pure PBMA sample annealed at 76 °C. The calculated slope is 0.46. The data was 111

annealed at 76 °C. The calculated slope is 0.46. The data was
---------- taken from Figure 4-9a in Chapter 4.

Figure 7-1 Plots of Area(0) (unfilled symbols) and efficiency of energy transfer ET (filled symbols) vs. the soft particle volume fraction; (a) for low molecular weight PBMA films, (b) for high molecular weight PBMA films. 119

Figure 7-2 Comparison of high M PBMA diffusion rates for pure PBMA films (○) and for films blended with 30 vol % PBA particles of different diameters (d_{PBA}): 56 nm (●),and 112 nm (▲). In part a) we plot the extent of mixing (f_m) vs annealing time, and in part b) we plot the apparent diffusion coefficient D_{app} vs. f_m. 123

Figure 7-3 Plots of f_m vs. $t^{1/4}$ for a pure PBMA film (○) and for films blended with 30 vol % PBA particles of different diameters (d_{PBA}): 56 nm (●), and 112 nm (▲). 124

Figure 7-4 Plot of $k_{1/4}$ vs $1/d_{PBA}$ in PBMA/ PBA blend films at 30 vol % PBA. The data were derived from Figure 7-3. 124

Figure 7-5 Plots of f_m vs. $t^{1/2}$ for a pure PBMA film (○) and for films blended with 30 vol % PBA particles of different diameters (d_{PBA}): 56 nm (●), and 112 nm (▲). 126

Figure 7-6 Plot $k_{1/2}$ vs. $1/d_{PBA}$ in PBMA/ PBA blend films at 30 vol % PBA. The data were derived from Figure 7-5. 126

Figure 7-7 Plot of the extent of mixing f_m for films blended with different amounts of PBA particles (d_{PBA}= 56 nm), expressed as volume percent (% PBA): 0 (○), 10 (▲), 30 (□), and 60 (■). Part a) 127

presents short time diffusion behavior, and part b) presents long time diffusion behavior.

Figure 7-8 Plots of : a) f_m vs. $t^{1/4}$ for films blended with different amounts of PBA particles (d_{PBA}= 56 nm), expressed as volume percent (% PBA): 0 (○), 10 (●), 30 (□), and 60 (■); and b) $k_{1/4}$ vs. vol % PBA. 128

Figure 7-9 Plot of the extent of mixing f_m vs. annealing time for films blended with different amounts of PBA particles (d_{PBA}= 56 nm), expressed as volume percent (% PBA): 0 (○), 3 (●), 6 (□). 130

Figure 7-10 Plots of f_m vs. $t^{1/4}$ for films blended with different amounts of PBA particles (d_{PBA}= 56 nm), expressed as volume percent (% PBA): 0 (○), 3 (●), 6 (□). 130

Figure 7-11 Dependence of parameter $k_{1/4}$ vs. volume fraction of filler (vol% PBA, d_{PBA}= 56 nm). 130

Figure 7-12 Plot of the extent of mixing f_m for films blended with different amounts of PBA particles (d_{PBA}= 56 nm), (% PBA): 0 (○), 3 (■), 6 (□) - series a; 0 (△), 10 (▲) - series b. The samples from series (a) and (b) were not annealed at the same time. 131

Figure 7-13 Plot $k_{1/4}$ vs. vol % PBA. 132

Figure 7-14 Plot log (D_{app}) vs. vol % PBA. The values of D_{app} were taken at constant f_m, f_m = 0.3. 132

Figure 7-15 Plots f_m vs $t^{1/2}$ for films blended with different amounts of PBA particles (d_{PBA}= 56 nm), expressed as volume percent (%PBA): 0 (○), 10 (●), 30 (□) and 60 (■). 133

Figure 7-16 Dependence of $k_{1/2}$ vs. vol % PBA: a) linear scale and b) log-log scale. 133

Figure 7-17 A model of latex film morphology in the presence of soft PBA fillers: a) at volume fractions of $\varphi_{PBA} \leq 0.06$ the filler particles are randomly distributed in the PBMA matrix; b) when $0.1 > \varphi_{PBA} > 0.06$ the formation of filler aggregates takes place; c) for $\varphi_{PBA} \geq 0.1$ we have two possibilities of the growth of aggregates with increasing volume of fillers; I) the aggregates are in form of a connected network which grows in contour length when the amount of filler is increased, II) the filler aggregates grow in volume. These domains consist of PBA only. 136

Figure 7-18 Influence of obstacles on polymer diffusion. The measured rate of diffusion decreases as the path of the diffusion increases in the presence of obstacles. 138

Figure 7-19 Comparison of low M PBMA diffusion rates for films blended with different amounts of PBA particles (d_{PBA}= 56 nm), expressed as volume percent (% PBA); 0 (○), 30 (□), and 60 (▲). In part a) we plot the extent of mixing (f_m) vs. square root of annealing time ($t^{1/2}$), and in part b) we plot the apparent diffusion coefficient D_{app} vs. f_m. 140

Figure 7-20 Plot of the first derivative of the heat capacity vs temperature for the high M PBMA sample, and its blends with 30 vol %, and 60 vol % of PBA. Part a) presents the heating scan from -125° C to 75° C; and in part b) the cooling scan from 75° C to -125° C. 141

Figure 7-21 Plot of the first derivative of the heat capacity vs temperature for the low M PBMA sample, and its blends with 30 vol %, and 60 vol % of PBA. Part a) presents the heating scan from –125 °C to 75 °C; and in part b) the cooling scan from 75 °C to –125 °C. 143

Figure 7-22 Drawing of a model for films with soft filler: the presence of soft PBA particles in the PBMA matrix induces wetting of the filler surface by the part of PBMA with lower M and the formation for PBMA of higher and lower mobility regions. This effect increases the average diffusion rate of PBMA 144

Figure A-1 a) The total heat flow calculated as the average of the modulated heat flow signal; b) the modulated heat flow and its amplitude Q_{amp}; c) the heating rate with its amplitude T_{amp}. 148

1. INTRODUCTION

1.1 Latex Film Formation

1.1.1 Description of the process

Latex film formation is a process by which an aqueous dispersion of polymer particles is transformed into a continuous coating material. This is a complex process, which can be divided into large number of steps. However, schematically we can distinguish three consecutive major steps that occur during film formation process. These steps are presented in Figure 1-1. First, evaporation of water brings the particles into close contact. Second, as more water evaporates, the particles undergo deformation to form a void–free solid structure, which is still mechanically weak. Finally, fusion occurs among adjacent particles to give mechanically strong film. At this point we would like to emphasize that stage two and stage three can only occur at temperatures higher than minimum film–forming temperature (MFT). The MFT commonly corresponds to the glass transition temperature of the latex in the presence of water. At T > MFT, the modulus of the polymer decreases by several orders of magnitude. Under these conditions the forces driving the latex deformation exceed the resistance to deformation.

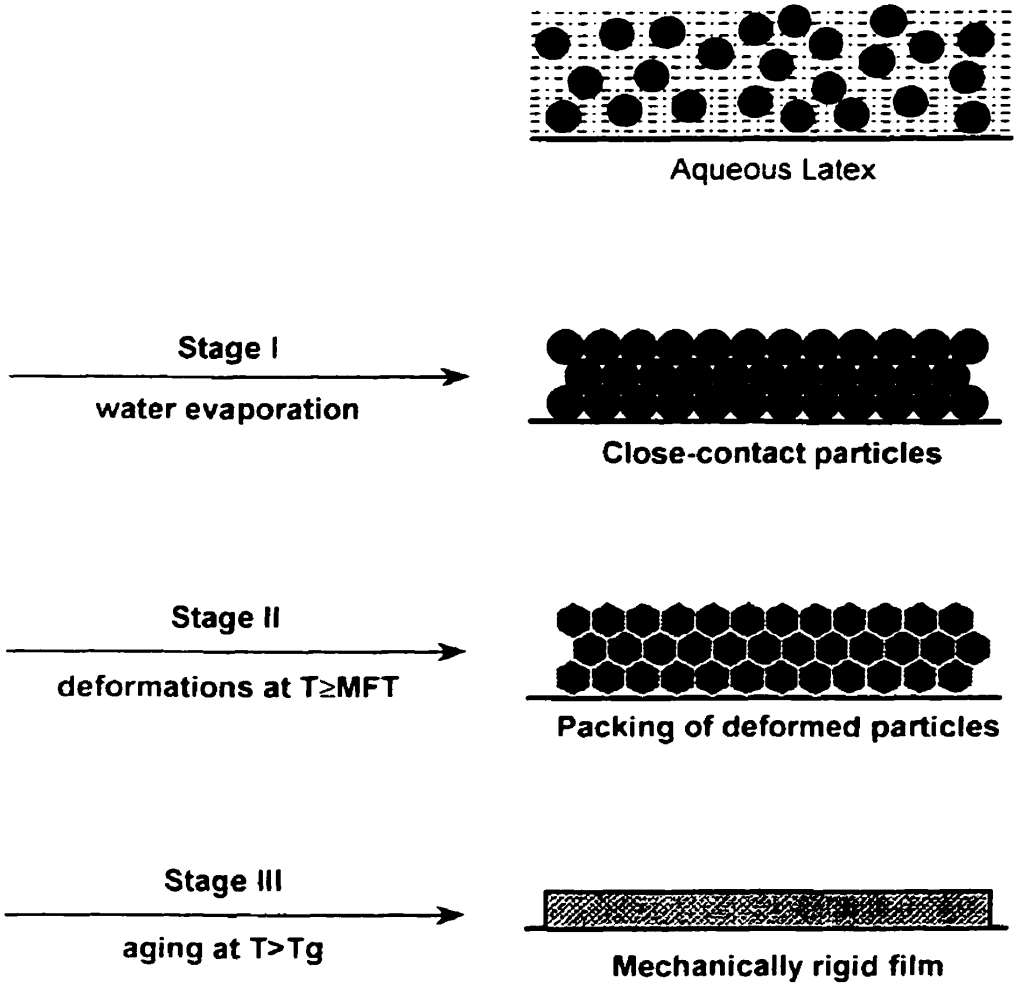

Figure 1-1 Representation of latex film formation process.

1.1.2 Drying Process.

The most well-known model of drying process is a simple model proposed by Vanderhoff.[1] He connected the changes in the water loss rate with the three steps of film formation process. In first stage, where the particles remain separated, the rate of water loss is constant. In second stage the particles deform, and they limit surface area of the air-water interface. The evaporation rate slows. Finally, in the stage third, the particle deformation process is finished, and the coalescence leads to sealing of the surface. The loss of the last traces of water is very slow, as the water has to diffuse through polymeric matrix.

The Vanderhoff model and other classic models[2,3] presume that drying process is uniform over the entire surface. However, when the dispersion is spread onto a flat surface, a flat liquid drop with a slightly convex surface forms immediately. In this case the drying occurs as a propagating front[4-7] from the edges to the center because water evaporates more rapidly from the high surface region at the wet – dry boundary than from the wet surface of the droplet itself. Water is constantly wicked through the pore structure at this boundary to these dry regions, and this in turn creates a flux of water and particles from the droplet to the dry edge. This drying process was first describing by Denkov et al.[5] who pointed out that the process depends sensitively on the shape of the meniscus, which is formed by the dispersion on the surface. Although the description by Denkov does not constitute a complete model of the drying process for latex dispersions, it describes two features of this process which other models can not explain. First, their picture is consistent with the observation that the drying front in the latex dispersion is in the plane of the substrate. Second, it explains the observation that films formed on flat quartz or glass substrates are much thicker at the edges than in the center.

1.1.3 Particle Deformation Mechanism and Packing Structure.

The nature of the forces ensuring particle deformation in the second stage of the latex film formation process has been much discussed in literature. There are in principle three types of forces that might drive particle deformation. For dry particles, the main force driving the coalescence of particles is associated with the polymer-surface (polymer-air) interfacial tension.[8] When particles compaction occur under water, the polymer-water interfacial tension will promote minimization of surface area[9] and cause particle deformation. Brown[10] pointed out the important role of the capillary forces, which are connected with air-water interfacial tension. These forces appear at the surface of the drying latex, when particles become partially exposed to the air. Water in capillaries between particles produces forces, which compress the packing of particles and make them coalesce. The forces are proportional to the air-water interfacial tension and inversely proportional to the size of the capillary to form. Finally, Eckersley and Rudin[11] have summarized the historical progression of film formation models. These authors proposed a theory in which capillary and interfacial forces act together to promote film coalescence. In this case, the interfacial forces may involve dry and/or wet sintering, depending on the details of the

drying process. Although huge progress has been made in the field of latex particle deformation and coalescence, the question of driving forces is still under active discussion. On the contrary, the general description of phenomena of particle resistance to deformation seems to have been achieved. The forces resisting the deformation are mainly related to the viscoelastic deformation and flow properties of polymer.[10-12]

When driving forces overcome resistance forces, the particle are transformed into space-filling polyhedra during the compaction process. It is generally thought that an ordered dispersion in water should form a film in which this order is maintained. There is a lot of experimental data showing that when the repulsion between particles are strong and the particles are monodisperse in size, they form a face centered cubic (fcc) structure in the dispersion[13] and this dispersion gives rise to a rhombic dodecahedral structure in the film.[14-18] When the coulombic repulsion forces between particles are screened (e.g. by the presence of salt or surfactant) no ordering occurs during drying. The particles will come into contact in a random closed-packed array.[17] The structure generated from randomly packed particles are predicted to form random Wigner-Seitz cells: polyhedra with typically 14 to 17 faces and each face having possibility of being 4 to 6 sided.[17,19]

1.1.4 Polymer Diffusion.

Polymer diffusion across latex particles occurs in newly formed latex film upon aging or annealing. Studies by electron microscopy revealed that with time (at temperatures above Tg) the film cellular microstructure of the original particles gradually disappears, leading to a smooth homogenous film.[1,20,21] This process is essential in producing a mechanically strong film.[22] For example, Sperling and Klein[23,24] compared the extent of polymer diffusion with the growth of tensile strength in latex films. They found that mechanical strength of the film increases with diffusion, and reaches a maximum value as the polymer molecules diffuse a distance equal to one radius of gyration across the interface.

As the theory of polymer diffusion across interference is discussed in further sections of this chapter, and most of the others chapters in this thesis concentrate on polymer diffusion in the presence of different kind of additives, I refer reader to these chapters to learn more about polymer diffusion in latex films. Here I would like only to point out two major techniques for measuring polymer diffusion in latex films: small angle neutron scattering (SANS) and the direct non-radiative energy transfer (DET). In both these

techniques, contrast is achieved by labeling. SANS measures the growth with time of radius of gyration (R_g) of deuterated microspheres dispersed in protonated matrix[25]. This growth can be fitted to a diffusion model and the diffusion coefficient of the polymer can be calculated from the evolution of R_g with time.

In the case of DET measurements, the latex particles are labeled by fluorescence dyes. Half of the particles are labeled with a donor dye and the other half with an acceptor dye. During the diffusion process, the donor-labeled polymer mixes with the acceptor-labeled polymer. As a consequence, energy transfer between donor and acceptor can take place. Energy transfer causes the Phe emission to be quenched, leading to a faster fluorescence decay. From the area under the fluorescence decay curve, one can calculate the quantum efficiency of energy transfer ϕ_{ET}. From ϕ_{ET}, one can calculate the extent of mixing. One can also calculate the apparent diffusion coefficient under the condition that the diffusion follows Fick's laws.

1.1.5 Materials

All latex films used in my thesis research are made from poly(n-butyl methacrylate) (PBMA) latexes. They were prepared by semi continuous emulsion polymerization method under monomer starved condition. For DET measurements the PBMA latex was labeled with either anthracene (An) or phenantrene (Phe). In Table 1-1 a typical recipe for the preparation of labeled PBMA latex is presented: For preparation of unlabeled particles, a similar procedure is employed, but without adding a dye comonomer. The procedure is described as follows: A small amount of PBMA latex seed (diameter d = 55 nm) was prepared in the first stage. Potassium persulfate (KPS), sodium dodecyl sulfate (SDS), and sodium bicarbonate ($NaHCO_3$) were used as the initiator, surfactant, and pH buffer, respectively. In some cases, a certain amount (e.g. 2 wt % based upon the monomer weight) of a chain transfer agent (i.e. dodecyl mercaptan, DM) was used to adjust the molecular weights for the latex polymers. In the second stage of polymerization, a monomer solution composed of 1 mol % of a fluorescent comonomer ((9-phenanthryl) methyl methacrylate (PheMMA), or 9 vinyl phenanthrene (V-Phe), or (9-anthryl) methacrylate (AnMA)), a certain amount of DM, and the rest of BMA were continuously fed into the seed latex dispersion. The monomer feeding rate was slow (< 0.1 ml/min). KPS and SDS dissolved in water were added into the reactor concurrently. A high conversion of the monomers (>

98.5%) was obtained for all reactions, as evaluated gravimetrically. The particle size was ca. 125 nm (with a narrow size distribution) where prepared by this recipe. The detailed characteristics of the latex particles used in particular experiments are shown in the successive chapters.

Table 1-1. Recipe for the preparation of labeled PBMA latex.

First stage		**Second stage**	
BMA (ml)	3.3	BMA (ml)	30
DM (ml)	0 – 0.074	DM (ml)	0 – 0.68
Water (ml)	60	PheMMA[a] (g)	0.58
KPS (g)	0.066	Water (ml)	24
SDS (g)	0.099	KPS (g)	0.540.06
$NaHCO_3$ (g)	0.066	SDS (g)	0.54
Temp (°C)	80	Temp (°C)	80
Time (h)	1	Time (h)	20-24

a) When using V-Phe dye comonomer this quantity becomes 0.48 g; For preparing the An-labeled latex, 0.62g AnMA was used to replace 0.58 g PheMMA.

1.2 Polymer Diffusion Measurements in Latex Films by Direct Energy Transfer (DET) method.

1.2.1 Polymer Diffusion Across Interface.

When two amorphous polymers are brought into good contact above T_g, the chain conformations at the interface tend to evolve towards those in the bulk, and the interdiffusion process take place due to Brownian motion. Such motion consists of random thermal jumps of segments of polymer chains between adjacent voids or "free volume elements." There are many factors that can change or influence polymer dynamics at an interface (molecular weight M, polydispersity in M, distribution of polymer chain ends, plasticization effect, etc.). Among these, the molecular weight is the most important factor affecting polymer diffusion rate. There are two models, the Rouse model[26] and the reptation model[27], describing the molecular weight dependence of polymer dynamics in various systems. The Rouse model takes account of the effect of chain connectivity on the friction

coefficient of a diffusing chain. The reptation model adds topological (entanglement) effects to the description of chain dynamics. When the molecular weight of polymer is not high $M < 2M_e$ (M_e is the critical entanglement molecular weight, and for PBMA, M_e = 30 000)[28] the Rouse model applies. The model corresponds to unperturbed coils with Gausian statistics of the end-to-end distance, and assumes that polymer chains consists of N beads connected by (N-1) springs. Each bead feels the same friction from the surrounding mediums, and has a frictional coefficient f. Since the N segments of the chain are hydrodynamically independent of each other, the molecular friction coefficient $f_{total} = Nf$, and the diffusion coefficient D is inversely proportional to the molecular weight M, $D \approx M^{-1}$ ($D = kT/f_{total}$ from the Einstein equation, where k is the Boltzman constant and T is the temperature). In the Rouse model, the chain relaxation time at the interface is very short, and polymer diffusion follows Fick's[29] laws. Fick's first law (eq. 1-1) defines the diffusion coefficient D (in units of cm^2/s), which is an important parameter characterizing the diffusion rate.

$$F = -D\,\partial C/\partial x \tag{1-1}$$

Here F is the flux or the rate of transfer of diffusing molecules through a unit cross-sectional area (in mole/cm^2s) and $\partial C/\partial x$ is the concentration gradient (in mole/cm^3/cm).

Fick's second law describes the mass transfer across the interface, and provides an expression for the concentration of the diffusing substance at certain position in the diffusing system in terms of the time t and the diffusion coefficient D. For example, for Fickian diffusion in spherical geometry, if the diffusing substance is initially distributed uniformly through a sphere of radius R with a concentration C_o, the concentration C(r,t) at radius r and time t is given by[30,29]

$$C(r,t) = \frac{C_0}{2}\left[\operatorname{erf}\left(\frac{R+r}{2\sqrt{Dt}}\right) + \operatorname{erf}\left(\frac{R-r}{2\sqrt{Dt}}\right)\right] - \frac{C_0}{r}\sqrt{\frac{Dt}{\pi}}\left\{\exp\left[-\frac{(R-r)^2}{4Dt}\right] - \exp\left[-\frac{(R+r)^2}{4Dt}\right]\right\} \tag{1-2}$$

A schematic drawing representing the concentration profile at time t = 0 and at a later time is shown in Figure (1-2)

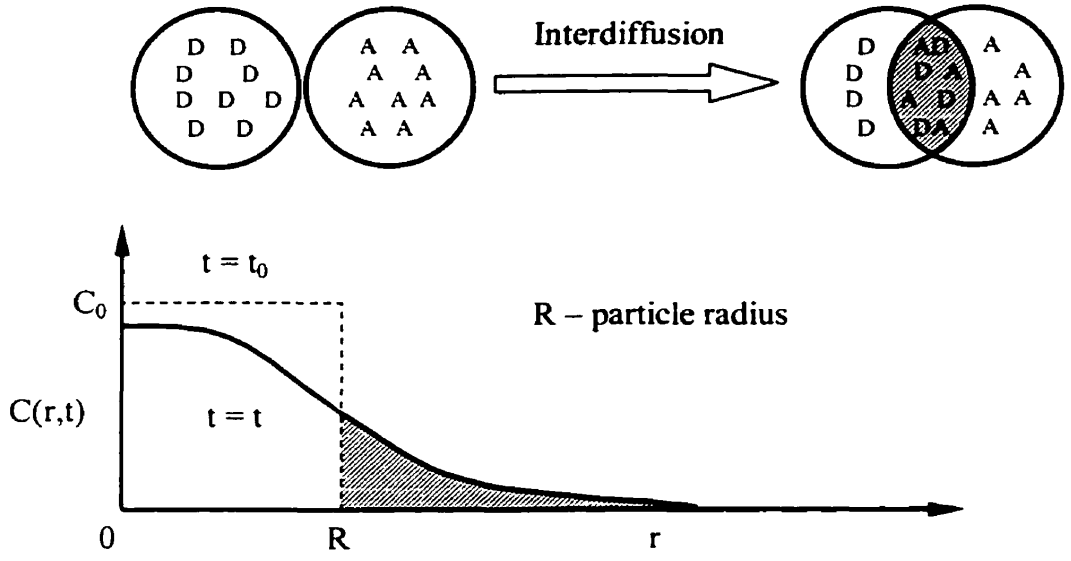

Figure 1-2. Schematic drawing depicting the concentration profile C(r,t) of polymers confined to a one latex particle with radius R at t = 0 and at some later time t.

The mass M_t, which has diffused across the interface after time t is shown in Figure 1-2 as a dashed area. The M_t is the difference between the mass of the polymer in the sphere with radius R at time t = 0, M_0 ($M_0 = 4/3\pi R^3 C_0$) and the mass which left within the sphere R after time t, so M_t can be described by the following equation:

$$M_t = M_0 - \int_0^R C(r,t)\pi R^2 dr \qquad (1\text{-}3a)$$

The fraction of the diffusing substance f_D that has diffused across the original boundary at time t is:

$$f_D = \frac{M_t}{M_0} = 1 - \frac{3}{4\pi R^3 C_0}\int_0^R C(r,t)\pi R^2 dr \qquad (1\text{-}3b)$$

and the mean square of displacement $\langle r^2 \rangle$ of the substance is 6Dt.

For high M polymers, where entanglements influence the polymer dynamics, the reptation model applies. In this model, neighboring chains are obstacles, restricting the lateral motion of a polymer chain, confining the chain to a "tube" where curvilinear, one dimensional, diffusion occurs along its contour, as shown in Figure 1-3a

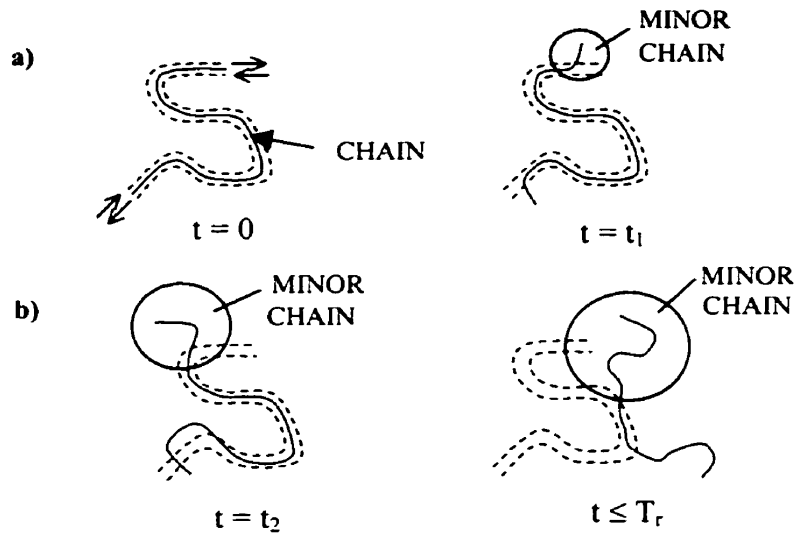

Figure 1-3. Minor chain reptation model[31]; a) diffusion along the tube and disengagement of a chain from its initial tube, b) the growth of minor chains up to reptation time T_r, where chains disengage from the initial tube and taking a new conformation.

Random motion occurs in both directions along the tube. Memory of the initial chain conformation (tube conformation) is gradually lost because motion of chain ends is random. Finally after reptation time T_r, a chain disengages itself from the initial tube, and takes a new conformation. For polymer diffusion across an interface, one has to take into account the influence of the interface as a dividing plane on the initial chain conformation. Prior to the onset of diffusion, the conformation of the polymer chains close to the interface is distorted from the normal Gaussian distribution of segments typifying polymer chains in the bulk state. This distortion is referred to us as confinement entropy. Diffusion of polymers across the interface leads to conformational randomization and recovery of Gaussian chain statistics. This process is well described by Wool in terms of his minor chain model[31]. For times less than the reptation time, the part of the chain that escapes from the initial tube is a random coil called a minor chain (see Figure 1-3b). This segment obeys Gaussian statistics, and a spherical envelope can be used to represent its static dimensions. The evolution of the minor chains at a polymer – polymer interface provides a convenient method of determining molecular properties and concentration profiles. Calculations based on the minor chain reptation model have been used to develop scaling laws for polymer interfaces.[31,32] For example, for times less than the reptation time, the average monomer interpenetration depth X(t), defined by equation (1-4) scales with time as $t^{1/4}$.

$$X(t) = \int_0^\infty xC(x,t)dx \Big/ \int_0^\infty C(x,t)dx \qquad (1\text{-}4)$$

C(x, t) is the concentration profile at time t, and at the x distance from the interface. The number of monomers crossing the interface, N (in other words, the mass transfer) is described by the expression:

$$N(t) = \int_0^\infty C(x,t)dx \qquad (1\text{-}5)$$

N scales with time as $t^{3/4}$ under the condition that the chain-ends are uniformly distributed in space. When chain-ends segregate at the surface prior to diffusion, N scales as $t^{1/2}$. At longer diffusion times ($t > T_r$), the molecular mixing becomes Fickian, and the total mass transferred becomes proportional to $t^{1/2}$.

In my experiments, I study polymer diffusion in latex films in which the polymer is poly(butyl methacrylate) PBMA. We should be able to use the Fickian spherical diffusion model to calculate the extent of polymer diffusion for low M PBMA samples. It is also possible to use this model for high M samples for diffusion times longer than the reptation time. In fact, because of the large polydispersity in molecular weight (M_w/M_n = 2-5) of latex polymer obtained in the emulsion polymerization, we do not know the exact concentration profile of diffusing polymer across the interface. To simplify the problem of calculating apparent diffusion constants, we will neglect the effects of reptation dynamics, and the effects of the recovery of Gaussian conformation by chains initially close to the interface. We assume that even for molecular weights as high as Mw = 4.0×10^5 (M_w/M_n = 3.2) the diffusion resembles Fickian diffusion at all stages of the diffusion process, and can be described by a spherical concentration profile as represented by equation (1-2). This assumption is strictly speaking not correct. I will show examples where deviations from Fick's law behavior occurs for DET measurements on high molecular weight samples. The influence of reptation effects on parameters characterizing polymer diffusion will be discussed further in sections of this Chapter and in Chapter 6.

1.2.2 Direct Non-radiative Energy Transfer

Direct non-radiative energy transfer (DET) involves the transfer of the excited state energy from a donor (D) molecule to an acceptor (A) molecule. This transfer is a results of

dipole – dipole interactions between the donor and acceptor[33]. If the transition dipoles are properly oriented and in resonance, the energy can be transfer over distance up to 100Å. In the presence of energy transfer, the decay rate of the excited donors increases. Scheme 1-4 shows deactivation paths of an excited donor to the ground state. Without acceptor, the donor will decay to the ground state through fluorescence emission with a rate constant k_f and by other non-radiative paths with a rate constant k_{nr}. In this case, the time-resolved decay of donor fluorescence $I_D(t)$ will follow a single exponential decay law as shown by equation (1-6)

$$I_D(t) = A\exp(-t/\tau_D{}^0) \tag{1-6}$$

where $\tau_D{}^\circ = 1/(k_f+k_{nr})$ is the fluorescence lifetime of the donor in the absence of acceptor. When acceptor molecules are present, the excited donor molecules can transfer their energy to acceptors with a rate k_{ET}.

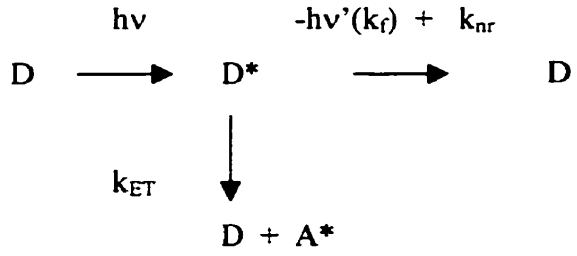

Scheme 1-4. The deexcitation pathways of an excited donor (D) in the presence of an acceptor (A) chromophore.

The rate of energy transfer $k_{ET}(r)$ depends on the extent of overlap of the emission spectrum of the donor with the absorption spectrum of the acceptor, the relative orientation of the D and A transition dipoles, and the distance r between these molecules.[34] For the case when donor-acceptor pairs are separated by a fixed distance r, the rate constant of energy transfer $k_{ET}(r)$ from a specific donor to an acceptor is given by[34,35]

$$k_{ET}(r) = 1/\tau_D^0(R_0/r)^6 \tag{1-7}$$

where τ_D^o is the lifetime of the donor in the absence of acceptor, and R_o is a characteristic distance, the Förster distance, at which the efficiency of energy transfer is 50%,[34] i.e. the transfer rate $k_{ET}(r)$ is equal to $1/\tau_D^o = (k_f + k_{nr})$. R_o is defined by

$$R_0^6 = [9000(\ln 10)\kappa^2 \phi^0{}_D / (128\pi^5 N_A n^4)] \int_0^\infty F_D(\nu)\varepsilon_A(\nu)d\nu / \nu^4 \qquad (1\text{-}8)$$

where $\phi^o{}_D$ is the quantum yield of donor fluorescence in the absence of acceptor, n is the refractive index of the medium, N_A is Avogadro's number, $F_D(\nu)$ is the corrected fluorescence intensity in the wave number range ν to $d\nu$, with the total intensity normalized to unity, $\varepsilon_A(\nu)$ is the extinction coefficient of the acceptor at ν, and κ^2 is a factor describing the relative orientation of the transition dipoles of the donor and the acceptor. The integral here expresses the degree of spectral overlap between the donor emission and the acceptor absorption. The κ^2 factor is equal be 2/3 for mobile, randomly distributed D and A molecules, and equals 0.475 for immobile, randomly distributed dyes.[33,36]

The $(1/r)^6$ dependence of DET on the distance between donor and acceptor molecule leads to high sensitivity of energy transfer to the concentration and concentration distribution of dye molecules in a system. One often describes this sensitivity in terms of a critical acceptor concentration C_{Ao}, which is the concentration of acceptor molecules at which an acceptor molecule is expected to be found inside a sphere of radius R_o and is given by [34,36]

$$C_{A_0} = 3000/(2\pi^{3/2} N_A R_0^3) \qquad (1\text{-}9)$$

A useful measure of the extent of energy transfer (ET) in the system is the quantum efficiency of energy transfer Φ_{ET}, which is defined by[33]

$$\Phi_{ET} = k_{ET}(r)/[k_f + k_{nr} + k_{ET}(r)] \qquad (1\text{-}10)$$

When D-A pairs are separated by a fixed distance, ET occurs with a single transfer rate $k_{ET}(r)$. Under these circumstances the decay of fluorescence intensity will be exponential with a lifetime $\tau_D = 1/[k_f + k_{nr} + k_{ET}(r)]$, shorter than the unquenched lifetime $\tau_D^o = 1/[k_f + k_{nr}]$. In cases where D and A molecules are separated by a random distribution of distances, the donor fluorescence decay is no longer exponential, and more complex expressions are required. Such expressions are generally derived by calculating the survival probability of

donor molecules, by integrating the transfer rate over the assumed distribution of acceptors around each donor. In case where D–A molecules are separated by a random distribution of distances, the time-resolved donor fluorescence decay follows Föster equation

$$I_D(t) = I_D{}^0 \exp[-t/\tau_D - 2p(t/\tau_D)^{1/2}] \tag{1-11}$$

where $I_D{}^0$ is the initial donor fluorescence intensity and $p = C_A/C_{Ao}$ is the ratio of acceptor concentration to the critical acceptor concentration.

The quantum efficiency of energy transfer Φ_{ET} is often calculated in the case of steady-state measurements, from the relative fluorescence yield as[33]

$$\Phi_{ET} = 1 - I_D / I_D{}^0 \tag{1-12}$$

where I_D, $I_D{}^0$ are the intensities of donor fluorescence in the presence and absence of acceptors, respectively. For the time-resolved donor decay, through δ-pulse excitation, the Φ_{ET} is calculated from donor fluorescence profiles I_D, expressed by the integrals of the decay function $I_D(t)$ as[33]

$$\Phi_{ET} = 1 - \frac{\left[\int_0^\infty I_D(t')dt'\right]}{\left[\int_0^\infty I_D{}^0(t')dt'\right]} \tag{1-13}$$

In this expression $I_D{}^0(t')$ is donor fluorescence decay in the absence of acceptor, with

$$\int_0^\infty I_D{}^0(t')dt' = \tau_D{}^0 \tag{1-14}$$

The integral of the donor emission, $\int_0^\infty I_D(t')dt'$, can be evaluated from the areas obtained experimentally under the donor decay curves (normalizing the decay curves at decay time zero), giving

$$\Phi_{ET} = 1 - \text{Area}_D / \text{Area}_D{}^0 \tag{1-15}$$

where $Area_D$, $Area_D^\circ$ are the areas under the normalized decay curves of donor fluorescence in the presence and absence of acceptor, respectively.

1.2.3 Analysis of Polymer Diffusion by DET

A PBMA latex film containing only phenanthrene (Phe) as a fluorescent label exhibits an exponential fluorescence decay with a lifetime τ_D of 45 ns. Latex films prepared from a mixture of donor- and acceptor-labeled PBMA latex, with Phe as the donor and anthracene (An) as the acceptor, exhibit non-exponential donor fluorescence decay profiles because of direct non-radiative energy transfer (DET) from Phe to An in the films. In annealed films, polymer diffusion mixes the Phe- and An-labeled polymers from adjacent cells, bringing the two chromophores into proximity. In freshly prepared films cast just above the minimum film forming temperature (MFT), little interdiffusion occurs, and the changes in the donor fluorescence decay profile $I_D(t')$ observed are due primarily to energy transfer across the interparticle boundary. The examples of fluorescence decays are presented in Figure 1-5.

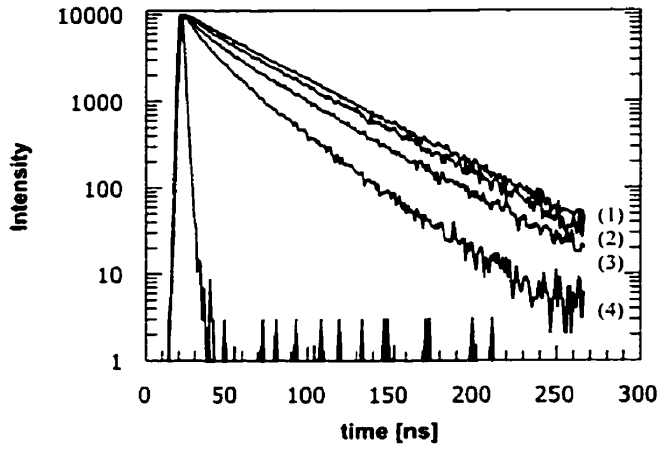

Figure 1-5. The examples of fluorescence decay for PBMA films: (1) containing only phenantrene (Phe); (2) for freshly formed film containing Phe as a donor and An as a acceptor with ratio Phe/An =1:1; (3) for the same film like in (2) but annealed at 80 °C for 4 hours; (4) for the same film like in (2) but fully mixed.

The quantum efficiency of energy transfer Φ_{ET}, which we calculate from the donor fluorescence decay profiles $I_D(t')$ for films in the presence and absence of acceptor, is a useful measure of the extent of energy transfer (ET) in a system.

$$\Phi_{ET} = 1 - \frac{\int_0^{\infty} I_D(t')dt'}{\int_0^{\infty} I_D^{o}(t')dt'} = 1 - \frac{Area(t)}{Area([An]=0)} \qquad (1\text{-}16)$$

Here, Area(t) represents the integrated area under the fluorescence decay profile of a latex film sample annealed for a time t, and Area([An] = 0) refers to the area under the decay profile of a film containing only donor. To calculate these areas, non-exponential decay profiles are fitted to the stretched exponential in equation (1-17).

$$I_D(t') = B_1 \exp\left[-\frac{t'}{\tau_D} - P\left(\frac{t'}{\tau_D}\right)^{1/2}\right] + B_2 \exp\left(-\frac{t'}{\tau_D}\right) \qquad (1\text{-}17)$$

The fitting parameters B_1, B_2 and p in equation (1-17) obtained from each profile are useful for area integration, but their physical meaning is not important here. These integrated areas have dimensions of time, and define an average decay time $<\tau_D>$ for the sample.

In newly formed films prepared near ambient temperature, values of Area (0) differ from that of Area ([An] = 0). Since little or no polymer diffusion takes place at room temperature, for most of our samples, we attribute this difference to trans-boundary energy transfer prior to the onset of polymer diffusion.[37] We have shown[38] that for a series of spherical high Tg donor-labeled particles, well-dispersed in a continuous acceptor-labeled matrix, the interfacial energy transfer efficiency increases with $1/d_p$, i.e., as the surface-to-volume ratio in the system, where d_p is the diameter of the latex. In a latex film prepared from a 1:1 mixture donor- and acceptor labeled particles, with a common level of acceptor label density, one expects a lower ET efficiency than in the case of the uniform acceptor-labeled surrounding matrix. For nascent films prepared from a 1:1 Phe/An mixtures of ca. 120 nm PBMA particles with the degree of labeling employed here, we often find $<\tau_D>$ values of 42 ns, corresponding to an ET efficiency of 7%.

To calculate the "extent of mixing" f_m that occurs upon annealing the samples, we have to correct for trans-boundary ET:

$$f_m = \frac{\Phi_{ET}(t) - \Phi_{ET}(0)}{\Phi_{ET}(\infty) - \Phi_{ET}(0)} = \frac{Area(0) - Area(t)}{Area(0) - Area(\infty)} \qquad (1\text{-}18)$$

where $[\Phi_{ET}(t) - \Phi_{ET}(0)]$ represents the change in DET efficiency between the initially prepared film and that aged for time t. f_m is an important parameter for characterizing the extent of polymer diffusion in latex films. Simulations show that, for the acceptor concentrations employed here, and for diffusion that satisfies Fick's laws, the fraction of diffusing substance (mass fraction of mixing) f_D from equation (1-3) is proportional to f_m for f_m values up to ca. 0.7. [39,40] The dependence of f_m on annealing time t will be discussed in detail in Chapter 6. Here we only want to emphasize that plots of f_m vs $t^{1/2}$ are linear for low M polymer, which is in agreement with Fickian diffusion. For high molecular weight samples, we observe a linear dependence of f_m on $t^{1/4}$. We believe that the $t^{1/4}$ dependence of f_m is a consequence of polymer reptation in polydisperse systems.

A new approach for characterization of polymer diffusion is developed in this thesis by introducing new parameters, $k_{1/2}$ and $k_{1/4}$, describing diffusion process in latex films. The diffusion rate parameter $k_{1/2} = f_m/t^{1/2}$ is defined as the slope of a straight line in the linear dependence f_m vs $t^{1/2}$ for low M polymer system; similarly the diffusion rate parameter $k_{1/4} = f_m/t^{1/4}$ is defined as the slope of a straight line in the linear dependence f_m vs $t^{1/4}$ for high M polymer systems. As f_m is proportional to the mass transfer for Fickian diffusion, $k_{1/2}$ characterizes the rate of mass transfer. We believe that the same relations apply for f_m and $k_{1/4}$ for entangled systems. The advantage of using the parameter $k_{1/2}$ ($k_{1/4}$) is that it can be easily and precisely calculated as a slope of a straight line, and it has a constant value throughout the whole diffusion process in a polydisperse polymer system. Its usefulness can be noted in the following example: In Chapter 4 we investigate the influence of oligomers on the rate of diffusion of high M polymers. The dependence of the parameter $k_{1/4}$ vs φ (volume fraction of oligomer) is presented in Figure 1-6. Figure 1-6 shows that the diffusion rate $k_{1/4}$ increases linearly with the amount of oligomers added. This result indicates that the effect of oligomers on the polymer diffusion is additive.

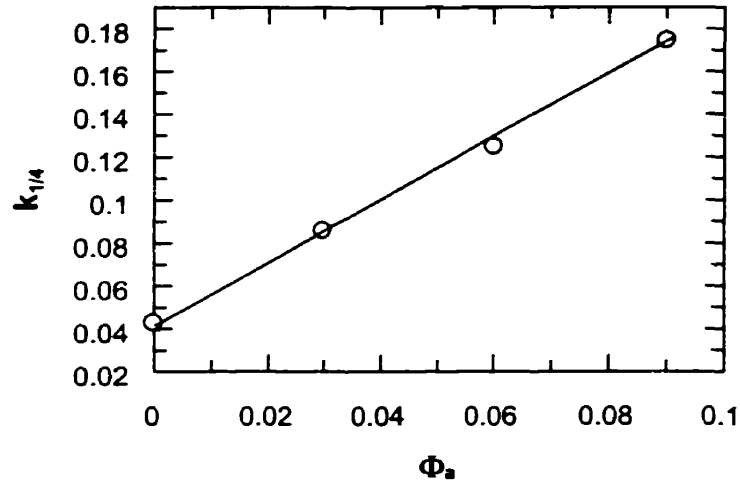

Figure 1-6. Dependence of $k_{1/4}$ vs φ for PBMA + BMA oligomers.

The other fundamental parameter characterizing the rate of polymer diffusion across the latex particle interface is the diffusion coefficient. It can be calculated at different levels of rigor and sophistication.[3,4] In our case, diffusion coefficients were calculated from f_m, assuming that $f_m = f_D$, where f_D is the fraction of mass that has diffused across the initial boundary, and fitting data to a spherical Fickian diffusion model,[41] (see eq. (1-2)). The details of this analysis, its convenience and its shortcomings, have been discussed previously.[42] The values we obtain are apparent mean diffusion coefficients D_{app}, which represent an average over the broad polymers molecular weight distribution in the sample, as well as the sample history. The importance of these numbers is that for samples with similar degrees of acceptor labeling, changes in D_{app}, compared at similar f_m values, correspond to changes in the true center-of-mass diffusion coefficients of the polymers. In other words the following relation is valid:

$$\frac{D_{app1}}{D_{app2}} = \frac{D_{True1}}{D_{True2}} \qquad (1\text{-}19)$$

Our D_{app} differs from D_{True} because f_m is only proportional to the mass transfer f_D across the particle boundary. When we apply this analysis to cases of high molecular weight polymers, we neglect the effects of entanglement. However, we found a general relationship between the $k_{1/4}$ parameter and D_{app},, which indicates that in the case of high molecular weight systems, the calculations of D_{app} are meaningful. In polymer systems in the presence of additives such as plasticizers, oligomers or fillers, we found that $\log(D_{app})$ depends linearly

on φ, where φ is the volume fraction of additive. For the same set of raw data analyzed differently, we find that $k_{1/4}$ also depends linearly on φ. Figure 1-7 shows the dependence of $\log(D_{app})$ and $k_{1/4}$ on φ, for BMA oligomers added to PBMA latex films. Figure 1-8 shows the same dependence for a system with soft filler particles. In the case of soft fillers, we observe a change in the slope for both $\log(D_{app})$ and $k_{1/4}$ at around 10 vol % of filler, which we interpret as a change in the latex film morphology (see Chapter 7). In conclusion, we can say that $\log(D_{app})$ and $k_{1/4}$ react to changes in the polymer system in the same way. We can therefore use them interchangeably to analyze polymer diffusion in latex systems. Calculations of $k_{1/4}$ are much easier and more straightforward than calculations of D_{app}. However, more experimental and theoretical work has to be done to calculate values of the free volume parameter or the apparent activation energy for polymer diffusion from values of $k_{1/4}$ or $k_{1/2}$ characterizing a polymer system.

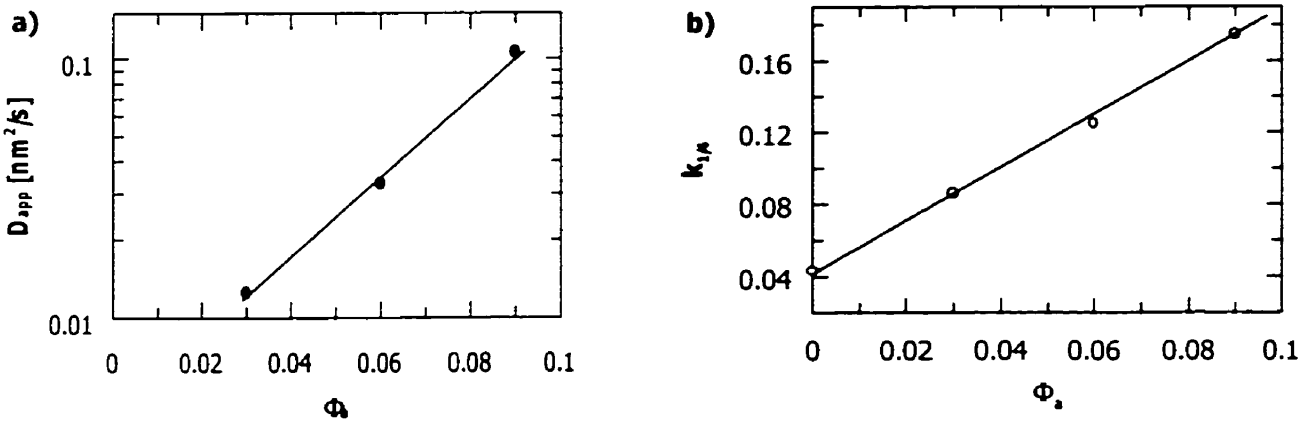

Figure 1-7. The changes of: a) $\log(D_{app})$, and b) $k_{1/4}$ vs. volume fraction of BMA oligomer φ in the PBMA film.

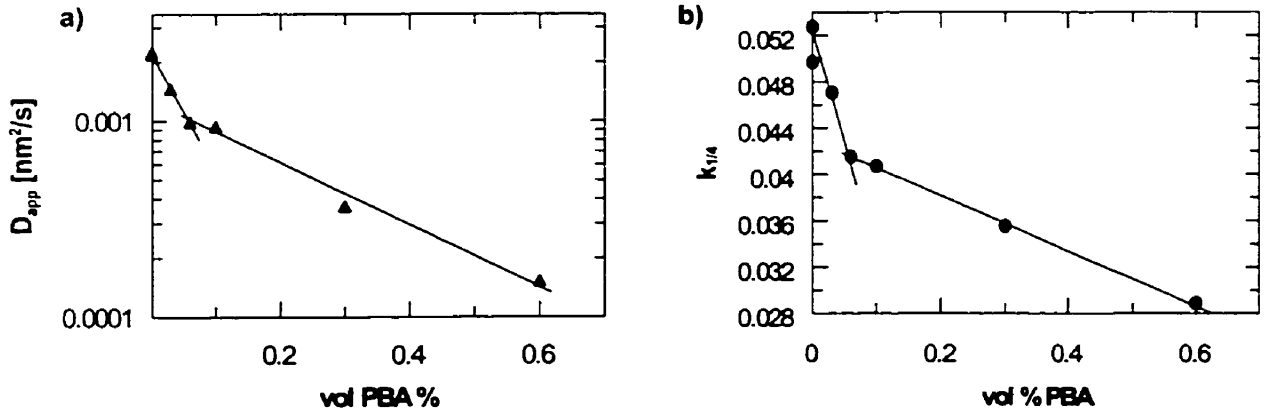

Figure 1-8. The changes of: a) $\log(D_{app})$, and b) $k_{1/4}$ vs. volume fraction of soft filler φ in the PBMA film.

1.2.4 Fluorescence Decay Measurements

All fluorescence decay profiles were measured by the time correlated single photon counting technique[43] in the same way. The measurements were conducted at room temperature. The donor phenanthrene was excited at 296 nm and its emission was recorded at 350-360 nm. The characteristic (Förster) energy transfer distance for Phe and An is 23 Å.[36] A bandpass filter (320-390 nm) was mounted in the front of phototube detector to minimize the scattered light and interferences due to the fluorescence from directly excited acceptors. For fluorescence decay measurement samples were placed to the small quartz test tube and kept under a nitrogen atmosphere. In case of annealed samples, before measurements, they were removed from the oven and cooled down to room temperatures. Finally the fluorescence decay profiles are measured and each decay trace provides a snapshot of the extent of diffusion to that point in the sample history. The areas under each decay curve were integrated and analyzed as described above.

1.3 Free volume theory

1.3.1 Historical background

When molecules pack together in the liquid state, not all spaces are occupied. The part of the volume of a body that is not occupied by the molecules has become known as the free volume of a substance, in contrast with the occupied volume, or proper volume, of the molecules themselves. The idea that molecular transport is regulated by free volume was first applied to liquids by Cohen and Turnbull[44-45] in 1959. Fujita adapted this theory to polymer-solvent diffusion.[46] Finally, Vertas and Duda[47] presented in 1977 a more general free volume theory, which successfully describes diffusion both above and below Tg, through the presumption that transport is controlled by the availability of free volume in the system[48].

1.3.2 Concept of free volume

The specific occupied volume of a liquid V_0 is defined to be the volume of the equilibrium liquid at 0 K. Hence the specific free volume V_F is given by

$$V_F = V - V_0 \tag{1-20}$$

where V is the specific volume of the liquid structure at any temperature T. As the temperature is increased from 0 K, the increase in volume is accompanied by the homogeneous expansion of the material due to increasing amplitude of vibrations with temperature, and also by formation of holes which are distributed discontinuously throughout the material at any instant. The expression for the self-diffusion coefficient of one component system derived from free volume theory is as follows:

$$D_1 = D_{01} \exp\left\{-\frac{V}{V_{FH}}\right\} \exp\left\{-\frac{E}{kT}\right\} \qquad (1\text{-}21)$$

Here D is the self-diffusion coefficient, D_{01} is a preexponential factor, V_{FH} is the average hole free volume per molecule in the liquid (or per gram of the polymeric liquid); V is the critical local hole free volume required for a molecule (or jumping unit in case of polymers) to jump to a new position; E is the critical energy a molecule must obtain in order to overcome the attractive forces holding it to its neighbors, T is the temperature and k is the Boltzman constant. The above equation reflects the dependence of the diffusion process on the probability that a molecule will obtain sufficient energy to overcome attractive forces (which depend on the chemical structure of the molecules) and on the probability that a fluctuation in the local density will produce a hole of sufficient size so that the diffusing molecule can jump[47].

For a binary mixture, it is assumed that the change in volume when two components are mixed is only due to a change in the available hole free volume. Under two additional conditions, that there is no volume change on mixing, and that the molecular weight of the solvent is equal to the molecular weight of a jumping unit of the polymer chain, Fujita[46] derived an expression for the diffusion coefficient D of a polymer in the presence of small molecular species:

$$D = ART \exp(-B/f) \qquad (1\text{-}22)$$

where f is a total free volume of the system. B is the minimum hole size or jump size required for the diffusion of a given molecule or molecular segment. A is a proportionality constant that depends on the size and shape of a jumping unit of the polymer chain. T is the absolute temperature, and R is the gas constant.

The free volume f of a two component system is in fact the sum of the fractional free volumes contributed by the individual components. In our case it will be polymer and surfactant,

$$f = f_p\Phi_p + f_a\Phi_a = f_p + \beta\Phi_a \qquad (1\text{-}23)$$

where Φ_p is the volume fraction of polymer with fractional free volume f_p. Φ_a is the volume fraction of additive with fractional free volume f_a. The term $\beta = f_a - f_p$ is the difference between the fractional free volume of an additive and a polymer.

Using equation (1-22) for expressing diffusion coefficients of a polymer in the presence and absence of low molecular weight species, and expressing the total free volume f in the form of equation (1-23) we can obtain the Fujita – Doolitle[46] equation (1-24) describing the influence of the additive, of volume fraction Φ_a, on the polymer diffusion coefficient at given temperature.

$$\left(\ln\frac{D(T,\Phi_a)}{D(T,0)}\right)^{-1} = f_p(0,T) + \frac{f_p^2}{\beta\Phi_a} \qquad (1\text{-}24)$$

where $D(T, \Phi_a)$ is the diffusion coefficient of a polymer at temperature T in the presence of Φ_a volume fraction of additive. D(T,0) is the diffusion coefficient of a polymer at temperature T in the absence of an additive. The terms f_p and β were defined in equation (1-23). By writing $f_p(T,0)$ instead of f_p we underline the fact that f_p is the fractional free volume of pure polymer $\Phi_a = 0$ at temperature T.

There are still a few more things important to mention when we deal with the concept of free volume. First of all, the free volume of a polymer is always smaller than the free volume of its monomer or oligomers. In addition, there is more free volume associated with the chain ends than with interior segments. Thus the lower molecular weight of the polymer, the more free volume is available in the polymer. This result can be easily explained by the fact that during polymerization, monomer molecules which have been at distances characteristic of intermolecular bonds (3-4) Å, begin to acquire the distances of chemical bonds (~1.54 Å). From this fact we can conclude that the most free volume is connected with the chain ends of polymer. However, the contraction which occurs during the polymerization process is not only due to the replacement of intermolecular distances with the distances of chemical bonds, but also because of the denser packing of polymer

chains in comparison with the packing of small molecules (the distance between the monomer segments belonging to different polymer chains decreases to some extent with increasing the length of a polymer chain). Tager, in his book, states[49] that the smaller fraction of contraction is due to the opening of double bonds, and the larger one due to the dense packing of polymer chains. For us the above facts can have important consequences. They indicate that there is a large fraction of free volume introduced by low molecular weight species to the polymer system, which is not connected with the chain ends of the species but with the fact that the short polymer chains are more separated from each other (less densely packed) than long polymer chains. This means that the free volume connected with the chain ends is only an additional, and not the major free volume introduced in to the system by small molecules. If the system were not sensitive to the small changes in its free volume we would not be able to observe a chain-end effect on polymer diffusion. We will see in Chapter 3 that a low molecular weight polymer system can be an example where surfactants with the same chemical structure but with different polymer chain lengths promote polymer diffusion in exactly the same way, and the chain-end effect is completely hidden.

1.4 References

1. Vanderhoff, J. W.; Bradford, E. B.; Carrington, W. K. *J. Polym. Sci.: Symp.* **1973**, No. 41, 155.
2. Sheetz, D. P. *J. Appl. Polym. Sci.*, **1965**, 9, 3759.
3. Croll, S. G. (a) *J. Coat. Tech.* **1986,** 58 (734), 411; (b) *J. Coat. Tech.* **1987**, 59 (571), 81.
4. (a) Joanicot, M.; Wong, K.; Maquet, J.; Chevalier, Y.; Pichot, C.; Graillat, C.; Lindner, P.; Rios, L.; Cabane, B. *Prog. Colloid Polym. Sci.* **1990**, 81, 175; (b) Chevalier, Y.; Pichot, C.; Graillat, C.; Joanicot, M.; Wong, K.; Lindner, P.; Cabane B. *Colloid Polym. Sci.* **1992,** 270, 806.
5. Denkov, N. D.; Velev, O. D.; Kralczevsky, P. A.; Ivanov, I. B.; Yoshimura, H.; Nagayama, K. *Langmuir* **1992**, 8, 3183.
6. (a) A. van Tent, K. te Nijenhuis, *J. Colloid Interfac. Sci.*, **1992,** 150, 97; (b) A. van Tent, K. te Nijenhuis, *Prog. Org. Coatings*, **1992,** 20, 459.

7. (a) Feng, J.; Winnik, M. A.; Shivers, R.; Clubb, B. *Macromolecules* **1995**, 28, 7671. (b) Winnik, M. A.; Feng, J. *J. Coat. Tech.*, **1996**, 68 (852), 39.
8. Dillon, R. E.; Matheson, L. A.; Bradford, E. B.; *J. Colloid. Sci.* **1951**, 6, 108.
9. Vanderhoff, J. W.; Tarkowski, H. L.; Jenkins, M. C.; Bradford E. B. *J. Macromol. Chem.* **1966**, 1, 361.
10. Brown, G. L. *J. Polym. Sci.* **1956**, 22, 423.
11. Eckersley, S. T.; Rudin, A. *J. Coating Tech.* **1990**, 62 no 780, 89.
12. Sperry, P. R.; Snyder, B.; O'Dowd, M.; Lesko, P. *Langmuir* **1994**, 10, 2619.
13. (a) Joanicot, M.; Wong, K.; Maquet, J.; Chevalier, Y.; Pichot, C.; Graillat, C.; Lindner, P.; Rios, L.; Cabane, B. *Prog. Colloid Polym. Sci.* **1990**, 81, 175; (b) Chevalier, Y.; Pichot, C.; Graillat, C.; Joanicot, M.; Wong, K.; Lindner, P.; Cabane, B. *Colloid Polym. Sci.* **1992**, 270, 806.
14. Henson, W. A.; Taber, D. A.; Bradford, E. B. *Ind. Eng. Chem.* **1953,** 45, 735.
15. Distler, D.; Kanig, G. *Colloid Polym. Sci.* **1978**, 256, 1052.
16. (a) Roulstone, B. J.; Wilkinson, M.; Hearn, J.; Wilson, A. *J. Polym. Int.* **1991**, 24, 87; (b) Roulstone, B. J.; Wilkinson, M.; Hearn, J. *J. Polym. Int.* **1992**, 27, 43.
17. Wang, Y.; Kats, A.; Juhue, D.; Winnik, M. A.; Shivers, R.; Dinsdale, C.; *Langmuir* **1992**, 8, 1435.
18. (a) Wang, Y.; Juhue, D.; Winnik, M. A.; Leung, O.; Goh, M. C. *Langmuir* **1992**, 8, 760; (b) Goh, M. C.; Juhue, D.; Leung, O.; Wang, Y.; Winnik, M. A.; *Langmuir* **1993**, 9, 1319.
19. Zallen, R. "*The Physics of Amorphous Solids*", Wiley-Interscience: New York, 1983.
20. Bradford, E. B.; Vanderhoff, J. W. *J. Macromol. Chem.* **1966,** 1, 335.
21. El-Aasser, M.; Robertson, A. *J. Paint Tech.* **1975**, 47 (611), 50.
22. (a) Voyutski, S. *J. Polym. Sci.* part A, **1958**, 32, 528; (b) Voyutski, S. "*Autohesion and Adhesion of High Polymers*", Wiley-Interscience: New York, 1963.
23. (a) Mohammadi, N.; Yoo, J. N.; Klein, A.; Sperling, L. H. *J. Polym.Sci. Part B: Polym. Phys.* **1992**, 30, 1311; (b) Mohammadi N.; Kim, K. D.; Klein, A.; Sperling, L. H. *J. Coll. Interfac. Sci.* **1993**, 157, 124; (c) Mohammadi, N.; Klein, A.; Sperling, L. H. *Macromolecules*, **1993** 26, 1019.
24. Kim, K. D.; Sperling, L. H.; Klein, A.; Wignall, G. D. *Macromolecules* **1993**, 26, 4624.

25. (a) Hahn, K.; Ley, G.; Schuller, H.; Oberthur, R. *Coll. Polym. Sci.* **1986**, 264, 1092; (b) Hahn, K.; Ley, G.; Oberthur, R. *Coll. Polym. Sci.* **1988**, 266, 631.

26. Doi, M.; Edwards, S. F. *The Theory of Polymer Dynamics*; Oxford University Press: Oxford, England, 1986.

27. de Gennes, P. G. *Scaling Concepts in Polymer Physics*; Cornell University Press: Ithaca, NY, 1979.

28. M_e value for PBMA was estimated according to Kavassalis, T. A.; Noolandi, J. *Macromolecules* **1989**, 22, 2709; For experimental value see Porter, R. S.; Johnson, J. *F. Chem. Rev.* **1966**, 66,1.

29. Crank, J. *The Mathematics of Diffusion*; Clarendon: Oxford, U.K. 1974.

30. (a) Zhao, C.; Wang, Y.; Hruska, Z.; Winnik, M. A. *Macromolecules*, **1990**, 23, 4082. (b) Wang, Y.; Zhao, C.; Winnik, M. A. *J. Chem. Phys.*, **1991**, 95, 2143; (c) Wang, Y.; Winnik, M. A.; Haley, F. *J. Coat. Technol.*, **1992**, 64 (811), 51; (d) Wang, Y.; Winnik, M. A. *J. Phys. Chem.*, **1993**, 97, 2507.

31. Wool, R. P.; *Polymer Inerfaces,* Hanser Publishers: **1995.**

32. Wool, R. P.; O'Connor, K. M.; *J. Appl. Phys.* **1981**, 52, 5953; Kim, Y.; H., Wool, R. P.; *Macromolecules* **1983**, 16, 1115; Zhang, H.; Wool, R., P.; *Macromolecules* **1989**, 22, 3018.

33. Lakowicz, J. R. "Energy Transfer", in *Principles of Fluorescence Spectroscopy*, Plenum Press: New York, 1983.

34. (a) Forster, T. *Ann. Phys.*,**1948**, 2, 55; (b) Forster, T. *Discuss. Faraday Soc.*, **1959**, 27, 7.

35. (a) Klafter, J.; Blumen, A. *J. Phys. Chem.* **1984**, 80, 875; (b) LeVitz, P.; Drake, J.; Klafter, J. Energy Transfer at Interfaces: Silica Gels as Model Systems", in: *Molecular Dynamics in Restricted Geometries*, John Wiley & Sons: New York, 1989.

36. Berlman, I. B. *Energy Transfer Parameters of Aromatic Compounds*, Academic Press, New York, 1973.

37. Feng, J.; Pham, H.; Stoeva, V.; Winnik, M. A. *J. Polym. Sci.: Polym. Phys.* **1998**, 36 (7), 1129.

38. Feng, J.; Winnik, M. A.; Siemiarczuk, A. *J. Polym. Sci.: Polym. Phys.* . **1998**, 36 (7), 1115.

39. Dhinojwala, A.; Torkelson, J. M. *Macromolecules* **1994**, 27, 4817; Liu, Y. S.; Feng, J.; Winnik, M. A. *J. Chem. Phys.* **1994**, 101, 9096; Kim, H.-B.; Winnik, M. A. *Macromolecules* **1995**, 28, 2033.

40. Yekta, A.; Duhamel, J.; Winnik, M. A. *Chem. Phys. Lett.* **1995**, 235, 119; Farinha, J.; Martinho, J. M. G.; Yekta, A.; Winnik, M. A. *Macromolecules* **1994**, 27, 1994.

41. Crank, J. *The Mathematics of Diffusion* (Clarendon, Oxford, **1975**).

42. Kim, H.-B.; Winnik, M. A. *Macromolecules* **1994**, 27, 1007.

43. O'Connor, D. V.; Phillips, D. *Time-Correlated Single Photon Counting*: Academic Press Inc.: London, U.K. 1984.

44. Cohen, M. H.; Turnbull, D. *J. Chem. Phys.* **1959**, 31, 1164.

45. Turnbull, D. J.; Cohen, M. H. *J. Chem. Phys.* **1961**, 34, 120.

46. Fujita, H. *Fortschr. Hochpolym.-Forsch.* **1961**, 3, 1.

47. Vertas, J. S.; Duda, J. L. *J. Polym. Sci.* **1977**, 48, 403-453.

48. Neogi, P.; Diffusion in polymers

49. Tager, A.; Physical chemistry of polymers, 1978

2 BINDING ISOTHERMS OF NP-(EO)$_n$ SURFACTANTS

2.1 Introduction

The interactions between polymer and surfactant in latex system can be characterized by measurements of adsorption isotherms of surfactants onto the surface of latex particles (e.g. the amount of surfactant adsorbed per a given area of surface over a range of surfactant concentration.). The driving force for the absorption of a surfactant molecule at the polymer-water phase is the decrease in free energy of the system associated with the transfer of the hydrocarbon portion of the surfactant molecule from the aqueous phase to the interface.

In mixture of surfactant and latex particles in water, above the critical micelle concentration (cmc), some surfactant molecules are dissolved molecularly in water phase and some are present in the form of aggregates of 50 – 100 molecules called micelles. The rest of the surfactant molecules are adsorbed at the particle-water and water-air interfaces. A dynamic equilibrium exists between the surfactant molecules in the micelles, in the bulk aqueous phase, and adsorbed to various surfaces in the system. The equilibrium can be represented by the following formula (2-1) and Figure 2-1.

$$\left\{\begin{array}{l}\text{Micella}\\ \text{Surfactant}\end{array}\right\} \underset{\longleftarrow}{\overset{K_1}{\longrightarrow}} \left\{\begin{array}{l}\text{Solute}\\ \text{Surfactant}\end{array}\right\} \underset{\longrightarrow}{\overset{K_2}{\longleftarrow}} \left\{\begin{array}{l}\text{Adsorbed}\\ \text{Surfactant}\end{array}\right\} \qquad (2\text{-}1)$$

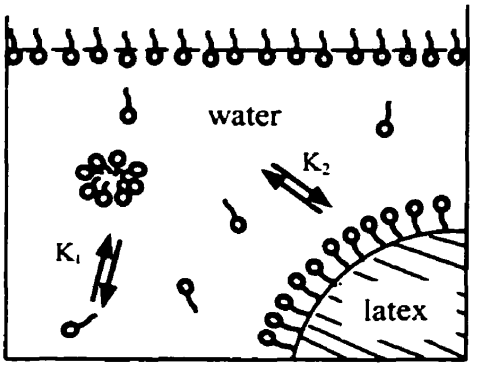

Figure 2-1. Schematic representation of the adsorption equilibrium of surfactant on latex.

K_1 and K_2 are equilibrium (association) constants that depend on the surface composition, structure of the particles and the chemical nature of the surfactant, including the nature of the hydrophilic part (nonionic, anionic cationic etc.) and that of the hydrophobe (length and nature of the chain, degree of branching, etc.). The equilibrium constants are related to the standard molar free energy of adsorption, $\Delta\mu^o$, through

$$\Delta\mu^o = -R \ln K \qquad (2\text{-}2)$$

where R is the gas constant, T is the absolute temperature, and K is the equilibrium association constant.

The larger the value of K, the more negative the standard molar free energy of adsorption, and the stronger the binding (affinity) of the surfactant to the surface.

2.2 Experimental

PBMA latex particles with diameters of 393 nm, 261 nm, and 141 nm were used for binding isotherm measurements. These latex dispersions were prepared and cleaned by ion-exchange resin of anionic surfactant remaining from the particle synthesis, as reported previously[9]. The binding isotherms were obtained by equilibrating known amounts of latex and NP-$(EO)_n$, n= 10, 20, 40, 100 surfactant, centrifuging the dispersion to sediment the latex, and measuring the concentration of surfactant in the supernatant (c_s) by UV-VIS spectroscopy. The measurements were made at the NP-$(EO)_n$ absorption peak at λ = 276. Different amounts of a stock solution (e. g. 5.054 x 10^{-3} M NP-20) were added to aliquots of a latex dispersion. Next the samples where shaken for a few hours and left overnight to equilibrate. The samples were then centrifuged for 10 min with an Eppendorf 5415C centrifuge, at 10,000 rpm for the 393 nm latex, and at 14,000 rpm for the 261 nm latex particles. For the latex with a diameter of 141 nm, a Beckman Instruments L550 B ultracentrifuge was used at 30,000 rpm. The centrifugation time was 20 min. In case of the 393 nm and 261 nm PBMA latex, after centrifugation, the supernatant was filtered through a 0.2 μm single-use filter from Gelman Sciences (product no. 4454). Finally the number of NP-$(EO)_n$ molecules per latex (Γ, the surface concentration) was calculated using the following equation: $\Gamma = (c_i - c_s)V/S$, where c_i is the initial concentration of NP-$(EO)_n$ in the latex dispersion; c_s is the concentration of the surfactant in supernatant calculated from UV absorption measurements; V is the volume of sample (0.2 mL); and S is the total surface

area (number of particles times the surface area per particle). A plot of Γ vs. c_s yields the binding isotherm curves for NP-$(EO)_n$. The plateau of the curve gives us the saturation value of Γ, Γ_{sat}, from which we calculate the mean area per surfactant of the NP-$(EO)_n$ molecules at saturation.

2.3 Results and Discussion

2.3.1 Influence of size of the PBMA latex on the binding isotherm for NP-20

Isotherms were measured for the binding of NP-20 surfactant to three samples of PBMA latex with different particle diameters (d = 393, 261, and 141 nm). We observe Langmuir type isotherms, but in this range of particle sizes, we do not see any size influence on the adsorption isotherm. The data are shown in Figure 2-2.

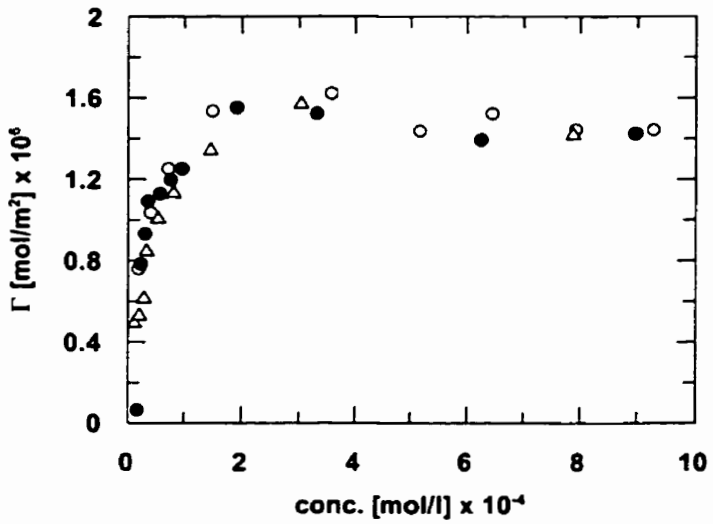

Figure 2-2. Binding isotherms of NP-20 with different diameters d of PBMA latex: (○) d=393 nm, (●) d=261 nm, (△) d=141 nm.

All three binding isotherms for different size of PBMA particles have the same shape, and they overlap. Similar results were obtained by Piirma and Chen[1] for polystyrene latex and ionic surfactants (sodium alkyl sulfate and potassium oleate). In the range of particle diameters, d = 77 – 178 nm they found no effect of particle size on the area occupied by a surfactant molecule (approximately 46 $Å^2$). In their work, they found a small decrease in area (36 $Å^2$) for the latex with d = 43 nm. One of the possible explanations for this deviation

can be the effect of particle curvature on the orientation of the surfactant. Due to the curvature of the particle surface, the area "occupied" by the surfactant molecule and the area of the surfactant itself may be quite different. This difference is directly related to the thickness of the surfactant monolayer (δ) and the diameter of the particle (d). For large particles, the magnitude of δ is negligible in comparison to d, and the difference is thus reduced. To avoid any possible deviations caused by the particle size, all the following experiments were done using PBMA latex with the average size 393 nm in diameter.

2.3.2 Influence of EO chain length on the binding isotherm of NP surfactants

For this experiment we used a series of NP-$(EO)_n$ with n = 10, 20, 40, 100 and PBMA latex with a diameter, d = 393 nm. In each case we observed Langmuir isotherms (Figure 1-3) and fitted data to the Langmuir equation:

$$\Gamma = \frac{\Gamma_{sat} \cdot [c_s]}{[c_s] + K_d} \tag{2-3}$$

Where Γ is the molar surface concentration of surfactant,

Γ_{sat} is the molar surface concentration of surfactant at saturation,

$[c_s]$ is the molar concentration of supernatant, and

K_d, is the dissociation constant.

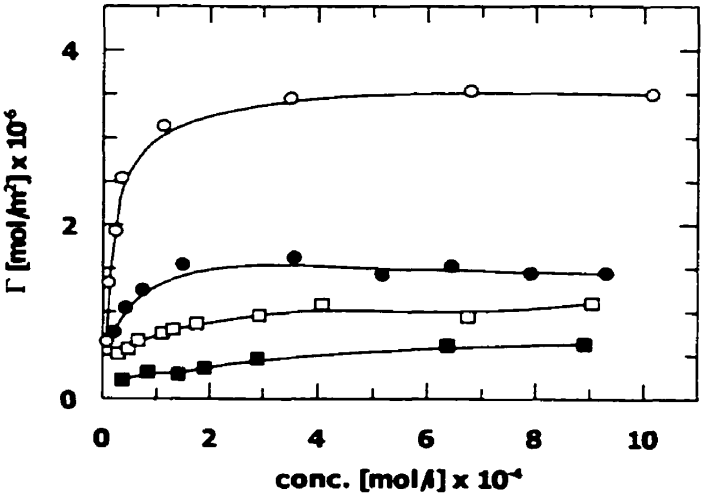

Figure 2-3. Binding isotherms of NP-$(EO)_n$ surfactants with PBMA latex (latex diameter d = 393 nm): (○) NP-10, (●) NP-20, (□) NP-40, (■) NP-100.

Figure 2-3 and Table 2-1 shows clearly that the amount of bound surfactant decreases with increasing EO chain length. As a consequence the occupied area per surfactant molecule increases significantly with the molecular weight of PEO.

Table 2-1 Adsorption data of NP-$(EO)_n$ surfactant on PBMA latex (d=393 nm)

	NP-10	**NP-20**	**NP-40**	**NP-100**
Area per molecule (Å)	46	107	147	232
Surfactant per latex particle, Γ_{sat} (μmol/m^2)	3.63	1.56	1.13	0.72

Table 2-2 Dissociation constants for NP-$(EO)_n$ bound to the PBMA latex. The values were obtained form fitting experimental data to the Langmuir isotherms.

Dissociation constant (mol/l) x 10^{-4}				
PBMA	**NP-10**	**NP-20**	**NP-40**	**NP-100**
(d = 393 nm)	0.187	0.195	0.48	1.57
(d = 261 nm)	-	0.23	-	-
(d = 141 nm)	-	0.2	-	-

In addition, we note (Table 2-2) that the dissociation constant K_d increases with the length of EO chain. This result implies that the strength of binding of the NP surfactant onto PBMA surface decreases with the increasing length of EO chain.

The results we obtained are consistent with those reported in the literature. Kronberg and coworkers[2] measured the adsorption of NP surfactants on polystyrene PS latex particles and obtained an area per molecule for NP-10 equal to 54 Å^2 and for NP-20 of 106 Å^2. However, the literature value of the area per molecule of NP-10 for PMMA latex is much higher (152 Å^2)[1]. This difference is explained in terms of a general trend found by a number of investigators[1,3,4] that the value of the molecular area of a surfactant increases with increasing polarity of the latex polymer. For nonpolar polymers such as PBMA or PS, the adsorption force of the hydrophobic portion on the polymer molecule is comparable to the association force of the hydrophobic tails themselves. The association of surfactant molecules on latex

particle surface is similar to their association in the micelles, and thus the surfactant molecules pack tightly on the latex particle surfaces. As the surface polarity of the particle increases, as in case of PMMA, the affinity between the surfactant hydrophobe and the particle surface is not as great as the affinity among the surfactant molecules themselves. The surfactant molecules prefer to stay in micelles, rather than tightly cover the particle surface. Under these circumstances, at saturation equilibrium, the polymer particle surface is still only partially covered with surfactant, and the average value of area occupied per surfactant molecule is much larger than in the case of PBMA or PS.

2.3.3 Effect of the nature and size of hydrophobe part of surfactant on binding isotherm

Although, we did not carry out systematic studies of the nature of hydrophobe part of surfactant on binding isotherm, we compared adsorption isotherms of two different surfactants, NP-40 and Ocenol-40, with the same $(EO)_n$ chain length, n = 40. The area occupied per molecule of surfactant in case of Ocenol-40 is 64 $Å^2$, less than half the area occupied by NP-40, (147 $Å^2$). This fact clearly shows that the nature of the hydrophobe has a significant influence on the binding process for adsorption to a nonpolar, hydrophobic surface, like that of a PBMA latex particle. In this case, adsorption occurs principally by dispersion interactions between the surface and the hydrophobic tail of the surfactant. It is reported[1] that even a difference in length, of four CH_2 units between sodium dodecyl sulfate and sodium hexadecyl sulfate, can result in a change of area occupied per surfactant molecule by a factor of two: from 52 $Å^2$/molecule for sodium dodecyl sulfate to 25 $Å^2$/molecule for sodium hexadecyl sulfate.

2.3.4 Conformation of NP-$(EO)_n$ surfactant molecules bound to the PBMA latex surface

In order to get information about the conformation of surfactant molecules bound to the latex surface we plot Γ_{sat}, calculated now in grams of surfactant per surface area of latex particles versus average molecular weight of EO_n, n=20, 40, 100. The dependence (Figure 2-4) is linear on a log-log scale.

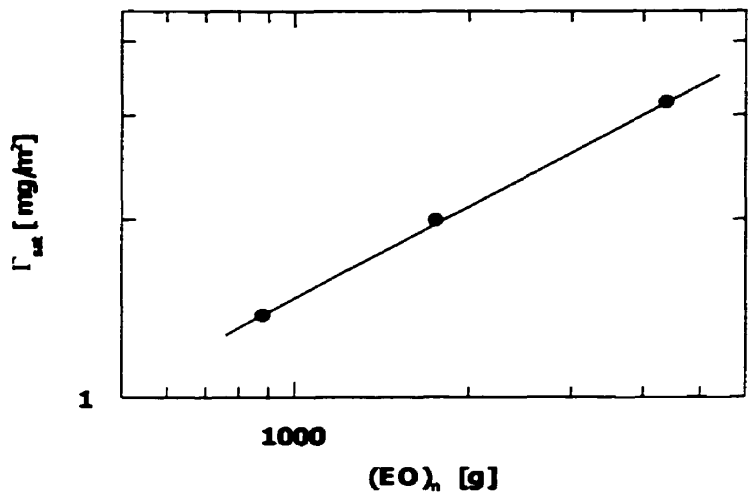

Figure 2-4. Dependence of the amount of bound surfactant per surface area at saturation Γ_{sat} vs. molecular weight of $(EO)_n$ – hydrophilic part of surfactant.

From the linear fit (correlation coefficient r = 0.9997), the adsorption data can be represented by the following equation:

$$\Gamma_{sat} = 0.0423 \cdot M_{(EO)n}^{0.5142} \qquad (2\text{-}4)$$

where $M_{(EO)n}$ is the average molecular weight of the hydrophilic part of the surfactant.
The fact that the amount of adsorbed surfactant varies linearly with the square root of the molecular weight, according to the equation (2-4), leads to some interesting conclusions concerning the conformation of the adsorbed surfactant. As an extreme limiting case, the EO_x polymer molecules could lie completely flat on the particle surface. At the other extreme, they could be present as essentially close-packed rigid rods oriented perpendicular to the surface. If the adsorbed molecules were flat against the surface, the weight adsorbed at saturation should be nearly independent of the molecular weight. In this case the amount of bound surfactant would be mostly dependent on the quantity of binding sites. If the surfactant had a rigid-rod perpendicular orientation, the weight of adsorbed surfactant at saturation should be directly proportional to the molecular weight. Another possibility, also suggested by many authors,[5,6,7] would be for the molecule to be anchored terminally but to have a random coil configuration similar to that found for the EO_x polymer in solution. This

situation would predict that the amount adsorbed be directly proportional to the square root of the molecular weight of the polymer. This is what we observe.

The radius of gyration, R_g, of PEO in water[8] (good solvent) scales to the power 0.57 of the molecular weight of PEO, so we can say that NP surfactants cover the surface of latex particles in the form of, at most, moderately distorted random coils. There are anchored to the surface by the hydrophobic part of the surfactant and finally packed to a complete monolayer. The question still remains as to whether the EO_x chains of the bound surfactant are at all extended. To answer this question we have to keep in mind that a snapshot of an individual polymer molecule in the solution would reveal a "cigar" shape; it is the time averaged random coil, which is spherical. When the polymer chains are bound to a surface, their motion is impeded by steric interaction with adjacent molecules. If packing is sufficiently dense, they tend to orient so that the long axis of the random coil is perpendicular to the surface. When the equation (2-4) applies, we know from the literature data[5,6,7] that the thickness of adsorbed layer , δ, is about 2 times the radius of gyration of the polymer coils in equilibrium solution. In this sense we can imagine that the absorbed NP surfactants on the latex surface have a somewhat stretched conformation.

Finally it is important to mention that NP-10 does not follow the behavior of equation (2-4). One explanation could be that only for surfactants with 20 EO units and more, do steric interactions of the EO_x chain influence the size of area occupied per surfactant molecule. In case of NP-10, the size of hydrophobic part is comparable with the size of hydrophilic part, and the steric effect may be negligible.

2.4 Conclusion

In this chapter we showed:

a) The surface area per NP surfactant molecule at complete coverage strongly increases with increasing EO chain length.
b) The affinity of nonionic NP surfactants to the PBMA surface decreases with increasing EO chain length.
c) The surfactant is bound to the latex surface in the form of packed random coils.
d) In the range of latex particle diameters of 141 –393 nm, the adsorption isotherm does not depend on the size of the latex.

e) The nature of hydrophobic part of the nonionic surfactant seems to have a pronounced effect on the area occupied per surfactant molecule at complete coverage.

2.5 References

1. Piirma, I.; Chen, Shih-R. *J. Colloid Interface Sci.* **1980**, 74, 90.
2. Kronberg, B.; Kill, L.; Stenius, P. *J. Dispersion Sci. Technol.* **1981**, 2(2&3), 215.
3. Vijayendran, B. R. *J. Appl. Polym. Sci.* **1979**, 23, 733.
4. Stutterlinn, N.; Kurth, K-J.; Markert, G. *Macromol. Chem.* **1976**, 177, 1549.
5. Elketov, Yu. A. *Pure & Appl. Chem.* **1989**, 61, 1987
6. Erich, F. R. *Colloidal & Interface Sci.*; Kerker, M.: New York **1977**, vol. 1
7. Stromberg, R. R.; Tutas, D. J.; Passaglia, E. J. *J. Phys. Chem.* **1965**, 69, 3955.
8. Stuart, M. A. C.; Waajen, F. H. W. H.; Cosgrove, T.; Vincent, B.; Crowley, T. L. *Macromol.* **1984**, 17, 1825.
9. Feng, J. Ph.D. Thesis, University of Toronto, **1996**.

3 THE EFFECT OF POST-ADDED SURFACTANTS ON POLYMER INTERDIFFUSION PROCESS IN LATEX FILMS

3.1 Introduction

Surfactants play an important role in latex coating systems. First, in the preparation of latex dispersions by emulsion polymerization, they act as emulsifiers. They can be employed to control particle size and its distribution and, under some circumstances, they determine the reaction mechanism.[1,2] Second, during storage and application of the coating, they stabilize the latex dispersion. They also serve as dispersing agents to prevent flocculation of pigment and other colloidal inorganic components, and as wetting agents to wet the substrate.[3] These surfactants remain in the system as the coating is formed. Thus it becomes very important to understand how surfactants affect the properties of the latex films. This is a subject that has received significant attention in the scientific literature. It has been shown, for example, that some surfactants significantly influence the glass transition temperature (T_g) of latex films,[4,5] their dynamic mechanical properties,[6] their peel strength[7] and their water resistivity.[8]

Over the past several decades, considerable effort has also been devoted to understanding the detailed behavior of these surfactants in latex films and the mechanism by which they affect the film properties. Early studies focusing on the location of surfactants in films were carried out by Bradford and Vanderhoff using electron microscopy.[9] In a poly(styrene-co-butadiene) latex system, they found that the post-addition of nonylphenol [NP]- ethylene oxide [EO] adducts of varying EO chain lengths resulted in different film surface morphologies and film properties. For instance, NP surfactants with 20 or 40 EO units (NP-20 and NP-40) were exuded to the film surface following coalescence, whereas no exuded species were found for the systems containing shorter EO chains, such as NP-4.

In many latex systems, exudation from latex films is often observed for anionic surfactants. Examples have been reported by Vijayendran[10] et al. More detailed information is available from experiments that employ spectroscopic methods to try to determine the concentration distribution of surfactants within the films. The classic experiments in this regard were carried out by the Lambla group in France[11] and the Urban group[12] in the US,

both using the Fourier transform infra-red-attenuated total reflection spectroscopy. These studies showed that the surfactant concentration is often higher at the film/air and film/substrate interfaces than in the bulk, and that for polyacrylate latex systems, this surface enrichment is more significant for ionic surfactants than for non-ionic surfactants.

Another important study of this issue by Hadicke[13] et al. employed the small angle neutron scattering technique [SANS]. They found that two deuterated surfactants, lauric acid (or its ammonium salt) and sodium dodecyl sulfate (SDS), gave different distribution patterns in PBMA latex films. The former was distributed homogeneously in the matrix, and the distribution was stable up to an annealing temperature of 150°C. The latter gave rise to scattering entities on the film surface with a mean radius of gyration (Rg) of 12 nm, and at high temperatures these surfactant domains aggregated into large clusters (Rg > 100 nm). The authors explained that lauric acid and its ammonium salt were miscible with PBMA, while SDS was immiscible and formed a separate phase as film formation and coalescence occurred.

Other studies examined the physical effects of these surfactants on the film formation process. Vijayendran[10a] et al. and Vandezande and Rudin[14] studied the influence of surfactant on the minimum film forming temperature (MFT) of the dispersions. They found that surfactants that were miscible with the latex polymer had a more pronounced effect on lowering the MFT, and hence led to a higher degree of film coalescence at the application temperature. Such surfactants likely act as plasticizers for the latex polymer. Padget and Moreland[15] reported that the presence of a triblock copolymer surfactant, poly(ethylene oxide-b-propylene oxide-b-ethylene oxide), accelerated film coalescence for their chlorine-containing vinyl acrylic latex dispersions. The rate of fusion increased with increasing block copolymer content up to the concentration at which monolayer coverage of the polymer particle surfaces occurred. Eckersley and Rudin[6] used dynamic mechanical analysis to examine whether common anionic and non-ionic surfactants have a plasticizing effect on a poly(methyl methacrylate-co-butyl acrylate) latex films. They found that the non-ionic surfactant NP-40 plasticized the polymer, promoting film coalescence and lowering the dynamic modulus of the films, while the anionic surfactant sodium dodecylbenzene sulphonate (NaDBS) had no such effect. In the scanning electron microscope images, some surfactant exudates appeared on films containing NaDBS. These results were attributed to miscibility between the NP surfactant and the polyacrylate, and immiscibility between the

anionic surfactant and the polymer. All these experiments suggested that the more miscible the surfactant is with the latex polymer, the more significantly it affects the film formation process. As the mechanism of surfactant influence on latex coalescence and polymer diffusion is not very well understood, we decided in this Chapter to investigate how the chemical structure of surfactants, their length, and miscibility with polymeric matrix change the polymer diffusion across latex particles.

3.2 Experimental

3.2.1 Sample Preparation and Fluorescence Decay Measurement

Phenanthrene-labeled (Phe-) and anthracene-labeled (An-) poly(butyl methacrylate) (PBMA) latex were prepared as described previously (Chapter 1). The latex dispersions were purified by stirring with a carefully washed mixed-bed ion exchange resin to remove surfactant and other free ionic substances. The characterization of these latexes is given in Table 3-1 in the case of high molecular weight PBMA latex and in Table 3-2 in the case of low molecular weight PBMA latex. The Phe-PBMA and An-PBMA latex spheres are mixed in a number ratio of AnPBMA:Phe-PBMA = 1:1.

Table 3-1. Latex particle characteristics –high M PBMA

Phe-PBMA	**An-PBMA**
M_w = 120,000	M_w = 133,000
M_n = 38,000	M_n = 42,000
M_w/M_n = 2.9	M_w/M_n = 3.16
d = 124 nm (0.04)[a]	d = 132 nm (0.037)[a]

a. size polydispersity

Table 3-2. Latex particle characteristics –low M PBMA

Phe-PBMA	**An-PBMA**
M_w = 33,900	M_w = 35,700
M_n = 18,300	M_n = 16,700
M_w/M_n = 1.85	M_w/M_n = 2.14
d = 119 nm (0.03)[a]	d = 119 nm (0.035)[a]

a. size polydispersity

We selected some commonly used surfactants for this study. The structures of these surfactants are given in Table 3-3. Most of them are non-ionic surfactants, NP-10 (TCI), NP-20 (TCI), NP-40 (Aldrich), NP-100 (Aldrich); A-20 ($C_{13.7}$-EO_{20}) (Dulux Australia); Ocenol-$EO_{9,\ 12,\ 15,\ 40}$ ((Dulux Australia); Undecenoate-$EO_{15,\ 40}$ ($C^{=}_{11}$-EO_n) (Dulux Australia); Octene-$EO_{7,\ 14}$ ($C^{=}_{8}$-EO_n) (Dulux Australia). Two of them, SDS (Aldrich) and C_{941} (Aldrich), are anionic surfactants.

Table 3-3. List of investigated surfactants.

SURFACTANT NAME	SURFACTANT STRUCTURE
NP-n	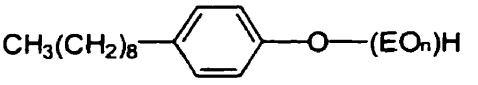
OCENOL- $(EO)_n$	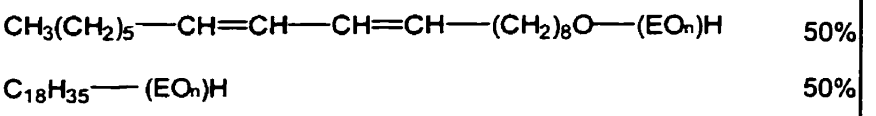 50% $C_{18}H_{35}$—$(EO_n)H$ 50%
A – 20 ($C_{13.7}$-EO_{20})	$CH_3(CH_2)_{12}$— $(EO)_{20}H$ 70% $CH_3(CH_2)_{14}$— $(EO)_{20}H$ 30%
OCTENE – $(EO)_n$ ($C^{=}_{8}$-EO_n)	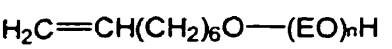
UNDECENOATE - $(EO)_n$ ($C^{=}_{11}$-EO_n)	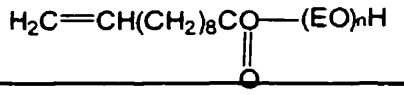
SDS (sodium dodecyl sulfate)	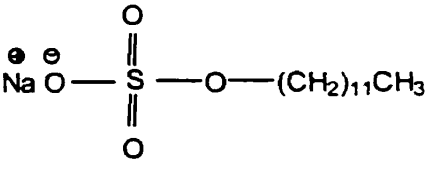
C_{941} (sodium dihexyl sulfosuccinate)	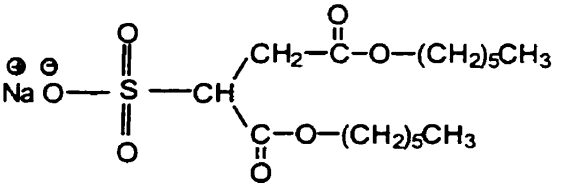

These surfactants were dissolved in deionized water and then mixed with the latex dispersion so as to give surfactant concentrations of 5 wt% relative to the solid latex. A few drops of the mixture of the latex dispersion, having a total solids content of about 7 wt%, were spread on thin quartz plates. The plates were then allowed to dry slowly at 32 °C (high M PBMA) or 22 °C temperature (low M PBMA) at high humidity for a few hours. After a transparent, crack free film was formed (the average thickness about 50 μm), the film was annealed at the desired temperature in an oven for a given period of time. For samples annealed for less than 20 minutes, the quartz plates were placed directly onto an aluminum slab in the oven. For longer annealing times, the quartz plate was placed in a quartz tube, flushed with ultra-pure Argon. The tube was then sealed with a rubber septum and placed in the oven. As a reference, a "fully mixed" sample was prepared by dissolving the polymer of a dried latex film in a good solvent for PBMA (here, toluene), and then recasting a film on a quartz plate.

Fluorescence decay measurements were carried out according to the description in Chapter 1. The calculations of extent of mixing f_m and apparent diffusion coefficient D_{app} are presented in Chapter 1.

3.3 Results and discussion

3.3.1 Influence of surfactants on diffusion of high molecular weight PBMA latex.

In Figure 3-1a I plot the extent of mixing f_m as a function of annealing time for a series of PBMA latex films containing different surfactants in the amount of 5 wt%, and annealed at 72°C. In Figure 3-1b these data are shown for longer annealing times. The lowermost two curves in Figure 3-1 are for experiments with the anionic surfactants SDS and C_{941}. These results show that for the polymer in the presence of the two anionic surfactants, the diffusion rates are not significantly affected, or just slightly reduced, compared to the surfactant-free sample. This result is probably connected with the fact that these surfactants do not mix with PBMA, and form separate domains in the polymer film[16].

In contrast, when non-ionic surfactants are present, the diffusion rates are increased. The enhancement is very large, and depends upon both the structure of the non-ionic surfactant and the amount of the surfactant present. For example, in order to reach the extent

of interdiffusion after 150 minutes in the sample with 5 wt% of NP-20, 4000 minutes of annealing at the same temperature are required for the samples without a surfactant. It is clear that post-added non-ionic surfactant may significantly promote polymer interdiffusion, and, what is most interesting, is that this enhancement occurs at all stages of the interdiffusion process. These observations suggest that non-ionic surfactant molecules are evenly distributed in the PBMA matrices during the experiment. If they were restricted to the boundary region of the individual latex particles, they would be effective only at the very early stages of the annealing process.

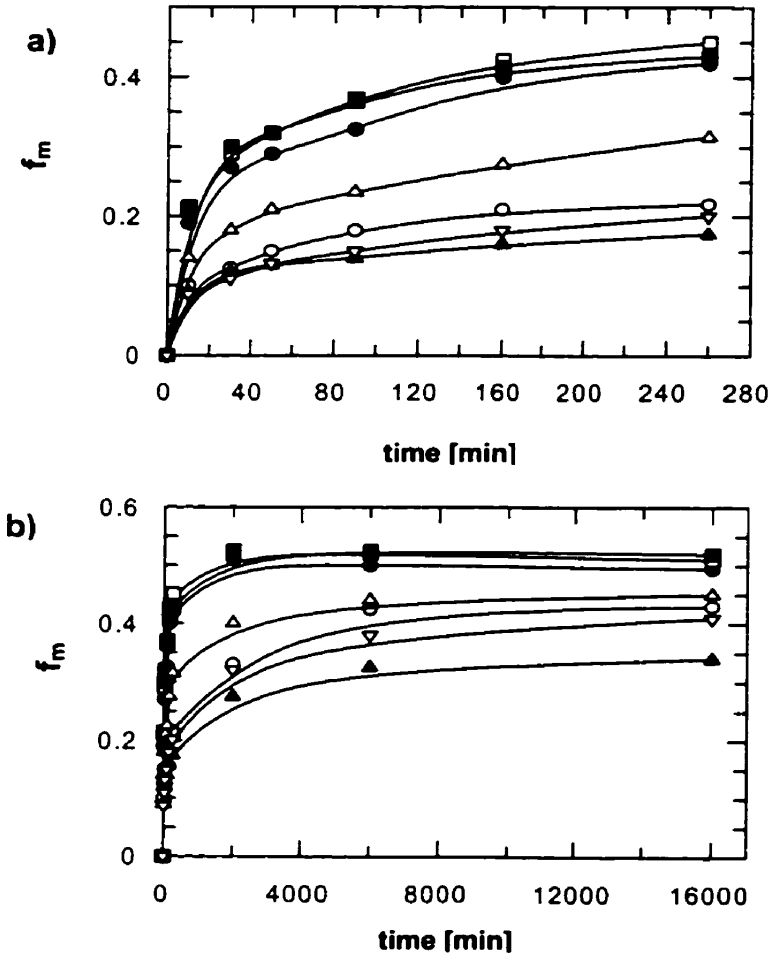

Figure 3-1. Dependence of extent of mixing (f_m) on annealing time (diffusion time) for pure high M PBMA film (○) and films with 5 wt % of different surfactants: NP-20 (●), A-20 (□), Ocenol-12 (■), Ocenol-40 (Δ), SDS (▲), C-941 (▽); (a) short time behavior, (b) long time behavior. The annealing temperature is 72 °C.

Ocenol-EO_{40} and Ocenol-EO_{12} have strikingly different effects on the polymer diffusion rate. Both enhance this rate, but the surfactant with the shorter PEG chains is far more effective for equal weights of added surfactant. The extent to which the rate of polymer interdiffusion is sensitive to the EO chain length is illustrated in Figure 3-2.

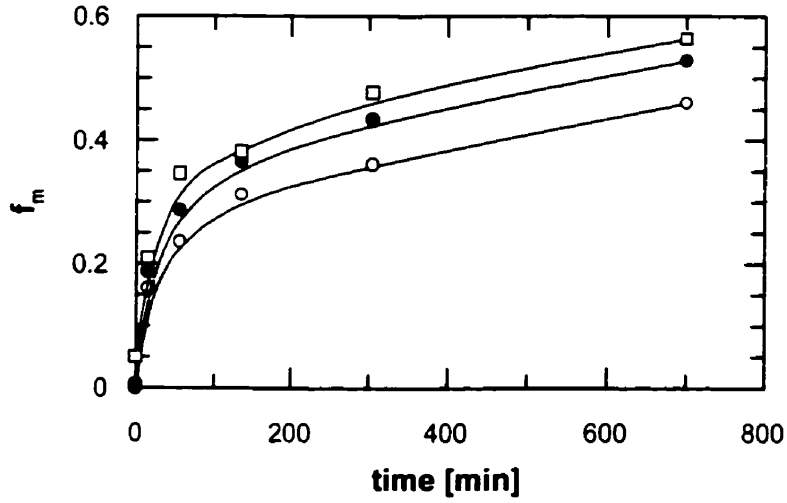

Figure 3-2. Dependence of extent of mixing (f_m) on annealing time for pure high M PBMA film (○) and films with the presence of 5 wt % Ocenol-9 (□), and Ocenol-15 (●). The annealing temperature was 76 °C.

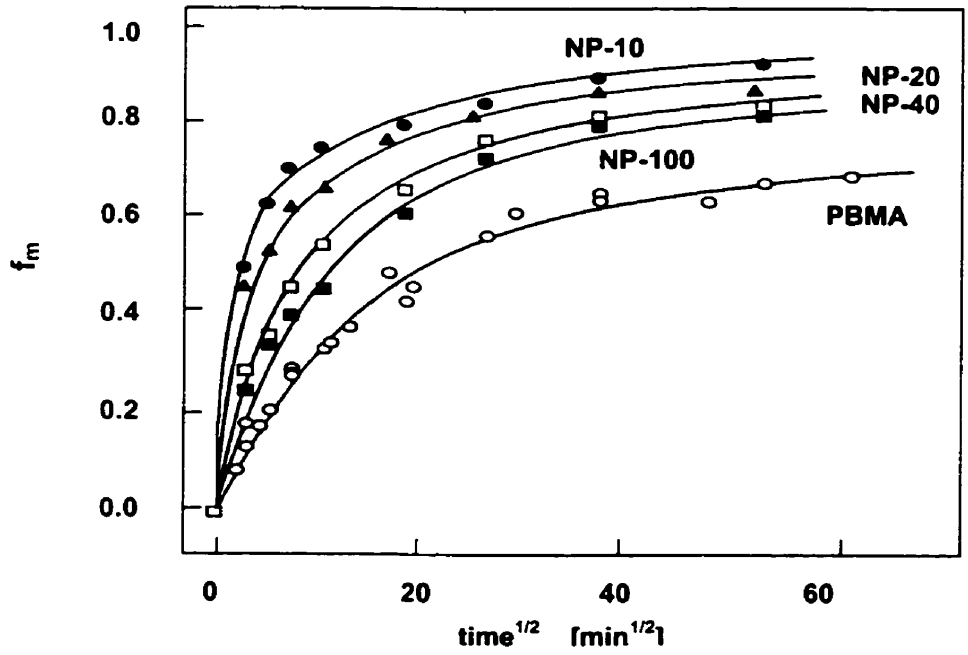

Figure 3-3. Plots of f_m vs. square-root of annealing time at the different NP-surfactants at 90°C. (○) 0 wt% NP; (■) NP-100, 15 wt%; (□) NP-40, 14.6 wt%; (▲) NP-20, 15.0 wt%, and (●) Np-10, 17.8 wt%.

In Figure 3-2 we compare the extent of mixing for PBMA samples containing 5 wt% of Ocenol-EO_9 and Ocenol-EO_{15}, annealed at 76 °C. The difference in size of the hydrophilic part of the nonionic surfactant, corresponding to an average of six EO units per molecule, influences the PBMA diffusion rate significantly. We have also noted similar effects of PEG chain length in a series of NP-EO_n surfactants, (n=10, 20 40, 100) (see Figure 3-3) on PBMA diffusion rate at 90 °C. However, in this experiment carried out by Kawaguchi[17a] the amount of surfactant in the film was high, 15 wt%. It is possible that in this experiment the observed effect of the surfactant size on polymer diffusion may be obscured by incomplete dissolution of the surfactants in the polymeric matrix at 90 °C. We know from Chapter 5 that the miscibility of the PBMA – nonionic surfactant system decreases drastically with increasing EO chain length. On the other hand, when we look back at Figure 3-1, we see that surfactants with different hydrophobic groups but similar hydrophilic size, such as NP-20, A-20 and Ocenol-EO_{12}, have on a weight basis similar effect on polymer diffusion.

The above results indicate that the chemical structure of the hydrophobic part of nonionic surfactants has less influence on polymer diffusion than the length of the EO chain, or simply speaking the size of the surfactant. This conclusion was the first indicator for us that it should be possible to treat the polymeric nonionic surfactants as conventional plasticizers. The surfactants can promote polymer diffusion by introducing free volume into the polymeric matrix, and in this way, provide more space for polymer chains to move. We have to emphasize, however, that in order to apply free volume theory to our system, the surfactant has to be miscible with the polymer. By changing the size of the nonionic surfactant via the length of the PEG chain, we also change its miscibility with the latex polymer (see Chapter 5). In order to test whether the free volume theory can describe the influence of surfactant concentration on the polymer diffusion rate, the conditions of the experiment (the annealing temperature, the amount of surfactant) have to be chosen properly so that the mixture is fully miscible under the conditions of the experiment.

3.3.2 Application of free volume theory to the high molecular weight polymer and nonionic surfactant system.

We have seen in previous sections that nonionic surfactants significantly promote polymer diffusion at elevated temperatures. Now we will consider how the polymer

diffusion rate changes with the amount of surfactant added to the latex film. This problem was considered by Kawaguchi,[17b] who carried out energy transfer experiment for PBMA latex films with different amounts of NP-20 surfactant, annealed at 90 °C. Characteristics of the latex used in his experiments are presented in Table 3-4. The sample preparation and ET experiment were carried out in a similar way as described in Chapter 1.

Table 3-4. Latex characteristics.

Phe-PBMA	An-PBMA
M_n = 140K	M_n = 133K
M_w = 495K	M_w = 353K
M_w/M_n = 3.54	M_w/M_n = 3.67
d = 138 nm	d = 132 nm

In Figure 3-4, the values of the apparent diffusion coefficient D_{app} for samples containing various concentrations of NP-20 are plotted against the extent of mixing f_m. One sees that there is a marked increase in the polymer diffusion rate by addition of NP-20 surfactants, and the extent of enhancement increases with increasing NP-20 concentration.

While NP surfactants might contribute in several ways to the enhancement of polymer diffusion, the most likely mechanism is one in which it acts as a plasticizer, to increase the free volume in the film. This idea was tested by fitting data to the Fujita-Doolitte equation (3-1) (see also Chapter 4).

$$\left[\ln\frac{D_p(T,\Phi_a)}{D_p(T,0)}\right]^{-1} = f_p(T,0) + \frac{f_p^2(T,0)}{\Phi_a\beta(T)} \qquad (3\text{-}1)$$

Here $f_p(T,0)$ is the fractional free volume of the polymer in the absence of surfactant, and Φ_a is the volume fraction of the surfactant. $\beta(T)$ represents the difference in fractional free volume between the surfactant and the polymer at temperature T, and D_p is the polymer diffusion coefficient. In Figure 3-5, the value of D_{app} obtained in the presence of NP-20 are superimposed on the corresponding data obtained in the absence of surfactant. In this way Kawaguchi calculated a shift factor which corresponds to the inverse of the term on the left hand side of equation (3-1). One sees that all data can be superimposed onto a single curve, to afford a master curve of D_{app} and f_m. He plotted the shift factor vs volume fraction of

surfactant Φ_a and obtained a linear relationship with an intercept $f_p(90°C, 0) = 0.089$, and a slope $f^2_p(90°C, 0)/\beta(T) = 0.038$. The value of $f_p(90°C, 0) = 0.089$ and $\beta(T) = 0.20$ are higher than the value I found for a similar PBMA system with BMA oligomers as the "solute" ($f_p(75°C, 0) = 0.029$, $\beta(T) = 0.05$, see Chapter 4). Fujita[17c] examined diffusion rates of high molecular weight poly(ethyl acrylate) in the presence of dissolved benzene in the polymeric matrix, and obtained $f_p(23°C, 0) = 0.046$, $\beta(T) = 0.07$.

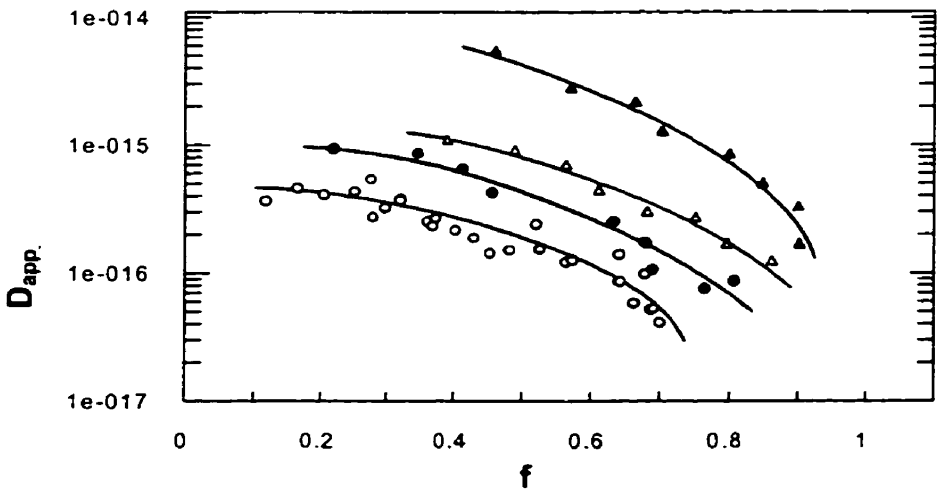

Figure 3-4. Plots of apparent diffusion coefficient (D_{app}) vs. extent of mixing (f_m) in the presence of NP-20 surfactant at 90 °C: (○) 0 wt%, (●) 3.34 wt%, (Δ) 9.9 wt%, (▲) 15 wt% NP-20.

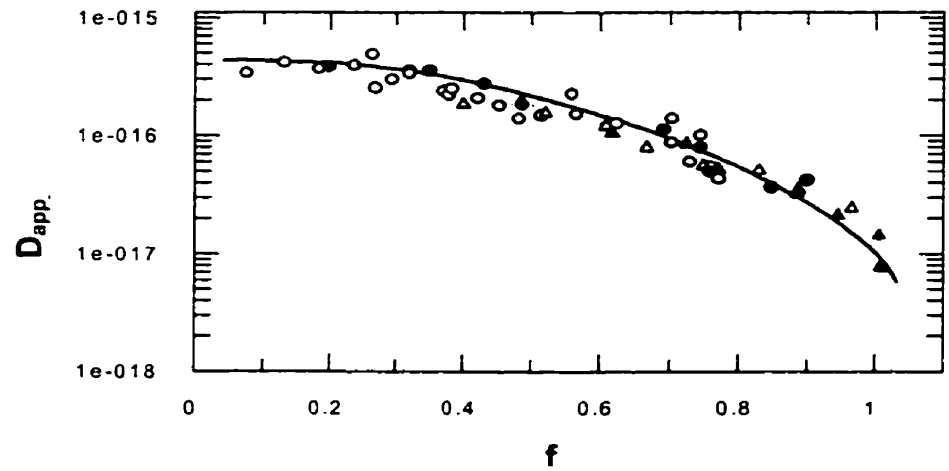

Figure 3-5. Master curve of D_{app} vs. f_m. The Master Curve was constructed from the data in Figure 3-4 using equation 3-1, and the values f_p(90 °C)= 0.089 and $\beta(t) = 0.20$ The symbols are the same as those in Figure 3-4.

In Kawaguchi's system β(T) has much higher value than β(T) for the other described systems. We do not know how to explain these differences. One of the reasons can be the difference in annealing temperatures in both experiments. However, the fact that Kawaguchi was able to superimpose all data onto one curve and obtain a Master Curve indicates that the free volume model can be applied to this polymer - surfactant system. NP-20 surfactant acts as a traditional plasticizer, increasing the rate of polymer diffusion by adding more free volume to the system.

3.3.3 Influence of nonionic surfactants on diffusion of low molecular weight PBMA.

Most polymer properties change with molecular weight. One example is the polymer mobility, which can increase by orders of magnitude with a decrease in the polymer molecular weight. In order to learn more about the polymer - surfactant system, we carried out ET measurements of polymer diffusion for our lower molecular weight PBMA samples in the presence of nonionic surfactants. We were mostly interested in how the diffusion of low molecular weight PBMA changes in the presence of nonionic surfactants and how it differs in comparison with the higher molecular weight sample.

3.3.3.1 Starting point for measurements of diffusion parameters for low M PBMA films.

In a newly formed latex film, there are two contributions to energy transfer. First, there is energy transfer across the boundary between donor and acceptor-labeled particles. Second, the early stages of polymer or segment diffusion can mix D- and A-labeled polymers. It is an important, though not easy, task to ascertain the onset time of polymer diffusion, and to distinguish energy transfer across a sharp interparticle interface from that associated with polymer diffusion and mixing. Under ideal circumstances, one would like diffusion to have a clear onset time, associated, for example, with raising the temperature of the sample.

We have found previously that in high molecular weight polymer films with similar particle size and label content, prepared under conditions which allow for complete particle deformation but negligible polymer diffusion, Φ_{ET} has a value of ca. 0.1 (Area(0) ≈ 42 ns). Our experience indicates that in newly formed latex films of low M PBMA (T_g = 21°C), $\Phi_{ET} \approx 0.17$ (Area(0) ≈ 38 ns). Feng[18]et al. analyzed the onset of diffusion for these low

molecular weight PBMA films at room temperature and found it helpful to plot Φ_{ET} vs. drying time of the film. The plot is shown in Figure 3-6 for Feng's data for the sample of low M PBMA. During the drying process (first 40 min) when particles come into the contact and deform, Φ_{ET} increases rapidly. Finally, when the drying process is over (e.g. when the sample is dry and transparent), the energy transfer efficiency has reached a value of 0.17, and the further rate of increase in energy transfer is much slower. This is why we identify $\Phi_{ET} \approx 0.17$ with the ET across the interfacial regions between adjacent cells in the films, and take this value as the extent of ET across sharp interparticle boundaries prior to the onset of diffusion in the low molecular weight PBMA films.

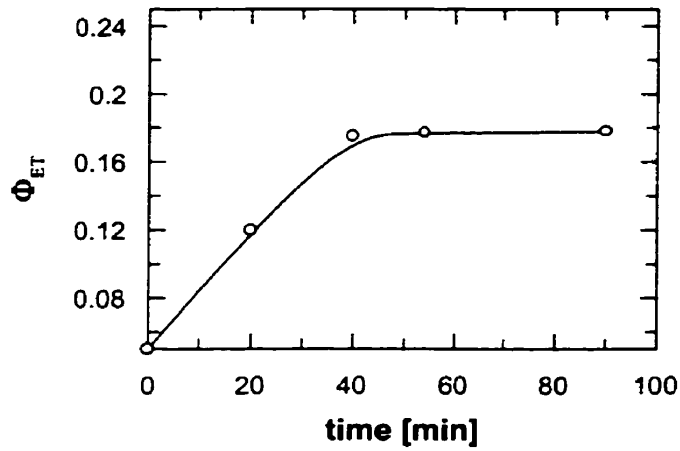

Figure 3-6. Efficiency of energy transfer Φ_{ET} vs. time of film formation for low M PBMA films. The data was taken from reference 18. After 40 min the process of water evaporation is finished and Φ_{ET} does not change with time up to 100 min.

3.3.3.2 Film formation and diffusion of low M PBMA in the presence of nonionic surfactants at room temperature.

In this section, we consider the nonionic surfactants with EO_n chain lengths less then n=15. These surfactants are liquids at room temperature, and promote diffusion of low M PBMA at ambient temperature. The efficiency of energy transfer Φ_{ET}, and the values of the area under the fluorescence decay Area (t) versus diffusion time for PBMA samples with and without 5 wt% of NP-10 and $C^{=}_{8}$-EO_7 are shown in Table 3-5 and in Figure 3-7. Time zero was chosen as the end of drying process (e.g. when sample first became dry and transparent to the eye). Table 3-5 shows that the diffusion of PBMA at room temperature in the presence of the surfactants occurs on a time scale of minutes while that for pure PBMA

occurs on a scale of hours. For example, for the sample with 5 wt% of $C^{=}_{8}$-EO_7 Area(t) decreases from 36.7 ns to 34.8 ns over 25 min. (see Table 3-5b). In the case of a PBMA film (Table 3-5a) consisting of pure polymer, approximately 25 hours (1485 min) are needed to obtain a change in Area(t) from 37.7ns to 36.7 ns.

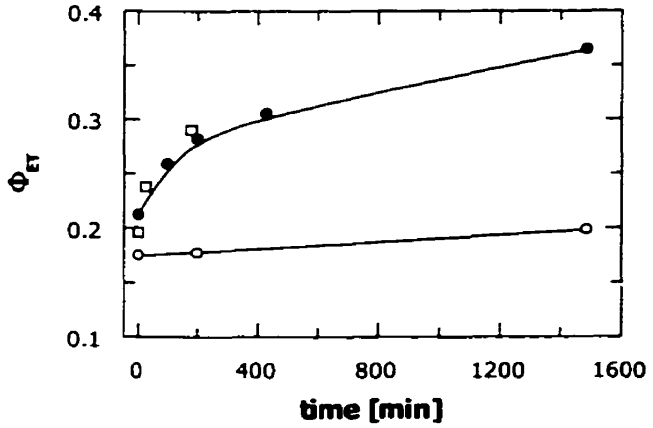

Figure 3-7. Efficiency of energy transfer Φ_{ET} vs. annealing time for pure low M PBMA film (○) and films with the presence of 5 wt% NP-10 (●), and Octene-7 ($C^{=}_{8}$-EO_7) (□). The diffusion process takes place at room temperature.

Table 3-5a. The change in the area under the fluorescence decay curves for various aging times at 23 °C, for a pure PBMA film and for a film containing 5 wt % NP-10.

	time [min]	0	100	200	430	1485
Area(t)	PBMA	37.68	-------	37.60	-------	36.65
	PBMA + 5 wt% NP-10	36.00	33.90	32.80	31.78	29.06

Table 3-5b. The change in the area under the fluorescence decay curves for various aging times at 23 °C, for a pure PBMA film and for a film containing 5 wt % $C^{=}_{8}$-EO_7.

time [min]		0	25	180	560
Area(t)	PBMA	37.68	-------	37.60	--------
	PBMA + 5 wt% $C^{=}_{8}$-EO_7	36.73	34.86	32.44	26.09

The efficiency of energy transfer for newly formed films with 5 wt % of NP-10 or $C^{=}_{8}$-EO_7 (see Fig. 3-7) increases from Φ_{ET} = 0.17, (Area(0) ≅ 38 ns, for pure PBMA) to Φ_{ET} = 0.2-0.215 (Area(0) ≅ 36 ns). These results indicate that some polymer interdiffusion takes place during film formation in the case of the samples with added NP-10 and $C^{=}_{8}$-EO_7.

It would be interesting to know exactly when the onset of diffusion occurred in these films, during the last stage of the drying step or later. I assumed that polymer diffusion is responsible for the changes in Area(0) for samples with NP-10 or $C^{=}_{8}$-EO_7 from 38 ns to 36 ns. To investigate this problem I prepared PBMA films with 5 wt% of $C^{=}_{8}$-EO_7 at low temperature (ca. 4°C). The samples were prepared as described in the experimental section, but with two major differences. First, they were prepared in a cold room at 4°C by placing an aliquot of dispersion on a quartz substrate. Second, the wet film was left uncovered in order to speed up the drying process. Under such conditions, the drying time was around 2h. The dry film was cloudy, which indicates that void closure during film formation during drying was not complete. I placed the sample in ice to carry the sample to the fluorescence decay apparatus and mounted the sample in a cooled sample holder. Measurements were carried out at ca. 7 °C. In this case, the measured Area (0) was 42 ns, which confirms the idea that the deformation and wetting stage of the film formation process was not complete. In the next step, I removed the cooling system and carried out the ET experiment (time of the experiment about 5 min) for the same sample at room temperature. For this run, the Area(0) was about 36 ns. Allowing the sample to sit for a few minutes at room temperature resulted in a transparent films. The decay profile was remeasured and gave the value of Area(0) = 36, the same value obtained previously for newly formed films with NP-10 or $C^{=}_{8}$-EO_7.

From the above experiment, we learned that we are not able to separate the stages of film formation during drying (close packing and particle deformation) from the onset of the interdiffusion process for low molecular weight PBMA films in the presence of these two surfactants. This result implies that there is not a well-defined time for these samples, that we could chose as a starting point for the onset of polymer diffusion.

In order to standardize the calculations of the diffusion rate of low M PBMA in the presence of nonionic surfactants, and to separate ET across the particle boundary from the ET connected with the polymer diffusion, we use equation (3-2) for calculations of the extent of mixing f_m.

$$f_m(t) = (38.5 \text{ ns} - \text{Area}(t))/(38.5 - \text{Area}(\infty)) \quad (3\text{-}2)$$

Where **38.5 ns** is the average value of the area under the fluorescence decay curve for the freshly formed pure PBMA films. This value of 38.5 ns represents ET across a sharp interfaces in these latex films.

Area(t) is the value of the area under the fluorescence decay curve after annealing time t for PBMA samples containing nonionic surfactant added.

Area(∞) is the area under fluorescence decay curve after infinite annealing time (≈13 h).

Equation (3-2) is a form of equation (1-18) from Chapter 1, adapted to the case of low molecular weight PBMA samples with nonionic surfactants.

3.3.3.3 Diffusion of low M PBMA in the presence of nonionic surfactants at elevated temperatures.

Here we analyze the diffusion in low molecular weight PBMA films in the presence of nonionic surfactants at two annealing temperatures: 50 °C and 60 °C. At 60°C the mixing process is complete in 90 min. Thus, 60 °C is the highest temperature at which we can analyze the diffusion of low molecular weight PBMA, without introducing significant errors connected with specifying short annealing times.

As our knowledge about the NP surfactant is the most complete, we analyze the experimental data starting with these surfactants. Figure 3-8a shows the extent of mixing f_m vs. annealing time, while Figure 3-8b shows the apparent diffusion coefficient D_{app} vs extent of mixing for low M PBMA samples with 5 wt% of NP-6, NP-20 and NP-40 surfactants, annealed at 60 °C.

Comparing Figure 3-8a with Figure 3-3, we see that the influence of NP surfactants on diffusion of low and high molecular weight PBMA is different. In the case of low molecular weight PBMA NP-6 and NP-20 promote polymer diffusion at 60 °C to the same extent, while NP-40 has a negligible influence on the PBMA diffusion rate. In the case of high M PBMA even NP-100 promotes polymer diffusion at 90 °C, and the effectiveness of the surfactant depends on the EO chain length. The fact that NP-40 does not promote diffusion of low M PBMA at 60 °C can only be explained by the lack of miscibility of NP-40 with PBMA at this temperature. When the NP surfactants are fully miscible with low M PBMA, like NP-6 or NP-20, then they have similar effects on the diffusion of low M PBMA. In

order to get more information about the system, we repeated the experiment with low M PBMA and 5 wt% of NP-6, NP-10 and NP-20 surfactants at lower annealing temperatures (50 °C). The results are presented in Figure 3-9.

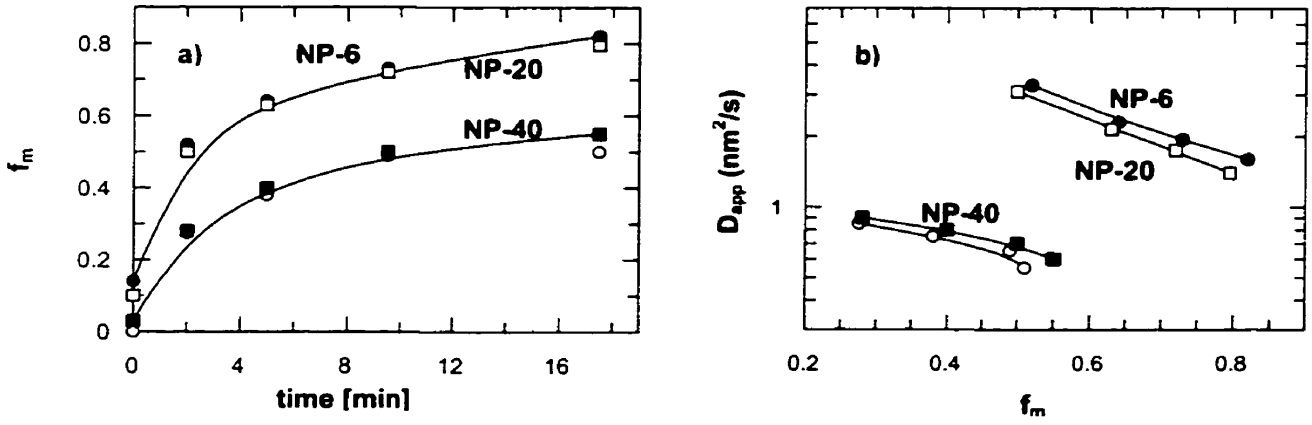

Figure 3-8. Dependence of extent of diffusion f_m (a) and apparent diffusion coefficient D_{app} (b) on annealing time (diffusion time) for low M PBMA film (○) and films with 5 wt % of NP surfactants: (●) NP-6, (□) NP-20, (■) NP-40. Annealing temperature is 60 °C.

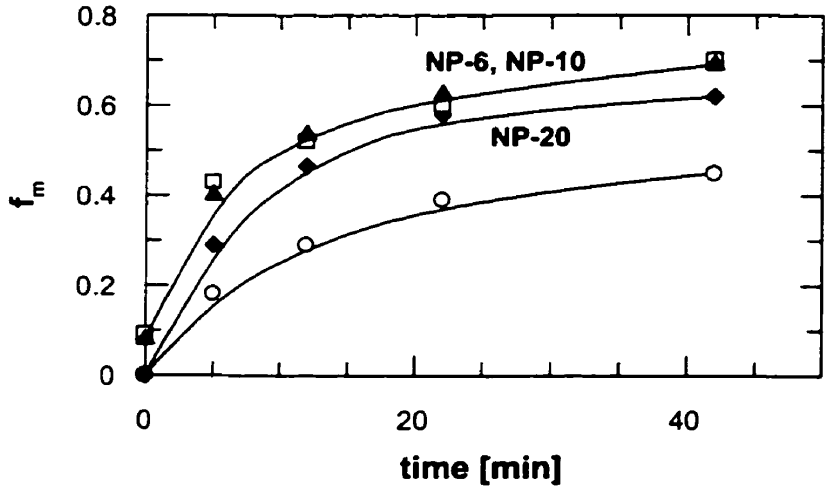

Figure 3-9. Dependence of extent of diffusion f_m on annealing time (diffusion time) for low M PBMA film (○) and films with 5 wt % of NP surfactants: (▲) NP-6, (□) NP-10, (◆) NP-20. Annealing temperature is 50 °C.

Now we see no difference between NP-6 and NP-10, but there is a clear difference between these two surfactants and NP-20. On an equal weight basis, NP-20 promotes polymer diffusion less effectively than NP-10 and NP-6. These results confirm the trend we

have already observed. The miscibility of the system drops drastically with temperature and is connected with the EO chain length of the surfactant.

Until now we concentrated mostly on the influence of NP surfactants on diffusion of low molecular weight PBMA. We will show now that other nonionic surfactants like Ocenol-EO_{16}, $C^{=}_{8}$-$EO_{7,\ 14}$ and $C^{=}_{11}$-$EO_{15,\ 40}$ influence the diffusion of low M PBMA in a similar way. In Figure 3-10 we present the dependence of the extent of mixing f_m on annealing time and the apparent diffusion coefficient D_{app} on the extent of mixing for these surfactants. The annealing temperature was 50 °C.

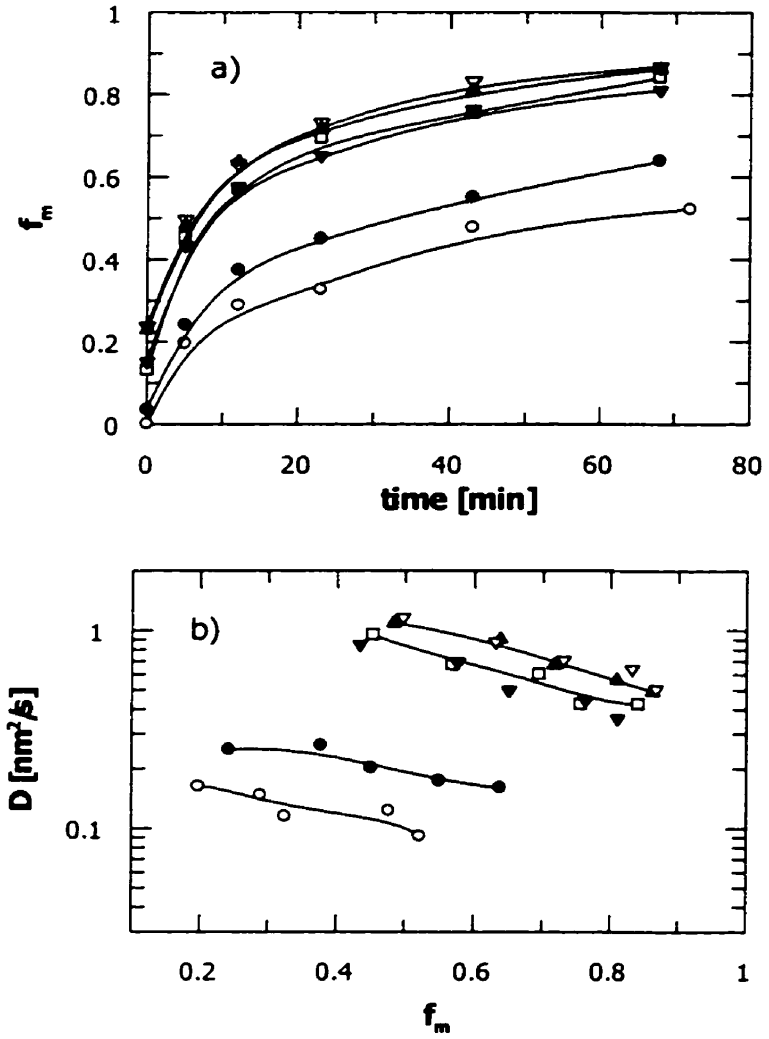

Figure 3-10. Dependence of extent of diffusion f_m (a), and apparent diffusion coefficient D_{app} (b) on annealing time (diffusion time) for low molecular weight PBMA film (○) and films with 5 wt % of the following surfactants: (●) $C^{=}_{11}$-EO_{40}, (□) $C^{=}_{11}$-EO_{15}, (▲) $C^{=}_{8}$-EO_{14}, (▼) OCENOL-EO_{16}, (▽) $C^{=}_{8}$-EO_{7}. The annealing temperature was 50 °C.

The $C^{=}_{8}$-EO_7 promotes PBMA diffusion to the same extent as $C^{=}_{8}$-EO_{14}, both at 5 wt %. Here the effect in promoting diffusion, does not depend on the size of the hydrophilic part of the surfactant. On the other hand, we see some influence of the hydrophobic part of the surfactants on the diffusion rate. $C^{=}_{8}$-EO_{14} is a better plasticizer than Ocenol-EO_{16} or $C^{=}_{11}$-EO_{15}. $C^{=}_{11}$-EO_{40} promotes PBMA diffusion only slightly at 50 °C, but this has to be connected with its low miscibility at this temperature.

Surprisingly, for surfactants that are completely miscible with low molecular weight PBMA at a given temperature and concentration (NP-6 or NP-20 at 60°C or $C^{=}_{8}$-EO_7 and $C^{=}_{8}$-EO_{14} at 50°C), we do not see an EO chain-length effect on the polymer diffusion rate at similar wt concentrations. Since the greatest free volume is connected with the chain ends of the polymer, it is perhaps expected that one should observe the same effect that was found for high molecular weight PBMA. The only explanation we can suggest is that the additional free volume connected with the chain ends of small molecules (see Chapter 1) is only a small part of the total free volume introduced to the system by small molecules. As the low M PBMA is a more mobile system than the high M PBMA, it is probably less sensitive to the small changes in the free volume of the system. We believe that this is the reason why we do not see the surfactant size effect on polymer diffusion in low molecular weight systems, and we observe, for example, that NP-10 promotes polymer diffusion in exactly the same way as NP-20.

Another way to investigate polymer diffusion in the presence of nonionic surfactants is to add surfactants to polymer films on an equal molar basis. In such films, we would have the same concentration of chain ends, so the surfactant effect on polymer diffusion would be only connected with the amount (on the weight basis) of the surfactant in the film (assuming full miscibility). On the other hand, we know that, for miscible surfactants in polymeric matrices, the more surfactant we add to the polymer film, the more significant the effect on polymer diffusion rate. In the case of low molecular weight systems, where we do not observe the surfactant EO chain-length effect on polymer diffusion we expect that nonionic surfactants with higher molecular weight will promote polymer diffusion better than equal molar amounts of nonionic surfactant with lower molecular weight, since the later experiments involve less surfactant on the basis of weight.

Unlike low molecular weight PBMA systems, high molecular weight PBMA systems are sensitive to the additional free volume connected with the chain ends of the nonionic

surfactants. In this case in order to get some quantitative data comparing different surfactants it could be interesting to chose a few concentrations of surfactant with, for example, shorter EO chain lengths, then try to find the concentration of surfactant with longer EO chain lengths that gives the same effect on polymer diffusion. The results obtained could give us a better understanding of the extent of the free volume effect connected with the chain ends of the surfactant, as well as describing wheather or not this effect changes with surfactant concentration.

3.4 Conclusions

1. Non-ionic surfactants post-added to a PBMA latex dispersion strongly enhance the rate of polymer diffusion in the latex films.
2. Their effectiveness depends on the amount of surfactant added, and the miscibility with the polymeric matrix.
3. When miscible, the nonionic surfactants act like a conventional plasticizer, and enhance polymer diffusion by introducing free volume to the system.
4. The energy transfer experiment indicates that the miscibility of the nonionic surfactants with PBMA decreases with increasing EO chain length of the surfactant and with decreasing temperature.
5. The miscibility of the PBMA with nonionic surfactant of EO chain length larger than 20 drastically changes in the range of the temperatures: 90-30°C. This result may be connected with the fact that the melting temperature for these surfactants is in the range of 30 - 60°C.
6. The surfactants with 15 or fewer EO units significantly promote diffusion in low molecular weight PBMA films at room temperature.
7. When system is fully miscible, on a weight basis, the diffusion of high M PBMA depends on the size of hydrophilic part (EO chain length) of nonionic surfactant, while the diffusion of low M PBMA does not show such a dependence.
8. The anionic surfactants (SDS and C_{94I}) do not enhance, and even slightly retard polymer diffusion in PBMA latex films. These surfactants are high melting solids ($T_m \approx 200$ °C),

and, in the range of the temperatures investigated exist as crystalline domains in the polymeric matrix. These crystallites may act as obstacles for diffusing polymer.

3.5 References

1. Basset, D. R.; Hamielec A. E. *"Emulsion Polymers and Emulsion Polymerization"*, ACS Symp. Ser. No. 165, Washington, D. C., **1981**.
2. El-Aasser, M. S.; Fitch, R. M. *"Future Directions in Polymer Colloids"*, NATO ASI, Series E, Applied Sciences No. 138, Nijhoff, The Hagne, **1987.**
3. Swarup, S.; and Schoff, C. K.; *Progress in Organic Coatings*, **1993,** 23, 1.
4. Tanaka, T.; Fujimoto, T.; Shibayanma, K. *J. Appl. Polym. Sci.*, **1979**, 23, 1131.
5. Haq, Z.; and Thompson, L. *Colloid Polym. Sci.*, **1982**, 260, 212.
6. Eckersley, S. T.; Rudin, A. *J. Appl. Polym.* **1993**, 1369.
7. Snuparek, J.; JR. A., Hanus, J.; Hajkova, B. *Polym. Sci.*, **1983**, 28, 1421.
8. Ikkaku, Y.; Kadowaki, T.; Okubo, M.; Matsumoto, T. *Kobunshi Ronbunshi*, **1982**, 39 (1), 35.
9. (a) Bradford, E. B.; Vanderhoff, J. W.; *J. Macromol. Chem.*, **1966**, 1, 335. (b) Bradford, E. B.; Vaanderhoff, J. W.; *J. Macromol. Sci.- Phys.*, B6, **1972**, 671.
10. (a) Vajayendran, B. R.; Bone, T.; Gajria, C.; *"Emulsion Polymerization of Vinyl Acetate"*, El-Aasser, M.S.; Vanderhoff, J. W.; Eds., Applied Science, Barking, Essex, U. K., **1981**.; (b) Vajayendran, B. R.; Bone, T.; Gajria, C.; *J. Appl. Polym.* Sci., **1981**, 26, 1351.; (c) Vajayendran, B. R.; Bone, T.; *J. Dispersion Sci. Technol.*, **1992**, 3(1), 81.
11. (a) Zhao, Ch.-L.; Holl, Y.; Pith, T.; Lambla, M.; *Colloid Polym. Sci.*, **1987,** 265, 823.; (b) Zhao, . Ch.-L.; Holl, Y.; Pith, T.; Lambla, M. *British Polym. J.*, **1989**, 21, 155.; (c) Zhao, Ch.-L.; Dobler, F.; Pith, T.; Holl, Y.; Lambla, M. *J. Colloid & Int. Sci.*, **1989**, 128, 437.
12. a. Urban, M.; Evanson, K. W. *Polym. Comm.*, **1990**, 31, 279.; b. Thorstenson, T.; Urban, M.; *J. Appl. Polym. Sci.*, **1993**, 47, 1387.; c. Thorstenson, T.; Tebelius, L.; Urban, M. *J. Appl. Polym. Sci.*, **1993**, 50, 1207.

13. Hadicke, E.; Hahn, K.; Ley, G.; Streib, J.; Lindner, P. *Prog. Colloid Polym.* Sci., **1990,** 81, 267.

14. Vandezande, G., A.; Rudin, A. *J. Coatings Tech.*, **1996,** 68, 63.

15. Padget, J. C.; Moreland, P. J. *J. Coatings Tech.*, **1983,** 55, 39.

16. Wang, Y.; Winnik. M. A. *J. Phys. Chem.* **1993**, 97, 2507.

17. a) Kawaguchi, S. *Lab Report*, University of Toronto, **1994**; b) Kawaguchi, S.; Odrobina, E.; Winnik, M. A. *Macromol. Rapid Commun.* **1995**, 16, 861.; c) Fujita, H. *Fortschr. Hochpolym. – Forsch.* **1961,** 3, 1.

18. Feng, J.; Pham, H.; Stoeva, V. *J. Polym. Sci. Part B Polym. Phys.* **1998**, 36, 1129.

19. Tager, A. *Physical chemistry of polymers,* English translation, Mir Publishers, **1978**, p 173.

4 EFFECT OF OLIGOMERS ON THE POLYMER DIFFUSION RATE IN POLY(BUTYL METHACRYLATE) LATEX FILMS

4.1 Introduction

We have seen in Chapter 3 that coalescing aids [1,2] and some non-ionic detergents[3] act as traditional plasticizers to accelerate the rate of polymer diffusion in latex films. In contrast, simple ionic surfactants such as sodium dodecyl sulfate (SDS) and sodium dihexyl sulfosuccinate (SHSS) have little effect (Chapter 3).

Here we are interested in the influence on polymer diffusion of a component of latex dispersions whose presence arises as a by-product of the latex synthesis, rather than as a formal additive. When latex particles are prepared by emulsion polymerization, some water-soluble oligomeric material is formed.[4] Larger amounts form when the polymerization is run under monomer-starved conditions, because the polymerization rate, which is first order in monomer concentration, is retarded relative to the chain-transfer and termination processes. Sometimes, water-soluble co-monomers such as acrylic acid or methacrylic acid are part of the monomer feed. They also promote the formation of a water-soluble component in the reaction. Our curiosity about the influence of this component was piqued by the fact that we observed its presence every time we analyzed the latex polymer by gel permeation chromatography (GPC). As a consequence, we decided to separate this component, analyze it, and add it in known amounts to latex dispersions which had been purified to remove all water-soluble oligomeric material. Thus we treat this component as an additive and show that it also acts as a plasticizer to promote polymer diffusion in poly(butyl methacrylate) (PBMA) latex films.

4.2 Experimental

4.2.1 Preparation of Oligomers

A surfactant-free emulsion polymerization of BMA was carried out to prepare a latex with significant amount of oligomers present in the water phase. To increase the content of oligomers in the sample, several strategies were considered for lowering the overall average

molecular weight of the latex product. A high initiator concentration and a small amount of a chain transfer agent (dodecyl mercaptan, 2 wt% based on the total monomer), were used during polymerization. The polymerization was carried out via a continuous process, with a very slow monomer addition rate (ca. 0.057 mL/min). The recipe for such a polymerization is as follow: KPS (0.44 g) dissolved in water (165 g) was precharged into the reactor and heated at 80°C. A monomer solution (BMA, 30 mL) containing dodecyl mercaptan (1.55 mL) was fed slowly into the reaction system. An additional amount of KPS (0.22 g) dissolved in water (30 mL) was fed concurrently. The total feed time for both the monomer and the aqueous solutions was ca. 9 h. After a feed ended the emulsion was warmed for 1 h to complete the polymerization.

The resultant latex dispersion was then centrifuged (at 20,000 rpm for 1 hour) to separate the particles from the water phase. The nearly clear liquid, containing a significant amount of water-soluble material, was stored for blending into the labeled PBMA dispersion for film formation. The oligomer species in the serum represent a complex mixture. This mixture was partially characterized by GPC analysis (were PS was used as a standard), by ^{1}H NMR (400 MHz) and by electrospray negative ion mass specroscopy using dried samples dissolved in an organic solvent (THF for GPC; $CDCl_3$ and DMSO-d_6 for the ^{1}H NMR, 1:1 acetonitrile-water for mass specroscopy). In the discussion that follows, we refer to this mixture as "oligomer."

4.2.2 Film formation and Characterization

Latex films were prepared from dispersion mixtures of 1 : 1 number ratio (N_{Phe}/N_{An}) of Phe- and An- labeled particles. The latex dispersions were cleaned by stirring at low solids (ca. 8 wt %) with an ion-exchange resin (AG-501-X8 Mixed-bed-resin, Bio-Rad, not purified before using) to remove the ionic surfactant and other ionic species present in the dispersion. Known amounts of the oligomer were added to aliquots of ion-exchanged PBMA latex dispersion. All films were formed by drying the dispersions (initial solids content 7.8 wt%) at 32° C on quartz plates. The wet film was covered by an inverted petrie dish to slow the water evaporation rate, and drying occurred over ca. 8 h. Fluorescence decay profiles were measured by the single-photon-counting timing technique.[5] The measurement conditions were similar to those described in Chapter 1. After each time interval of annealing, the samples were cooled to room temperature, and the fluorescence decay profile

of each film was measured. Fluorescence decay measurements were carried out as described in Chapter 1. The calculations of areas under each decay curve, extent of mixing f_m and apparent diffusion coefficient D_{app} are also described in Chapter 1.

4.3 Results and Discussion

4.3.1 Characterization of the Latex Polymer.

The films we examine were prepared from a dispersion containing a 1:1 blend of Phe- and An-labeled PBMA latex particles, referred to as Phe-PBMA and An-PBMA, respectively. Some important characteristics for these samples are listed in Table 4-1. Since the two labeled latex dispersions were prepared using nearly identical recipes and under strictly identical conditions, we obtained particles of similar size and size distribution. More important, the molecular weight and molecular weight distribution of the two types of particles are very similar.

Table 4-1. Latex characteristics.

Phe-PBMA	An-PBMA
M_n = 130,000	M_n = 133,000
M_w = 377,000	M_w = 421,000
M_w/M_n = 2.91	M_w/M_n = 3.16
d = 124 nm (0.040)[a]	d = 132 nm (0.037)[a]

a. size polydispersity

We used gel permeation chromatography (GPC) measurements to characterize the latex polymers. Figure 4-1 displays the refractive-index (RI) signals of GPC traces of one of our PBMA latex samples, before and after cleaning by ion exchange (Bio-Rad, AG-501-X8 mixed bed resin, 3 g resin per 100 mL of latex). One observes that there is a small peak at 25 min in both samples. It is likely that this peak is caused by the presence of a small amount of oligomers.

Figure 4-2 shows a GPC trace for the An- labeled PBMA sample. The continuous line represents RI signal, while the fluorescence (FL) signal is shown as dashed line. The FL signal exhibits a peak (at 13-20 min) which appears in the same range as the polymer peak

in the RI signal. The two signals in this region also have a similar shape (a similar intensity distribution) indicating random dye distribution in the polymer. In the low-molar-mass region there is an additional peak in the RI trace for which there is no signal in the FL trace. Thus there is no low molar mass fluorescent species in the sample. We can conclude from this result that all of the dye co-monomer is incorporated into the polymer. This fact is important for us to obtain high quality data in our diffusion analysis.

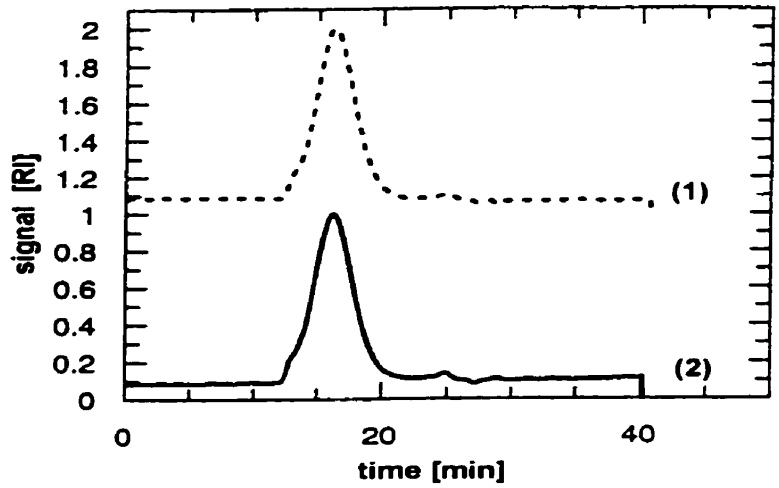

Figure 4-1. GPC (RI) curves for an unlabeled PBMA sample with (1) and without (2) cleaning.

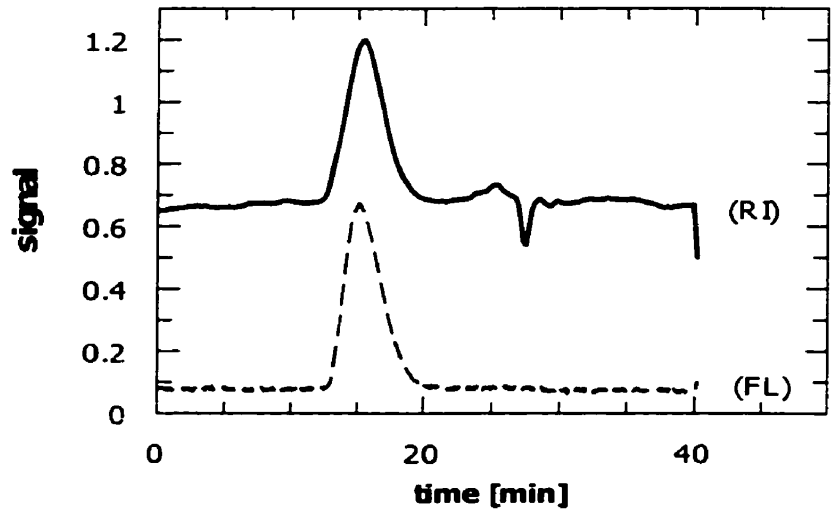

Figure 4-2. GPC curves for a labeled (An-PBMA) sample: refractive index (RI) signal, fluorescence (FL) signal

4.3.2 Characterization of the oligomeric species.

We expect that a significant fraction of the end groups of our oligomers should be the sulfate group, which results from the initiation of polymerization by sulfate ion-radicals formed by the decomposition of persulfate ion:

$$S_2O_8^{2-} \longrightarrow 2SO_4^{\bullet} \qquad (4\text{-}1)$$

Termination by combination leads to oligomer (or polymer) molecules with two sulfate end groups. Termination by disproportionation or chain transfer leads to molecules with one sulfate end group. In the dissociated form, these oligomers can act as anionic surfactants and add additional stability to the latex. However, Kolthoff and Miller[7] have shown that the sulfate ion-radical can attack water to generate sulfuric acid and hydroxyl radical:

$$SO_4^{\bullet} + H_2O \longrightarrow HO^{\bullet} + HSO_4^- \qquad (4\text{-}2)$$

The hydroxyl radical can initiate polymerization to form polymer and oligomer with hydroxyl end groups. Hydrolysis of sulfate end groups can also yield hydroxyl end groups plus bisulfate ions, and in this way reduce the number of sulfate groups bound to the oligomer or polymer.

$$ROSO_3^- + H_2O \longrightarrow ROH + HSO_4^- \qquad (4\text{-}3)$$

The oligomers lacking a sulfate end group should not act as a surfactant. We would not expect to remove them from the latex dispersion with the ion exchange resin.

Rudin at al[8,9] report characterization of oligomers obtained in the surfactant-free emulsion polymerization of methyl methacrylate and of methyl methacrylate/butyl acrylate mixture. In their experiments, the polymerization was initiated by amonium persulfate, and in some cases, isooctyl mercaptopropionate was used as a chain transfer agent. They were able to separate their surface-active oligomers from crude latex by a combined centrifuge and filtration method. Conductometric and potentiometric titrations on cleaned latexes and crude latexes show that for every mole of sulfate groups added as persulfate in the

polymerization, about 0.1 mol of sulfate groups became bound to macromolecular chain ends. In addition about 0.13 mol of sulfuric acid salt (in the form shown in eq. (4-2) was generated, and about 0.50 mol of initial sulfate groups were attached to oligomers, which behave in a way similar to traditional surfactants. Under these reaction conditions about 0.27 mole of initiator remained undecomposed.

Based on their results we can expect that our experiments produce some BMA oligomer. This component is in its active – surfactant form with a sulfate group at the end, and some amount is hydrolysed. In order to try to characterize the oligomers, we analyzed them first by GPC.

Figure 4-3 displays the RI signal of a GPC trace of the isolated oligomers. This oligomer fraction comes only from the water phase of the PBMA latex. They were obtained by centrifugation of the latex, followed by drying of its aqueous phase. Next, the dry oligomers were dissolved in THF and the GPC measurements were carried out. Under these conditions, not all the solid dissolves in THF. The insoluble part may be only inorganic salts. It is also possible that the GPC trace represents only a part of oligomers, the part that dissolved in THF. The insoluble part was easily separated from the rest of the solution by centrifugation.

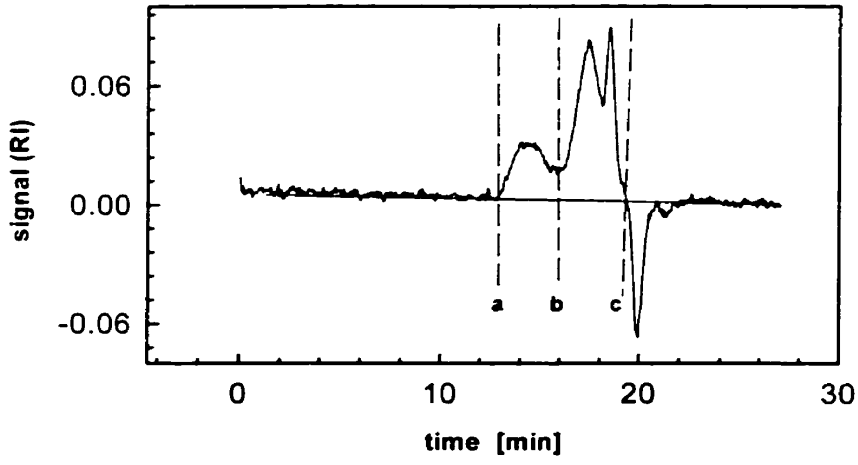

Figure 4-3. GPC signal for BMA oligomer separated from PBMA latex (Figure 4-4a) by centrifugation, then dried and dissolved in THF.

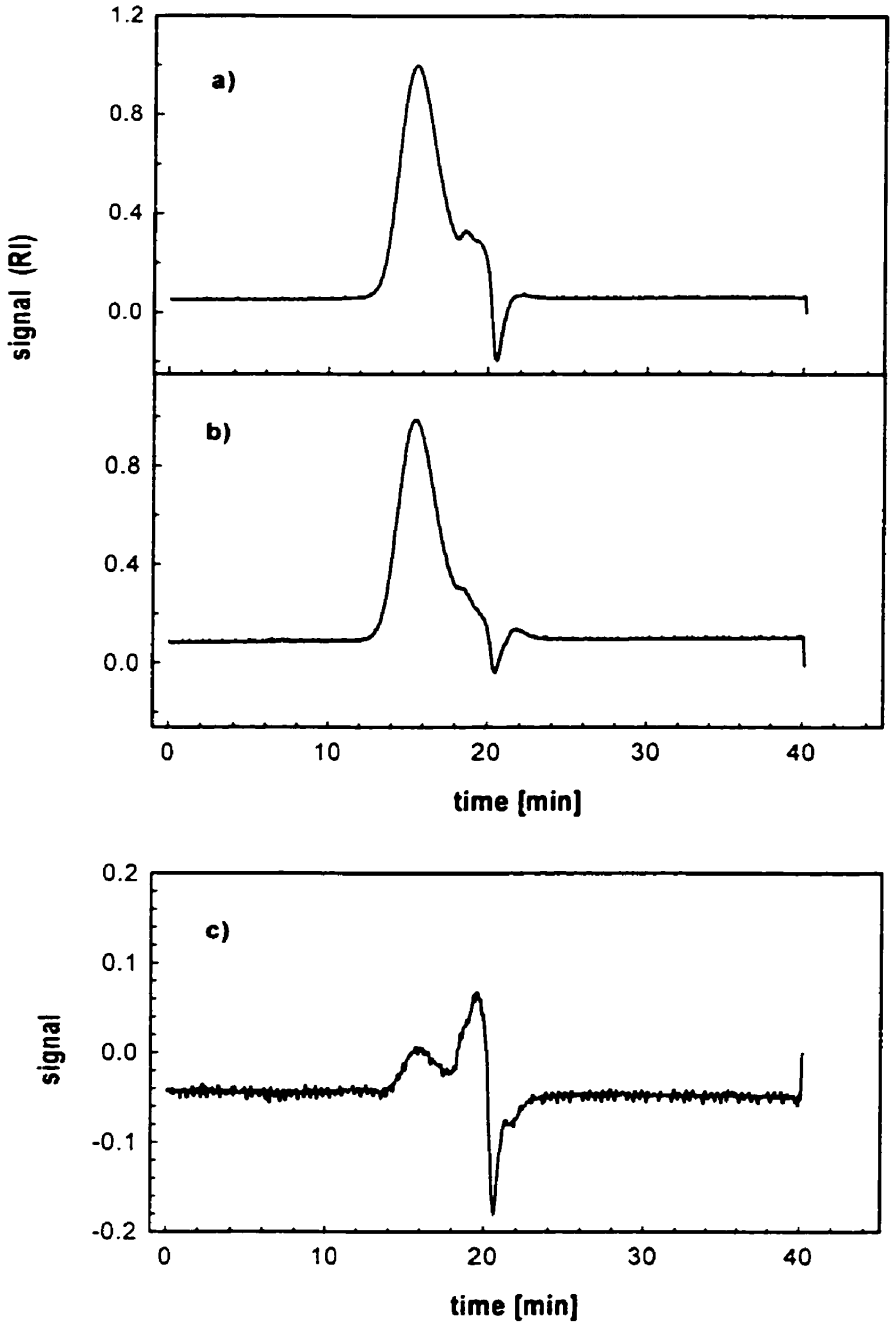

Figure 4- 4. GPC (RI) curves for (a) crude PBMA sample with oligomers (a), and (b) the same sample after cleaning by ion exchange. The two traces are normalized to the same peak height for the polymer peak at t = 16 min. (c) The difference signal obtained by subtracting curve (b) from curve (a).

Figure 4-3 shows that the mass distribution of the oligomers is bimodal, and the second peak, which represents the part of the lower molecular weight species overlaps with the solvent peak. We calculated the molecular weight of each peak separately, using polystyrene standards. The baseline chosen for calculations is shown in Figure 4-3 as a straight line. The integration limits are represented by dashed vertical lines, (a) and (b) for the first peak, and (b) and (c) for the second peak. The calculated molecular weight for the first peak is M_n = 10,000 and M_w = 16,000, M_w/M_n = 1.57, and for the second peak M_n = 365 and M_w = 680, M_w/M_n = 1.87. We also attempted to obtain the molecular weight of the oligomer fraction using GPC with light scattering and viscosity detectors (a DAWN triple detector). These experiments did not yield useful results. The signals confirm the existence of the two peaks observed by RI detector, but they were very noisy. It was impossible to carry out any useful analysis of the data.

Although we can not get an accurate molecular weight of our oligomer by GPC, we can certainly draw the conclusion that the oligomer used as an additive in polymer diffusion measurements consists of very low molecular weight species of the order of one, two, or three BMA monomer units, as well as, some part of low molecular weight polymer. This conclusion is also confirmed by comparison of GPC traces (Figure 4-4) of crude PBMA latex with oligomers (Figure 4-4a), and the same latex cleaned by ion exchange resin (Figure 4-4b). The GPC signal is normalized in both cases to the maximum of the peak. The difference between the two normalized signals is shown in the Figure 4-4c, and represents only the mass distribution of the water-soluble oligomer.

We also report the spectroscopic data for the oligomer component and attempt to assign aspects of its structure. We first present the ^{1}H NMR spectrum of PBMA in $DCCl_3$ in Figure 4-5. In the polymer, both methyl groups (6H) appear at 0.7 to 1.1 ppm, and the O-CH_2- group appears without structure at 3.9 ppm. The three remaining CH_2 groups appear as three sets of closely spaced peaks in the range of 1.2 to 2.0 ppm, although the intensity is less for the peak at highest field.

The ^{1}H NMR spectrum of PBMA oligomer in $DCCl_3$ is presented in Figure 4-6. As in the polymer, the intensity in the range of (0.7 – 1.7) ppm is due to aliphatic CH, but the CH_3 signal at 0.87 ppm appears as a fairly well-defined triplet. The carboxyl ester –OCH_2- should appear at ca. 3.6 – 3.9 ppm and the –CH_2-$OSO_3^{(-)}$ would be expected to appear at ca. 4.0 ppm.[10] In our case we have a slim peak at 3.9 ppm without structure, as in the polymer

spectrum, and additional peaks at 3.7, 4.1 ppm and at 4.6 with some structure. All these peaks are likely to be connected with O-CH_2- group. There is little evidence for a significant amount of –CH_2OH groups, because the protons in this group should appear at 3.6 – 3.8 ppm. The three remaining CH_2 groups appear as three sets of closely spaced peaks in the range of 1.2 to 2.0 ppm. The ratio of the proton intensity in the range (0.7 – 2) ppm to that at (3.6 – 4.6) ppm is 4.8. The peak at 7.3 ppm is the solvent peak, and the peak at 6.8 is likely to be a water peak. Some small peaks at 2.2 and 2.8 ppm also appear in NMR spectra of PBMA oligomers in chloroform. Assuming that triplet at 4.6 ppm comes from –CH_2-$OSO_3^{(-)}$ (the coupling should be 7 Hz, but we found 11 Hz) and comparing the intensity of this peak with the intensity of the triplet at 0.87 ppm representing methyl groups we obtained the average number of monomer units per oligomer chain equal to 4.4.

Since the solid containing the PBMA oligomer is not completely soluble in chloroform, we also measured NMR spectrum in DMSO. The ^1H NMR spectrum of the oligomer mixture in DMSO-d6, with a trace of DMSO at 2.5 ppm as a reference, is shown in Figure 4-7. DMSO is more viscous than $CDCL_3$. As a consequence, the peaks are broader. The insert shows an expanded view of the region between 0 to 2 ppm. In the oligomer NMR, we find peaks at 0.87, 1.07 (broad), 1.32 (broad), 1.54 (broad) and a weaker, broader band at ca. 2 ppm. There are, in addition, peaks at 3.7 (broad, but some structure) and 4.0 (broad) plus a very broad peak of low amplitude. As in the polymer, the intensity in the range of (0.7 – 1.7) ppm is due to aliphatic CH, but the CH_3 signal at 0.87 ppm appears as a fairly well-defined triplet. The carboxyl ester –OCH_2- appear at ca. 3.6 – 3.9 ppm and the –CH_2-$OSO_3^{(-)}$ would be expected to appear at ca. 4.0 ppm.[10] All these peaks overlap and it is impossible to calculate the value of the signal from the end groups separately. The ratio of the proton intensity in the range (0.7 – 1.7) ppm to that at (3.3 – 4.2) ppm is 2.4. We suspected that the broad peak at > 4.2 ppm may be due to –O<u>H</u>, and added increasing amounts of pyridine to the sample to sharpen and to shift this peak. As expected, this band disappears, but is replaced by a broad singlet at 4.2 ppm.

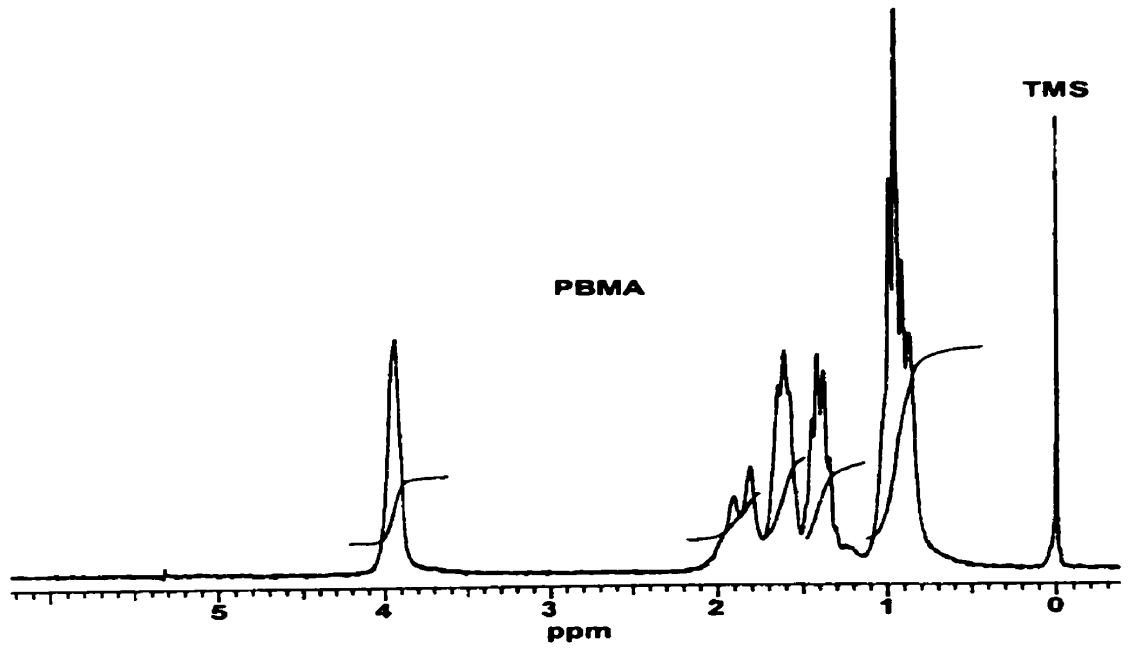

Figure 4-5. ^{1}H NMR spectrum of poly(butyl methacrylate) in $CDCl_3$.

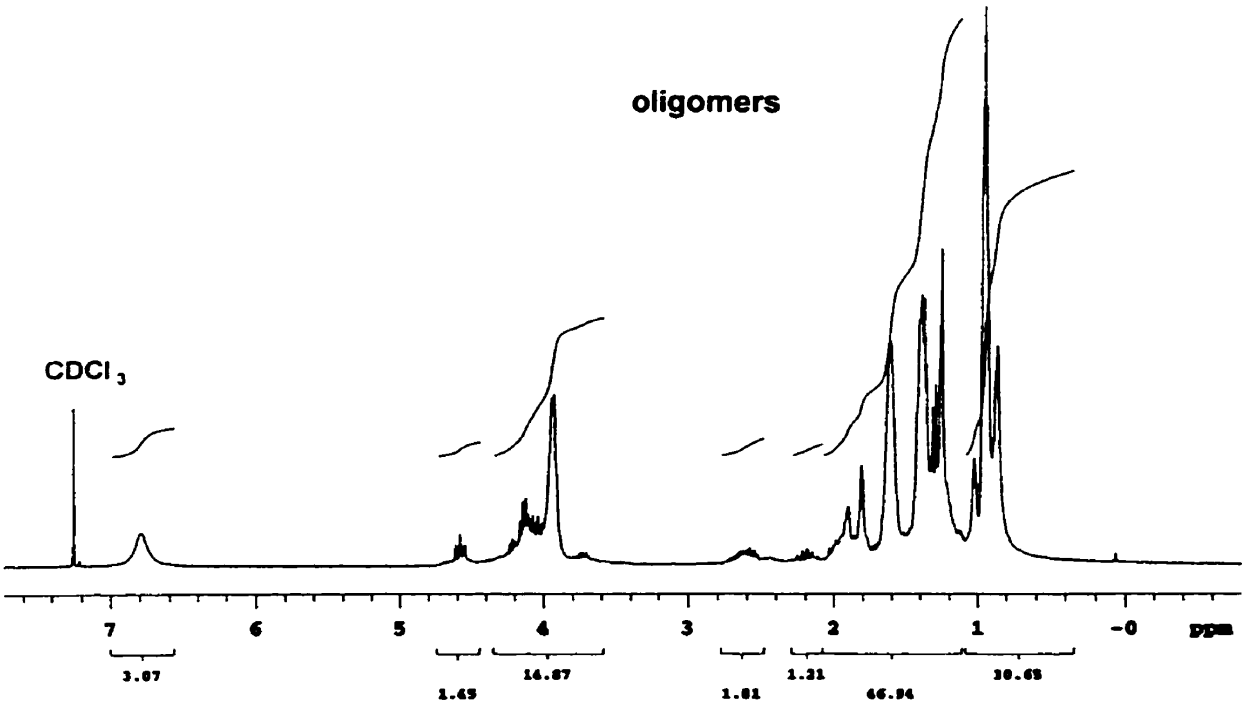

Figure 4-6. ^{1}H NMR spectrum of a freeze-dried sample of the oligomer in $CDCl_3$.

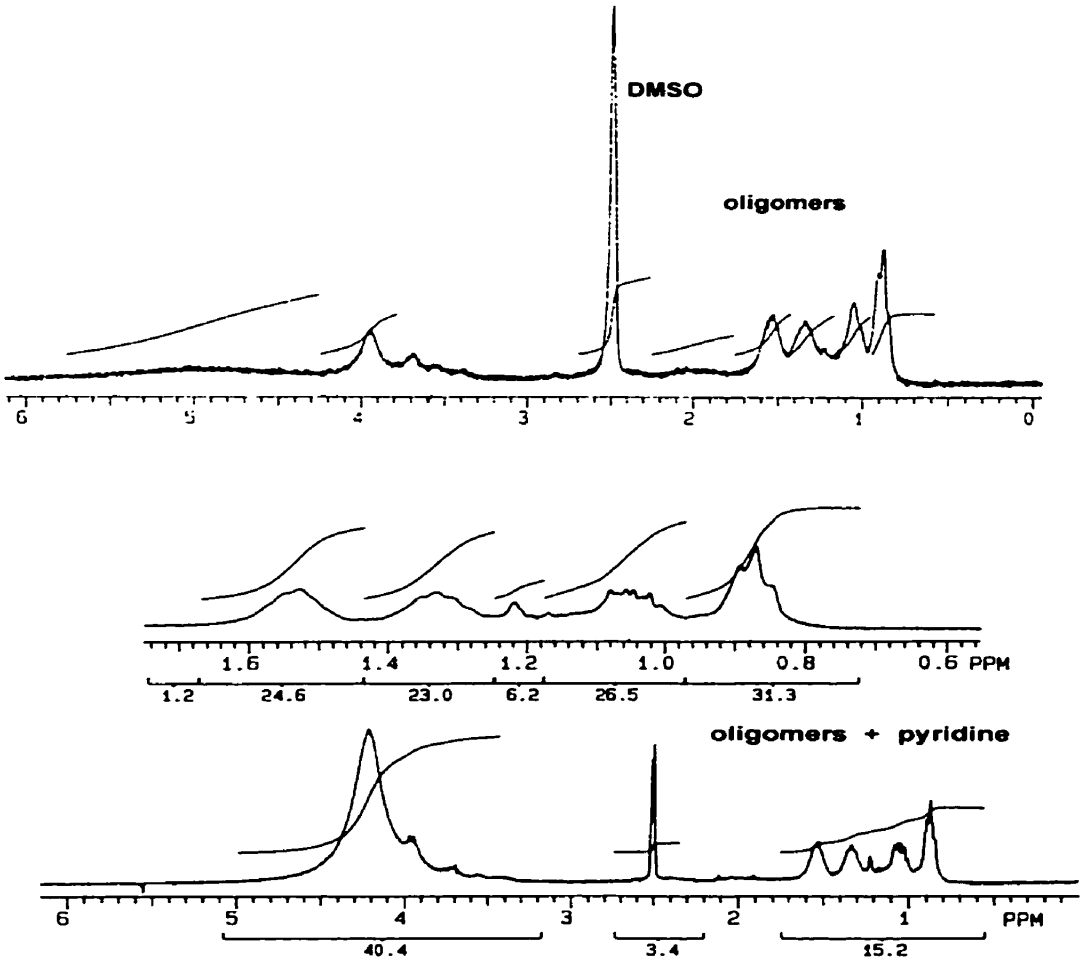

Figure 4-7. (top) ^{1}H NMR spectrum of a freeze-dried sample of the oligomer fraction employed in the experiments described above. The sample is dissolved in DMSO-d6 to which a trace of DMSO is added as a reference. (bottom) ^{1}H NMR spectrum of the same sample to which a few drops of pyridine have been added. The inset presents the aliphatic region of this spectrum on an expanded scale.

Electrospray ionization[11] is a very gentle way of ionizing molecules and ions with relatively little fragmentation. The negative-ion spectrum of the oligomer shows a base peak (for m/e > 100) at m/e 325, with significant intensity at 380 (14%), 379 (7%), 309 (40%), 238 (27%), 237 (9%), and 210 (16%). The strongest peak is at m/e 97, corresponding to $HSO_3^{(-)}$. One also sees weak peaks in the mass spectrum at higher mass values, up to m/e 483. These mass values can be rationalized in terms of the structures shown below. The other isomer with a $C{=}CH_2$ group adjacent to the ester is also possible for the ion with m/e 379.

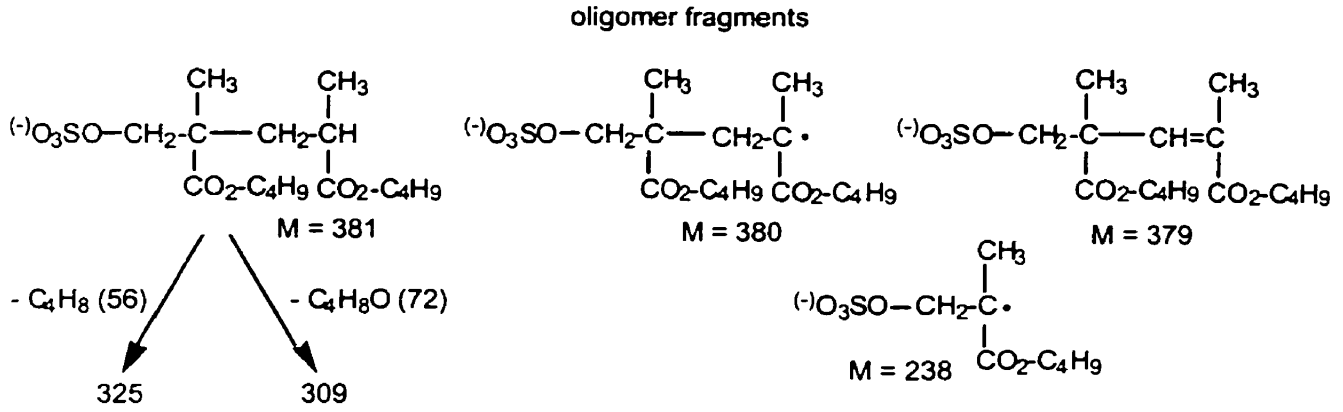

The structure shown for m/e 379 is unlikely to be a major constituent of the oligomer because one does not observe in the NMR the olefinic protons of the unsaturated structure, nor a singlet at ca. 2 ppm for the methyl group attached directly to the double bond. We see only a weak peak at m/e 381 in the mass spectrum, but two of the fragment peaks (m/e 309 and 325) may have this dimer ion as their parent. The spectroscopic data confirms the GPC results that the oligomer consists primarily of dimer, trimer and higher homologues.

4.4 Effect of oligomer on PBMA diffusion.

Measured quantities of BMA oligomers in aqueous solution were added to ion-exchanged dispersions of labeled PBMA latex (M_w = 370,000; M_n = 130,000), and the solutions were dried to form films. In Figure 4-8 we compare the GPC traces for the PBMA latex samples before and after addition of oligomers. In Figure 4-8 we present the RI signals for a latex polymer sample consisting of 1:1 mixture of the Phe- and An-labeled PBMA, first for the sample cleaned by ion exchange, and for the same sample after adding 9 wt% of oligomers. For the sample with the oligomers added, we see an additional peak in the RI signal that confirms the presence of low molecular species. The integrated area of the small peak is about 20% of that of the larger peak at high molar mass, even though we have added only 9 wt% of oligomers. This discrepancy is likely connected with the possibility that the small-molar-mass species have a different RI sensitivity than the polymer. Rudin et al.[6] compared the GPC traces from RI, light scattering and viscosity detector for polyethylenes with wide molecular weight distribution, and found that the RI detector is the most sensitive

for the low molecular weight species, but its sensitivity for high molecular weight polymers drops significantly with comparison to the other detectors.

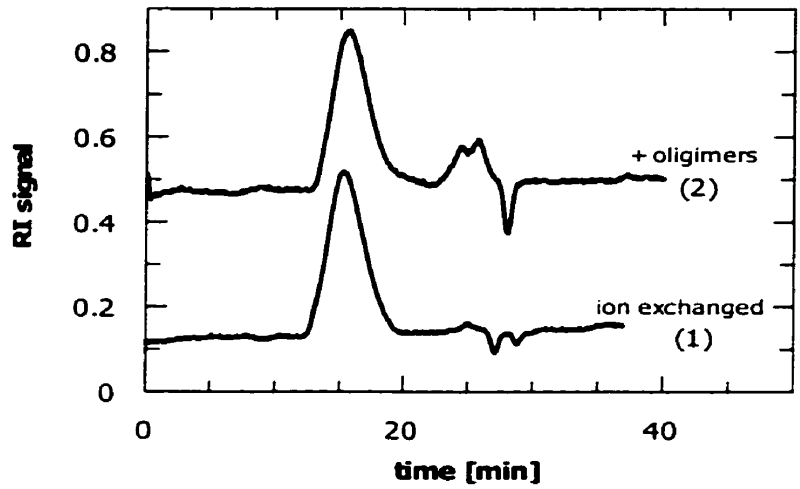

Figure 4-8. GPC signals for 1:1 mixture of the Phe- and An-labeled PBMA without (1) and with (2) post-added oligomers (9 wt %).

For energy transfer measurements, the dry PBMA films with and without oligomers, were annealed at 76° C for various periods of time, cooled to room temperature, and their fluorescence decay profiles were measured. From the decay profiles, f_m values were calculated, providing us with a measure of the polymer diffusion rates. From the f_m values, apparent diffusion coefficients for the polymers were calculated. Figure 4-9 compares the diffusion rates determined for PBMA with different amounts of BMA oligomers present in the system. One observes a clear trend that with increasing amount of oligomer, the diffusion rate of the polymer increases. The D_{app} values have increased about 6 times upon addition of only 3 wt% oligomers, and are much higher for films with 6 or 9 wt% oligomers. This indicates that the oligomers can plasticize the polymer and enhance its diffusivity. The presence of the oligomers does not have a large effect on the minimum film forming temperature of the latex, nor does it seem to promote diffusion at room temperature, approximately 12° C degree below the glass transition temperature of PBMA itself (Tg = 34 °C). We also do not observe differences in the area under the donor decay profile (the Area(0) value) due to the presence of oligomer in the sample. If the oligomer were to form a continuous membrane phase that separated the Phe-and An-labeled cells in the nascent film, we might expect the Area(0) values to increase from 42 ns toward 45 ns.

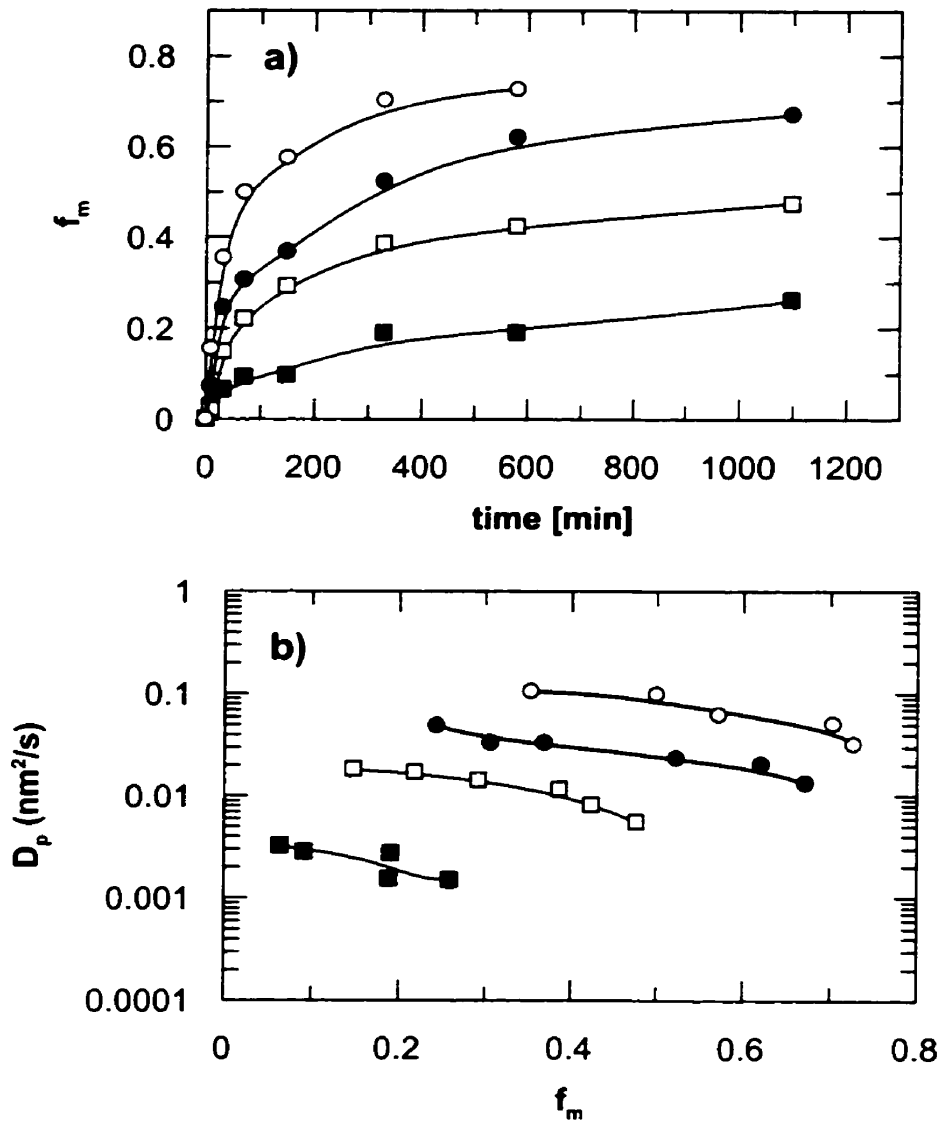

Figure 4-9. Comparison of diffusion rates for PBMA (M_w=370K) at 76°C without post-addition (■) and with addition of 3 wt% (□), 6 wt% (●), and 9 wt% (○) of BMA oligomers. In (a) and (b) the plots of extent of mixing (f_m) vs. time (in min) and the mean diffusion coefficient (D_p, in nm^2/s) vs. fm, respectively, are shown.

At higher temperatures the oligomer might contribute in many ways to enhancement of polymer diffusion. If the oligomer acts as a traditional plasticizer to increase the free volume in the sample, and is uniformly distributed in the polymer matrix at the annealing temperature, its influence on the polymer diffusion rate should follow the Fujita-Doolittle equation. [2,3,12]

$$\left[\ln\frac{D_p(T,\Phi_a)}{D_p(T,0)}\right]^{-1} = f_p(T,0) + \frac{f_p^2(T,0)}{\Phi_a\beta(T)} \qquad (4\text{-}4)$$

Here D_p is the polymer diffusion coefficient; Φ_a is the volume fraction of the plasticizer; $f_p^2(T,0)$ is the fractional free volume of the polymer with no added plasticizer; and $\beta(T)$ is the difference in fractional free volume between the plasticizer and the polymer at temperature T. From Figure 4-9, the magnitude of the term $\{\ln [D_p(T,\Phi_a)/D_p(T,0)]\}^{-1}$ can be calculated for each set of data, with Φ_a ranging from 3 to 9 vol%. This calculation assumes that the oligomers have a density of 1.0 g/mL, close to the value of 1.06 g/mL for PBMA. We equate D_p with D_{app}. Since the plots of (log D_{app}) vs. f_m in Figure 4-9b are essentially parallel for all sets of data for different values of Φ_a, the term $\{\ln [D_p(T,\Phi_a)/D_p(T,0)]\}^{-1}$ is almost constant at different f_m values.

In Figure 4-10 we plot values of $\{\ln [D_p(T,\Phi_a)/D_p(T,0)]\}^{-1}$ vs. $1/\Phi_a$. A straight line is obtained, confirming that the system follows the behavior predicted by the Fujita-Doolittle model [eq. (4-4)]. The intercept yields a $f_p(T,0)$ value of 0.029, and the slope gives a $\beta(T)$ value of 0.051. The $f_p(T,0)$ and $\beta(T)$ calculated here are quite reasonable, compared to values for plasticizers in polymer systems found in literature. For example, Fujita[12] gives values of $f_p(T,0) = 0.046$ and $\beta = 0.07$ for the system of high molecular weight poly(ethyl acrylate) (T_g = -28 °C) – benzene at 23° C. In our lab we have previously used this kind of analysis to describe the effect of the coalescing aid Texanol™ (trimethylpentanediol monoisobutyrate) on the diffusion rate of PBMA at 36 °C, for a sample of $M_w \approx 8.9\times10^4$, where we found $f_p = 0.025$ and $\beta = 0.07$.[2] From Figure 4-9, we calculate $\log[D_p(T,\Phi_a)/D_p(T,0)]$, a shift factor which allow us to superimpose data obtained with a fraction of additive Φ_a to that for $\Phi_a = 0$. One sees that all the data can be superimposed onto a single master curve, Figure 4-11. This result confirms that the oligomer acts in a similar way to traditional plasticizers in these latex films.

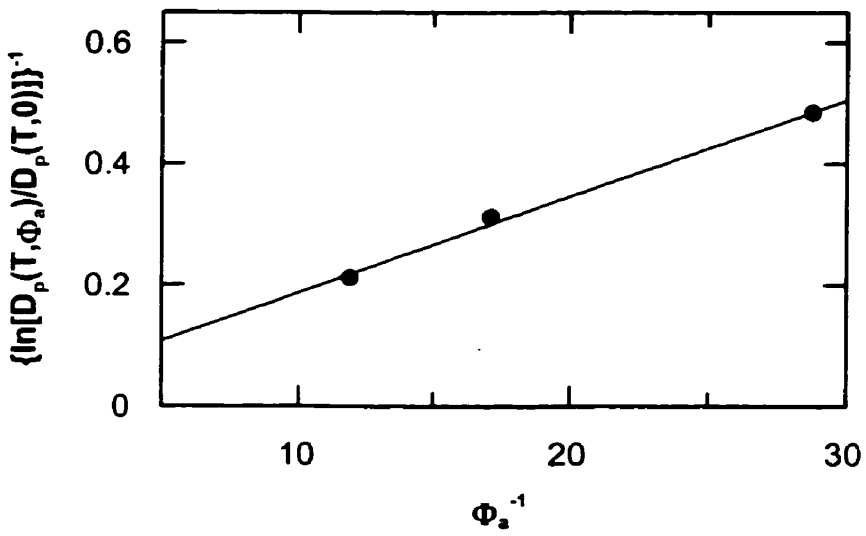

Figure 4-10. Plot of $1/Ln[D_p(T,\Phi_a)/D_p(T,0)]$ vs $1/\Phi_a$.

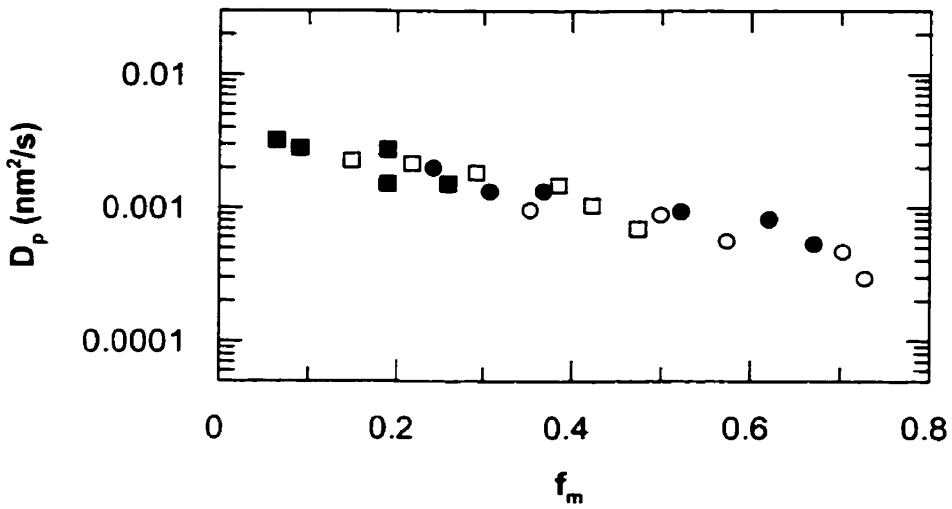

Figure 4-11. Master curve of D_p vs. f_m for PBMA latex films with 0 wt% (■), 3 wt% (□), 6 wt% (●), and 9 wt% (○) of BMA oligomers.

4.5 Conclusions

We analyzed diffusion rates of a high molecular weight polymer in latex films prepared from PBMA latex dispersions to which different amounts of ionic plus hydrolyzed oligomers in water was added. We found that the presence of a small amount of oligomer in the film can greatly enhance the diffusion rate of the polymer. The behavior follows the

Fujita-Doolittle free volume model, which predicts the increase of polymer diffusion coefficients in the presence of a plasticizer.

4.6 References

1) Wang, Y.; Winnik, M. A.; Haley, F. *J. Coat. Techn.* **1992,** 64(811), 51-61.

2) Juhué, D.; Wang, Y.; Winnik, M. A. *Makromol. Chem., Rapid Commun.* **1993,** 14, 345.

3) Kawaguchi, S.; Odrobina, E.; Winnik, M. A. *Macromol. Rapid Commun.* **1995**, 16, 861.

4) Wang, Z.; Paine, A. J.; Rudin, A. *J. Polymer Sci.: Polym. Chem.* **1995,** 33, 1597.

5) O'Connor, D. V.; Phillips, D. *Time-Correlated Single Photon Counting*: Academic Press Inc.: London, U.K. **1984.**

6) Pang, S.; Rudin, A. *Polymer*, **1992**, 33, 1949.

7) Kolthoff, I. M.; Miller, I. K. *J. Am. Chem. Soc.*, **1951**, 73, 3055.

8) Wang, Z.; Paine, A. J.; Rudin, A. *J. Polym. Sci.*, **1995**, 33, 1597.

9) Thomson, B.; Wang, Z.; Paine, A. J.; Lajoie, G.; Rudin, A. *J. Polym. Sci.*, **1995**, 33, 2297.

10) Simons, W. W.,editor, *The Sadtler Handbook of Proton NMR Spectra*; Spectroscopist Sadtler Research Laboratories Inc.: Philadelphia, **1978**; p 581-582.

11) Cole, R. B., editor, *Electrospray Ionization Mass Spectroscopy*, John Wiley & Sons., Inc.: New York, **1997.**

12) Fujita, H. Fortschr. Hochpolym.-Forsch. **1961**, 3, 1.

5 LOCATION OF NONIONIC SURFACTANTS AND PEG OLIGOMERS IN PBMA LATEX FILM.

5.1 Introduction.

The presence of surfactant in a latex film can affect various properties of the film, including its glass transition[1,2], its dynamic mechanical properties[3], its peel strength,[4] and its water resistance[5]. The magnitude of these effects depends sensitively on the location of the surfactant in the film. If miscible with the latex polymer, the surfactant can dissolve in the film resin and can act as a plasticizer.[6-8] If the miscibility is low, the excess surfactant can form occlusions in the film or migrate to the air or substrate surfaces.[9-11] In this chapter we try to understand how the chemical structure of the nonionic surfactants influences the latex film formation process and its morphology, and how the length of the hydrophilic part of the nonionic surfactants influences the morphology of the film.

As a model system in our experiments we used PBMA latex films with NP-20 surfactant and poly(ethylene glycol) (PEG) oligomers. We measure the miscibility of such a system and distribution of NP-20 and PEG oligomers by Modulated Differencial Scanning Calorimetry (MDSC), DET and Laser Scanning Confocal Fluorescence Microscopy (LSCFM) method.

5.2 Experimental

5.2.1 Materials

Unlabeled poly(butyl methacrylate) (PBMA) aqueous latex particles were employed in the MDSC and Confocal Microscopy experiments. By gel permeation chromatography (GPC, poly(methyl methacrylate) standards) the PBMA had $M_w = 3.85x10^5$ with $M_w/M_n = 2.67$, and $M_w = 4.4x10^5$ with $M_w/M_n = 3.68$ respectivelly. Polymer diffusion experiments were carried out on labeled PBMA samples, of both high molecular weight ($M_w = 4 \times 10^5$) and low molecular weight ($M_w = 3.5 \times 10^4$) (PBMA). For both sets of polymers $M_w/M_n = 2.5$ - 3, and had a degree of labeling of 0.8 mol%. Film samples were prepared from a 1:1 mixture of donor- (phenanthrene) and acceptor- (anthracene) labeled polymer, referred to as

Phe-PBMA and An-PBMA, respectively, matched as closely as possible in molecular weight, molecular weight distribution, and particle size. In case of anthracene labeled PEG - An$(EO)_{38}$, we used only phenanthrene labeled Phe-PBMA with M_w=4.95x10^5 and M_w/M_n=3.5. The synthetic procedure for preparing labeled and unlabeled latex dispersions was described in Chapter 1 The characteristics of the latex particles and An$(EO)_{38}$ employed here are presented in Tables 5-1a,b,c,d.

Table 5-1a. Latex particle characteristics –high M PBMA

Phe-PBMA	**An-PBMA**
M_w = 120,000	M_w = 133,000
M_n = 38,000	M_n = 42,000
M_w/M_n = 2.9	M_w/M_n = 3.16
d = 124 nm (0.04) [a]	d = 132 nm (0.037) [a]

a. size polydispersity

Table 5-1b. Latex particle characteristics –low M PBMA

Phe-PBMA	An-PBMA
M_w = 33,900	M_w = 35,700
M_n = 18,300	M_n = 16,700
M_w/M_n = 1.85	M_w/M_n = 2.14
d = 119 nm (0.03) [a]	d = 119 nm (0.035) [a]

a. size polydispersity

Table 5-1c. High M PBMA latex + An-$(EO)_{38}$ characteristics. (DET measurements)

Phe-PBMA	**An-$CH_2(EO)_{38}OH$**
M_w = 495,000	M_w = 1907
M_n = 141,000	M_n = 1688
M_w/M_n = 3.5	M_w/M_n = 1.13
d = 144 nm (0.03) [a]	

a. size polydispersity

Table 5-1d. High M PBMA latex + An-$(EO)_{38}$ characteristics. (LSCFM) measurements

Phe-PBMA	**An-$CH_2(EO)_{38}OH$**
M_w = 440,000	M_w = 1907
M_n = 120,000	M_n = 1688
M_w/M_n = 3.5	M_w/M_n = 1.13
d = 141 nm (0.04)[a]	

a. size polydispersity

Surfactant (sodium dodecyl sulfate) and low molecular weight salts used in the preparation of the latex dispersions, were completely removed by ion exchange (Bio-Rad, AG-501-X8 mixed bed resin, 3 g resin per 100 mL of latex). The procedure was repeated three times. Nonylphenoxypoly(ethylene oxide) NP-20 (TCI) and polyethylene glycol (PEG-n, EO_n); n = 10, 20, 45, 68, 100 (Aldrich) were used without further purification. The anthracene labeled PEG was received as a gift from Dr. Trevor Blease at ICI Surfactants. It was prepared by ethoxylation of 9-anthrylmethanol. In Toronto, this surfactant was purified by recrystallization from ethyl acetate and analyzed by NMR and GPC (polystyrene was used as a standard and THF (tetrahydrofuran) as a solvent). We found that only half of the PEG chains have an anthracene at the end, the other half is not labeled. The surfactant has a bright yellow color.

5.2.2 Sample Preparation

NP-20 surfactant was added to the PBMA latex dispersions to obtain samples with 2, 5 or 10 wt% of surfactant based upon latex solids. The mixtures were gently shaken for a few hours and left overnight to equilibrate. Then the dispersions were cast onto glass plates each covered with an inverted Petri dish, and placed in an oven at 32° C to form dry and transparent films. Because the wet films are covered in this way during drying, water evaporation is slow (e.g., 6h), and most of the drying occurs at 100% relative humidity. Films containing EO_{10}, EO_{20}, EO_{48}, EO_{68}, EO_{100}, and An$(EO)_{38}$ were prepared in the same manner, but for DET measurements, the dispersions were cast onto quartz plates. Samples with low M_w PBMA were dried at 25° C. In some experiments with NP-20 surfactant, films were prepared through more rapid drying at 65% relative humidity. In this case the samples were simply left open to the air (drying time e.g. 0.5 h). The other conditions were the same

as for the slow drying films. Generally, the thickness of the films was in the range of 30 - 50 μm. However, for DSC measurements films with the thickness about 0.5 mm were used. These films were cut off of the glass substrate and placed in the DSC pan (in the form of small pieces). Some NP-20 surfactant-containing samples were annealed for 1 hour at 90° C, prior to the DSC analysis.

5.2.3 Modulated Differential Scanning Calorimetry (MDSC) Measurements.

MDSC measurements were carried out using a Universal VI.6I TA DSC Instrument. The samples were run under N_2 with a 2 °C/min average heating and cooling rate. The modulations had amplitude of ± 1°C every 60 sec. For most samples three scans were performed: scan 1 (heating from –60 °C to 75 °C); scan 2 (cooling from 75 °C to –60 °C); scan 3 (reheating from –60 °C to 75 °C). The total measurement required about 5 h. T_g values were calculated automatically using the instrument software.

5.2.4 Laser Scanning Confocal Fluorescence Microscopy (LSCFM).

The images were obtained using a ZeissLSM 510 confocal instrument with a water immersion C-Apochromat 63x/1.2w corrected objective. Anthracene was excited with the 364 nm band of an Enterprise ENTC-653 laser. A 385 nm cut-off filter was used to prevent excitation light from reading to the detector. The confocal pinhole was set at 79 μm, which corresponds to an optical slice thickness of 0.6 μm. The investigated film area was 73.1 x 73.1 μm. The resolution of confocal microscopy in the x,y plane is 0.5 μm.

The film samples were transferred to a cuvete and put on a top of a drop of water in order to suppress light scattering. The stained, bright phase should be due to fluorescence from "An" labeled PEG, and the dark phase should represent domains of the PBMA films where no anthracene is located. However, because water is a good solvent for PEG, we recognize that the darkest spots in the films near the surface represents places where surfactant rich phase was present in the film before the PEG was dissolved by the water used to immerse the lens.

5.2.5 Fluorescence Decay Measurements

Fluorescence decay measurements were carried out as described in Chapter 1. The calculations of areas under each decay curve, the extent of mixing f_m and the apparent diffusion coefficient D_{app} are also described in Chapter 1.

5.3 Results and discussion.

5.3.1 Latex films in the presence of NP-20.

In Chapter 3 of my thesis I described the effect of NP-20 on polymer interdiffusion rates in PBMA latex films at 90 °C. Using a fluorescence energy transfer method, we measured the influence of this surfactant on the rate of mixing of polymers in adjacent cells in latex films. We observed that small amounts (3 wt%) of NP-20 in the dry film accelerated the polymer diffusion rate significantly, and increasing the amount of surfactant to 15 wt% led to a two-order-of-magnitude increase in the diffusion rate. We showed that the influence of NP-20 on the calculated apparent diffusion coefficients (D_{app}) could be analyzed quantitatively in terms of the Fujita-Doolittle free volume model. In this model, the diffusion coefficient increases with the volume fraction φ_a of additive, and all the data can be shifted to generate a master curve with a single fitting parameter that describes the difference in free volume between the polymer and the plasticizer additive.

From these results we deduced that the surfactant and polymer were miscible at 90 °C for the range of compositions examined, which means that NP-20 surfactant is uniformly distributed in PBMA matrix at elevated temperature. Other questions remain. For example, what happens at room temperature? When does the surfactant enter the polymer phase? What drives the miscibility, the PEG chain or the NP-hydrophobic group? To address some of these questions, we have extended our interdiffusion studies to examine the effect of PEG oligomers on the PBMA diffusion rate, and we have carried out modulated differential scanning calorimetry (DSC) measurements on PBMA latex films, in the presence and absence of these additives.

5.3.2 DET in Nascent Films containing NP-20.

Because DET operates over such a short range (10 to 40 Å for Phe/An), the presence of unlabeled membrane material in the latex films will separate the donor- and acceptor-labeled polymer, and decrease the efficiency on interparticle energy transfer. Under these circumstances, the mean Phe decay time $<\tau_D>$ will increase toward its unquenched value of 45 ns. The value of $<\tau_D>$ is often known with great precision (better than ± 1%) because it is obtained by integrating the area under the entire donor decay profile. The presence of interstitial material in newly formed latex film which causes a significant decrease in the area of contact between adjacent cells in the film should cause a measurable change in $<\tau_D>$. On occasion we observe this effect for anionic surfactants such as sodium dodecyl sulfate (SDS)[12]. On the other hand, some coalescing aids promote interdiffusion during film formation, leading to higher values of $\phi_{ET}(0)$ than expected for sharp intercellular interfaces.

Crack-free transparent films are formed from all PBMA dispersions containing NP-20 or EO_n dried at 32° C. In these freshly prepared films, we observe a measurable amount of DET. We plot our data in Figure 5-1, where we observe no change, within experimental error, in the magnitude of Area(0) over a broad range of NP-20 concentrations.

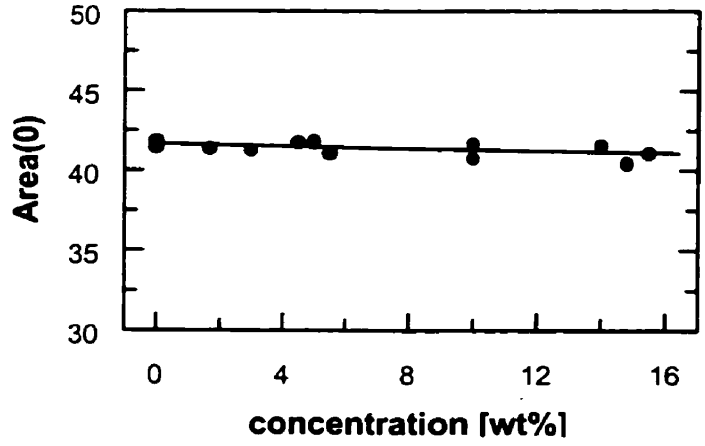

Figure 5-1. Plots of Area(0) values (obtained from integration of the normalized Phe fluorescence decay profiles) vs. concentration of NP-20 surfactant molecules.

From our binding isotherm measurements for NP-20 (Chapter 2), we know that 6.5 wt% surfactant corresponds to monolayer coverage of the PBMA particles. The value of $<\tau_D>$ = 42 ns, compared to τ_D = 45 ns in the acceptor-free film indicates that there are two possible explanations for this result. The first, which had a strong appeal for us, was that the

surfactant was able to diffuse into the latex polymer even at 32° C. We will see below that this explanation is incorrect. Alternatively, expulsion of the surfactant from the interstitial spaces would lead to surfactant domains within the film. Under these circumstances, the surfactant occlusions might have a negligible effect on the cell surface area probed by the DET experiments in the newly formed films.

5.3.3 Miscibility of PBMA with NP-20 and PEO oligomers examined by MDSC

MDSC is a recent variation of differential scanning calorimetry in which a sinusoidal temperature perturbation is applied[13,14]. The theory of MDSC is presented in Appendix 1. The advantages of MDSC include the ability to separate overlapping phenomena, as well as to improve measurement resolution and sensitivity[13]. Various applications have been reported. These include separation of the recrystallization peak of a polymer from the glass transition[15], separation of physical aging annealing peaks from the glass transition[15,16] measurements of absolute heat capacity[17, 18] and the measurements of thermal conductivity [19]. An example of the total, reversing, and nonreversing heat flow for pure PBMA is shown in Figure 5-2.

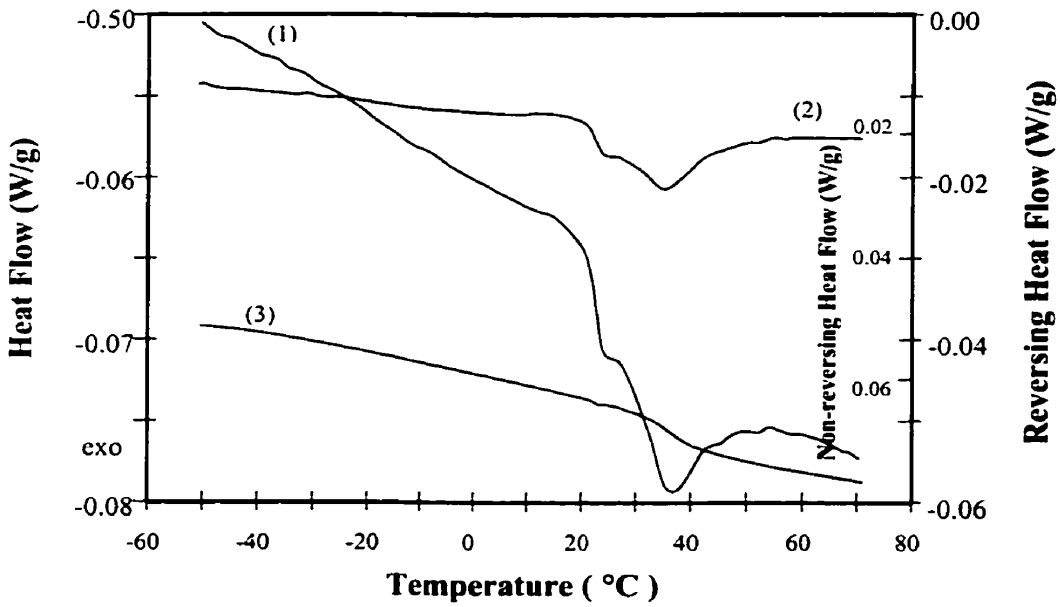

Figure 5-2. Plots of heat flow (1), nonreversing heat flow (2), and reversing heat flow (3) vs. temperature for pure PBMA. The reversing heat flow shows a glass transition at 34 °C. The peak in the scan of nonreversing heat flow is due to enthalpy relaxation reflecting prior sample history.

The term "reversing" refers to the part of the process that is reversible on the time scale of the oscillations. From reversing heat flow we see very clearly the glass transition T_g = 34 ° C. From the nonreversing heat flow we observe the peak which comes only from the sample's preparation history. NP-20 is a crystalline material, and the formation of surfactant occlusions in the polymer films should lead to a melting transition measurable by DSC. Since the melting temperature occurs in the same temperature range as the glass transition of PBMA, we turned to modulated DSC, which allows us to separate the glass transition from other interfering transitions in the sample.

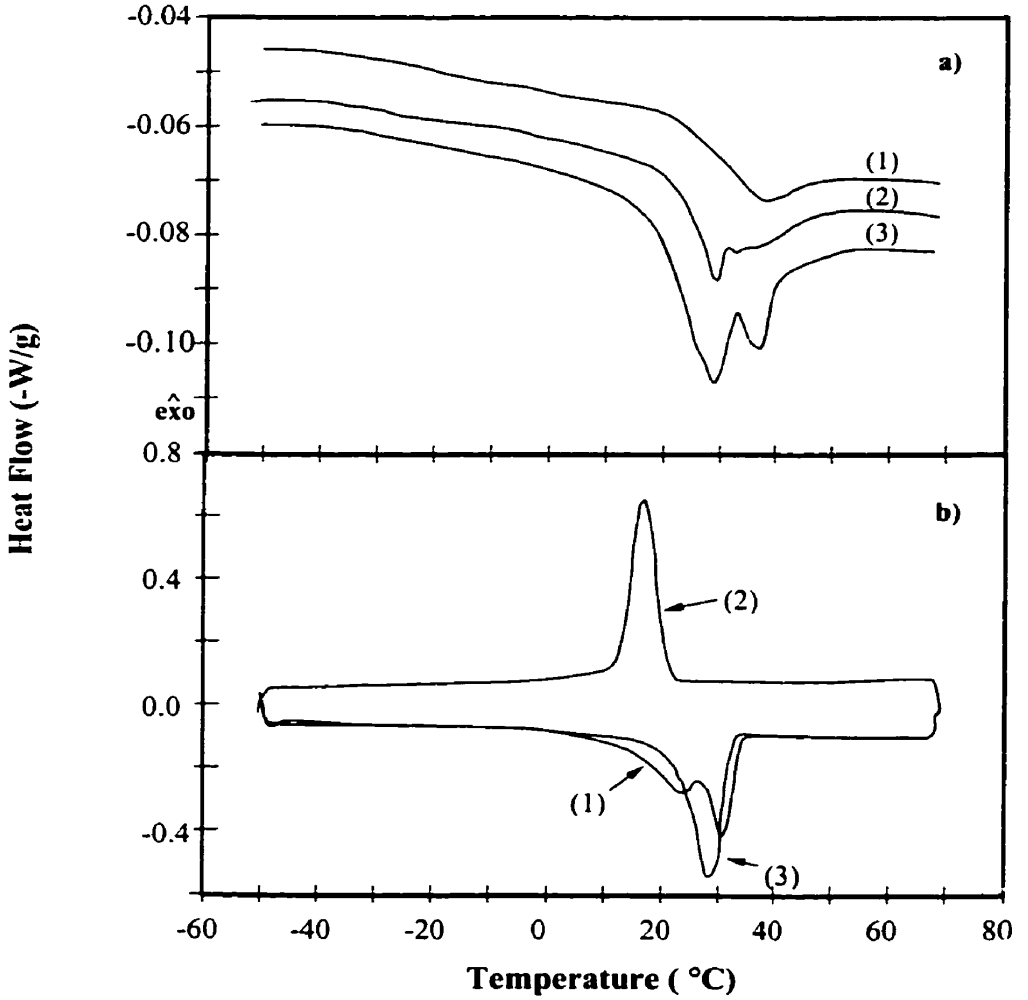

Figure 5-3. (a) MDSC first scan (heating) for pure PBMA (1), PBMA + 5 wt% NP-20 (2), and 10 wt% NP20 (3). (b) MDSC scans (first heating (1), second cooling (2), and third reheating (3) for pure NP-20 surfactant.

In Figure 5-3a we show typical MDSC first heating scans for pure PBMA, and for PBMA latex films containing 5 wt% and 10 wt% of NP-20 surfactant. Figure 5-3b shows

the MDSC first heating scan (melting), second cooling scan (crystallization), and third scan (melting) for the pure NP-20 surfactant.

Over the same range of temperatures (between 20 °C and 40 °C) one can observe three overlapping events: the glass transition of the polymer, the exotherm peak from enthalpy relaxation in the sample, and the melting transition for the surfactant. The glass transition is a reversible transition superimposed upon the melting transition and the non-reversing part of the heat flow due to sample preparation history. In order to separate these events, we consider the cooling scan (Figure 5-3b), where the crystallization exotherm for pure NP-20 is detected in the non-reversing component of the total heat flow. We note that the crystallization exotherm has a similar area to that of the melting endotherm seen on the reheating scan, and is shifted somewhat to lower temperature. The temperature shift depends upon the relative temperature ramp (cooling, heating rate) compared to the time required for crystallization to take place.

We see remarkably different behavior in MDSC traces of PBMA + NP-20 mixtures. For example, when we add 5 wt% of NP-20 to the PBMA, a crystallization exotherm can be observed in the cooling scan. It appears at very low temperatures (e.g. – 40 °C). An example is given in Figure 5-4a. When we look at Figure 5-4b for the cooling scan for sample with 10 wt% we see two crystallizations peaks, one at around 15 °C, like as is found in pure NP-20, and another at – 40 °C, as in case of the sample with 5 wt % surfactant. The shift in the position of the crystallization exotherm at –40 °C compared to the melting endotherm is at first surprising. We explain this behavior as follows: In the newly formed film, most of the NP-20 is present in its crystalline form. As the sample is heated, the substance melts. We know that at sufficiently high temperature (90° C), the NP-20 molecules diffuse into the PBMA polymer phase and mix molecularly with the polymer. As the sample is cooled, demixing occurs. This takes time. The exact position of the crystallization endotherm, and its breadth, depend upon the rate of demixing compared to the rate of cooling of the sample. In this sense, the crystallization endotherm at -40° C differs significantly from that observed for the pure surfactant, which crystallizes more rapidly on cooling. The PBMA sample with 10 wt% of NP-20 has two crystallization peaks, implying that during the heating scan in which the sample was heated up to 75 °C, not all the surfactant became molecularly mixed with the polymer matrix. Some of the surfactant remained as discrete occlusions and gave a crystallization peak at 15 °C.

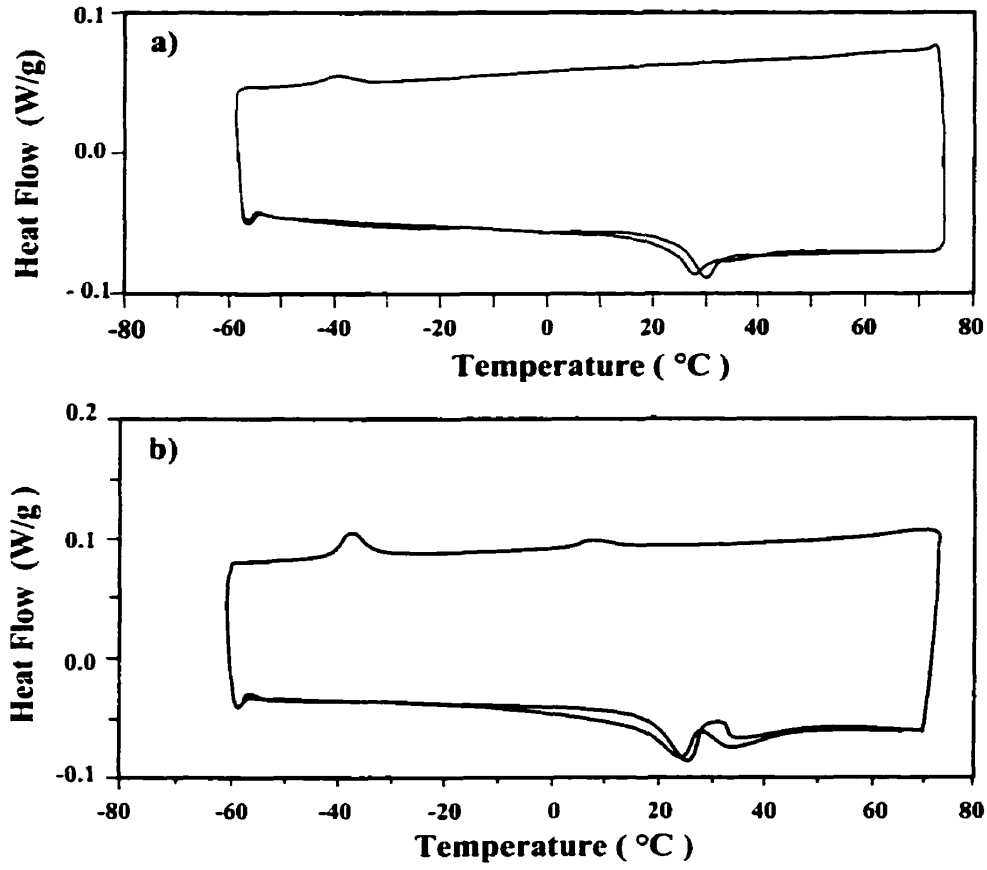

Figure 5-4. Plot of total heat flow vs. temperature (three scans) for: (a) PBMA + 5 wt % NP-20, and (b) PBMA + 10 wt % NP-20. We identify the peak exotherm at – 40 °C in the cooling scans with the crystallization of NP-20 after it demixes from the polymer. In case (b) we also observe broad NP-20 crystallization peak at 15 °C indicating that not all surfactant became molecularly mixed with polymer matrix.

We are particularly interested in the influence of NP-20 on the glass transition temperature of the PBMA matrix. Films containing only 2 wt % surfactant exhibit no melting or recrystallization transitions for the surfactant, either on heating or cooling. There is, however, a measurable decrease in the T_g of the polymer, which can be observed in all three scans. In Table 5-2 we report values of T_g for PBMA and for PBMA containing 2 wt% NP-20. For PBMA itself, we find a small decrease in the calculated T_g values on successive scans, a sample history effect. There are similar effects of sample history on the sample containing 2 wt% NP-20, with lower T_g values in the presence of this small amount of surfactant. We note that the NP-20 has a larger effect on lowering T_g in the second and third scans than in the first scan, where the change in T_g is only 1.6 °C. For the second and third

DSC scans, the change has increased to 3.6° C. While this difference is not large, and the estimated precision in T_g is ± 0.5°, these observations are consistent with only partial mixing of the surfactant and polymer during the film formation. More extensive mixing and a more uniform distribution of the surfactant in the polymer phase takes place following the first heating scan. During the first heating scan and subsequent cooling scan, the sample spends about 40 min at temperatures between 50° to 75 °C. In our view, it is during this time that the surfactant diffuses into the PBMA phase.

Table 5-2. Summary of T_g values for PBMA and PBMA + 2 wt% NP-20 blends

scan	Tg (° C)[a]	
	PBMA	**PBMA + 2 wt% NP-20**
1st - heating	36.3°	34.8°
2nd - cooling	34.1°	30.5°
3rd - heating	33.6°	30.4°

a. The estimated error in all Tg measurements reported here is ± 0.5 °C

To study the influence of larger amounts of NP-20 on the polymer T_g, we obtain information from the reversing component of the cooling scan. In the first heating scan and in the reheating scan, the glass transition is masked by the melting of the NP-20. In Figure 5-5 we show the reversing heat flow for the cooling scan for a sample of PBMA itself, and for PBMA samples containing 2, 5 and 10 wt% of NP-20. These latex films were all prepared under slow drying conditions. The results are summarized in Table 5-3.

Table 5-3. Summary of T_m values[a] for NP-20 and T_g values[b] for PBMA (in °C) for NP-20 and for mixtures of PBMA with various amounts of NP-20.

material	NP-20	PBMA	PBMA + NP-20 2 wt%	PBMA + NP-20 5 wt%	PBMA + NP-20 10 wt%
T (° C)	16 [a]	34 ± 0.5[b]	30.5 ± 0.5[b]	29 ± 0.5 [b]	29 ± 0.5 [b]

a. crystallization peak obtained on the cooling scan
b. glass transition temperatures obtained on the cooling scan

We find that 2 wt % NP-20 causes a 4 °C decrease in the T_g of the polymer, whereas further addition of NP-20 leads to only a small additional decrease (1 °C) in T_g. These results suggest that at temperatures near room temperature, the system has reached the limits of miscibility at a surfactant content between 2 wt % and 5 wt %. Even this conclusion is subject to sample history effects. When the sample containing 5 wt% NP-20 is annealed for 1 hour at 90 °C, the polymer exhibits a T_g = 27.3 °C (ΔT_g = 7 °C) on the subsequent cooling scan. These results establish that for NP-20 in PBMA latex films near room temperature, some of the surfactant dissolves in the polymer, and some is present in the form of aggregates or occlusions sufficiently large to exhibit both melting and crystallization transitions.

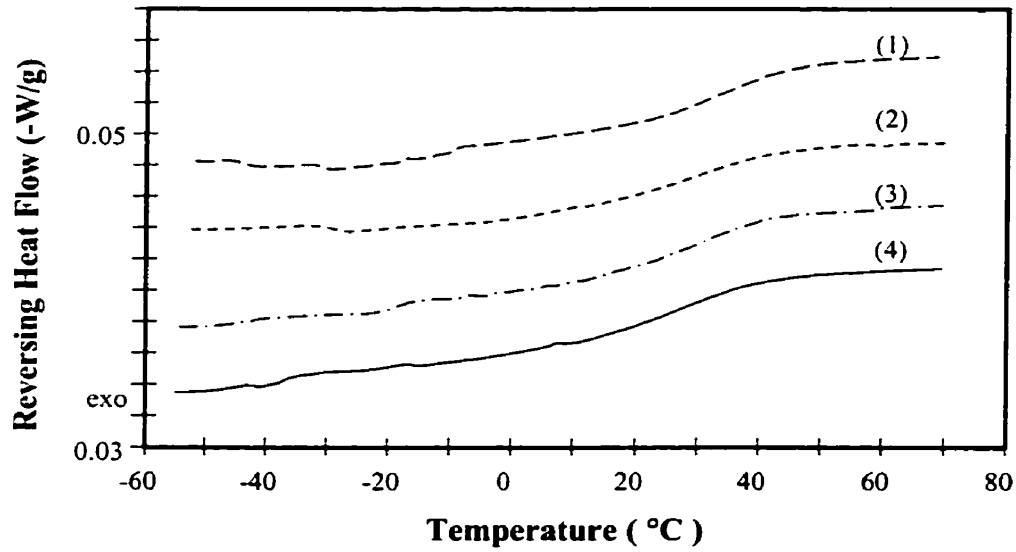

Figure 5-5. Plots of reversing heat flow (W/g) for the cooling scan vs. temperature for PBMA (1), PBMA + 2 wt % (2), PBMA + 5 wt % NP-20 (3), and PBMA + 10 wt % NP-20 (4).

5.3.4 Mixtures of PBMA with EO_{10} and EO_{20} Examined by MDSC

The results for PBMA latex films prepared in the presence of the PEG oligomer EO_{20} are presented in Table 5-4. For all of the samples, containing 3.8 wt%, 5 wt%, and 10 wt% EO_{20}, the measured T_g's are identical to that of the PBMA polymer itself. From this result, we could conclude that EO_{20} and PBMA are essentially immiscible over the temperature range of our measurements. Although from the cooling scan for PBMA samples with EO_{20} oligomers in Figure 5-6 we see that crystallization process take place at two

different temperatures, similarly like for sample with 10 wt% of NP-20 surfactant. One is the temperature of crystallization of pure EO_{20}, +25 °C the other one is much lower, -30°C

Table 5-4. Summary of T_g and T_m values (in ° C) for EO_{20}, and (PBMA + EO_{20})

scan	EO_{20}	T_g PBMA + EO_{20}		
		3.9 wt%	5.1 wt%	9.4 wt%
Heating	32.6° [b]	—[a]	—[a]	—[a]
Cooling	24.9° [c]	32.9°	32.2°C	32.0°C

a. The PBMA T_g is obscured by contributions of EO_{20} melting to the reversing heat flow.
b. Melting peak
c. Crystallization peak

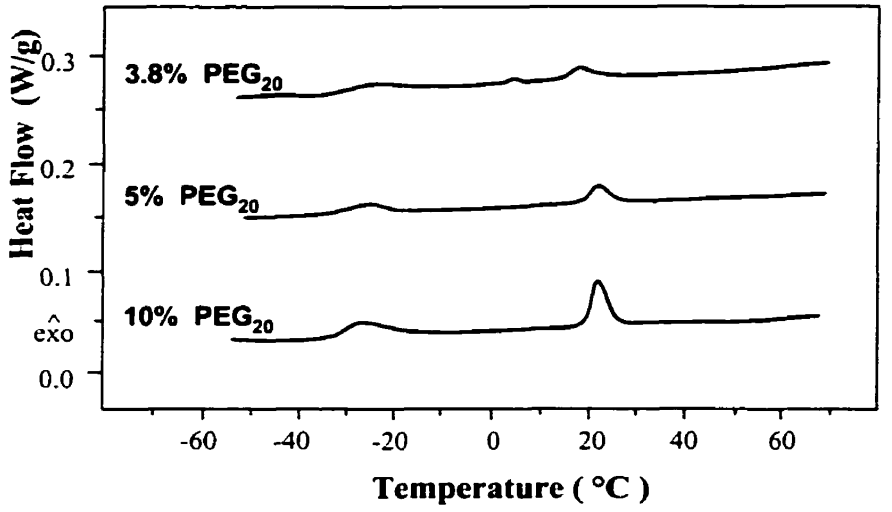

Figure 5-6. Plots of total heat flow for cooling scans vs. temperature for PBMA samples with 3.8 wt %, 5 wt %, and 10 wt % PEG_{20}. The two crystallization peaks observed in these scans are approximately at –30 °C and 25 °C. The peak at 25 °C is the crystallization peak of pure PEG_{20} (not mixed with PBMA). The peak at –30 °C is the crystallization peak of PEG_{20} after it demixes from the polymer.

We can explain the mechanism of crystallization of EO_{20} in the PBMA film in the same way as for the NP-20 surfactant. Some amount of EO_{20} mixes with PBMA at elevated temperatures. During cooling, the unmixed part crystallizes at 25° C, but the oligomer that mixed with the PBMA needs time to separate and to form domains large enough to crystallize. This oligomer is responsible for the additional crystallization peak we observe at

low temperature. The fact that we do not see any change in T_g for the cooling scan suggests that the mixing process only take place on the surface of latex particle and leaves the bulk of the PBMA unchanged. Most of the EO_{20} remains in the unmixed state. The height of the peak at 25 °C increases with increasing content of EO_{20} in the film.

In polymer diffusion studies described below, we observed that the presence of EO_{20} in PBMA latex films retards PBMA diffusion in the film. An important question is whether this retardation effect is due to the unmixed EO_{20} or the EO_{20} dissolved in regions of the PBMA. If the mixing of PEG with PBMA is a result of mixing of polar components at the latex particle surface, this mixture can serve as a membrane barrier to retard further polymer diffusion. We examined this problem by investigating the influence of EO_{20} on film formation by PBMA. We found that the minimum film forming temperature (MFT) is lower for PBMA samples with EO_{20} present than for pure PBMA dispersions. For the PBMA dispersions containing EO_{20}, we were able to get nice transparent films without any cracks at 29 °C, whereas pure PBMA films obtained at this temperature were full of cracks. This result indicates that the EO_{20} present at the PBMA latex surface acts to plasticize the surface rather than acting as a barrier. As we will see below, when we combine these observations with the diffusion results, we will conclude that a fraction of the PEG oligomers slightly plasticize the PBMA polymer in the PBMA-PEG interface zone, while the remaining part of PEG is the major source of retardation of polymer diffusion.

The results for films prepared from PBMA latex + EO_{10} are presented in Table 5-5. The melting transition of the EO_{10} (T_m = 0.8° C) is well separated from the glass transition of PBMA (see Figure 5-7), so that we were able to obtain PBMA T_g values from all three MDSC scans. Here a small but significant decrease of T_g (about 3.5 °C) is observed during the cooling scan (i.e., after the sample has been heated); but no change in T_g can be detected on either the first or second heating scan. Diffusion experiments show that EO_{10} causes a slight increase in the diffusion rate of polymer for annealed samples. These results suggest that there is some miscibility between the two components at high temperature, but they phase separate at low temperature.

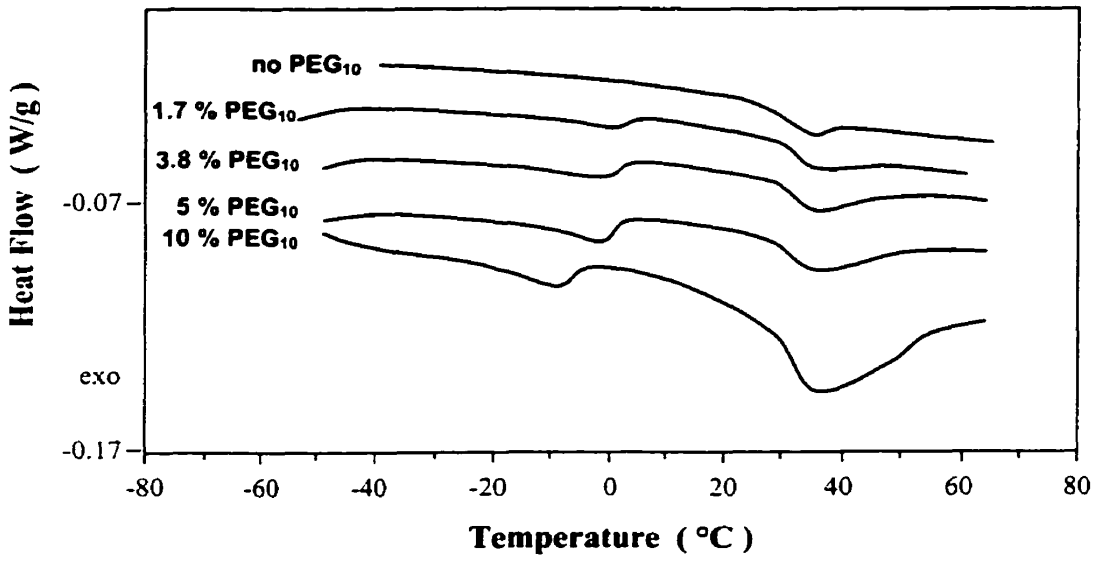

Figure 5-7. Plots of total heat flow for first heating scans vs. temperature for PBMA samples with 0 wt %, 1.7 wt %, 3.8 wt %, 5 wt %, and 10 wt % PEG_{10}. The peak around 0 °C is the melting peak of PEG_{10}. The peak at 35 °C is due to enthalpy relaxation, and obscures the PBMA glass transition region.

Table 5-5. Summary of T_g and T_m values (in °C) for EO_{10}, and (PBMA + EO_{10})

scan	EO_{10}	T_g PBMA + EO_{10}		
		1.7 wt%	3.6 wt%	5.1 wt%
1. heating	0.8° [a]	34.0°	34.5°	34.0°
2. cooling	--	29,5°	30,8°	29,5°
3. heating	--	34.5°	33.8°	31.7°

a. melting peak

5.3.5 DET investigation of the effects of An-EO_{38} in latex films.

To learn more about the behavior of PEG oligomers in the latex film, we carried out DET experiment on phenanthrene labeled PBMA films with different contents of the anthracene labeled EO_{38}. We measured the fluorescence decay of samples with different amounts of An-EO_{38} and calculated the area under the fluorescence decay and efficiency of energy transfer, for freshly formed films and for films annealed at 50 and 90 °C. From the DSC data, we learned that PEG itself is only poorly miscible with PBMA, but we were not

able to draw conclusions about how much of PEG can penetrate into the film. With the An–labeled PEG, we can obtain further information about miscibility, and we also hope to be able to say something about the kinetics of PEG phase separation.

The system discussed in this section is shown schematically in Figure 5-8. We imagine that in the Phe-labeled PBMA latex film, the An-labeled PEG domains are located between latex particles. Energy transfer can take place between donor-labeled PBMA particles and acceptor-labeled PEG domains. The amount of $An(EO)_{38}$ in the film, the size, and shape of $An(EO)_{38}$ domains should influence the results of this ET experiment. We monitored changes in the amount of ET in these films as a function of processing conditions. From the data obtained, we try to draw some conclusions about features of latex film morphology in the presence of low molecular weight PEG-containing species.

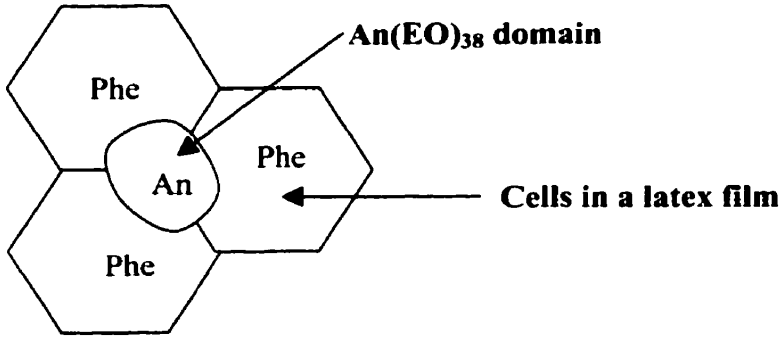

Figure 5-8. The schematic representation of An-labeled PEG domains (An-EO_{38}) in the Phe-labeled latex film. The energy transfer takes place between donor-labeled latex particles and acceptor labeled PEG domains.

Anthracene-labeled EO_{38} is bright yellow powder. The PBMA samples with a content of An-EO_{38} less than 10 wt% (we always consider the total amount of PEG in the film; labeled and unlabeled) were transparent and colorless. Films with 10 wt% of An-EO_{38} were still transparent but slightly yellow. Samples with 15 wt% of EO_{38} and more were yellow and start to become turbid. The turbidity appears initially only at the edges of the samples where the films were the thickest (samples with 15 and 20 wt % of EO_{38}). Finally with further increasing concentration of EO_{38} in the film (25 or 30 wt %) the entire samples are turbid. Moreover we found that annealing decreases the turbidity of the samples and speeds up the exudation of An-EO_{38} to the surface. We were able to observe large droplets of An-EO_{38} liquid on the surface of the annealed film after short times of annealing.

In Figure 5-9 we present values of the area under the fluorescence decay curves (Area) and the efficiency of energy transfer Φ_{ET} for freshly formed PBMA latex films (○), and for films annealed at 50 °C for 30 hours (■) in the presence of different amounts of An-EO_{38} (up to 30wt%). For freshly formed films we observe that the Area (Figure 5-9a) decreases with increasing amount of An-EO_{38} up to 33 ns for the film with 30wt % of EO_{38}. This results means that Φ_{ET}, increases from 0 (no An-PEG) up to 0.27 (30 wt% PEG) (see Figure 5-9b). Even 30 hours of annealing at 50 °C does not cause any change in values of the Area and Φ_{ET} for the samples with an An-EO_{38} content no greater than 15 wt %. For samples with an amount of An-EO_{38} larger than 15 wt %, the area increases with annealing time until, it reaches a constant value of 38 ns. Figure 5-10 shows the changes of Area and Φ_{ET} with annealing time for samples with different amounts of An-EO_{38}.

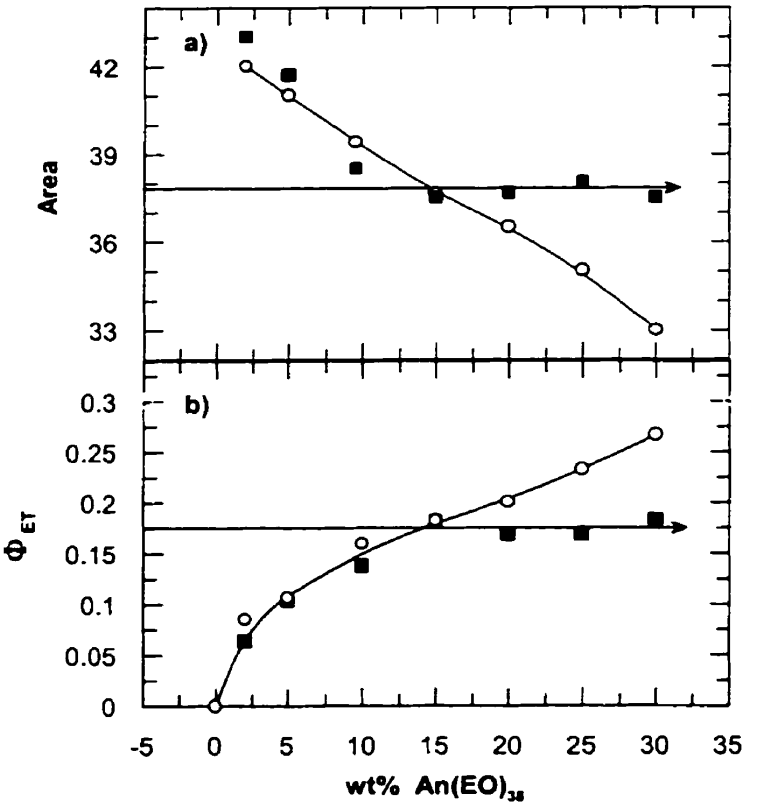

Figure 5-9. Area under the fluorescence decay (a), and efficiency of energy transfer Φ_{ET} (b) vs. An-EO_{38} concentration for PBMA + An-EO_{38}: (○) freshly formed films, (■) films annealed for 30 hours at 50 °C.

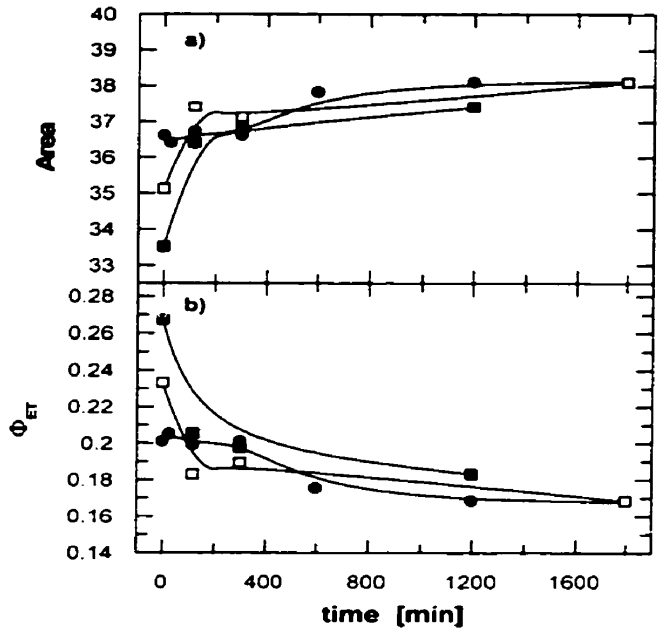

Figure 5-10. The area under the fluorescence decay (a), and the efficiency of energy transfer Φ_{ET} (b) versus annealing time at 50 °C for films with: 20 wt% (●), 25 wt% (□), and 30 wt% (■) An-EO_{38} in the Phe-PBMA latex film.

For example, the sample with 20 wt% of An-EO_{38} needs 500 min of annealing at 50 °C for us to observe a change of area from 36.6 ns to 37.8 ns (or a change in Φ_{ET} from 0.20 to 0.175). For samples with 25 and 30 wt% of EO_{38} approximately, 100 min of annealing at 50°C is enough to induce a significant increase in the area values, from 35 ns (33.5 ns) to approximately 37 ns. In this case Φ_{ET} decreases from 0.27 (30 wt% PEG) and 0.235 (25 wt% PEG) to approximately 0.18 for both samples. The further increase in the area value to 38 ns and decrease in Φ_{ET} to 0.17 is very slow.

We interpret these results as follows: The area under the fluorescence decay decreases for freshly formed films with increasing amount of An-EO_{38} because ET between an An-EO_{38} and Phe-PBMA increases as a result of a growing number of An-EO_{38} domains between the latex particles. The annealing process at 50° C does not change anything in the samples up to 15 wt % of EO_{38}. Although at this temperature the EO oligomer is already melted, it is buried in the film as the separate domains. The mobility of the PBMA at 50° C is negligible even for annealing times as large as 30 hours, so there is no driving force for the PEG to be expelled to the surface of the film. If there is some exudation of EO oligomers for samples containing 10 or 15 wt % of An-EO_{38}, it must take place during the

film formation process. A different situation occurs for samples with more than 15 wt% of An-EO_{38}. After approximately 1 h of annealing at 50° C (we did not examine shorter times), we observed a decrease in the energy transfer signal for samples with 25 and 30 wt% of An-EO_{38} compared to the samples prior to annealling. After 1 h of annealing at 50 °C, the area under the fluorescence decay changed from 35.1 ns to 37.4 ns for the sample with 25 wt% An-EO_{38} and from 33.5 ns to 36.4 ns for the sample with 30 wt% An-EO_{38} (see Figure 5-10). This change suggests that there is a rapid exudation process, which takes place probably just after melting of the PEG. In the case of samples with 20 wt % of An-EO_{38}, the observable increase in the area under the $I_D(t)$ decay profile takes over more than 5 hours, and the change in area is from 36.6 ns to 37.8 ns. Finally, the areas increase to constant a value of about 38 ns for all samples annealed for sufficiently long times (30 h).

As the exudation of PEG oligomers is fast at the beginning of annealing process for samples with high concentration of EO_{38}, we believe that in these samples, there exist separate PEG domains that are connected to one another. The connections form "channels", which allow rapid flow of the molten surfactant to the surface. The rate of exudation depends on the amount of these channels and their size. When smaller amounts of $AnEO_{38}$ are present, the EO-rich domains are isolated "lakes". Even in the melt state, diffusion or flow to the polymer surface is inhibited.

Now let us consider what happened when the samples were annealed at 90° C. At this temperature not only the PEG is very mobile, but diffusion of PBMA polymer molecules can be measured easily on the time scale of this experiment. Does the mobility of the matrix affect the exudation and phase separation of the PEG? The experimental results are present in Figure 5-11. Recall that the Φ_{ET} values for these experiments are determined after rapidly cooling the films to room temperature.

At first the results are surprising. For short annealing times (5-15 min) we observe increases in the values of Φ_{ET}. The increase in Φ_{ET} can be only explained as an increase in the miscibility of the two components with increasing annealing temperature. On the other hand for longer annealing times (5 -11 hours) the value of Φ_{ET} decreases for all samples investigated, from 5 to 30 wt% of An-EO_{38} in the film. These results reflect the kinetics of phase separation of the two components in the system. Phase separation of An-EO_{38} resulting in exudation to the surface is a kind of macrophase separation. The decrease in the ET signal (increase in area) can also be connected with microphase separation, in which the

shape of PEG domains evolve from elongated to round ones, or the fusion of small PEG domains into bigger ones. In other words, each process that causes that the ratio of the surface-to-volume of the PEG domains to decrease, decreases the amount of ET occurring in the system. In comparison with samples annealed at 50 °C the phase separation process is much faster at 90 °C. At 90 °C we are able to observe the phase reorganization process even for the sample with 5 wt% of An-EO_{38}. No change in this sample was observed upon annealing at 50 °C.

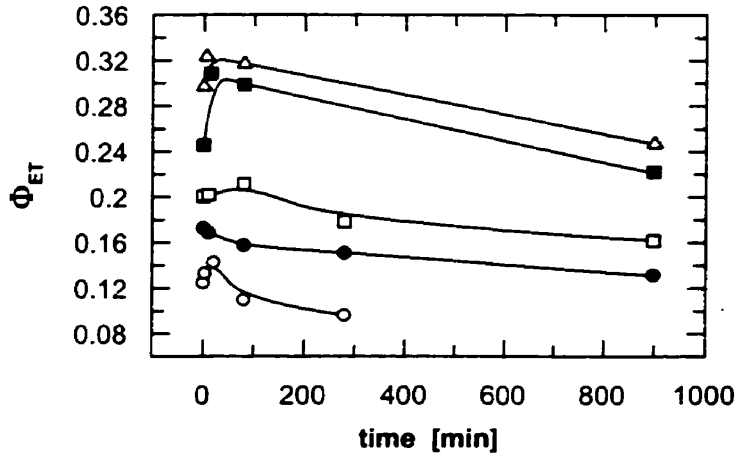

Figure 5-11. The efficiency of energy transfer versus annealing time at 90° C for Phe-PBMA films containing: 5 wt% (○), 10 wt% (●), 15 wt% (□), 25 wt% (■), and 30 wt% (Δ) An-EO_{38}.

The results from annealing experiment at 90°C indicate that at this temperature we have two competing processes: phase separation and a limited extent of mixing. Since we observe the decrease in area values for short annealing times, we conclude that diffusive mixing of An-EO_{38} is a rapid process, and is already completed after 5 – 10 min of annealing at 90° C.

By eye and with a microscope we observe some exudation of An-EO_{38} to the film surface following short annealing times for samples with 25 and 30 wt% of PEG derivative. The An groups in this phase do not affect Phe fluorescence. Thus diffusive mixing has to be the source of the decrease in area of the donor decay profile. As the mixing process is fast and is completed after a few minutes of annealing, we conclude that the contribution from the mixed part of the EO_{38} to the DET signal is the same at each stage of annealing process. However, the phase separation process (the change in shape and in size of PEG domains), is continued during the whole annealing time. This is why with increasing annealing times (1 h

or more), finally, this process dominates, and the area under the fluorescence decay starts to increase.

5.3.6 Morphology of PBMA films with $AnEO_{38}$ in the light of Laser Scanning Confocal Fluorescence Microscopy(LSCFM).

Confocal microscopy has a resolution of 0.5 μm. Thus we are limited to the observations of objects larger than 0.5 μm. In other words, if the PEG is present in domains smaller than 0.5 μm we can not resolve these domains. More specifically, if the An-PEG is distributed as a membrane between the latex particles, we would not see any structure of the film. The film would appear as a homogeneous bright area.

5.3.6.1 Images for freshly formed films and films annealed at 50 °C.

PBMA films containing 7, 10 , and 15 wt% of An-EO_{38} look like homogenous bright films in the confocal microscope. The images are similar for the freshly formed films and for films annealed at 50 °C for even 30 hours. The brightness of each film increases with depth, indicating that surfactant is not uniformly distributed in the film. The lower concentration of the surfactant near the surface of the film may be due to leaking of the surfactant during the microscopic measurement. During the experiment, the sample is immersed in water, which is good solvent for the PEG. If the surfactant forms a kind of network, so that water can penetrate into the film, water can remove the PEG from the film. Lost of fluorescent material may explain why the film is darker close to the air surface than in the bulk. These images indicate a high concentration of PEG at the quartz substrate – film surface. As a confirmation of this location for the surfactant we find that the latex film in the samples with high concentrations of PEG (e.g. 30 wt%), when immersed in water, very easily separate from the substrate.

The images of a freshly formed film with 30 wt% of An-EO_{38} differs substantially from the homogeneously bright images of samples with up 15 wt% of PEG, and are shown in Figure 5-12. The first image shows the surface of the film, and the following images are the subsequent optical slices of the sample with depth intervals 5 μm. The surface of this sample is less bright than images from inside the film. The next image (5 μm from the surface) shows an inhomogeneous morphology, with dark spots on a bright background. We believe that the dark spots represents holes distributed randomly in the film. They were formed

when the PEG-rich phase located at the spot dissolved in the water during the LCFM measurements. Deeper into the film, the images are more homogenous.

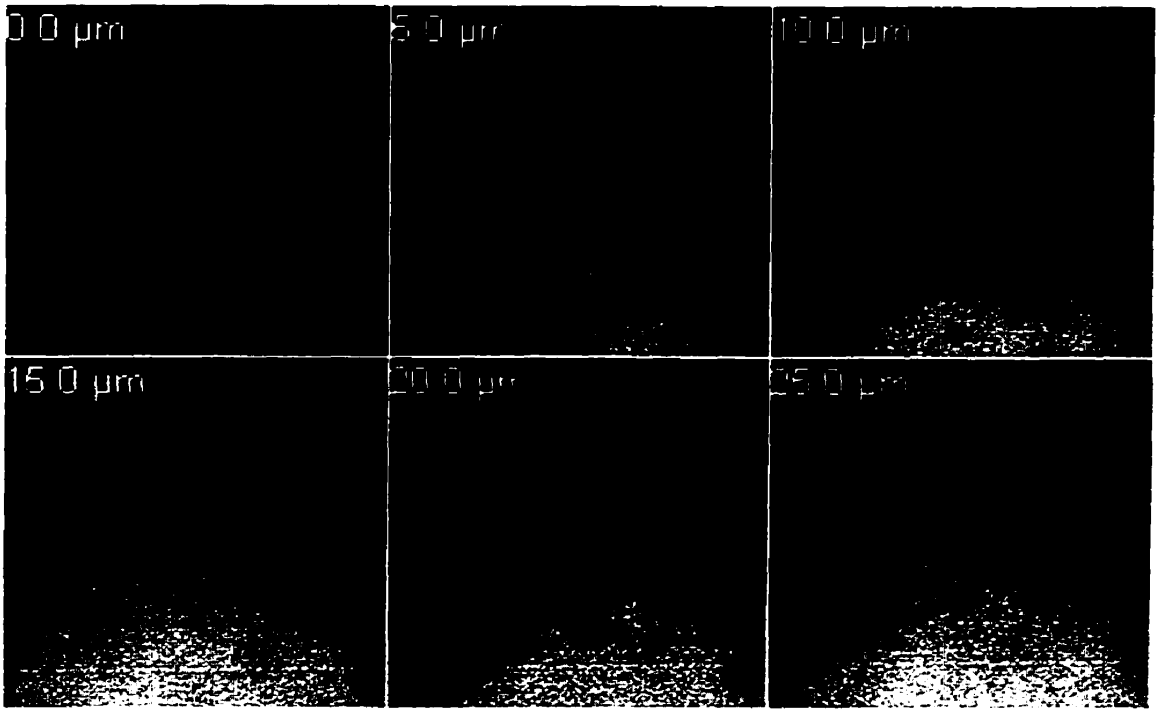

Figure 5-12. Confocal images of freshly formed PBMA sample with 30 wt% of $An(EO)_{38}$. The top right image is the surface of the sample, next ones are the subsequent slices with the depth interval 5µm. The size of each image is 73.1 x 73.1 µm

The images support the conclusion we drew from DET, the existence of some PEO-rich structures ("channels"), which lead to the surface for samples with PEG concentration higher than 15 wt %. From confocal microscopy, we learn that these "channels" can be micron size objects.

5.3.6.2 Images for films annealed at 90 °C.

Samples of PBMA films with 7, 15, and 30 wt% of $AnEO_{38}$ were annealed at 90 °C for 3 h before the images were taken. The annealed film with 7 wt% of PEG (Fig 5-13) does not show any structure and looks the same as the not-annealed samples.

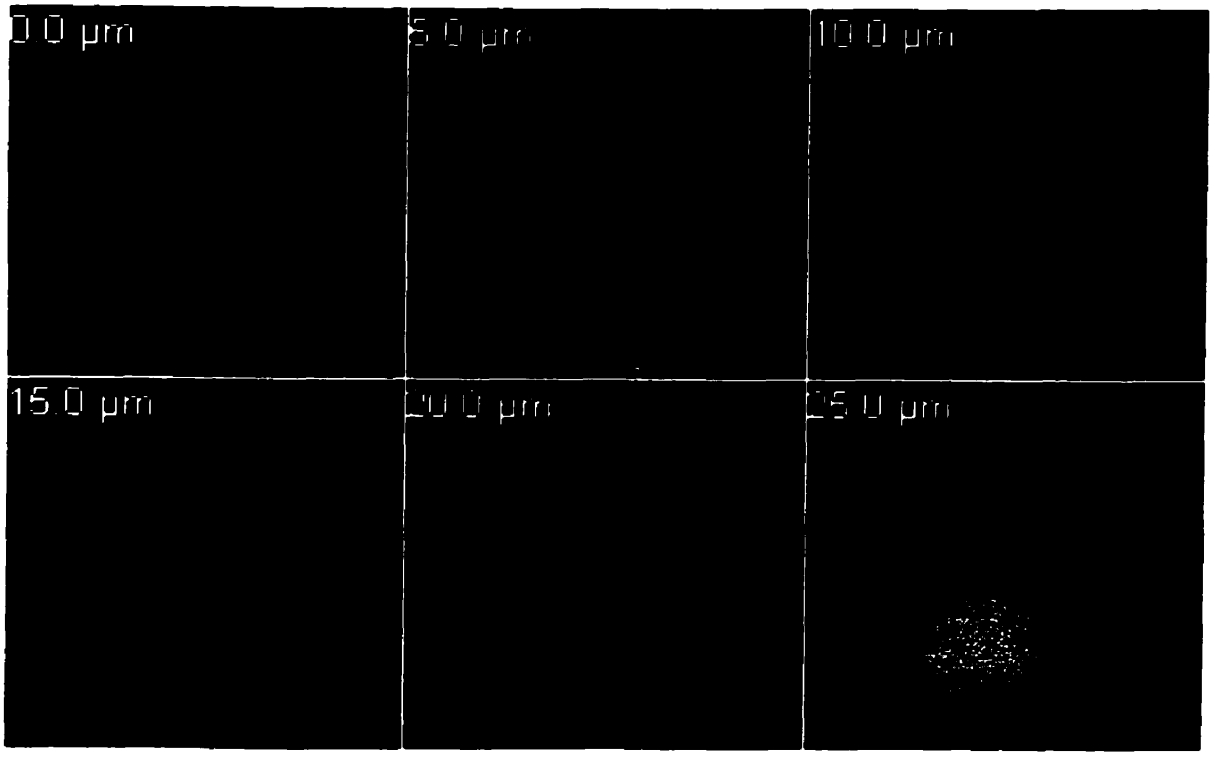

Figure 5-13. Images of PBMA sample with 7 wt% of $AnEO_{38}$, annealed at 90 °C, 3 hours. The images are from the surface (right top) of the film into the bulk with 2 µm depth interval. The size of each image is 73.1 x 73.1 µm

The film with 15 wt% of PEG after annealing 3 h at 90 °C, shows already an interesting morphology (see Figure 5-14a). In Figure 5-14a we present 5 successive images from the surface of the film into the bulk at 5 µm depth intervals. The surface of the film shows six huge holes, with an average diameter of 4.5 µm. These holes are also seen in the next two images, implying that the holes are connected in the vertical direction. The images from deeper in the film show phase separation in the film as a mixture dark and bright areas. For comparison in Figure 5-14b we show images of sample with 15 wt% PEG without annealing. The images do not reveal any structure, and looks like images of a homogenous film.

A

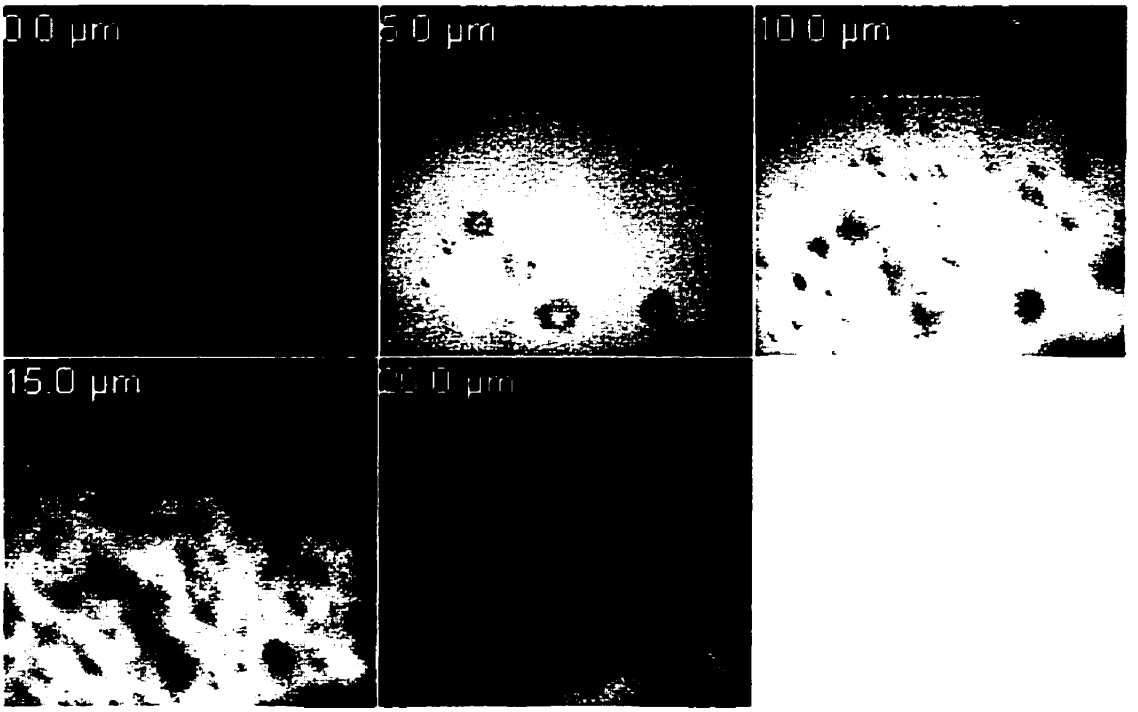

B

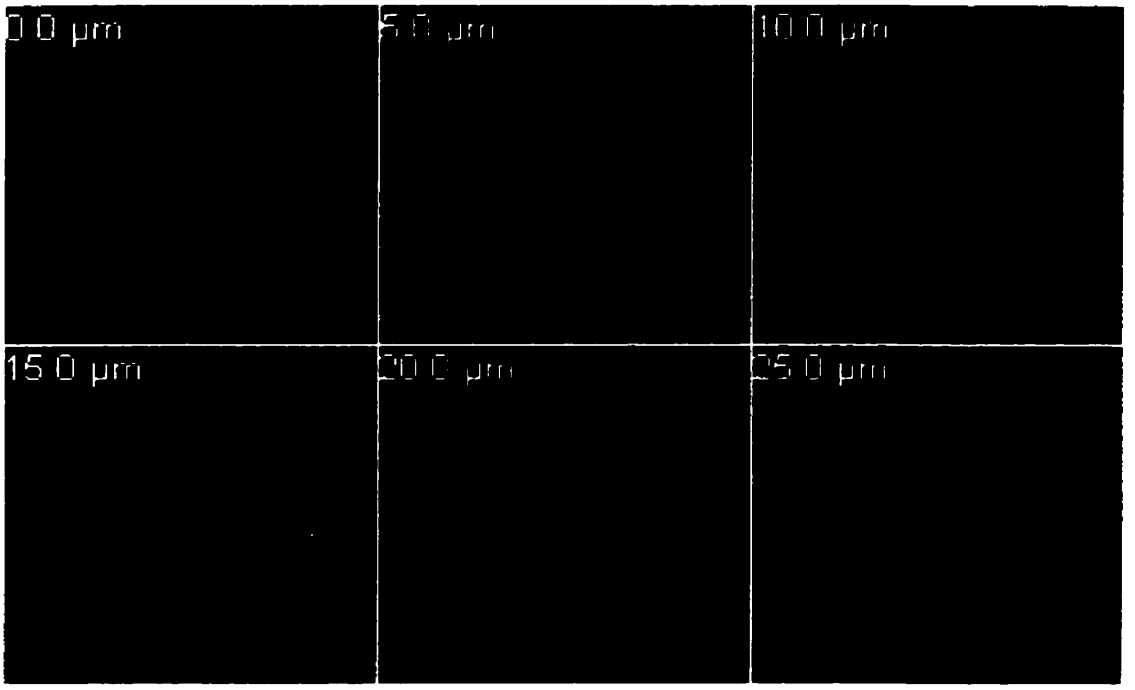

Figure 5-14. Images of PBMA sample with 15 wt% of $AnEO_{38}$: (A) annealed at 90 °C for 3 hours, (B) for freshly formed film. The images are from the surface (right top) of the film into the bulk at 5 µm depth intervals. The size of each image is 73.1 x 73.1 µm

The sample with 30 wt % PEG, annealed 3 h at 90 °C, reveals a pattern of holes near the surface structure which disappears when one looks deeper into the film. In Figure 5-15 we see a pattern of dark spots which we believe are due to channels representing the surfactant-rich phase. Deeper in the film the dark spots disappear and the film is more or less homogenous.

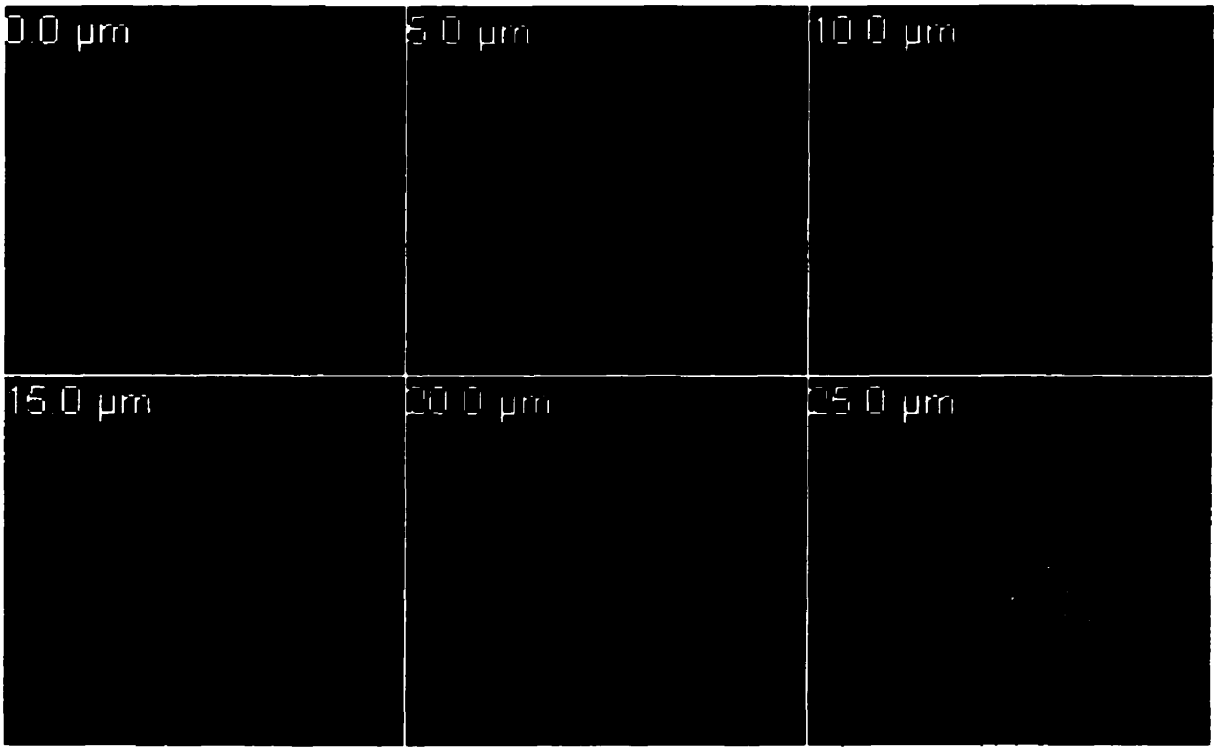

Figure 5-15. Images of PBMA sample with 30 wt% of $AnEO_{38}$, annealed at 90 °C, 3 hours. The images are from the surface (right top) of the film into the bulk at 5 µm depth intervals. The size of each image is 73.1 x 73.1 µm

The effect of increasing homogeneity of the film with the depth is observed for all samples. We do not know if this is a real effect and phase separation occurs more rapidly in the vicinity of the air surface where the surfactant can exude onto the surface, or if this is an effect connected with the contrast between two phases. (With increasing depth it is more difficult for water to reach the PEG-rich phase). We did one control experiment to check the influence of water on sample images. In Figure 5-16 we present the image of the PBMA film with 30 wt% PEG annealed for 3 h at 90 °C, but in this case the sample was immersed in silicon oil instead of water. The silicon oil does not dissolve the PEG-rich phase. The images are very different in comparison with Figure 5-15. Now we see on a dark

background micron-size bright round spots, which appear over the whole sample. We believe that these bright spots represent pure PEG crystalline material. Because of the high brightness of these spots, the rest of the film is dark and its structure is hidden.

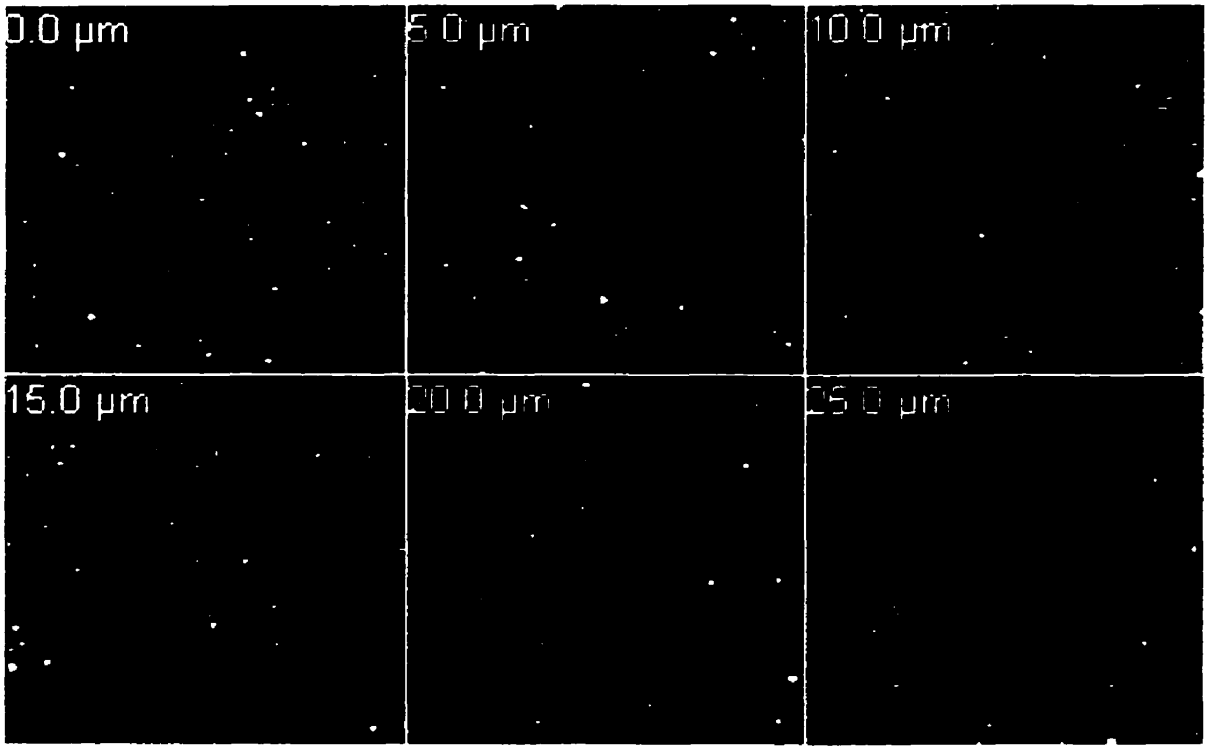

Figure 5-16. Images of PBMA sample with 30 wt% of $AnEO_{38}$, annealed at 90 °C for 3 hours, and immersed in silicon oil. The images are from the surface (right top) of the film into the bulk at 5 µm depth intervals. The size of each image is 73.1 x 73.1 µm.

Combining the results from DET with the images of PBMA films containing $AnEO_{38}$ we believe that the transport of the $AnEO_{38}$ to the surface is associated with existence in the film connected, micron size channels, round or oval in shape, and leading to the film surface. The size, number, and length of the channels depend on the amount of $AnEO_{38}$ in the PBMA film, and influence the rate of PEG exudation.

5.3.7 Effect of EO_n on Interdiffusion in PBMA Latex Films

Because of the limited miscibility observed by MDSC and DET for the EO_n oligomers with the high molecular weight PBMA sample, we examined the influence of these oligomers on both high and low molecular weight PBMA latex films, and we also carried out experiments at two different temperatures. The results for films prepared from the high

molecular weight PBMA sample, annealed at 76° C in the absence and presence of 5 wt% PEG are shown in Figure 5-17. In Figures 5-17a and 5-17b we plot the time-dependence of the extent of mixing f_m and the calculated apparent diffusion coefficients D_{app}, respectively; and in Figure 5-17c we plot D_{app} as a function of f_m.

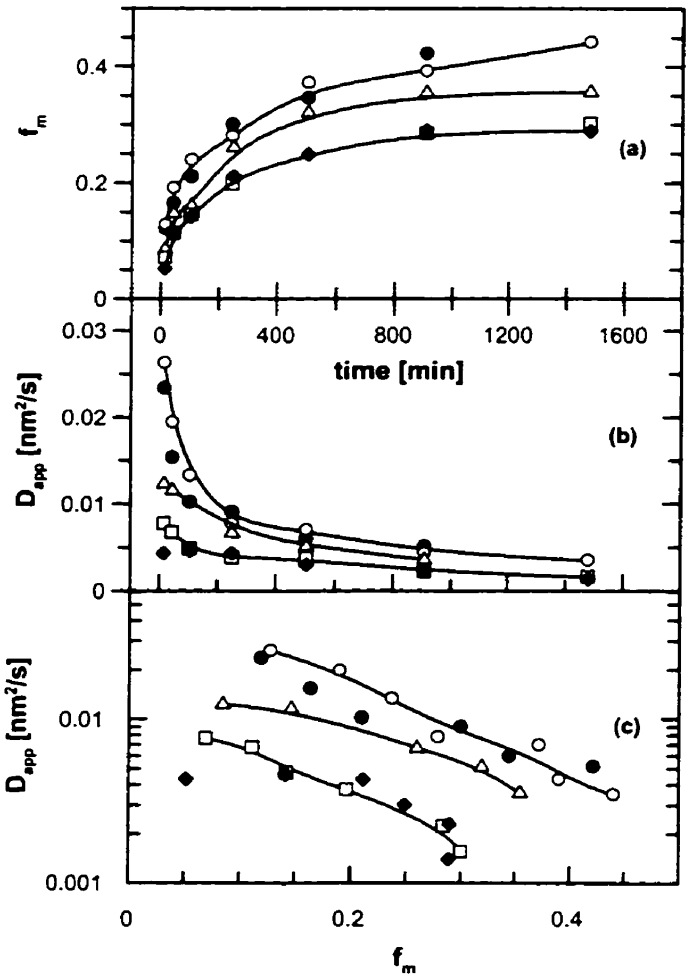

Figure 5-17. Dependence of extent of diffusion f_m (a) and apparent diffusion coefficient D_{app} (b) on annealing time (diffusion time). (c) Dependence of diffusion coefficient on extent of mixing for pure PBMA film (●) and films with the presence of 5 wt % PEG of different molecular weight (○) EO_{10}, (△) EO_{20}, (□) EO_{68}, (◆) EO_{100}. Annealing temperature: 76 °C.

For the sample without added PEG, one observes a very rapid drop in D_{app} values at early stages of polymer interdiffusion. This drop is especially pronounced in the plot of D_{app} vs. time (Figure 5-17b) for the pure PBMA film and the film containing 5 wt % EO_{10}. The mixing at early stages of polymer interdiffusion involves the lowest molecular weight components of the latex polymers. The presence of a labeled low molecular weight tail in

the PBMA molecular weight distribution can be seen in gel permeation chromatography experiments and is a consequence of our preparing the latex under monomer-starved conditions. The broad molecular weight distribution of the sample also contributes to the continuing decrease in D_{app} values at later times, as seen in Figures 5-17b and 5-17c. Once the most mobile components of the polymer have intermixed, the increase in ET measured in the experiment is due to interdiffusion by somewhat less mobile polymer, and near the end of the experiment, as f_m approaches unity, the slowest diffusing polymer contributes to the growth in ET. We have to keep in mind that the ET experiment is sensitive to diffusion on the length scale of the particle diameter. Diffusion can occur over much longer distances, but the ET experiment loses sensitivity once all the Phe-PBMA has mixed with An-PBMA. Additionally, only in the plot of D_{app} values as a function of f_m (Figure 5-17c) can we make quantitative comparisons of diffusion rates among the different samples. The plots of D_{app} vs time, however, emphasize that a significant amount of interdiffusion occurs at early times.

From the data in Figure 5-17, it is clear that at 76 °C, the presence of PEG at 5 wt% retards the rate of polymer diffusion, and that this effect is more pronounced with the higher molecular weight oligomer. For EO_{10}, the effect is too small to be observed, whereas longer chain derivatives (EO_{20}, EO_{68}, EO_{100}) have an increasingly larger effect on the rate of mixing. In Figure 5-17b we see that there is a particularly large effect on the interdiffusion rate at early times in the diffusion process. These could be consistent with the formation of a polar hydrophilic membrane by the PEG in the PBMA latex film, which could serve as a barrier to polymer diffusion across the intercellular boundaries. Based upon arguments described previously, we would expect that if the PEG oligomers form a hydrophilic membrane, we would observe an increase in Area(0) from 42 ns with the increasing amounts of PEG. The results are presented in Figure 5-18.

We do not observe a change in Area(0) with increasing amount of PEG in the freshly prepared films. This result indicates that the film is characterized by separate domains of PEG between latex particles rather than a continous membrane. The PEG domains do not cause a large decrease in the contact area between Phe and An labeled cells in the film. Additionally, we will see later in Chapter 7 that separate domains in the latex film can act as a obstacles to retard polymer diffusion. Obstacles appear to have their most pronounced retardation effect on polymer diffusion at the beginning of the annealing process, as it is observed for PEG domains.

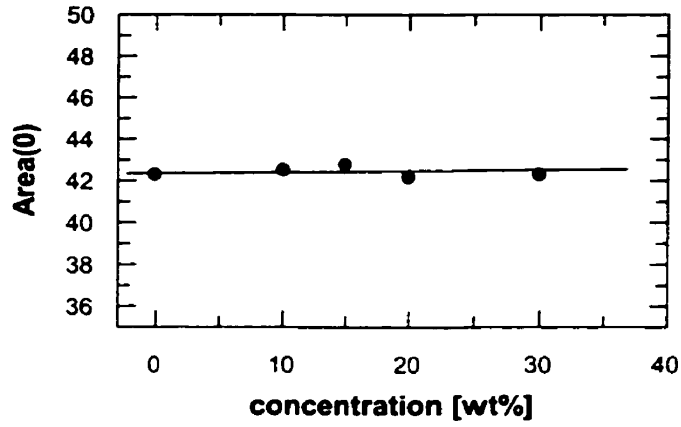

Figure 5-18. Plots of Area(0) vs. concentration of EO_{20} in the PBMA films

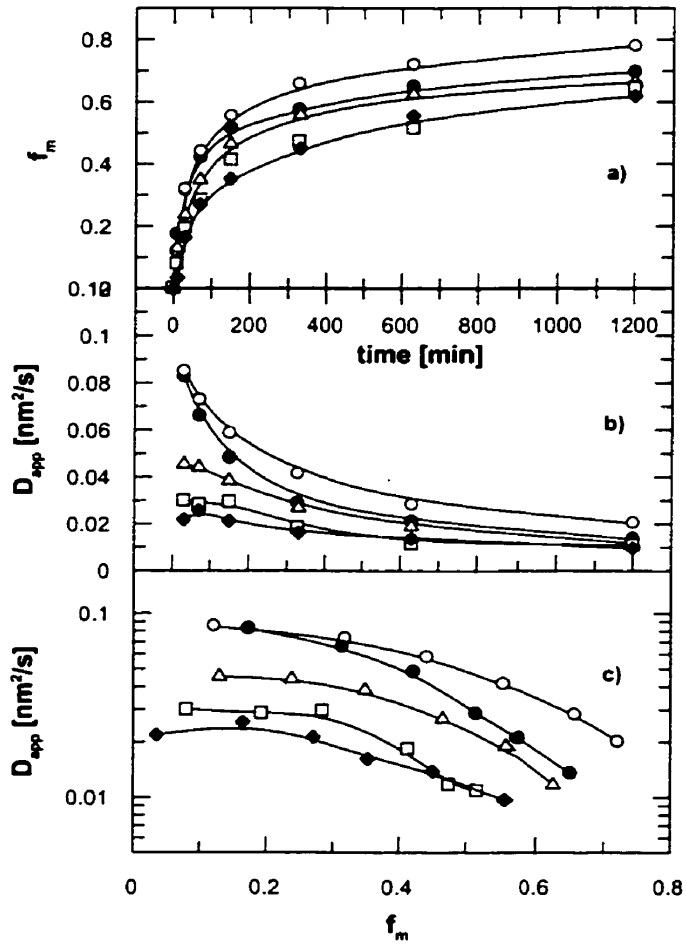

Figure 5-19. Dependence of extent of diffusion f_m (a) and apparent diffusion coefficient D_{app} (b) on annealing time (diffusion time). (c) Dependence of diffusion coefficient on extent of mixing for pure PBMA film (●) and films with the presence of 5 wt % PEG of different molecular weight (○) EO_{10}, (△) EO_{20}, (□) EO_{68}, (◆) EO_{100}. Annealing temperature: 90 °C.

A second set of experiments carried out at 90 °C gave similar results. The data is presented in Figure 5-19. At 90 °C, the presence of 5 wt% EO_{20}, EO_{68}, or EO_{100} suppresses the polymer interdiffusion rate. Here we found that EO_{10} actually increases the diffusion rate to a small extent. These results are consistent with limited miscibility of the short PEG oligomer with PBMA at elevated temperatures.

Three experiments were carried out with the low molecular weight PBMA sample (M_w = 35,000). Because of the much faster polymer diffusion rate for this sample, the films were annealed simultaneously at 60° C. In Figure 5-20 we plot f_m vs. time for these samples. Here we see that EO_{10} acts as a plasticizer to promote the polymer mixing rate whereas 5 wt% EO_{45} causes a small retardation. The shorter the EO oligomer and the PBMA polymer, the greater their miscibility, a situation typical of polymers of borderline immiscibility.

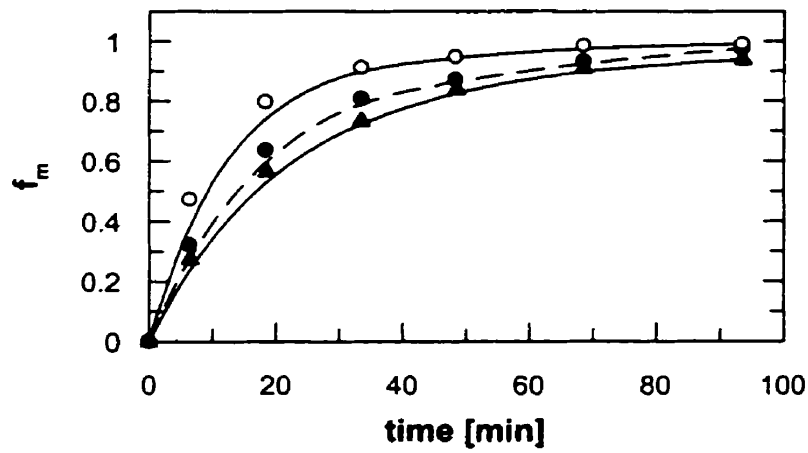

Figure 5-20. Dependence of extent of diffusion (f_m) on annealing time (diffusion time) for pure low M PBMA film (●) and films with the presence of 5 wt % PEG of different molecular weight (○) EO_{10}, (▲) EO_{45}. Annealing temperature: 60 °C.

From our diffusion and miscibility studies we conclude, that there are two opposing effects, which influence polymer diffusion in the presence of PEG oligomers. The first is an obstacle effect. Separate PEG domains in the PBMA latex film act as obstacles to retard polymer diffusion (see Chapter 7). The second is a surface plasticization effect. A fraction of PEG oligomers plasticize the polymer at the PBMA–PEG interface and speed up polymer diffusion. The miscibility is very limited (for most of the PEG samples I examined, there is no change in T_g of the PBMA phase) and strongly dependent on the EO chain length and temperature. Depending upon which effect dominates, obstacles or plasticization, one can observe a retardation or an increase of the polymer diffusion rate. Under certain

circumstances, these two effects cancel, and we see nearly no PEG effect (EO_{10} at 76 °C) on the polymer diffusion rate.

In Figure 5-17 and 5-19 we see that the retardation effect depends on the EO chain length. Miscibility decreases as the PEG chain length increases. The smaller the miscibility, the larger obstacle effect. In the case of EO_{68} and EO_{100}, for samples annealed at 76° C (Figure 5-17), there is likely to be almost no miscibility. Obstacle effects dominate. In this way, we explain why the influence of these two oligomers on polymer diffusion at this temperature is the same. When we increase the temperature, the miscibility of EO_{68} increases, and now EO_{100} retards PBMA diffusion more than EO_{68}.

The conclusion that PEG is located in the latex film in the form of separate domains rather than as a hydrophilic membrane is also consistent with the work of Chevalier[9] at al. on a latex film formation process in the presence of hydrophilic material. These authors investigated by small-angle neutron scattering the coalescence of soft latex particles covered by hydrophilic material. When the particles were covered with a shell of covalently bound poly(acrylic acid) the hydrophilic material formed an interconnected membrane that persisted in the film. When the particles were coated with short–chain surfactant molecules, the membrane that formed initially broke up into discrete domains as neighboring particles deformed into polyhedral cells during film formation.

5.4 Conclusions

The non-ionic surfactant NP-20 has only limited miscibility with PBMA at room temperature. Miscibility at room temperature is detected as a lowering of the polymer T_g, and the limit of miscibility inferred from these measurements is slightly more than 2 wt%. As the samples are heated, the components become more miscible, and at 90 °C the surfactant is fully miscible with the polymer in amounts up to at least 15 wt%, as was shown in polymer diffusion experiments (Chapter 3). Thus these components are characterized by an upper critical solution temperature.

We are interested in the location of the NP-20 in the latex film as a function of sample history. The smaller change in polymer T_g on the first heating scan (ΔT_g = 1.5 °C) for the 2 wt% sample, compared to the change that occurs following sample annealing (ΔT_g = 3 °C),

suggests that there is limited diffusion of the surfactant into the surface regions of the latex during film formation at 32 °C. More extensive mixing occurs once the sample is heated. Attempts to repeat these measurements in the presence of higher concentrations of NP-20 are frustrated by poor data when the melting endotherm occurs in the same temperature range (e.g., on heating) as the glass transition. The miscibility increases with temperature significantly, and the crystallization endotherm observed on the cooling scan for sample with 5 wt% of NP-20 is due to surfactant which demixes and then crystallizes in the sample. The implication of this result is that in the polymer interdiffusion experiments described in Chapter 3, the components mix rapidly when the samples are heated to 90 °C. Each time we removed samples from the oven and cooled them to room temperature for the fluorescence decay measurements, the NP-20 must have demixed, but these phase-separated domains caused no interference with the fluorescence decay measurements of polymer interdiffusion.

A drawing depicting our view of this process is presented in Figure 5-21.

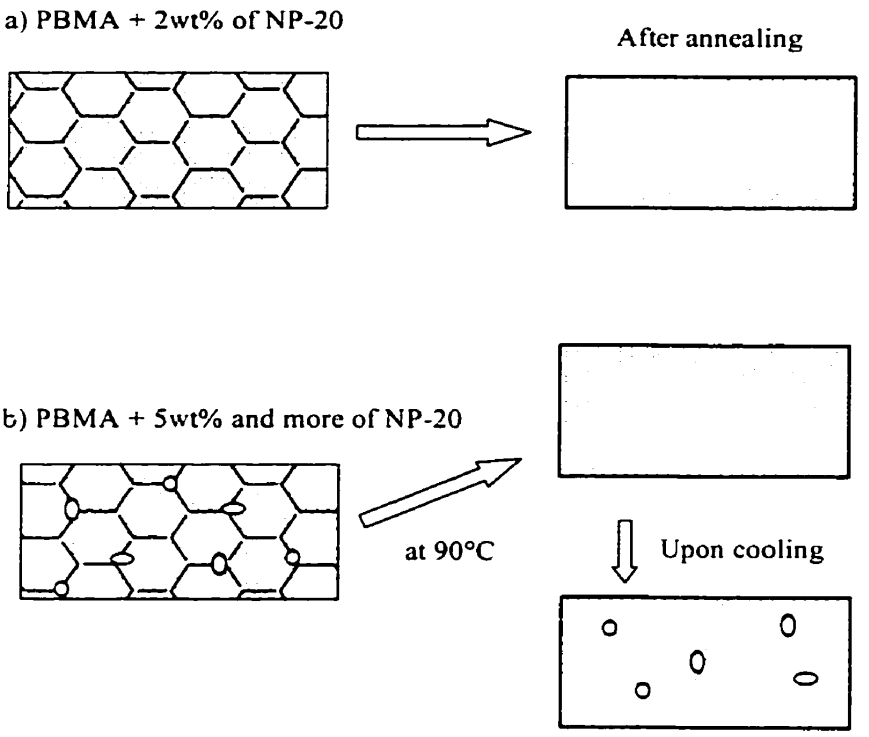

Figure 5-21. Model of NP-20 surfactant distribution in PBMA latex films with varying surfactant content. (a) For PBMA films with 2 wt % or less of NP-20 surfactant. Before annealing, the surfactant is distributed only in the top surface of the polymer. After annealing, the surfactant is uniformly

distributed in the film. (b) For PBMA films with 5+ wt % NP-20 surfactant. Before annealing, the surfactant is distributed only in the top surface of the polymer. During annealing at 90 °C, the surfactant diffuses uniformly inti the polymer phase. Upon cooling, part of the surfactant remains in the polymer phase, but the rest of the NP-20 phase separates and forms local domains in the film.

By MDSC, neither EO_{10} nor EO_{20} show any evidence for miscibility with PBMA near room temperature, for freshly prepared samples. For annealed samples containing EO_{10}, we observe in the cooling scan a small drop in T_g, about 3.5 °C, indicating some miscibility of these two components at elevated temperatures. The diffusion studies also confirm some miscibility of EO_{10} with PBMA at elevated temperatures. EO_{10} promotes the diffusion of high molecular weight PBMA (M_w = 450,000) at 90 °C (but not at 76 °C), and has an even larger effect on the diffusion of low molecular weight PBMA (Mw = 35,000) at 60° C. In case of PBMA films with EO_{20}, there is no change in T_g in the cooling scan, but we observe two crystallization peaks. As in the case of the NP-20 surfactant, the crystallization peak shifted to lower temperatures is connected with the demixing process. Our results on EO_{20} suggest a very limited miscibility of these two components, which takes place primarily near the surface of the latex particles. ET measurements of polymer interdiffusion show that all EO oligomers of 20 or more EO units act to retard polymer diffusion. We believe that this retardation is caused by an obstacle effect. The existence of separate EO domains interferes with polymer diffusion. With increasing temperature and the decreasing EO chain length, the miscibility of the system increases, reducing the obstacle effect or even causing it to disappear.

From DET measurements of PBMA latex films with anthracene-labeled EO_{38}, we confirm the very limited miscibility of PEG oligomers with PBMA polymer at 90° C.

Here we find that substantial amounts of this amphiplitic oligomer exude to the polymer surface. Much of this exudation of PEG from the film takes place during film formation process, or at the beginning of annealing. We think that the "fast exudation" is connected with the existence in the latex film of interconnected domains or channels of $AnEO_{38}$, leading to the surface. The existence of such channels is confirmed by Confocal Microscopy measurements. Through these channels the $AnEO_{38}$ can easily flow to the film surface after melting. This process become important only when the amount of $AnEO_{38}$ exceeds 15 wt%. Under these circumstances, percolation of the minor domains in the film can provide the connectivity needed for flow to the surface. The subsequent process of phase separation and

exudation, which results in a slower expulsion of An-EO_{38} from the film to the surface depends on the mobility of the polymeric matrix, and is prominent at 90 °C. At 50 °C the mobility of the high molecular weight PBMA is negligible, and the slower pathway for $AnEO_{38}$ exudation is suppressed.

5.5 References.

1. Tanaka, T.; Fujimoto, T.; Sibayama, K. *J. Appl. Polym. Sci.* **1979**, 23, 1131.
2. Haq, Z.; Thompson, L. *Colloid Polym. Sci.* **1982**, 260, 212.
3. Eckersley, S. T.; Rudin, A. *J. Appl. Polym. Sci.* **1993**, 48, 1369.
4. Snuparek, J.; Hanus, Jr. A.J.; Hajkova, B. *J. Appl. Polym. Sci.* **1983**, 28, 1421.
5. Roulstone, B. J.; Wilkinson, M. C.; Hearn, J. *Polymer International* **1992**, 27, 43.
6. (a) Kawaguchi, S.; Odrobina, E.; Winnik, M. A. *Macromol. Rapid Commun.* **1995**, 16, 861; (b) Fujita, H. *Fortschr. Hochpolym.-Forsch.***1961**, 3, 1.
7. Bradford, E. B.; Vanderhoff, J. W. *J. Macromol. Chem.*, **1966**,1, 335.
8. Bradford, E. B.; Vanderhoff, J. W. *J. Macromol Sci.-Phys.*, **1972**, B6, 671.
9. Chevalier, Y.; Pichot, C.; Grailat, C.; Joanicot, M.; Wong, K.; Maquet, J.; Lindner, P.; Cabane, B. *Colloid Polym. Sci*, **1992**, 270(8), 806.
10. Voyutskii, S. S. *J. Polym. Sci.*, **1958**, 32, 528.
11. Wang, Y.; Kats, A.; Juhué, D.; Winnik, M. A.; Shivers, R. R.; Dinsdale, C. J. *Langmuir* **1992**, 8, 1435.
12. Feng, J.; Winnik, M. A.; Siemiarczuk, A. *J. Polym. Sci.: Polym. Phys.* . **1998**, 36 (7), 1115.
13. Reading, M. *Trends Polym. Sci.* **1993**, 8, 248.
14. Gill, P. S.; Sanerbrunn, S. R; Reading, M. *J. Therm. Anal.* **1993**, 40, 931.
15. Reading, M.; Elliott, D.; Hill, V. L. *J. Therm. Anal.* **1993**, 40, 949.
16. Hourston, D. J.; Song, M.; Hammiche, A.; Pollock, H. M.; Reading, M. *Polymer* **1996** 37 (2), 243.
17. Boller, A.; Jin, Y.; Wunderlich, B. *J. Therm. Anal.* **1994**,42, 307.
18. Varma-Nair, M.; Wunderlich, B. *J. Therm. Anal.* **1996**, 46, 879.
19. Marcus, S. M.; Blaine, R. L. *Thermochimica Acta* **1994**, 243, 231.

6 THE f_m VS $t^{1/2}$ AND f_m VS $t^{1/4}$ DEPENDENCE OBSERVED IN POLYDISPERSED LATEX FILMS.

6.1 Introduction

A description of the theory of polymer diffusion across interfaces was presented in Chapter 1. In general, we assume that diffusion follows Fick's law when the molecular weight of polymer is low. In addition, the theory of polymer diffusion predicts that the diffusion will follow Fick's law when the diffusion time is larger than the reptation time (T_{rep}) for an entangled polymer system. For Fickian diffusion, the mass transfer scales with time as $t^{1/2}$, while for reptation dynamics at $t < T_{rep}$, it scales as $t^{3/4}$ when the chain ends are uniformly distributed in space, or as $t^{1/2}$ for chain ends concentrated at the surface.[1,2] When diffusion satisfies Fick's law, the extent of mixing parameter f_m, which we calculate from energy transfer experiments, is proportional to the mass transfer.[3] In the past we have also assumed that this proportionality holds for polymers whose diffusion is influenced by reptation, but we have had no means to test this assumption. If f_m is proportional to mass transferred for reptating chains, we should expect, based on the theory of polymer diffusion across interfaces, that the f_m parameter will scale as $t^{3/4}$ or $t^{1/2}$ for entangled high molecular weight polymers at $t < T_{rep}$.

In this Chapter we examine the dependence of f_m on annealing time t for low and high molecular weight PBMA samples. For low molecular weight samples, f_m has a power law time dependence and scales as $t^{1/2}$. For high molecular weight samples, we found a change in the dependence of f_m on t. We attribute the crossover from $t^{1/2}$ to $t^{1/4}$ behavior to the large molecular weight polydispersity of our samples. In our view, the lowest molecular weight components contribute to mixing at early times. Their diffusion follows Fick's law. At longer times, the experiment detects the reptation-diffusion of the higher molecular weight components in the sample.

6.2 Experimental

Most of the experimental data from DET measurements was taken from Chapter 7, so the details of latex film formation process and condition of DET experiment can be found in

Chapter 7 and 1. Data presented in Figure 6-4 comes from Chapter 4. The PBMA samples investigated had either high molecular weight ($M_w \geq 10^5$, $2.5 < M_w/M_n < 3.5$) or low molecular weight ($M_w = 3.5x10^4$, $M_w/M_n = 2.5$), and were annealed at 60 °C (low M), 70 °C, and 76 °C (high M). Some films contained fully crosslinked PBA latex particles as a filler. However, here we concentrate only on the f_m vs. t relationship, which is general for latex films and does not depend on the filler particles present. The influence of filler effects on polymer diffusion is described in detail in Chapter 7.

6.3 Results and discussion

Three sets of experimental data are presented in Figure 6-1. These plots refer to three separate energy transfer experiments on films prepared from the low molecular weight ($M_w = 3.5x10^4$, $M_w/M_n = 2.5$) PBMA samples annealed at 60°C.

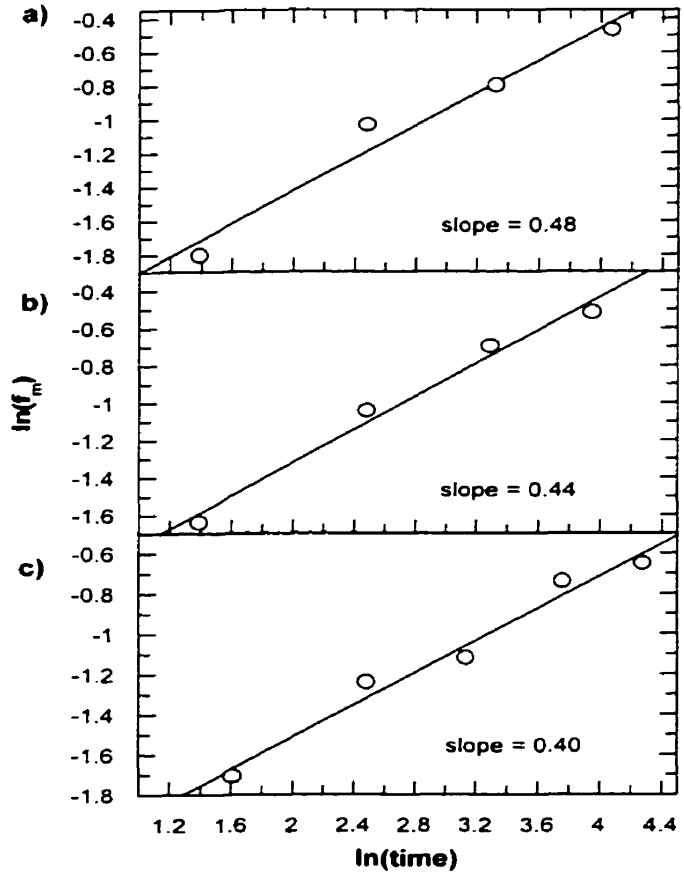

Figure 6-1. Dependence of $\ln(f_m)$ vs. $\ln(t)$ (f_m is the extent of mixing, and t is the annealing time) for three different latex film samples prepared from the low molecular weight ($M_w = 3.5x10^4$) PBMA particles, annealed at 60 °C.

The three different samples were prepared from the same latex but annealed separately. In Figure 6-1 we plot (ln f_m) vs (ln t), where t is the annealing time. The dependence is linear with an average slope of 0.44. We interpret these results to be consistent with f_m scaling with time as $t^{1/2}$, in agreement with Fickian diffusion. Furthermore, a plot of f_m vs. $t^{1/2}$ for these data are linear.

For the high molecular weight latex samples ($M_w \geq 10^5$, $2.5 < M_w/M_n < 3.5$), we obtain different results. Here we see a crossover in the time-dependence of f_m. The extent of mixing appears to increase as $t^{1/2}$ for the early stages of diffusion e.g. $f_m \leq 0.2$, and as $t^{1/4}$ for $f_m > 0.2$. Examples of such behavior are shown in Figure 6-2.

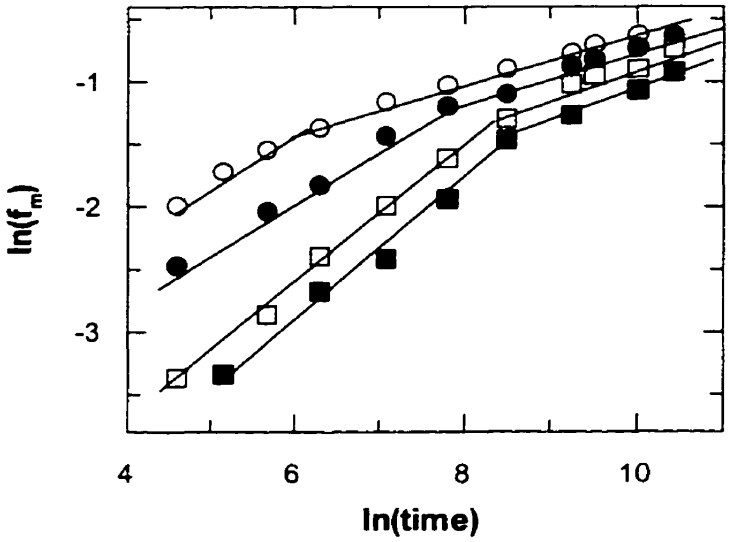

Figure 6-2. Dependence of ln(f_m) vs. ln(t) (f_m is the extent of mixing, and t is the annealing time) for high molecular weight ($M_w = 4x10^5$) PBMA sample and its blends, annealed at 70 °C: (○) in the absence of presence of crosslinked poly(butylacrylate) (PBA) microspheres, (●) 10 % PBA, (□) 30 % PBA, (■) 60 % PBA.

In Figure 6-2 we present (ln f_m) vs (ln t) for four samples annealed at 70 ° C and described in Chapter 7: (○) pure PBMA, (●) PBMA+10% PBA filler, (□) PBMA+ 30% PBA filler, (■)PBMA+60% PBA filler. For each of the samples, the dependence is linear. In each case, the line changes slope from 0.25 to 0.47 (on average) at approximately $f_m \cong 0.2$ to 0.22 [ln(0.2) = -1.61, ln(0.22) = -1.51].

In Figure 6-3 we present an expanded view of the linear dependence of (ln f_m) on (ln t) using the data taken from Figure 6-2. In Figure 6-3a we show data for the region with $f_m \leq 0.2$, and in Figure 6-3b we show the data for the region with $f_m > 0.2$.

The polymer in the latex samples has a broad molecular weight distribution ($M_w/M_n \approx 3.5$). To explain the linear dependence of f_m vs $t^{1/2}$ at early stages of the diffusion process, I imagine that the fastest diffusing species are the low molecular weight components. These polymers diffuse according to Fick's law. At longer diffusion times, the diffusive mixing of high molecular weight polymer starts to dominate the energy transfer measurements. Here entanglement effects influence the polymer mobility. As a consequence, the dependence of the f_m parameter on time changes from $t^{1/2}$ to $t^{1/4}$. Such behavior is not predicted by the Wool reptation model[1,2] for the conformational relaxation of surface chains. On the other hand, we do not know how to explain the crossover from $t^{1/2}$ to $t^{1/4}$ behavior in our samples.

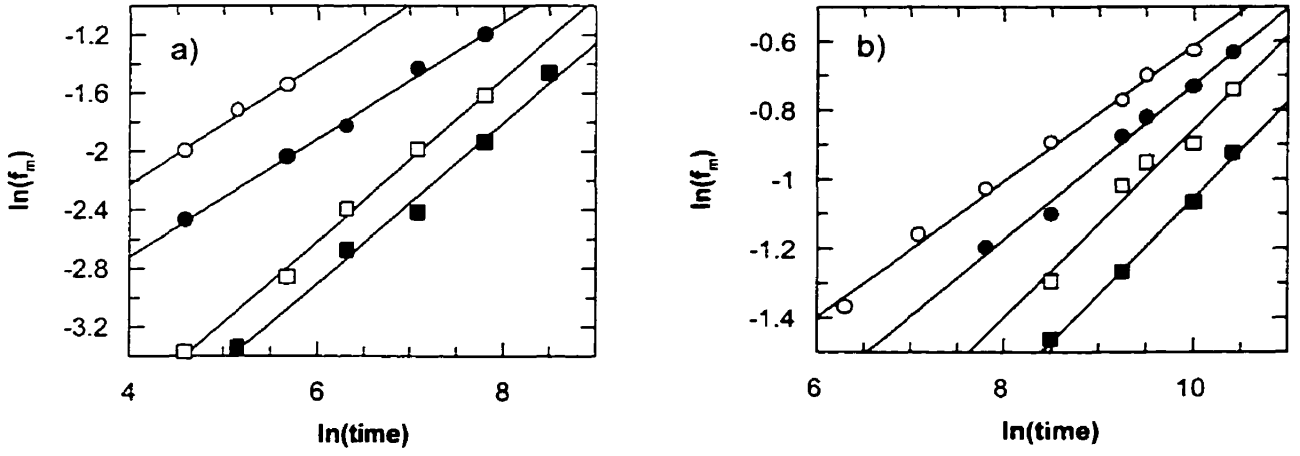

Figure 6-3. Dependence of $\ln(f_m)$ vs. $\ln(t)$ for samples from Figure 2: a) expanded region for $f_m \leq 0.2$, (○) pure PBMA (slope = 0.41), (●) 10 % PBA (slope = 0.4), (□) 30 % PBA (slope = 0.56), (■) 60 % PBA (slope = 0.55); b) expanded region for $f_m > 0.2$, (○) pure PBMA (slope = 0.20), (●) 10 % PBA (slope = 0.22), (□) 30 % PBA (slope = 0.27), (■) 60 % PBA (slope = 0.28).

The experimental data for other PBMA samples, (e.g. films prepared from pure PBMA latex dispersions; data taken from Chapter 4) provide support for the idea of Fickian diffusion at early times. In these samples we also observed a linear dependence of ($\ln f_m$) on ($\ln t$) with a slope in the range of 0.4 to 0.56 for $f_m \leq 0.2$ (see also Figure 6-4), and 0.2 to 0.3 for $f_m > 0.2$. The $t^{1/4}$ dependence for high molecular weight latexes is very reproducible, and others in our lab made similar observations for high molecular weight PBMA polymers several years ago[4]. At this point I would like to emphasize that this is the first time that we observed a crossover from $t^{1/2}$ to $t^{1/4}$ in the f_m vs. t dependence of high molecular weight

latex films. To observe this crossover, we need to choose properly the annealing times and annealing temperatures. Normally, we choose the annealing temperature in such a way that we are able to monitor the entire diffusion process over a reasonably short period of time (a maximum of a few days). In the past we chose the annealing temperatures sufficiently high that we had at most two values of f_m in the range of $0 < f_m < 0.2$. Thus we neglected the contribution to mixing of the low molar mass components of the latex polymer. Here we are more careful. By lowering the annealing temperature, and by carrying out measurements over long periods of time we can get several data points in the region $0 < f_m < 0.2$, and at longer times obtain additional data for $f_m > 0.2$. Under these conditions, to obtain meaningful data over the whole diffusion process (up to $f_m > 0.6$), we need to follow the diffusion process for times on the order of several weeks. Only in this way we were able to observe the crossover from $t^{1/2}$ to $t^{1/4}$ dependence in the polymer diffusion process.

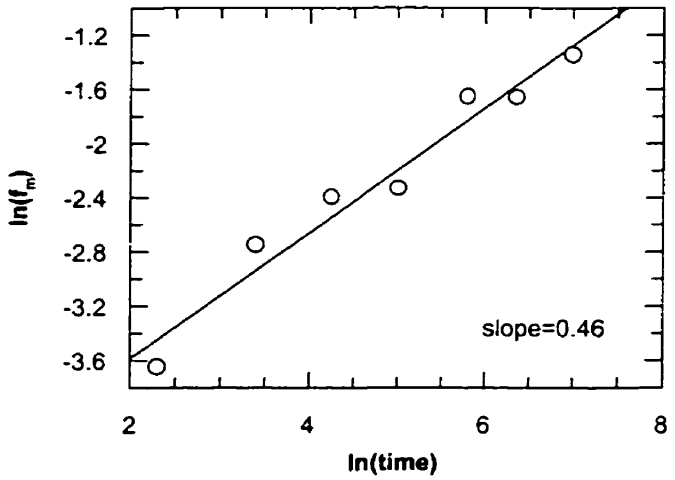

Figure 6-4. Dependence of $\ln(f_m)$ vs. $\ln(t)$ in the range of f_m parameters $0 < f_m \leq 0.2$ for high molecular weight ($M_w = 4x10^5$) pure PBMA sample annealed at 76 °C. The calculated slope is 0.46. The data was taken from Figure 4-9a in Chapter 4.

Kim, Sperling and Klein[5] used an emulsification procedure to prepare spherical polystyrene particles from monodisperse polystyrene and deutero – polystyrene (M_n values ranged from 150,000 to 200,000 with $M_w/M_n \leq 1.03$). They prepared films from these "latex" particles, and used SANS measurements to investigate the polymer diffusion process across the particle-particle interface. These authors found that the diffusion rates they measured were consistent with Wool's minor-chain reptation model. In their experiments, they found that the average interpenetration depth X increased with the one-fourth power of

the annealing time up to the reptation time. For times longer than the reptation time, the dependence crossed over to a one-half power dependence, as predicted by Wool[2] for the case of uniformly distributed chain ends in space.

Our system has a broad molecular weight distribution. It is also likely that the chain ends are not uniformly distributed in space. Some of the chains contain polar end groups from the $-OSO_3^-$ initiator, and these groups will tend to be on the latex particle surface. In cases where the chain ends are segregated at the interface, some molecular properties are predicted to change, and some not.[2a] For example, the predicted average interpenetration depth is unaffected, but the number of monomers crossing the interface N(t) (mass transfer) has a scaling law for segregated chain ends different from that for uniformly distributed chain ends. This is probably why most authors who attempt to test the reptation model in their system examine the average interpenetration depth and not the mass transfer across the interface. Of course neutron scattering experiments do not measure the amount of mass transferred. They measure the radius of gyration of the deuterated latex for various annealing times. Thus SANS experiments are not sensitive to the issue of the chain ends distribution in space.

In our ET experiment, we measure a quantity related to mass transfer through the extent of mixing. The scaling law appropriate to our experiments is sensitive to the polymer chain-end distribution. Generally speaking, depending on the specific shape of the distribution function, the power law exponent may no longer be constant with time, or it may take an intermediate value between ¾ (uniform) and ½ (segregated) for different chain end distributions.

The effect of molecular weight polydispersity on polymer dynamics at interfaces was considered by Tirrell[6] and Wool[2]. Assuming independent chain diffusion, the contributions to the concentration profile from individual reptating chains can be determined for any molecular weight distribution.[2b] We need only realize that at a given interdiffusion time, part of the polymer chains will have already reached their equilibrium state (their chain conformation is Gaussian, their interdiffusion time $t > T_r$), while the longer chains are still in their non-equilibrium state. In case of emulsion polymers, however, we would have to determine the absolute molecular weight distribution experimentally. Since we do not have this information, we are not able to calculate the scaling law for molecular properties of our

emulsion polymers. In addition, the lowest molar mass components of the sample are not much longer than one or two entanglement lengths.

6.4 Conclusions

The crossover from $t^{1/2}$ to $t^{1/4}$ in f_m vs. t dependence is now a well-established feature of polymer diffusion latex films made up of high molecular weight polymer with a broad molecular weight distribution. This phenomenon needs to be investigated in more detail in order to understand the molecular origin of this behavior. In particular, one needs to carry out "baseline DET experiments" with high molecular weight latex samples of narrow molecular weight polydispersity. Such experiment would allow us to compare the f_m vs. t dependence for systems with narrow and high molecular weight polydispersity.

6.5 References:

1. Wool, R. P.; O'Connor, K. M. *J. Appl. Phys.* **1981**, 52, 5953: Kim, Y. H.; Wool, R. P. *Macromolecules* **1983**, 16, 1115: Zhang, H.; Wool, R. P. *Macromolecules* **1989**, 22, 3018.
2. Wool, R. P. *Polymer Inerfaces*, Hanser Publishers: **1995**; a) page 69 -72; b) page 75.
3. Farinha, J. P. S.; Martinho, J. M. G.; Yekta, A; Winnik, M. A. Macromolecules **1995**, 28, 6084; Dhinojwala, A.; Torkelson, J. M. *Macromolecules* **1994**, 27, 4817; Liu, Y. S.; Feng, J.; Winnik, M. A. *J. Chem. Phys.* **1994**, 101, 9096
4. Wang, Y., Zhao, CH.-L., Winnik, M., A. J. Chem. Phys. **1991**, 95, 2143.
5. Kim, K., D., Sperling, L., H., Klein, A. Hammouda, B. Macromolecules **1994**, 27, 6841.
6. Tirrell, M. Rubber Chem. Technol. **1984**, 57, 523.

7 THE EFFECT OF SOFT POLYMER FILLER PARTICLES ON POLYMER DIFFUSION IN PBMA LATEX FILMS.

7.1 Introduction

Additives affect the final properties of latex films. Some additives like plasticizers dissolve in the latex polymer. Other additives form separate domains (occlusions) within the film. The effect of hard fillers on the mechanical properties of polymers[1] and on polymer diffusion[2] has been explored extensively. The addition of hard fillers to elastomers can increase the strength and hardness of the material and its resistance to deformation. These particles also act to retard polymer diffusion.

The change in the properties of polymer films in the presence of fillers is, to some extent, connected with the fact that polymer chains near a filler surface have substantially different properties than those in the bulk.[3-9] This is due to chain conformational changes attributed to the presence of a boundary, and specific interactions between the polymer and the interface, which, in certain cases, can propagate away from the surface up to $50R_g$[10] or even "tie" portions of the chain to the interface. Additionally, the geometry of a random environment created by the distributions of filler particles is also an important factor influencing the polymer diffusion. The presence of filler increases the diffusion path of the polymer (tortuousity effect), and can produce some energetic barriers for diffusing polymer chains, when the chains are confined to the restricted space between the filler particles. If size of the confinement is less than radius of gyration of the polymer chain, there will be an entropy barrier for the chain to enter this space. In this case the diffusion of the polymer chain into this space proceeds by overcoming the entropic bottlenecks generated by the random media[10].

Most studies of polymer diffusion near a solid substrate have indicated a reduction in polymer mobility closer to the substrate[11-13]. For example Zheng et al.[12], using dynamic scanning ion mass spectrometry, interpreted data to find that the diffusion rates of polystyrene (PS) perpendicular to a silicon oxide substrate were as much as an order of magnitude slower than in bulk even up to 80 nm (10 R_g). Smaller, but substantial, decreases in lateral polymer diffusion coefficients were found by Frank et al.[11] in PS films with

thickness up to 150 nm (50 R_g) cast on silicon oxide substrate. Work by Lin et al.[13] on poly-(methyl methacrylate) (PMMA) diffusion away from a silicon oxide surface found that the range of influence of the substrate on polymer diffusion was at most 40 nm (4 R_g). These results have been interpreted as being associated with an increase in the effective T_g. However, the enhancement in polymer mobility in the presence of solid surface, and a decrease in T_g was also observed[14-16] in similar systems. Orts et al.[14] and Keddie et al.[15] observed that ultrathin polystyrene films on silicon oxide surfaces (with a weakly attractive interaction energy) exhibit a lower glass transition temperature than the bulk polymer. Additionally, Reiter[16] observed that polystyrene films dewetted silicon oxide surfaces at temperatures below the bulk polymer T_g, providing the evidence of enhanced chain mobility.

In contrast, the air-polymer interface or "free" surface is thought of as a region of enhanced mobility. Simulations indicate that this free surface region may have decreased density compared to the bulk.[5] It has also been argued that chain-end segregation to a surface due to conformational entropy considerations may increase local free volume and thus increase polymer mobility.[6] Brillouin scattering studies of freely standing, ultrathin polystyrene films by Dutcher and coworkers[17,18] indicated substantial reductions in T_g as thickness is reduced. In summary, the type of the surface and the morphology it creates in the polymeric matrix has significant influence on the polymer mobility in the regions of the polymer close to the surface.

It seems clear that the presence of the surface changes the polymer dynamics. However, differences in the results obtained by different research groups for similar systems indicate that there are many parameters that influence the mobility of polymers close to the surface. As this topic seems to be very interesting from both a theoretical and an applications point of view, we decided to examine how soft elastic spherical fillers with different diameters affect the mobility of polymers in a latex film, and how the mobility depends on the morphology of these films.

7.2 Experimental

7.2.1 Latex samples

Two samples of unlabeled fully crosslinked poly(butyl acrylate) (PBA) latex particles with Tg = - 43 °C and diameters, d = 56 and 112 nm, respectively, were prepared by conventional emulsion polymerization using the recipes presented in Table 7-1. The 56 nm PBA latex was obtained by batch polymerization. Part of this sample was used as the seed in the semicontinous polymerization used to prepare the 112 nm diameter PBA latex. In both reactions, 3.75 wt% of 1.6-hexanediol diacrylate (HDA) was added as the crosslinker.

Table 7-1. Recipe for the preparation of crosslinked PBA latex

First Stage (56nm crosslinked PBA seeds)		Second Stage (112nm crosslinked PBA)	
BA (mL)	16.062	BA (mL)	10.657
Crosslinker[a] (g)	0.626	Crosslinker (g)	0.387
KPS[b] (g)	0.358	KPS (g)	0.06
SDS[c] (g)	1.154	SDS (g)	0.4
Water (g)	372	Water (mL)	28
Temp. (°C)	80	Temp. (°C)	80
Time (h)	1	Time (h)	3

a) 1.6-hexanediol diacrylate; b) KPS: potassium persulfate; c) SDS: sodium dodecyl sulfate.

Using the data in Table 7-1, and density of BA monomer ζ, ζ = 0.894g/cm^3 we calculated M_c, the mean molecular weight between cross-links assuming that both $H_2C{=}CHCO_2$ group of HDA react. The calculated M_c is 2600 (20 BA units). The gel content was not measured, but it was assumed to be 100%. For the d = 56 nm PBA latex, some attempts to determine the gel content were carried out. A PBA film prepared at room temperature was transferred to a centrifuge tube filled with THF solvent. The film was left for 24 h in the solvent for swelling. Under these conditions the film fell apart. The PBA fragments coming from the latex film redispersed in THF, and the obtained cloudy solution

could not be sedimented by centrifugation. Based on this experiment we assumed that PBA latex is fully crosslinked.

This PBA latex particles were used as a soft fillers in poly(butyl methacrylate) (PBMA) latex films. The PBMA samples were labeled with a fluorescence dye, either a donor, phenanthrene (Phe), or an acceptor, anthracene (An), referred to Phe-PBMA and An-PBMA, respectively. We prepared both high (high M) and low (low M) molecular weight dye-labeled PBMA latex particles. Some important characteristics of PBMA latexes are present in Table 7-2.

Table 7-2. Characteristics of PBMA latexes.

high M	**Mw (g/mol)**	**Mn (g/mol)**	**d (nm)**	**Tg (°C)**	**Dye content (mol%)**
Phe-PBMA	380,000	130,000	124	34	0.9
An-PBMA	420,000	130,000	132	34	0.9
low M					
Phe-PBMA	35,000	16,000	120	21	0.9
An-PBMA	34,000	17,000	120	21	1

All the latex samples have a narrow particle size distribution, as indicated by dynamic light scattering.

7.2.2 Modulated Differential Scanning Calorimetry (MDSC) Measurements.

The glass transition temperature T_g of the homopolymers and their blends were determined by MDSC measurements using an Universal VI.6I TA DSC Instrument. The samples were run under N_2 with a 2° C/min average heating and cooling rate. The modulations had an amplitude of ± 1°C every 60 sec. For most samples three scans were performed: scan 1 (heating from -125° C to 75° C); scan 2 (cooling from 75° C to -125° C); scan 3 (reheating from -125°C to 75°C). The total measurement required about 7 h. The Tg values were obtained as the maximum in the heat capacity derivative curves. The heat capacity and its derivative were calculated automatically using the MDSC software. The

description of the MDSC technique itself, and the calculations of the reversing and nonreversing heat flows, are presented in Appendix A.

7.2.3 Film formation and measurements

For both diffusion and MDSC measurements, latex films were prepared in the same way from a mixed dispersion containing a 1:1 number ratio of Phe- and An- labeled PBMA particles and a varying volume fraction of soft crosslinked PBA particles. The volume ratios in blends were calculated based on the weights of solids of the various types of particles, using density values of 1.05 g/mL for PBMA, and 1.08 g/mL for crosslinked PBA. The mixtures of latex dispersions were gently shaken for 10 minutes and then cast onto quartz (diffusion measurements) or glass slides (MDSC measurements). The plates were covered with an inverted Petri dish, and placed in an oven for about 4h to form dry, crack free, and transparent films. Films with the higher contents of PBA in the sample (30 or 60 wt%) were slightly cloudy. The film formation temperature was 34°C for the high M PBMA samples and 22°C for the low M PBMA. After the films were dry, they were either cut from the glass substrate and placed in the DSC pan (in the form of small pieces) or for diffusion measurements left on the quartz plate and annealed at 55 °C (low M PBMA) or at 70 ° and 80 °C (high M PBMA). The thickness of the films was in the range of 30 to 50 μm. Polymer diffusion was monitored as a function of annealing time, by fluorescence decay measurements of the extent of energy transfer (ET). The technique and measurement conditions are described in Chapter 1. For each series of samples to be compared, the films were dried and annealed simultaneously. After each time interval of annealing, the fluorescence decay profile of each film was measured. The areas under each decay curve were integrated. ET quantum yields, Φ_{ET}, extent of mixing, f_m, as well as the apparent diffusion coefficient D_{app} were calculated, and analyzed as described in Chapter 1 and below.

7.3 Results and Discussion.

7.3.1 Initial Energy Transfer in Nascent Films.

We begin by examining the efficiency of energy transfer in newly formed low molecular weight films $\Phi_{ET}(0)$, which provides a measure of the interfacial area of the system. Feng et al[19,20] found that the amount of energy transfer across the interparticle boundary in nascent films is proportional to the total contact area of donor-acceptor labeled particles divided by the volume of donor-labeled phase. We wanted to see if the presence of soft fillers changes the interfacial area between the donor– and the acceptor-labeled particles. Our results are shown in Figure 7-1a. We find that the amount of ET is almost independent of the soft-particle fraction from 0 to 0.6, with the Area(0) value ranging from 38.7 to 39.6 ns, corresponding to $\Phi_{ET}(0)$ varying from 0.15 to 0.13.

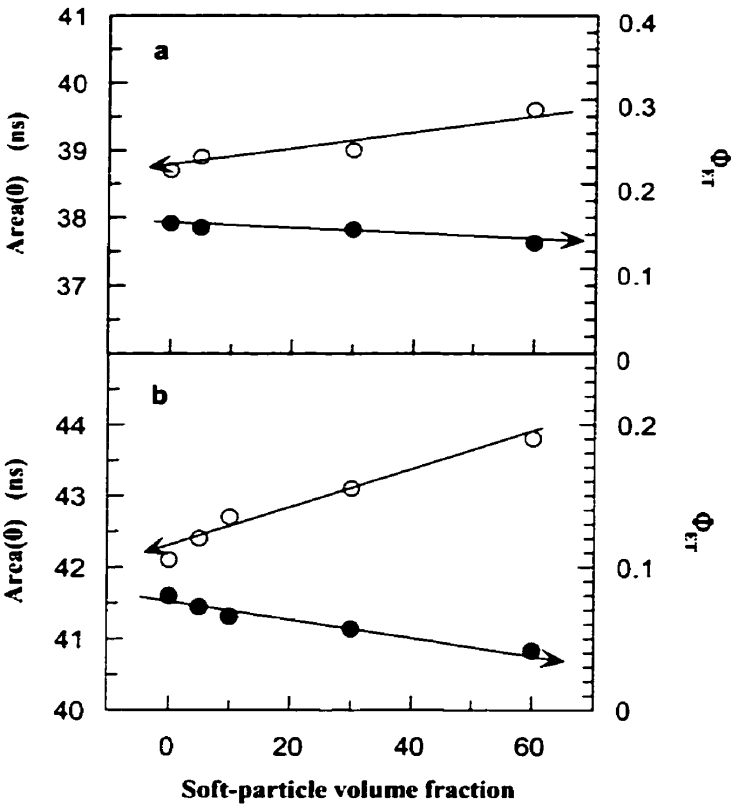

Figure 7-1. Plots of Area(0) (unfilled symbols) and efficiency of energy transfer ET (filled symbols) vs. the soft particle volume fraction; (a) for low molecular weight PBMA films, (b) for high molecular weight PBMA films.

There is no trend for changes in $\Phi_{ET}(0)$ over a wide composition range (especially from 0 to 30 vol % of soft filler). This result indicates that the ratio of the D/A interfacial area to the volume of the D-labeled particles does not change significantly, even when a large fraction of unlabeled soft particles is present. In filled films, a significant fraction of the labeled PBMA surface area must be in contact with the unlabeled filler particles. No ET can take place at this interface. The above results imply that the mean surface area of each PBMA particle is increased as more soft particles are incorporated into the film, so that the presence of PBMA / soft-particle contacts does not decrease significantly the interfacial area between D- and A- labeled PBMA particles. We should mention that the same trend was observed by Feng et al.[2] for the same PBMA latex sample containing hard particles (PMMA microspheres) as the filler.

In case of the high M PBMA films with soft PBA particles, we observe an increase of Area(0) and a decrease of Φ_{ET} with increasing volume fraction of soft filler. For this system the value of Area(0) increases monotonically, on average, from 42 ns for the PBMA sample itself to 43.8 ns for the PBMA sample containing 60% PBA, corresponding to a decrease in Φ_{ET} from 0.08 to 0.04 (see Figure 7-1b). These results indicate that for high M PBMA films with soft fillers, the interfacial area between D/A labeled particles decreases with increasing volume fraction of soft particles. I would like to stress that, especially for the samples with 60% of PBA, the Area(0) values showed significant scatter for different samples, and ranged for similar samples from 43 ns to 45 ns. Since the unquenched lifetime of the phenanthrene chromophore in PBMA films is 45.7 ns, a value of Area(0) = 45 ns means that the donor and acceptor labeled PBMA particles for some samples with 60 vol% of PBA were nearly completely separated by the PBA filler particles. However, for these samples, even very short annealing times, such as 7 min at 70 °C changes the area from 45 ns to 43 ns. In contrast, under the same annealing conditions, we did not observed any changes in the initial area 42.4 ns for sample with 10 vol % PBA. From these findings we conclude that at the beginning of the annealing process, some morphology changes take place, leading mainly to a change in the amount of interfacial area between donor and acceptor-labeled particles. These changes precede the beginning of polymer diffusion, and can be easily

observed for samples when larger amount of PBA is present. This is why we chose as the Area(0) value for samples with 60 % of PBA equal to 43.5 ns.

The above results show that for the low M PBMA latex plus soft PBA particles, the interfacial area does not change significantly with the amount of PBA added, while for the same system with high M PBMA, the interfacial area decreases monotonically. This difference in behavior suggests that changes in interfacial area depend on how flexible the polymer matrix is in comparison with the elasticity of filler during the film formation process. If the matrix is more flexible than the filler particles, then PBMA particles deform more easily and surround the filler. If the filler particles are easier to deform, then they surround the PBMA particles and decrease the interfacial area between donor/acceptor labeled PBMA particles.

7.3.2 Maximum Energy Transfer in Well-Mixed Films.

To examine whether the filler particles were able to suppress diffusion for some fraction of the polymer, we examined the effect of long annealing times on the extent of polymer diffusion. We measured the extent of energy transfer for films of different blend compositions annealed for sufficiently long times that the ET values approached their maximum value $\Phi_{ET}(\infty)$. At this point, the diffusion approaches its final, equilibrium state where all the D- and A-labeled molecules are well-mixed. In case of low M PBMA samples, we could anneal the films at relatively low temperatures (60 °C) for relatively short times, ranging from a 1- 2 days, to obtained fully mixed films.

In high M PBMA samples, where the polymer diffusion during annealing is much slower than in low molecular weight films, we employed a different procedure to obtain well-mixed films. In this case, to get Area(∞) values, we placed a few drops of an organic solvent (tetrahydrofuran, THF) on top of the freshly formed PBMA\PBA film to swell the film and promote mixing. After solvent evaporation, we measured the fluorescence decay of each dried film.

In both cases, for low and high M PBMA plus PBA, the Area(∞) values for the blends are slightly higher than that for pure PBMA itself. These differences are rather small, with the area values ranging from 15.9 ns (pure PBMA) to 17.5 ns (60 vol% PBA), and Φ_{ET} values ranging from 0.67 to 0.62 for low M PBMA films. For high M PBMA films, the

Area(∞) values change from 17.6 ns (pure PBMA) to 19.3 ns (60 vol% PBA); and Φ_{ET} values, from 0.61 to 0.58. It is clear that all the above samples undergo sufficient interdiffusion to reach close to their full-mixing state. The small differences in the Area(∞) and Φ_{ET} values among the well-mixed films are not considered to be significant in our data analysis, and they do not interfere with our comparison of diffusion rates for the different samples examined here. This difference may arise from the possibility that in the blend some PBMA particles can be totally separated by PBA particles and polymer mixing in this case is not possible. Although we claim the sample is fully mixed there may be some domains in the film not mixed. Another possible explanation for the higher value of Area(∞) for samples with large amounts of PBA filler in comparison to the pure PBMA film is the mixing of tiny fraction of PBMA segments with PBA at the interference between these components.

7.3.3 Effect of the size of soft PBA particles on diffusion rate of high Mw PBMA.

To test the effect of the PBA particles on the mobility of the surrounding matrix, and how this effect depends on the size of PBA particles, we examined diffusion rates at 80 °C for the high M PBMA samples. These films contained 30 vol % of PBA, but different soft particle diameters. Our analysis implicitly assumes that there is no significant PBMA diffusion into fully cross-linked PBA particles. This assumption is confirmed by our measurements of Area(∞), which showing only small differences between pure PBMA samples and samples containing 60 % vol of PBA. We know from the work of Briber et al.[21] that even linear homopolymers and cross-linked polymers of the same composition will phase separate if the mesh size of the cross-linked polymer is less than the radius of gyration R_g of the linear polymer. Thus we expect very little mixing of the PBMA and cross-linked PBA components. The volume of the PBMA phase and the final dye concentrations should not change substantially when soft particles are present.

Figure 7-2 shows the PBMA diffusion data for a pure PBMA film and films with 30 vol % PBA particles of different diameters, d_{PBA} = 56 and 112 nm. From Figure 7-2 we see clearly that diffusion rate is more retarded with the PBA particles of smaller size. For an extent of mixing f_m = 0.2, the value of apparent diffusion coefficient D_{app} for the pure PBMA sample is 0.012 nm^2/s. This value decreases to 0.005 nm^2/s in case of the sample

with d_{PBA} = 112 nm, and to 0.002 nm^2/s for sample with d_{PBA} = 56 nm. Our results on PBMA diffusion indicate that the diffusion rate depends on the size of the soft particles.

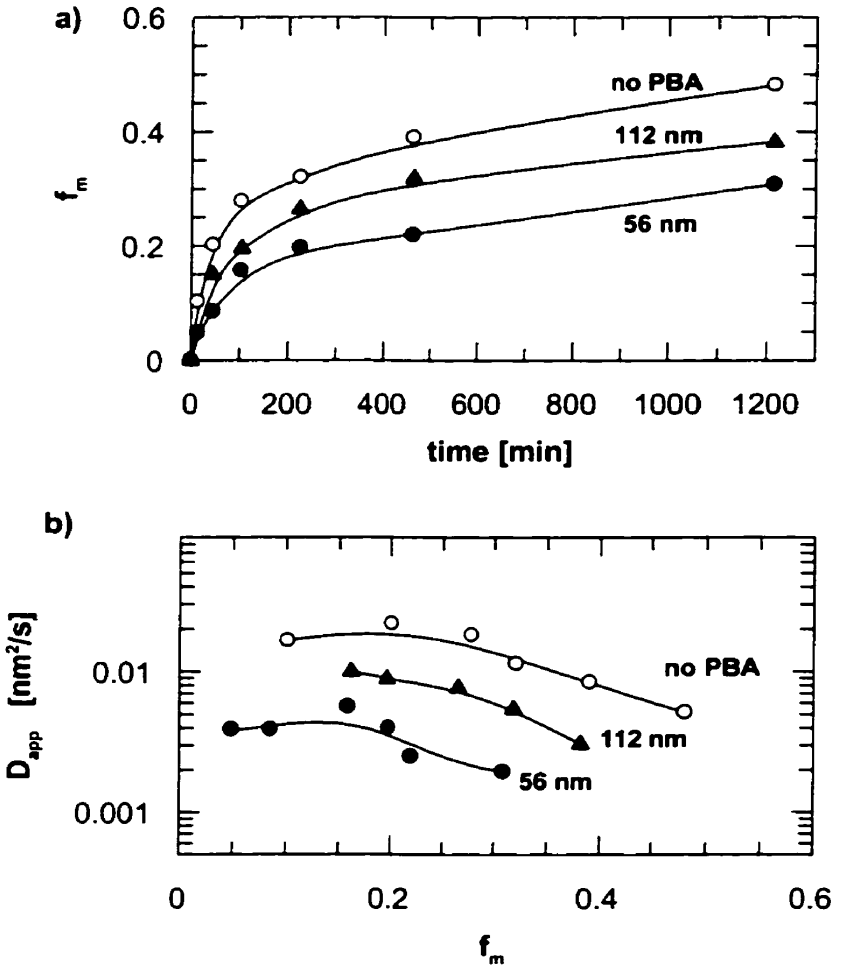

Figure 7-2. Comparison of high M PBMA diffusion rates for pure PBMA films (○) and for films blended with 30 vol % PBA particles of different diameters (d_{PBA}): 56 nm (●),and 112 nm (▲). In part a) we plot the extent of mixing (f_m) vs annealing time, and in part b) we plot the apparent diffusion coefficient D_{app} vs. f_m.

Another way to compare these diffusion rates is to plot f_m as a function of $t^{1/4}$ or $t^{1/2}$, where t is the annealing time. We know from the previous Chapter that for the case of high M PBMA f_m varies linearly with $t^{1/2}$ for $f_m \leq 0.2$, and linearly with $t^{1/4}$ for $f_m > 0.2$. We will start our analysis with the results for the case where $f_m > 0.2$.

Figure 7-3 shows the f_m vs. $t^{1/4}$ plot for the PBMA film itself and for two PBMA/PBA blend films with different PBA particle diameters. To proceed with the data analysis, we calculate a mobility parameter $k_{1/4}$, characterizing the rate of diffusion, as the slope in the f_m

vs. $t^{1/4}$ plot. Next we plot the values of the parameter $k_{1/4}$ vs. $1/d_{PBA}$ as shown in Figure 7-4. A straight line is obtained. The linear dependence of $f_m/t^{1/4}$ vs. $1/d_{PBA}$ plot in Figure 7-4 indicates that the decrease of diffusion rate is inversely proportional to the diameter of the filler particles. For spherical particles the ratio of surface-to-volume S/V = 6/d, where d is the diameter of the particle, so keeping volume as a constant, V = const, S = const/d. This result tells us that, at a given volume fraction of filler, the retardation effect increases with the total surface area of the filler particles.

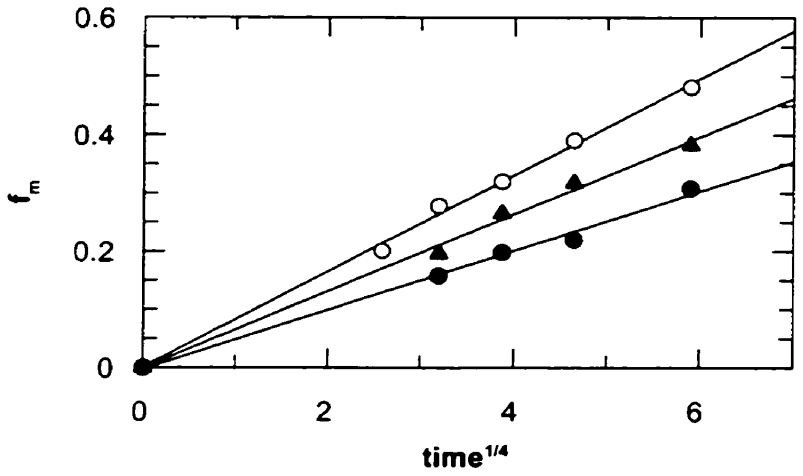

Figure 7-3. Plots of f_m vs. $t^{1/4}$ for a pure PBMA film (○) and for films blended with 30 vol % PBA particles of different diameters (d_{PBA}): 56 nm (●), and 112 nm (▲).

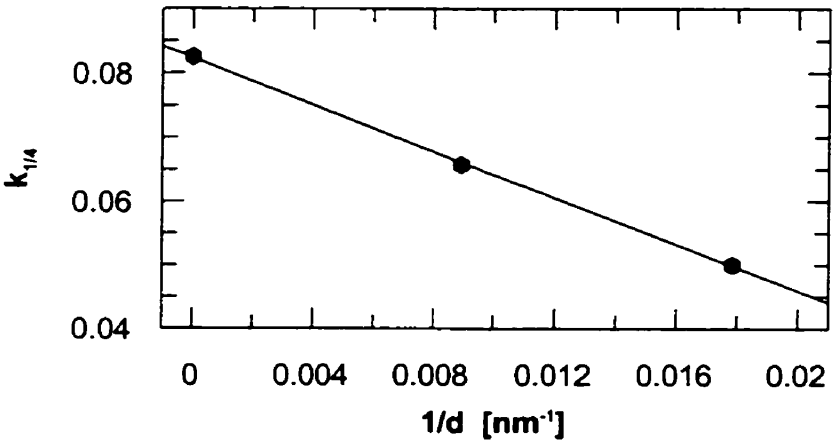

Figure 7-4. Plot of $k_{1/4}$ vs $1/d_{PBA}$ in PBMA/ PBA blend films at 30 vol % PBA. The data were derived from Figure 7-3.

A similar effect of filler-size on the rheological properties of LDPE melts containing a dispersed elastic filler was observed by Serenko et al.[22] In their case the elastic filler was a

rubber powder prepared by grinding the worn treads of used tires, containing up to 50 wt % of polyisoprene rubber and 30 wt % of carbon black. The rubber powder was sifted using a standard set of sieves to select the fractions with particle sizes with $0.1<d<0.2$, $0.2<d<0.315$, $0.315<d<0.4$, and $0.4<d<0.6$ mm. The specific surface S of the particles was determined by the nitrogen adsorption method on a Gazometer GKh-1 setup. The polymeric compositions were obtained by mixing the melts in a laboratory extruder at average temperature of 140 ° C. The rheological measurements were done at 120 °C on a Polymer K-1 capillary viscometer with constant flow rate.

The authors present the dependence of the viscosity of LDPE at constant wt % of filler on the specific surface (g/m^2) of the rubber powder. At a given wt % of filler, the viscosity increases linearly with increasing total surface area of the filler (decreasing filler diameters). The size effect of filler particles is observed at filler contents only above 60 wt%, and increases at higher concentrations of filler. In our case, the effect of size of filler particles on polymer diffusion can be observed at lower concentrations of filler (e.g. 30 wt% PBA). This difference in behavior is likely related to the fact that the diameter of our filler is much smaller (56 nm), in comparison to that (0.1 mm) used by Serenko et al.[22] We introduce a larger specific surface area into the system. As a consequence, the system is more sensitive, and the effect can be observed at lower filler concentrations.

Now we will consider the early stages of polymer diffusion when $f_m \leq 0.2$. In this case f_m is linear with $t^{1/2}$, and this dependence is shown in Figure 7-5. Figure 7-6 presents the mobility parameter $k_{1/2} = f_m/t^{1/2}$ vs 1/d (d is the diameter of filler particles). In this case it is difficult to judge if the relation is linear or not. If it is linear, the fit is not as good as in case of $f_m > 0.2$ (Figure 7-4). If the real plot is not linear, it could mean that at the beginning of annealing - diffusion process, the system is not in its equilibrium state, and processes other than polymer diffusion also take place, e.g. relaxation of soft filler particles from a squeezed to a more round shape. Certain evidence for this kind of relaxation process was reported earlier on page 7 and 8. If the filler particles are distorted in the nascent film, during the equilibration process they will relax. The ratio of their surface-to-volume will decreases to value $S/V = 6/d$ of a sphere. If the rate of this decrease is different for different size filler particles, then the expected linear relation $k_{1/2}$ vs 1/d would be disturbed at early stages of polymer diffusion.

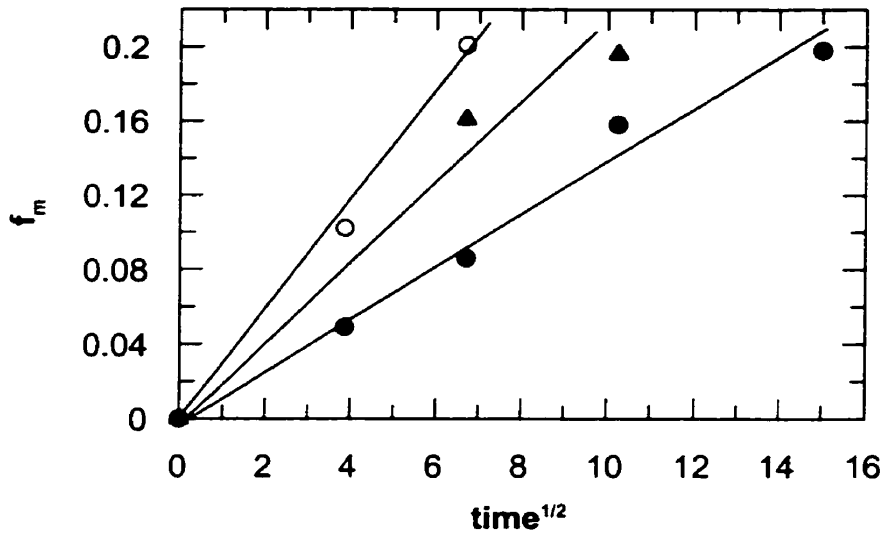

Figure 7-5. Plots of f_m vs. $t^{1/2}$ for a pure PBMA film (○) and for films blended with 30 vol % PBA particles of different diameters (d_{PBA}): 56 nm (●), and 112 nm (▲).

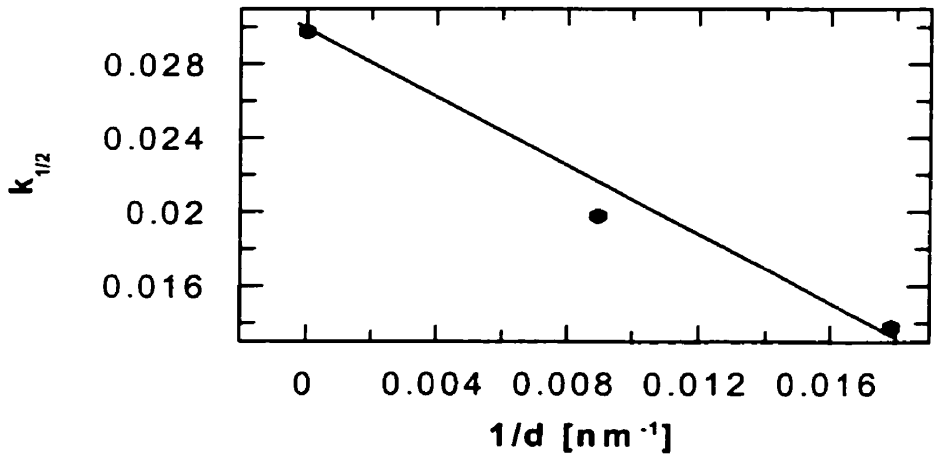

Figure 7-6. Plot $k_{1/2}$ vs. $1/d_{PBA}$ in PBMA/ PBA blend films at 30 vol % PBA. The data were derived from Figure 7-5

7.3.4 Effect of soft PBA particles on high Mw PBMA diffusion. Varying the blend composition.

In this section, we examine the diffusion rates of the high M PBMA samples at 70 °C in films containing different amounts of soft particles with a diameter, d_{PBA} = 56 nm. Keeping in mind the conclusion from previous section, we should expect that by increasing the amount of the PBA particles in the film, we should more efficiently decrease the diffusion rate of the surrounding polymer. In Figure 7-7a we plot the extent of mixing f_m vs.

annealing time for the first 5,000 min of annealing, and in Figure 7-7b we plot the same relation but we present data for f_m values up to annealing times of 60,000 min (1000 h). Figure 7-7 shows explicitly that the more soft filler we introduce into the film, the more the diffusion rate of PBMA decreases. This effect is most pronounced at earlier stages of diffusion. Figure 7-7b indicates that the PBMA diffusion is not suppressed, only retarded in the presence in the soft fillers. After a long enough time, f_m reaches the same extent of mixing as in samples without fillers.

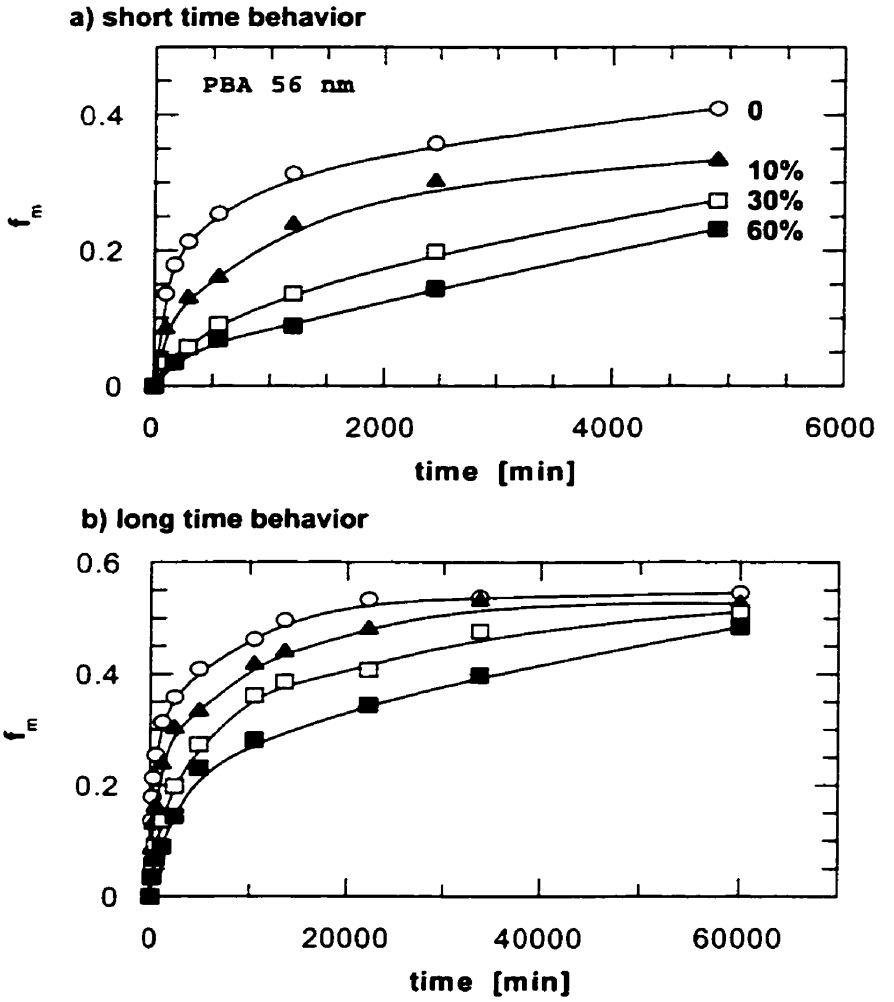

Figure 7-7. Plot of the extent of mixing f_m for films blended with different amounts of PBA particles (d_{PBA}= 56 nm), expressed as volume percent (% PBA): 0 (○), 10 (▲), 30 (□), and 60 (■). Part a) presents short time diffusion behavior, and part b) presents long time diffusion behavior.

The dependence of f_m vs. $t^{1/4}$, for $f_m > 0.2$ is presented in Figure 7-8a, and is linear. When we plot the mobility parameter $k_{1/4}$ vs. the volume fraction of PBA particles, we again observe a linear dependence (Figure 7-8b) excluding point for 0 % of filler. The mobility

parameter $k_{1/4}$ decreases linearly (slope = -0.0213, intercept = 0.0417) with the increasing volume fraction φ of the soft filler. Since all particles have the same diameters (here d =56 nm) the parameter $k_{1/4}$, in fact, decreases linearly with the total surface of the filler particles.

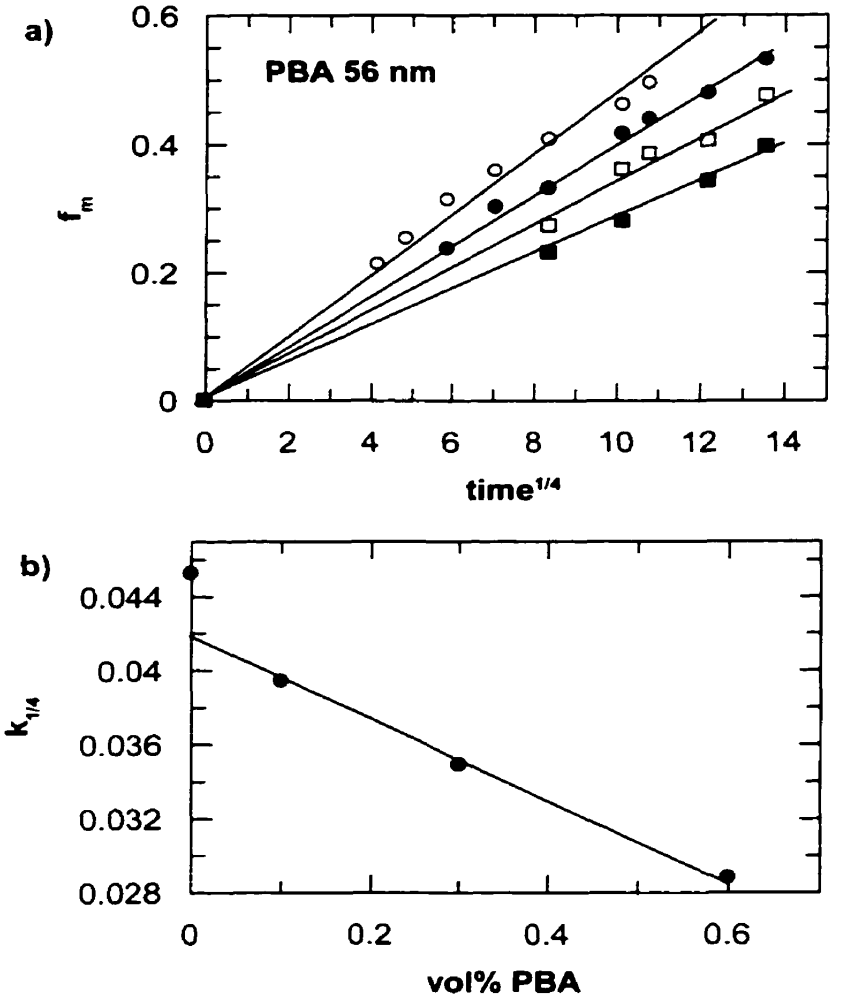

Figure 7-8. Plots of: a) f_m vs. $t^{1/4}$ for films blended with different amounts of PBA particles (d_{PBA}= 56 nm), expressed as volume percent (% PBA): 0 (○), 10 (●), 30 (□), and 60 (■); and b) $k_{1/4}$ vs. vol % PBA.

Summarizing the results from this and the previous section we can say that the influence of soft filler particles in the range of volume fraction (0.1 – 0.6) on polymer diffusion depends on the total area of the filler surface, and the relation $k_{1/4}$ vs. S_{TF} (S_{TF} total surface of fillers) is linear. We can increase the total surface of the filler in the sample in two ways: at constant filler diameter we can increase the amount of the filler, or at constant volume fraction of the filler, we can decrease its diameter. Another important conclusion resulting

from the linear dependence $k_{1/4}$ vs. φ, is that the decrease in $k_{1/4}$ ($\Delta k_{1/4}$) caused by increase in total volume of filler ΔV_{TF} has constant value, $\Delta k_{1/4} / \Delta V_{TF}$ = constant, so each particle contributes to the retardation of polymer diffusion in the same way. This effect depends on the amount of surface added to the system, our results imply, that each particle makes a similar and independent contribution of its surface to the total filler surface in contact with the polymer.

It would be interesting to find a relationship between $k_{1/4}$ and the vol % PBA for the range of small filler concentrations ($0 < \varphi < 0.1$). We found that, in most cases, samples in this range of concentrations annealed at 80 °C do not have a large effect on polymer diffusion, and they all retard polymer diffusion in nearly the same way. On the other hand, for the sample with 10 vol% PBA, we always observed a significant retardation effect on polymer diffusion, but this effect was nearly the same as for the samples with 20% or 30 vol% of filler. Based on these results, I believe that some morphology changes in the latex film take place at about 10 vol % PBA. However, this is the only conclusion I can draw from the experiment carried out at 80 °C. I think that, at this temperature, the mobility of the polymer matrix is high enough for the filler to aggregate during the experiment, even at early stages of polymer diffusion. This is my explanation for why the reproducibility and resolution of the data was poor.

To examine the system in more detail, we repeated experiments with 3 and 6 vol % of filler at a lower annealing temperature, 70 °C. The plot of f_m vs. annealing time is shown in Figure 7-9. The sample with 6 vol % PBA shows more retardation of polymer diffusion than the sample with 3 vol% PBA, but for 5000 min annealing time, the difference between the 3 vol% and 6 vol% samples disappears.

In Figure 7-10 we plot f_m vs. $t^{1/4}$, omitting the data points at 5000 min annealing time where the two lower curves in Figure 7-9 meet. The plots are linear. In Figure 7-11 we plot the slopes, $k_{1/4} = f_m / t^{1/4}$ vs. volume fraction of filler. Here we also found a linear dependence of $k_{1/4}$ on φ with a slope = - 0.19, and intercept = 0.053. The slope has a much higher value than that for samples with 10 and more vol % PBA (slope = - 0.021). The parameter $k_{1/4}$ for the sample without filler now falls on the line for the linear dependence presented in Figure 7-11.

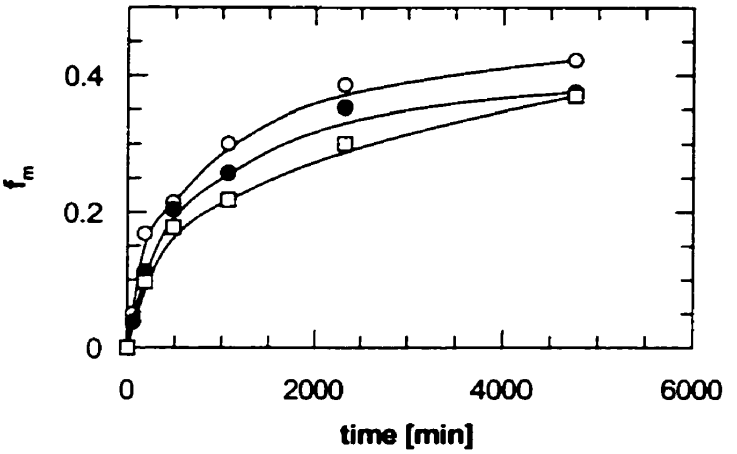

Figure 7-9. Plot of the extent of mixing f_m vs. annealing time for films blended with different amounts of PBA particles (d_{PBA}= 56 nm), expressed as volume percent (% PBA): 0 (○), 3 (●), 6 (□).

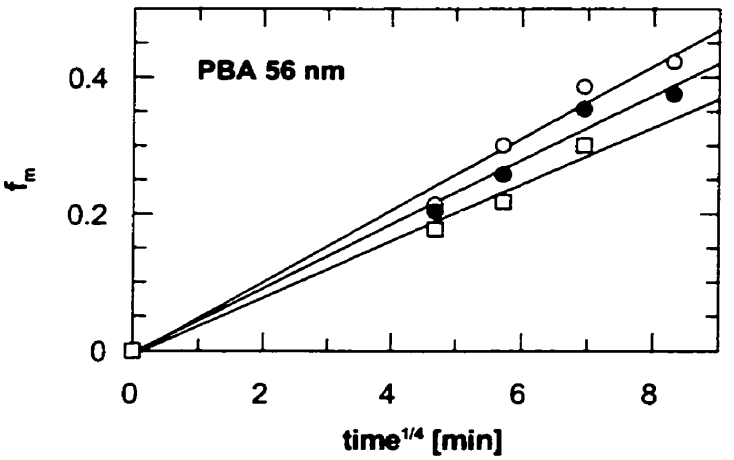

Figure 7-10. Plots of f_m vs. $t^{1/4}$ for films blended with different amounts of PBA particles (d_{PBA}= 56 nm), expressed as volume percent (% PBA): 0 (○), 3 (●), 6 (□).

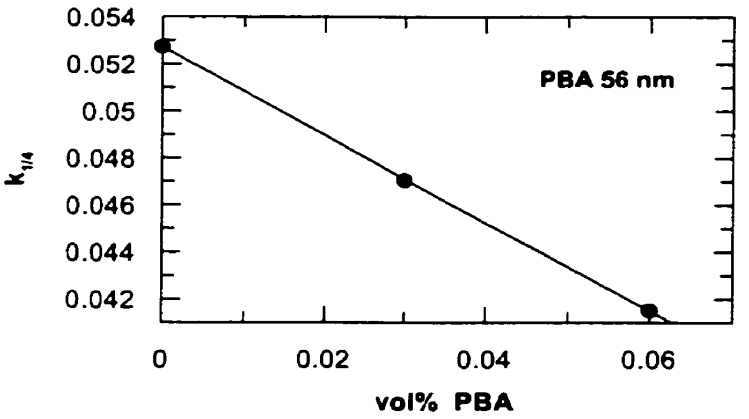

Figure 7-11. Dependence of parameter $k_{1/4}$ vs. volume fraction of filler (vol% PBA, d_{PBA}= 56 nm)

As the samples with low filler concentration ($0 \leq \varphi < 0.1$) were not annealed at the same time as samples with the higher concentration of filler $\varphi \geq 0.1$, and some changes in oven temperature can occur between measurements, we have to make sure that the results from these two ranges of filler concentration can be compared. In order to do this we plot data from both experiments on the same graph (Figure 7-12): the extent of mixing f_m vs t for 0, 3, 6 vol % PBA films (series a), and for films with 0, 10 vol% PBA (series b). The results for PBMA samples without filler (for both series) overlap, indicating that samples from two series were annealed under the same conditions, and that the results obtained in these two series can be compared. Another interesting finding is that the f_m values for sample with 6 vol% PBA nearly overlap those of the sample with 10 vol% PBA.

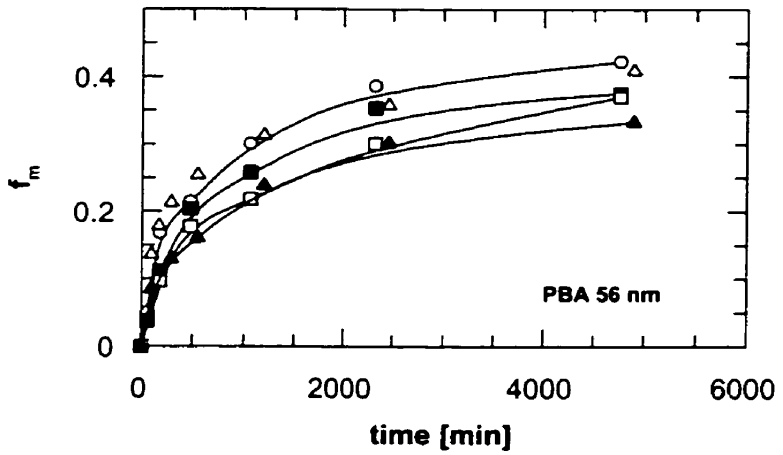

Figure 7-12. Plot of the extent of mixing f_m for films blended with different amounts of PBA particles (d_{PBA}= 56 nm), (% PBA): 0 (○), 3 (■), 6 (□) - series a; 0 (△), 10 (▲) - series b. The samples from series (a) and (b) were not annealed at the same time.

Values of $k_{1/4}$ vs. vol % PBA are plotted in Figure 7-13. Figure 7-13 shows a crossover in linear behavior of parameter $k_{1/4}$ vs. volume fraction of filler φ at $\varphi = 0.06$. The value of the slope $k_{1/4}$ vs φ is larger for filler concentrations $\varphi \leq 0.06$ than for $\varphi \geq 0.1$. These results indicate that filler effectiveness in the retardation process decreases for higher filler concentrations ($\varphi \geq 0.1$).

The same change in the slope of linear dependence is observed for log (D_{app}) vs. φ (see Figure 7-14). Here the values of apparent diffusion coefficient D_{app} were taken at constant f_m, f_m= 0.3. As we will see later, we connect the change in the slope of $k_{1/4}$ (log(D_{app})) dependence vs. filler concentration with the change in film morphology.

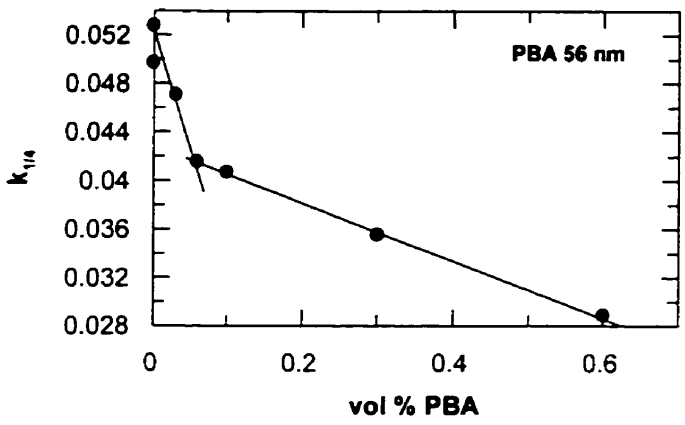

Figure 7-13. Plot $k_{1/4}$ vs. vol % PBA.

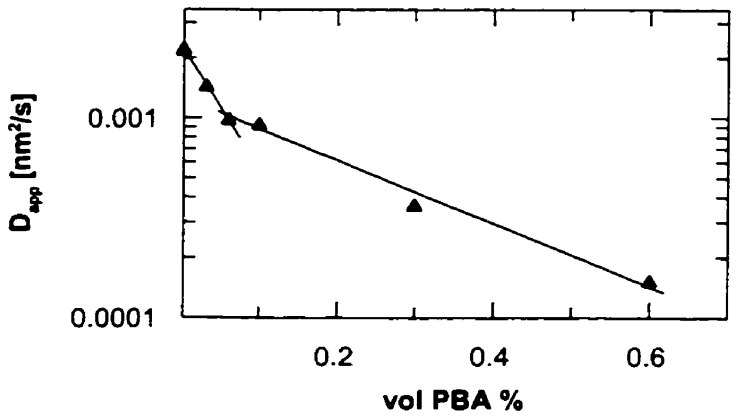

Figure 7-14. Plot log (D_{app}) vs. vol % PBA. The values of D_{app} were taken at constant f_m, f_m = 0.3.

Next, we will consider the early stages of polymer diffusion ($f_m < 0.2$) for the samples described above without and with 10, 30, 60 vol % of filler. The f_m dependence vs. $t^{1/2}$ is linear and is presented in Figure 7-15. The dependence of $k_{1/2}$ vs. vol % of PBA is presented in Figure 7-16a and is not linear. However, the log-log plot is linear with a slope n = 0.475 (Figure 7-16b) and indicates that at the beginning of the diffusion process the influence of soft filler on polymer diffusion is different than during the later stages of polymer diffusion.

We do not know why parameter $k_{1/2}$ behaves differently than parameter $k_{1/4}$ with increasing volume fraction of filler. We can only speculate, as we did in the previous section describing early stages of polymer diffusion for samples containing filler particles with different diameters, that the lack of a linear dependence of $k_{1/2}$ on φ_{PBA} is connected with the filler relaxation process in the first stages of annealing. The filler particles in freshly formed latex films are squeezed between latex particles. During the annealing process, when

polymer matrix is mobile, they can easily relax to their original round shape and decrease the surface-to-volume ratio. If the rate of this process depends on the amount of the filler, the $k_{1/2}$ vs. vol % PBA dependence would not be linear.

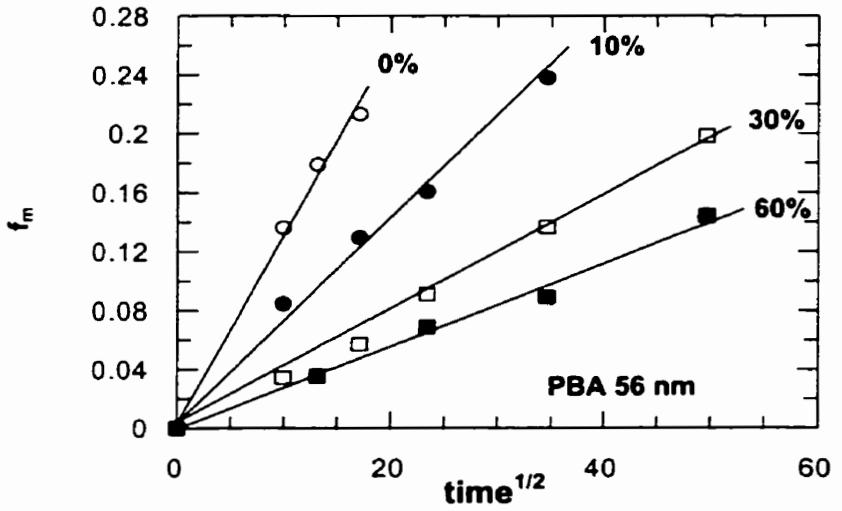

Figure 7-15. Plots f_m vs $t^{1/2}$ for films blended with different amounts of PBA particles (d_{PBA}= 56 nm), expressed as volume percent (%PBA): 0 (○), 10 (●), 30 (□) and 60 (■).

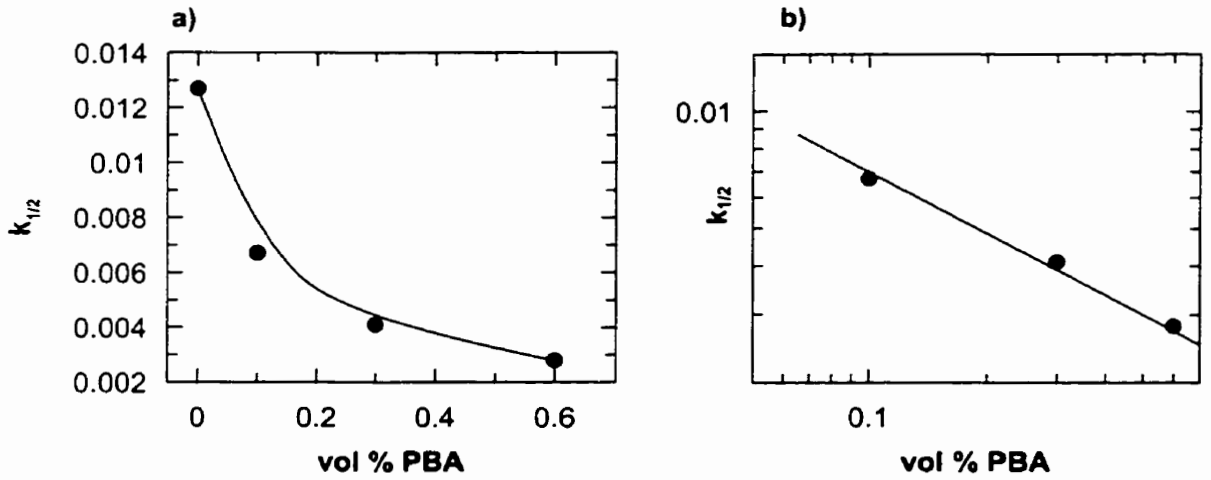

Figure 7-16. Dependence of $k_{1/2}$ vs. vol % PBA: a) linear scale and b) log-log scale.

7.3.5 DET as a method for probing local morphology in latex films.

DET is an experimental method that probes polymer properties over small length scales. In the study of polymer diffusion in latex films the ET experiment loses sensitivity when the

donor-labeled PBMA is "fully mixed" with the acceptor-labeled PBMA, involving diffusion over the length of a particle radius. This is why our technique is not able to probe the morphology changes on a macroscopic scale, e.g. the formation of a continuous network of filler throughout the whole sample. Nevertheless, DET experiments can be sensitive to the formation of smaller structures like aggregates on the microscopic scale. In order to measure the macroscopic changes in the film morphology, we have to image the structure using microscopy or measure the macroscopic properties of the film, which are sensitive to these changes, like conductvity[22], the elastic[25] or the tensile[1a] modulus of the film.

Recently, Chevalier et at.[25] examined aggregations in latex blend films by dynamic mechanical analysis (DMA) and SANS[23,24]. These two experimental methods give complementary information about the morphology of latex films by providing structural information on very different scales. Chevalier et at.[25] examined the structure of composite films made of high T_g polystyrene (PS) latex particles dispersed in a low-T_g poly(butyl acrylate) latex film. For SANS experiments, they investigated samples with two filler concentrations: 10 wt% and 45 wt% PS. The important experimental result was that the position and shape of the scattering peak was identical for both samples, indicating that the local morphology of the films at the two different concentrations is the same. From SANS experiments, they found that the PS particles were not randomly distributed in the PBA film. The separation between PS particles was shorter than that expected for a random distribution, indicating that PS particles were aggregated into relatively open clusters. The structure of the film was made of regions that were enriched in PS particles, at the expense of remaining regions containing fewer PS particles than the average. The composition of the PS-rich domains (60 vol % PS) was similar, regardless of the overall composition. This type of behavior resembles features of phase separation where the separate phases do not consist of pure components.

From the DMA measurements (sensitive to the large-scale structure-topological arrangement)[26] of the elastic moduli G', the authors found that the percolation threshold connected with efficient mechanical reinforcement of the investigated film occured at 32 wt% PS. This result indicates that the formation of a continuous network of PS particles in the whole film takes place at 32 wt% PS. DMA measurements, however, were not sensitive to the formation of PS clusters below the percolation threshold. The influence of the aggregates on mechanical properties was manifested only above the percolation threshold.

On the other hand, SANS, as a local method, was not able to monitor the formation of continuous PS phase in the whole film, but was sensitive to the formation of local structure like the PS clusters present at 10 vol % PS.

From our result on high T_g fillers[2], and results described in earlier sections of this Chapter we know that the filler effect on polymer diffusion in latex film, measured by DET, depends on the total filler surface-to-volume ratio. If this ratio decreases, the extent of the effect decreases too. The formation of filler aggregates is understood as a decrease in filler surface-to-volume ratio, and should be seen by DET. In this way we think that DET measurements can also be sensitive to local morphology changes in latex films.

7.3.6 Latex film morphology in the presence of soft PBA filler.

We will start our consideration of latex film morphology from the analysis of Figure 7-13, where we plot the diffusion rate $k_{1/4}$ vs. the volume fraction of filler φ. The slope of the line representing samples up to 6 vol % PBA is much steeper than the slope of the line representing samples with more than 10 vol % of PBA. As described above, we have interpreted the linear dependence of $k_{1/4}$ on the vol % of PBA to mean that each particle adds the same contribution to the retardation of polymer diffusion, by adding the same increment to the total filler surface area in contact with the diffusing polymer.

In Figure 7-13 we are confronted with a new problem, a change in slope at approximately 10 vol % soft filler. This result indicates that above this value, added filler is less effective at retarding polymer diffusion. The slope of the straight line reflects what part of the surface of each particle is in contact with the diffusing polymer, and in this way contributes to the retardation of polymer diffusion. Our picture of this process is shown in Figure 7-17. For low concentrations of filler ($\varphi < 0.06$) we assume that PBA particles are distributed randomly in the film and do not aggregate (Figure 7-17a). In this case, the total surface of each particle participates in the retardation process, and the linear dependence $k_{1/4}$ vs. vol % PBA starts from zero filler concentration. For higher concentrations of filler, ($\varphi >$ 0.06), the slope of $k_{1/4}$ vs. vol % PBA decreases, which means that the contribution of each PBA particle to the retardation process of polymer diffusion is smaller. We can imagine such a situation in the case in which the aggregates of filler particles start to form (Figure 7-17b). Then, only part of each filler particle is in contact with the diffusing polymer and the rest is in contact with the other filler particle. We believe that in the region of filler

concentrations $0.06 < \varphi < 0.1$, the beginning of filler aggregation takes place, and this is why the difference between samples with 6 and 10 vol % PBA is very small (see also Figure 7-12).

Above 10 vol% PBA, the structure of aggregates is established and from the linear dependence of $k_{1/4}$ vs. vol % PBA we conclude that again each filler particle contributes to the retardation process in the same way. Figure 7-17c shows two possibilities of how aggregates of filler can grow with increasing amounts of filler particles. Case c-II shows the situation when the aggregates grow in size as pure PBA domains. The situation is not consistent with experimental data because in this case we should not observe the linear dependence $k_{1/4}$ vs. φ, as the filler volume-to-surface ratio increases with increasing filler concentration.

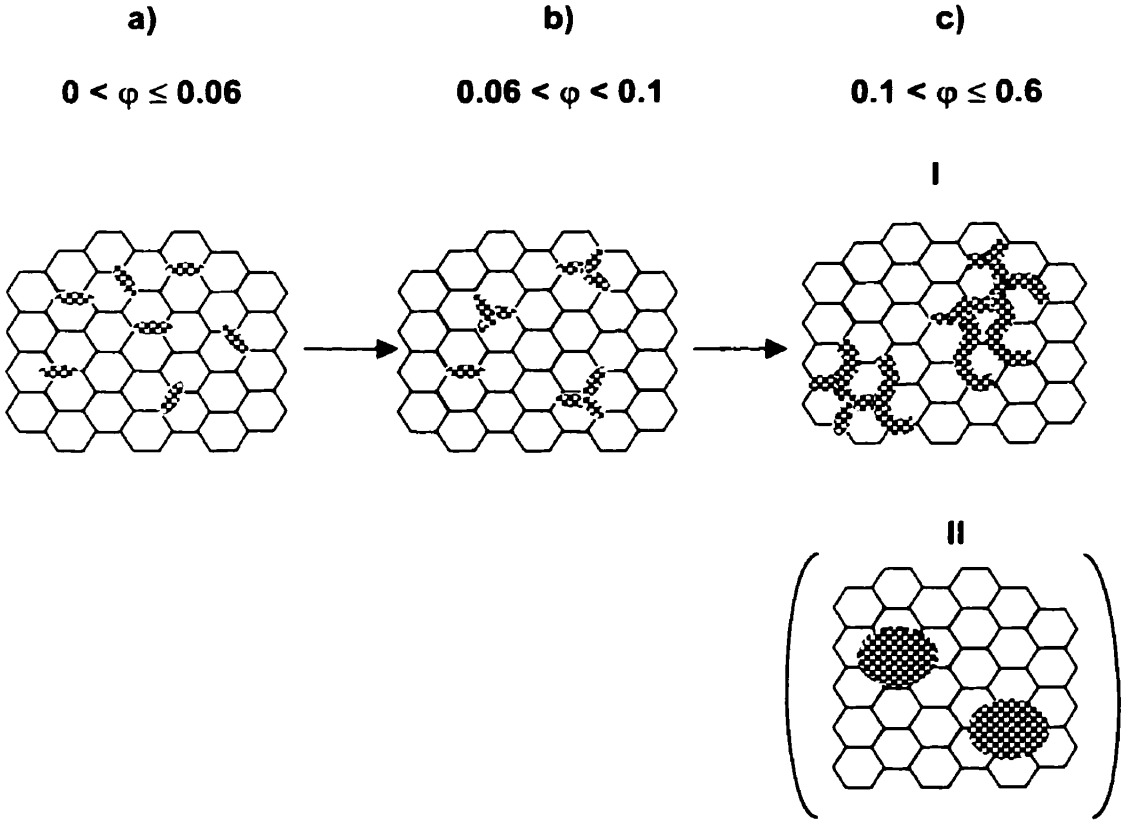

Figure 7-17. A model of latex film morphology in the presence of soft PBA fillers: a) at volume fractions of $\varphi_{PBA} \leq 0.06$ the filler particles are randomly distributed in the PBMA matrix; b) when $0.1 > \varphi_{PBA} > 0.06$ the formation of filler aggregates takes place; c) for $\varphi_{PBA} \geq 0.1$ we have two possibilities of the growth of aggregates with increasing volume of fillers; I) the aggregates are in form of a connected network which grows in contour length when the amount of filler is increased, II) the filler aggregates grow in volume. These domains consist of PBA only.

The other more realistic possibility, (case c-I), shows the aggregates growing in size as a kind of growing network of fillers. Here we can easily imagine that each element of the network (though as a separate filler particle or small group of filler particles) participates in the obstacle effect in the same way, by adding the same part of its surface to the total filler surface area in contact with diffusing polymer. This case is similar to that of Chevalier et at.[25], mentioned above, in the way that their PS aggregates in the PBA matrix seem to have the shape of a connected network. Their PS aggregates consist of 60 % PS, and 40 % PBA matrix. The PS particles have to be connected within the cluster as the percolation threshold for this system is at 32 vol % PS.

Another aspect of the morphology of latex blends was pointed out by Eckerslay et al.[27]. In their work they emphasize that not only the composition of the latex blends, but also the ratio of hard and soft particle sizes has a significant effect on latex film morphology. The smaller the filler diameter, the less is needed to form a continuous phase in the film, and the more easily the filler aggregates into connected domains. Therefore we have to keep in mind that some aspects (e.g. ranges of concentrations) of the proposed model of latex film morphology from Figure 7-17 can change with changing the ratio of particle size (soft/hard) in our films.

Summarizing, we think that case c-I shown in Figure 7-17 is the most likely structure of PBA aggregates in PBMA latex films. However, it is difficult to say if in the considered range of filler concentrations ($0.1 \leq \varphi \leq .0.6$) the elements of such a network can be thought of as individual particles, or rather as small aggregates consisting of a few filler particles. Although the suggested model of latex film morphology seems to be reasonable, in future we wish to get images from freeze fracture transmission electron microscopy (FFTEM) in order to see the real structure of these films and determine the validity of this model.

For very high filler concentrations ($\varphi > 0.6$), we expect that the dependence $k_{1/4}$ vs. φ has to change. Figure 7-13 confirms this conclusion. Using the linear dependence $k_{1/4}$ vs. φ to calculate the φ value at which $k_{1/4} = 0$, we find $\varphi = 1.85$! However, the volume fraction can not be larger than 1. For high concentrations of PBA, we expect a crossover to a dispersion of individual PBMA particles in a PBA matrix. In such a case, the interdiffusion between latex particles would be more and more suppressed. Thus the $k_{1/4}$ vs. φ dependence would change again for very high filler concentrations.

7.3.7 Obstacle vs. Free Volume models.

Up to now, we only considered the influence of the morphology of the latex film on the polymer diffusion rate. This does not, however, tell us anything about the nature of the interaction between the two polymers. There are two general models one can use to explain the change of diffusion rate in the presence of filler particles. These models differ in their description of the interactions between filler particles and the matrix. One model is the obstacle model. Obstacles decrease the apparent diffusion rate by increasing the tortuosity of the diffusion path (see Figure 7-18) without affecting the friction experienced by the diffusing species.

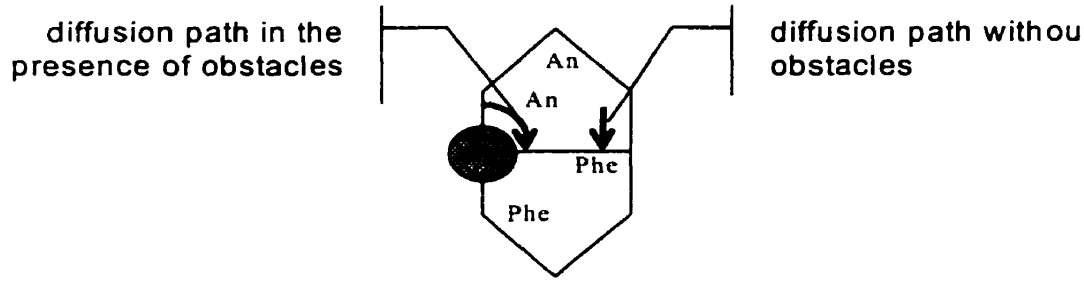

Figure 7-18. Influence of obstacles on polymer diffusion. The measured rate of diffusion decreases as the path of the diffusion increases in the presence of obstacles.

The second model is based on the concept of free volume. Free volume models ascribe the changed diffusion rate to an increase (or decrease) in the microscopic friction coefficient of the diffusing species. This change is caused by the influence of the surface of the filler on the mobility of diffusing polymer in the vicinity of the filler particles through specific polymer – filler interactions. In other words, close to the filler surface we have a polymer layer with an average thickness δ, which has a different mobility than the mobility of the polymer in the bulk.

However, the concept of two mobility regions can be applied to both models described above. ET in latex films as a method for measuring local polymer diffusion over distances up to 100 nm does not measure polymer diffusion on a macroscopic scale. The diffusion process measured is not sensitive to macroscopic changes in the film morphology. The macroscopic changes in the film morphology can contribute significantly to the obstacle effect on long term polymer diffusion. If this is so, "the local obstacle effect" on polymer

diffusion can be explained, as in the case of free volume theory, in terms of "two mobility regions". The polymer close to the filler surface, which is not further from the surface than an average distance δ_1 ($\delta_1 \approx R_g$), feels the tortuosity effect, and to reach a given point in space has to travel a longer path than the other polymer chains, which are further from the filler surface than δ_1. In this way, we have again two mobility regions: a "lower mobility" region close to the filler surface and a "higher mobility" region in the bulk. This means that the linear dependence of the diffusion rate parameter $k_{1/4}$ vs $1/d_{PBA}$ does not prejudge which model should be applied in our case. This is the reason we decided to learn more about our system. In new experiments we carry out diffusion measurements on low M PBMA films in the presence of PBA particles and also measure the glass transition temperature for PBMA + PBA blend films.

7.3.8 Influence of Soft PBA Particles on low M PBMA.

In reference 2 Feng et al. described the effect of hard fillers on the diffusion rate of the polymer in low M PBMA latex films. In these films, f_m is proportional to $t^{1/2}$. To examine the effect of filler size on polymer mobility they defined a mobility parameter $k_{1/2} = f_m/t^{1/2}$. They found that the hard fillers retard polymer diffusion. The effect is in many ways similar to that of the soft fillers in the high M PBMA matrix. At the same volume fraction of filler, the diffusion rate decreases with decreasing the size of the filler. In both systems, for constant volume fraction of filler, the diffusion rate k was founded to be inversely proportional to the size of the filler. Here we wish to see if we obtain a similar behavior for the low M PBMA sample in the presence of soft fillers.

These experiments were carried out with 30 and 60 vol % of PBA latex. The films were annealed at 55 °C. The results are presented in Figure 7-19, where we plot (a) the extent of mixing f_m vs square root of annealing time $t^{1/2}$, and (b) the apparent diffusion coefficient D_{app} vs f_m for pure PBMA sample and samples with different amounts of PBA filler.

Figure 7-19 shows that 30 vol % PBA clearly promotes polymer diffusion, while 60 vol % of PBA has a negligible effect on PBMA diffusion. The results are very different than those for the high M PBMA in the presence of soft fillers, and also different than those for the same low M PBMA in the presence of hard fillers. The results from Figure 7-19 indicate that two opposite and overlapping phenomena influence the PBMA diffusion rate in the

presence of soft PBA fillers. The presence of soft fillers in the film, on one hand, speeds up the diffusion process, perhaps by influencing the free volume of the film. On the other hand, the soft fillers retard diffusion by acting as obstacles. In the case of the sample with 60 vol % of PBA, the two effects cancel.

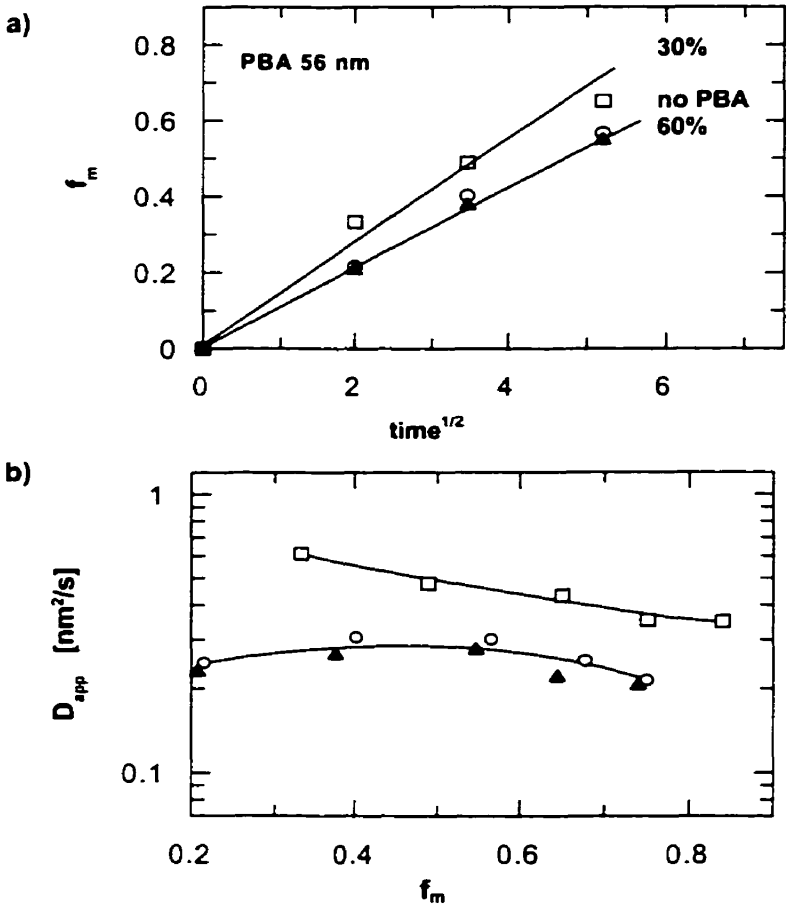

Figure 7-19. Comparison of low M PBMA diffusion rates for films blended with different amounts of PBA particles (d_{PBA}= 56 nm), expressed as volume percent (% PBA); 0 (○), 30 (□), and 60 (▲). In part a) we plot the extent of mixing (f_m) vs. square root of annealing time ($t^{1/2}$), and in part b) we plot the apparent diffusion coefficient D_{app} vs. f_m.

7.3.9 MDSC Measurements of the Glass Transition Temperature T_g in the PBMA + PBA blends.

The presence of soft filler particles in latex films can speed up or slow down polymer diffusion depending on the amount of filler present in the sample and the molecular weight of the polymeric matrix. When the changes in mobility are due to changes in the friction

coefficient of the diffusing species, we should be able to monitor changes in mobility via changes in the glass transitions of the latex blends with respect to its pure components.

a) High M PBMA + PBA

In Figure 7-20 we present a plot of the first derivative of the heat capacity vs. temperature for the high M PBMA sample itself and for its blends with 30 and 60 vol % of PBA. The maximum of the peak in the DSC scan indicates the value of T_g. The only difference between Figure 7-20a and 7-20b is the sample history.

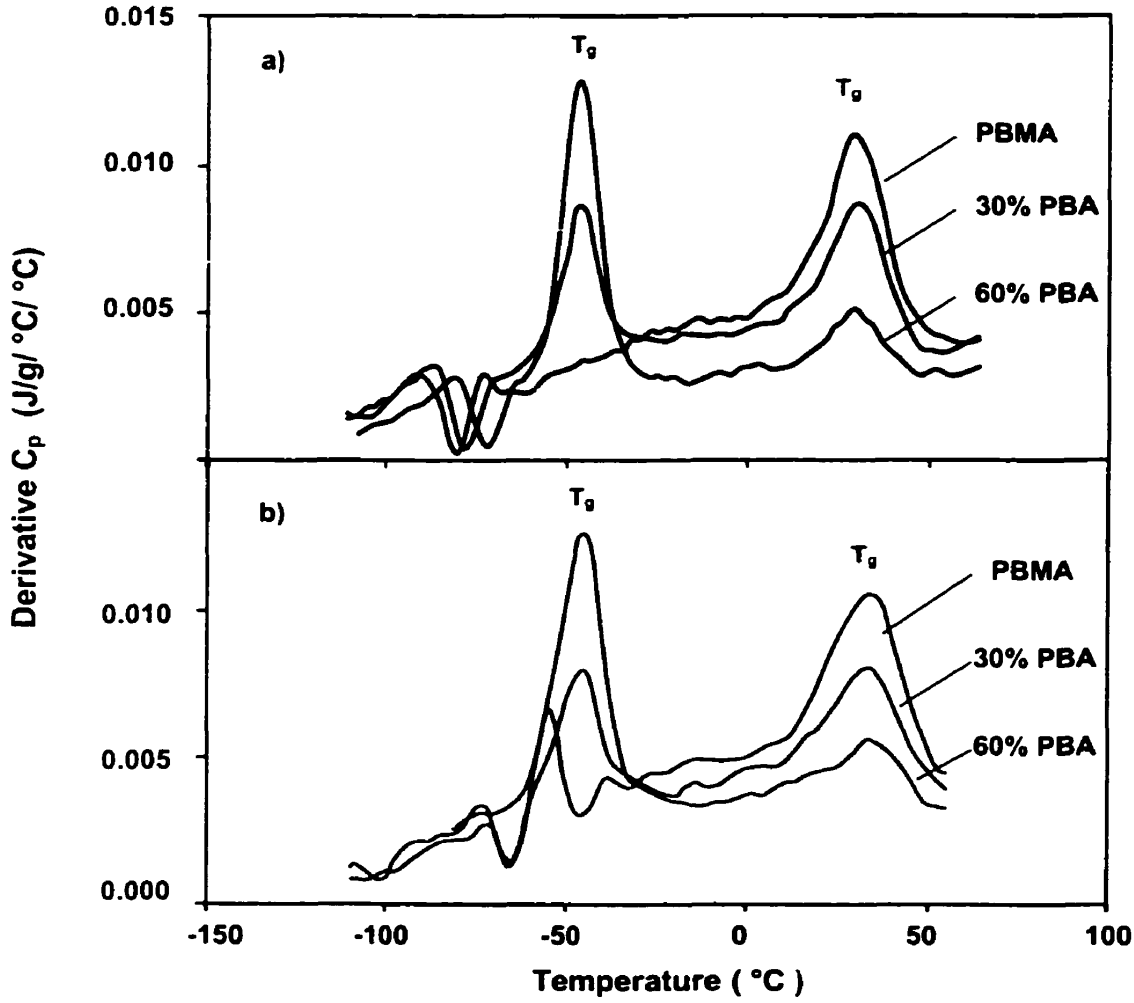

Figure 7-20. Plot of the first derivative of the heat capacity vs temperature for the high M PBMA sample, and its blends with 30 vol %, and 60 vol % of PBA. Part a) presents the heating scan from -125° C to 75° C; and in part b) the cooling scan from 75° C to -125° C.

Figure 7-20a presents a heating scan where samples were cooled from room temperature to –125 °C, and measurements of T_g were taken during sample heating from –

125 °C to 75 °C. Figure 7-20b shows the DSC curves for the case where samples were cooled from 75 °C to -125°C. For samples consisting of PBMA and PBA blends, DSC scans show two peaks. Figure 7-20 shows that the T_g of PBMA in the presence of PBA particles does not change in comparison to the T_g of pure PBMA (34 °C). The same invariance was observed for the T_g of PBA. The T_g of pure PBA is equal to - 43 °C and does not change in the presence of PBMA polymer. An important feature of the glass transition peaks is that they are symmetric. Only the T_g peak for the PBMA sample with 60 vol % of PBA is asymmetric in the cooling scan. For this sample, the peak has a tail on the side of lower T_g values. However, we have to point out that the range of temperatures at which the glass transition takes place and the maximum of the peaks is the same for all samples, which indicates that there is no miscibility or evidence for special interaction between high M PBMA and the cross-linked PBA particles. Combining the DSC results with the fact that diffusion of high M PBMA is retarded in the presence of PBA particles, we conclude that the retardation of polymer diffusion is due to an obstacle effect.

b) Low M PBMA + PBA.

In the case of low M PBMA films, we investigated the same blend compositions in the same range of temperatures. Figure 7-21a shows the heating scan (samples heated from -125°C to 75 °C) for pure low M PBMA films and films with 30 and 60 vol % PBA particles, while Figure 7-21b shows the DSC scans for the same samples, for a run carried out from 75 °C to -125°C (cooling scan).

In Figure 7-21, we do not see any change in the position of the PBA peak for films consisting of PBA – PBMA blends. Its maximum is at - 43°C, and is the same as that for the pure PBA film. This indicates that there is negligible miscibility between cross-linked PBA and PBMA. The glass transition region of low M PBMA alone occurs in the same temperature range (-10 to 50 °C) as its blends. However, the maxima of the PBMA peaks for samples with 30 and 60 vol % of PBA move slightly to higher temperatures compared with those of the pure PBMA sample (T_g = 24.5 °C), and are at ca. of 26 °C and 29°C, respectively. This result seems very surprising upon first consideration. We know from energy transfer experiments that PBA particles promote diffusion of low M PBMA. If the

filler increases the free volume in the blend film, we expect a decrease in the PBMA T_g in the presence of PBA particles.

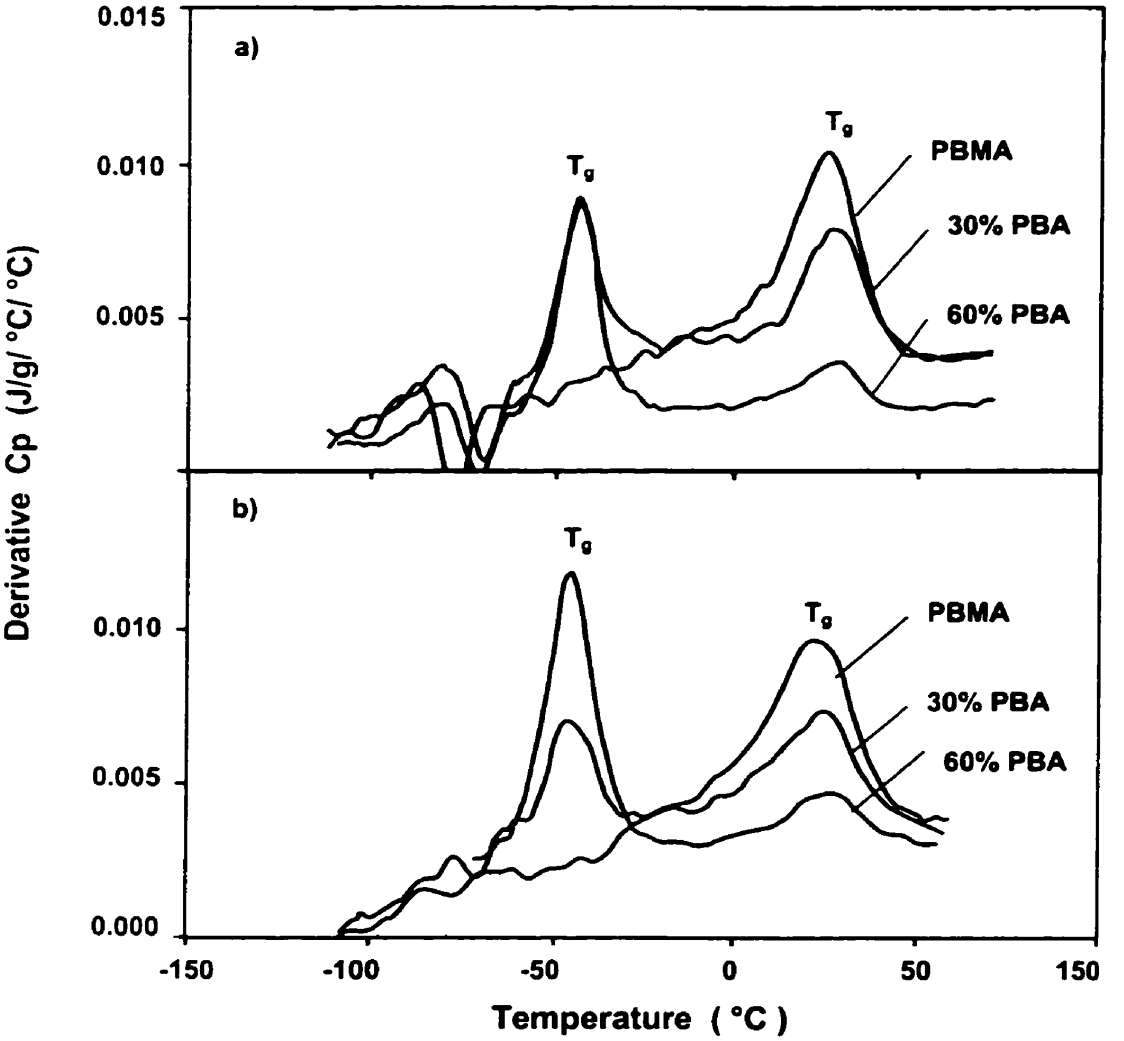

Figure 7-21. Plot of the first derivative of the heat capacity vs temperature for the low M PBMA sample, and its blends with 30 vol %, and 60 vol % of PBA. Part a) presents the heating scan from –125 °C to 75 °C; and in part b) the cooling scan from 75 °C to –125 °C.

However, other features of the PBMA glass transition region for PBMA and PBA blends help us to understand the observed phenomena. The peaks for the samples with increasing PBA content become asymmetric in shape, suggesting two overlapping peaks. On the side of higher temperatures, the transition peaks are steeper than on the side of lower temperatures. The asymmetry of the peaks for samples with PBA fillers indicates the existence of two different mobility regions in these films. As the range of glass transition

temperatures is the same for PBMA samples with and without fillers, we conclude that the presence of soft PBA particles in the PBMA matrix induces wetting of the filler surface by lower-M PBMA and segregation of PBMA into higher and lower mobility regions. This effect increases the average diffusion rate of low M PBMA, as presented in Figure 7-22.

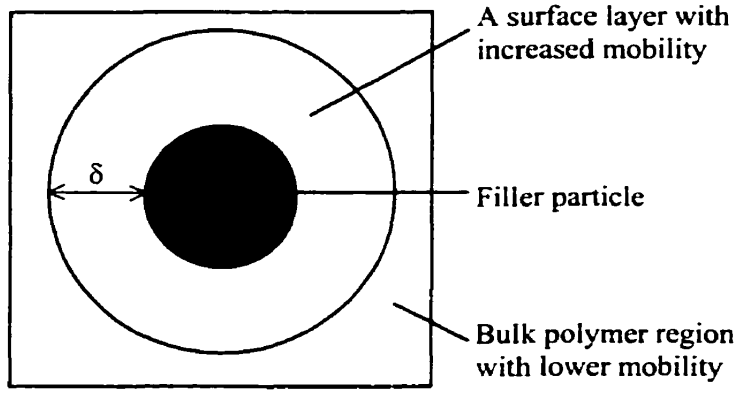

Figure 7-22. Drawing of a model for films with soft filler: the presence of soft PBA particles in the PBMA matrix induces wetting of the filler surface by the part of PBMA with lower M and the formation for PBMA of higher and lower mobility regions. This effect increases the average diffusion rate of PBMA.

In Figure 7-22, we present a drawing indicating key features of our explanation. The higher mobility region consisting of lower molecular weight PBMA surrounding the filler particle. The rest of the PBMA has lower mobility, as the molecular weight of this region is higher. The PBMA from the higher mobility region mixes faster than the PBMA from the lower mobility region, or PBMA in the absence of filler particles. This effect influences the whole diffusion process by increasing the average diffusion rate of low M PBMA.

7.4 Conclusions

1. The presence of soft, elastic particles in a latex film decreases the diffusion rate of high M PBMA latex polymer. The retardation effect depends on the total surface of filler particles being in contact with diffusing polymer.

2. The presence of soft, elastic particles in the low M PBMA latex film increases the diffusion rate of the PBMA polymer.
3. The overall effect of soft filler particles on polymer diffusion is a combination of an obstacle effect, a wetting phenomenon, and an influence on the morphology of the film. Depending on which of these effects dominates, we can observe an increase or decrease in the polymer diffusion rate. The diffusion rate in low M PBMA films is speeded up in the presence of 30 vol % PBA particles, and we do not observe any effect on polymer diffusion when the amount of PBA particles is increased to 60 vol % PBA.

7.5 References

1. a) Hsu, W. H.; Wu, S. *Polym. Eng. Sci.* **1993**,vol.33, No. 5, 293. b) Tsagaropolous, G.; Eisenberg, A. *Macromolecules*, **1995**, 28, 6067. c) Vollenberg, P.; Heinkens, D. *Polymer*, **1989**, 30, 1659. d) Lucis, S.; Kovacevic, V.; Hace, D. *International J. Adhesion & Adhesives*, **1998**, 18:(2), 115.
2. Feng, J.; Odrobina E.; Winnik M. A. *Macromolecules* **1998**, 31, 5290.
3. Lipatov, Y. S.; Sergeeva, L. M. *Adsorption of Polymers*; Wiley: New York, 1974.
4. Bitsanis, I.; Hadziioannou, G. *J. Chem. Phys.* **1990**, 92, 3827.
5. Mansfield, K. F.; Theodorou, D. N. *Macromolecules* **1991**, 24, 6283.
6. Mayes, A. M. *Macromolecules* **1994**, 27, 3114.
7. Baschnagel, J.; Binder, K. *Macromolecules* **1995**, 28, 6808.
8. Baschnagel, J.; Binder, K. *J. Phys. I* **1996**, 6, 1271.
9. Brown, H. R.; Russell, T. P. *Macromolecules* **1996**, 29, 798.
10. Honeycutt, J. D.; Thirumalai, D.; Klimov, D. K. *J. Phys. A: Math. Gen.* **1989**, 22, L169. Printed in UK.
11. Frank, B.; Gast, A. P.; Russell, T. P.; Brown, H. R.; Hawker, C. *Macromolecules* **1996**, 29, 6531.
12. Zheng, X.; Rafailovich, M. H.; Sokolov, J.; Strzhemechny, Y.; Schwarz, S. A.; Sauer, B. B.; Rubinstein, M. *Phys. Rev. Lett.* **1997**, 79, 241.
13. Lin, E. K.; Wu, W. L.; Satija, S. K. *Macromolecules* **1997**, 30, 7224.
14. Orts, W. L.; , van Zanten, J. H.; Wu, W. L.; Satija, S. K. *Phys. Rev. Lett.* **1993**, 71, 867.
15. Keddie, J. L.; Jones, R. A. L.; Cory, R. R. *Europhys. Lett.* **1994**, 27, 59.

16. Reiter, G.; *Macromolecules* **1994**, 27, 3046.
17. Forrest, J. A.; Dalnoki-Verres, K.; Dutcher, J. R. *Phys. Rev. Lett.* **1996**, 77, 2002.
18. Forrest, J. A.; Dalnoki-Verres, K.; Dutcher, J. R. *Phys. Rev. E* **1997**, 56, 5705.
19. Feng, J. *Ph.D. Thesis*, University of Toronto, **1997.**
20. Feng, J.; Yekta, A.; Winnik, M. A. *Chem. Phys. Lett.* **1996**, 260, 296.
21. Briber, R. M.; Liu, X.; Bauer, B. J. *Science*, **1995**, 268, 395.
22. Serenko, O. A.; Goncharuk, G. P.; Knunyants, M. I.; Kryuchkov, A. N. *Polym. Sci. Ser. A*, **1998**, Vol. 40, No. 7.
23. Linder, P.;2 Zemb, Th., Eds. *Neutron, X-ray and Light Scattering: Introduction to an Investigative Tool for Colloidal and Polymeric Systems*; North-Holland: Amsterdam, 1991.
24. Chevalier, Y. *Trends Polym. Sci.* **1996**, 4, 197.
25. Chevalier, Y.; Hidalgo, M.; Cavaillé, J. Y.; Cabane, B. *Macromolecules*, **1999**, 32 7887.
26. (a) Cavaillé, J.-Y.; Pérez, J. *Macromol. Chem., Macromol. Symp.* **1990**, 35/36, 405. (b) Cavaillé, J.-Y.; Vassoille, R.; Thollet, G.; Rios, L.; Pichot, C. *Colloid Polym. Sci.* **1991**, 269, 248. (c) Ouali, N.; Cavaillé, J.-Y.; Pérez, J. *Plast., Rubber Compos. Process. Appl.* **1991**, 16, 55. (d) Favier, V.; Chanzy, H.; Cavaillé, J.-Y. *Macromolecules* **1995**, 28, 6365.
27. Eckersley, S. T.; Helmer, B. J. *J. Coat. Technol.*, **1997,** vol 69, No 864, 97.

APPENDIX A

The theory of modulated differential Calorimetry

The theory supporting modulated DSC can be easily understood by comparing it to conventional DSC. In both techniques the difference in temperature between the sample and a reference is measured as a function of time, and from the Newton's Law of cooling (A-1) the heat flow between the sample and reference is calculated:

$$\frac{dQ_{1-2}}{dt} = K(T_1 - T_2) \tag{A-1}$$

where dQ_{1-2}/dt is the calculated heat flow between the sample and reference, T_1 and T_2 are the temperatures of sample and reference, respectively, measured experimentally, and K is a constant.

DSC and MDSC differ in the way the sample is heated. In the case of conventional DSC, the sample and reference are heated with a constant heating rate β, so that the temperature is a linear function of time:

$$T(t) = T_0 + \beta t \tag{A-2a}$$

where T(t) is the programmed temperature, T_0 is the starting temperature, t is time, β is the constant heating rate (°C/min), is defined by equation (A-2b).

$$\beta = \frac{dT}{dt} \tag{A-2b}$$

In the case of MDSC, the change of programmed temperature follows the equation

$$T(t) = T_0 + \beta t + A_T(\sin \omega t) \tag{A-3a}$$

where A_T is the Amplitude of temperature modulation; $\omega = 2\pi/P$ is the modulation frequency (sec^{-1}); P is the period (sec), and β is the overall (average) heating rate.
The MDSC heating rate calculated from equation (A-3a) is:

$$\frac{dT}{dt} = \beta + C\cos \omega t \tag{A-3b}$$

where $C = A_T\omega$, which is a constant.

The heating rate consists of two components: β, the average heating rate, and the modulated heating rate equal to $C\cos\omega t$. Applying the temperature changes with time (eq. A-3a) to the calculations of heat flow (eq. (A-1)), we see that the heat flow from equation (A-1) has the form of a modulated heat flow. The total heat flow in MDSC is the average of the modulated heat flow signal. An example of modulated heating rate, modulated and total heat flow, for an EO_{20} sample is shown in Figure A-1.

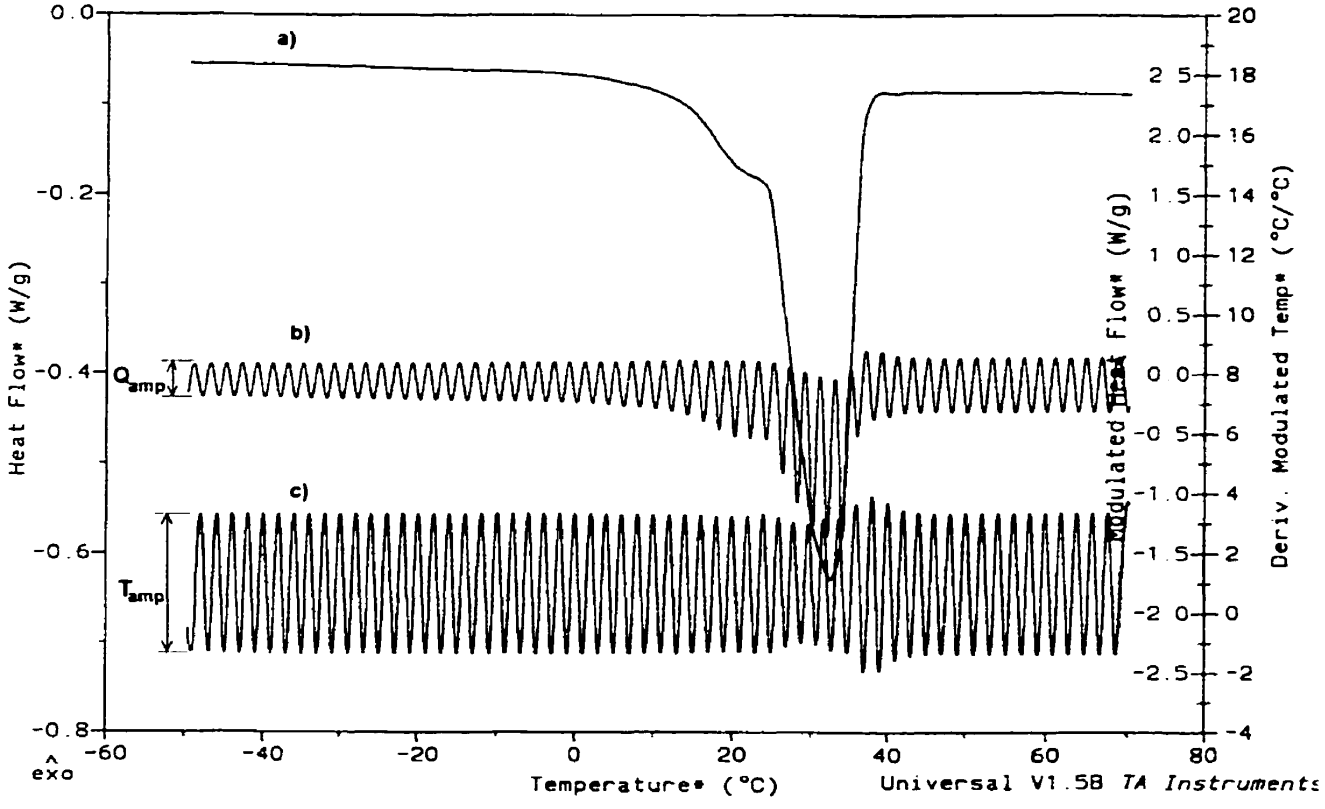

Figure A-1. a) The total heat flow calculated as the average of the modulated heat flow signal; b) the modulated heat flow and its amplitude Q_{amp}; c) the heating rate with its amplitude T_{amp}.

The general equation, which describes the total heat flow at any point in a DSC or MDSC experiment is:

$$\frac{dQ}{dt} = Cp\beta + f(T,t) \qquad \text{(A-4)}$$

where dQ/dt is the total heat flow, Cp is the heat capacity, β is the average heating rate, and $f(T,t)$ is the heat flow from the kinetic (absolute temperature- and time-dependent process).

As can be seen from equation (A-4), the total heat flow (dQ/dt) consists of two components. One component is a function of the sample's heat capacity and the rate of temperature change, whereas the other is a function of absolute temperature and time. Conventional DSC determines only total heat flow, while modulated DSC determines the total, as well as these two individual heat flow components. MDSC is able to do this based on the two heating rates seen by the materials (equation (A-3b)): the average heating rate β, and the sinusoidal heating rate. The individual heat flow components are often referred to by different names. We use the terms "heat capacity component" [Cpβ] and "reversing heat flow" interchangeably. Likewise "kinetic component" [f(T,t)] and "nonreversing heat flow" are use interchangeably. Reversing heat flow represents the changes in the heat capacity, so from the reversing heat flow we are able to calculate the glass transition temperature. Nonreversing heat flow represents all events that are nonreversing on the time scale of the temperature modulations. As an example of non-reversing heat flow, we point out sample thermal history, evaporation, or cold crystallization. In real life, the glass transition, represented by reversing heat flow, is nearly always obscured by non-reversing events. In the case of conventional DSC, where we can measure only the total heat flow, we are not able to separate reversing from non-reversing heat flow, and we can not analyze complex transitions. In the case of MDSC, we are able to analyze these complex transitions.

We have already explained that the total heat flow is an averaged modulated heat flow. To calculate the reversing component of total heat flow, we first have to calculate the heat capacity C_p of the sample, and then convert the heat capacity into heat flow using the equation (A-5).

$$\text{Reversing Heat Flow} = (-C_p) \times \text{Average Heating Rate} \qquad \text{(A-5)}$$

The kinetic (non-reversing) component of the total heat flow is determined as the arithmetic difference between the total heat flow and the heat capacity component.

$$\text{Nonreversing Heat Flow} = \text{Total Heat flow} - \text{Reversing Heat Flow} \qquad \text{(A-6)}$$

The approach of calculating the heat capacity C_p in MDSC is based on one of the well-accepted procedures for determining C_p by conventional DSC. In conventional DSC, C_p is generally calculated from the difference in heat flow between a blank (empty pan) run and a sample run under identical conditions:

$$C_p = K_{Cp} \frac{\text{Heat Flow(sample)} - \text{Heat Flow(blank)}}{\text{Heating Reate}} \qquad \text{(A-7)}$$

where K_{Cp} is a calibration constant.

However, C_p can also be calculated by comparing the difference in the heat flow between two runs on an identical sample at two different heating rates. In this case:

$$C_p = \bar{K}_{Cp} \frac{\text{Heat Flow at Heat Rate 2 - Heat Flow at Heat Rate1}}{\text{Heating Rate 2 - Heating Rate 1}} \qquad \text{(A-8)}$$

where $\bar{K}_{Cp}$ is a diffrent calibration constant.

In MDSC, the heating rate changes during the modulation cycle. The amplitude of the modulated heating rate (Figure A-1c) is the difference between the smallest and the largest heating rate with which the sample is heated, and in general can be thought of as the difference between two different heating rates. The amplitude of modulated heat flow (Figure A-2b) is the difference between the heat flow at the highest heating rate and at the lowest heating rate, and can be thought of as the difference between heat flow at rate 1 and heat flow at rate 2. Taking the amplitude of modulated heat flow and dividing it by the amplitude of the modulated heating rate is equivalent to the conventional DSC approach using two different heating rates and equation (A-8), so the final equation for heat capacity C_p in MDSC is:

$$C_p = K_{Cp}(Q_{amp} / T_{amp}) \qquad \text{(A-9)}$$

where C_p is the heat capacity, K_{Cp} is the heat capacity calibration constant, Q_{amp} is the heat flow amplitude, T_{amp} is the temperature amplitude, $T_{amp} = 2C$, where C is the constant from equation (A-3b).

References

Modulated DSC™ Compendium – Basic theory and experimental considerations, edited by TA Instrument Thermal Analysis and Rheology.